11th Human Amyloid Imaging

January 11-13, 2017
Miami, Florida

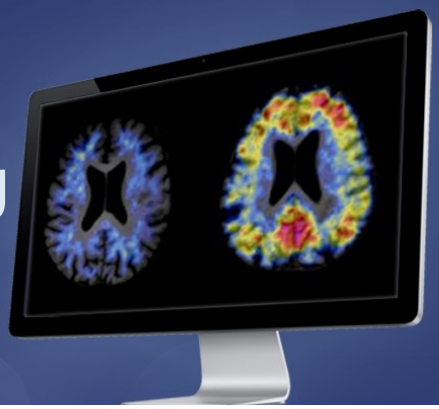

Co-Organizers:
Keith A. Johnson, MD ● William J. Jagust, MD ● William E. Klunk, MD, PhD ● Chester A. Mathis, PhD

Conference Program and Abstracts

www.worldeventsforum.com/hai

Table of Contents

PRESENTER INDEX

POSTER INDEX *(www.worldeventsforum.com/hai/posters)*

WEDNESDAY

Abs. ID	Board #	Poster Title	Authors	Presenter
125	**1**	Kinetic modeling of the tau PET tracer [18F](S)THK-5351 in healthy controls and Alzheimer's disease subjects	Barret | Constantinescu | Buckley | Dalsgaard | Gibson | Purohit | Beaver | Seibyl | Tamagnan | Marek | Jennings | Salinas-Valenzuela	**Barret**
183	**2**	A cortical cluster-based measure of change in longitudinal 18F-T807 FTP PET	Becker | Cosio | Lee | Andrea | Sperling | Johnson	**Becker**
157	**3**	Comparison of region of interest segmentation methods for extraction of 11C-PiB SUVR in the Down syndrome population	Betthauser | Lao | Tudorascu | Price | Bulova | Hartley | Hardison | Tumuluru | Minhas | Laymon | Murali | Mathis | Cohen | Barnhart | Devenny | Klunk | Johnson | Handen | Christian	**Betthauser**
172	**4**	A comparison of DVR and SUVR methods for THK5317 and THK5351	Betthauser | Lao | Murali | Barnhart | Furumoto | Okamura | Stone | Johnson | Christian	**Betthauser**
87	**5**	[18F]flutemetamol â€“ quantification on the centiloid scale	Buckley | Battle | Smith | Van Laere | Vandenberghe | Lowe	**Buckley**
101	**6**	Evaluation of Caspase-3 Activation in AD using [18F]ICMT-11 PET/CT	Calsolaro | Femminella | Fan | Dani | Kozlowski | Aboagye | Edison	**Calsolaro**
76	**7**	Cerebral Brain Perfusion in Cognitively Normal Elderly: Measured with Arterial Spin Labelling and [18F]Flutemetamol PET	Carter | Parkes | Hinz | Pendleton | Herholz	**Carter**
70	**8**	Selection of reference region for 18F-THK-5351 PET imaging analysis	Chen | Hsiao | Lin | Huang	**Chen**
104	**9**	Head-to-head comparison of tau-specific tracers in Alzheimer's disease: [11C]THK5351 vs [11C]PBB3 PET imaging	Chiotis | Stenkrona | Almkvist | Arakawa | Takano | Stepanov | Varrone | Higuchi | Halldin | Nordberg	**Chiotis**
107	**10**	Flow changes affect SUVr but not binding potential in an AD clinical trial	Groot | Timmers | Ossenkoppele | Yaqub | Prins | Lammertsma | Scheltens | van Berckel	**Groot**
14	**11**	Optimization of early phase [18F]flutemetamol scanning window as a proxy for relative tracer delivery	Heurling | Van Laere | Vandenberghe | Buckley | Farrar | Lubberink	**Heurling**
99	**12**	In vitro binding of [3H]RO6958948, [3H]AV-1451, [3H]THK5351 and [3H]T808 to tau aggregates in non-AD tauopathies	Honer | Gobbi | Muri | Borroni	**Honer**
174	**13**	Measuring amyloid change using florbetapir over a 4 year interval in SUVR and Centiloid units	Joshi | Navitsky | Kennedy | Pontecorvo | Mintun | Devous Sr., | ADNI	**Joshi**
72	**14**	Noise reduction algorithm for amyloid imaging without loss of image resolution	Kimura | Fujii | Yamada | Hosokawa | Sakata | Murakami | Ishii	**Kimura**
94	**15**	Binding of a tau positron emission tomography ligand, PBB3, to alpha synuclein pathology as assessed by fluorescence and autoradiographic labeling	Koga | Ono | Sahara | Higuchi | Dickson	**Koga**
102	**16**	Considerations for defining a striatal region of interest in amyloid PET studies within the Down syndrome population	Lao | Betthauser | Price | Klunk | Bulova | Hartley | Hardison | Tumuluru | Murali | Mathis | Cohen | Barnhart | Tudorascu | Devenny | Laymon | Johnson | Handen | Christian	**Lao**
151	**17**	High quantitative accuracy amyloid PET imaging with precision estimation	Markiewicz | Erlandsson | Schott | Scott | Cash | Barkhof | Fox | Ourselin	**Markiewicz**
141	**18**	The quantitative impact of emission-transmission scan misalignment and region selection upon amyloid measurement accuracy	Matthews | Matthews | Smith	**Matthews**
132	**19**	Longitudinal Centiloid Change in ADNI [18F]Florbetapir PET Data: Implications for Clinical Trials	McLaren | Carbonell | Auclair | Zijdenbos | Joshi | Navitsky | Mintun | Chiao | Bedell	**McLaren**
133	**20**	FreeSurfer approach to the Centiloid standardization method: evaluation of	Minhas | Lopresti | Aizenstein | Laymon | Campbell | Yu | Tudorascu | Mathis | Klunk	**Minhas**

Abs. ID	Board #	Poster Title	Authors	Presenter
		alternative cortical target regions and partial volume correction		
187	**21**	Selegiline reduces brain [18F]THK5351 binding	Ng | Massarweh | Soucy | Gravel | Pascoal | Mathotaarachchi | Kang | Shin | Therriault | Levasseurr | Horowitz | Gauthier | Rosa-Neto	**Ng**
8	**22**	Development of novel tau PET tracers, [18F]AM-PBB3 and [18F]PM-PBB3	Ono | Kitamura | Shimada | Sahara | Takuwa | Yoshiyama | Trojanowski | Lee | Suhara | Zhang | Jang | Tamagnan | Marek | Higuchi	**Ono**
24	**23**	Validation of the semi-quantitative static SUVR method by pharmacokinetic modeling on dynamic cross-sectional [18F]-AV45 data	Ottoy | Verhaeghe | Niemantsverdriet | Wyffels | Somers | De Roeck | Struyfs | Soetewey | Deleye | Van den Bossche | Van Mossevelde | Ceyssens | Versijpt | Stroobants | Engelborghs | Staelens	**Ottoy**
28	**24**	A simulation study on the quantification of the blood flow-dependent component in [18F]-AV45 SUVR differences between the MCI and AD stage	Ottoy | Verhaeghe | Stroobants | Engelborghs | Staelens	**Ottoy**
117	**25**	Developing a tracer agnostic pipeline for amyloid and tau PET data	Hobel | Baker | Ellis | Pa	**Pa**
65	**26**	Implementation of the Centiloid transformation for 18F-florbetaben	Rowe | Jones | Dore | Baxendale | Mulligan | Stephens | De Santi | Masters | Dinkelborg | Villemagne	**Rowe**
59	**27**	Quantitative analysis and correlation with clinical endpoints of [18F]MK6240 targeting neurofibrillary tangles (NFTs) in healthy volunteers and subjects with AD	Salinas | Chiao | Purohit | Schmidt | Beaver | Sur | Struyk | Bennacef | Lohith | Evelhoch | Hiatt | Tamagnan | Jennings | Marek | Hargreaves	**Salinas**
3	**28**	Kinetics of [18F]GTP1 (Genentech tau probe 1) in the basal ganglia of Alzheimer's patients and healthy controls	Sanabria Bohorquez | Bentsson | Barret | Tamagnan | Alagille | de Crespigny | Ayalon | Ward | Kerchner | Jennings | Seibyl | Marek | Weimer | Marik	**Sanabria**
95	**29**	A computationally efficient method for making PET measurements: the T1-GTM approach.	Schultz | Sperling | Johnson	**Schultz**
21	**30**	Rigid registration contributes significant imprecision to amyloid PET SUVR measurements	Schwarz | Jones | Gunter | Lowe | Vemuri | Senjem | Petersen | Knopman | Jack	**Schwarz**
159	**31**	Comparison of tau distribution according to tau tracers in various neurodegenerative diseases: Using [18F]AV1451 and [18F]THK-5351	Jang | Rabinovich | Kim | Lee | Kim | Seo	**Seo**
22	**32**	18F-Flortaucipir SUV normalization using a Parametric Estimate of Reference Signal Intensity (PERSI)	Southekal | Devous Sr. | Kennedy | Navitsky | Lu | Joshi | Pontecorvo | Mintun	**Southekal**
93	**33**	Blood-brain barrier disruption in AD measured by PiB PET: a preliminary study	Su | Vlassenko | Raichle | Morris | Benzinger	**Su**
50	**34**	18F-PM-PBB3 a novel imaging tracer for visualization and quatification of TAU pathologies with Positron Emission Tomography	Tempest | Jang | Tamagnan | Marek | Seibyl | Alagille | Barret | Higuchi | Shimada | Ono | Suhara | Zhang	**Tamagnan**
96	**35**	Simplified reference tissue methods in [18F]AV1451 PET	Timmers | Golla | Ossenkoppele | Groot | Verfaillie | Scheltens | van der Flier | Schwarte | Mintun | Devous | Schuit | Windhorst | Lammertsma | Boellaard | Yaqub | van Berckel	**Timmers**
129	**36**	Longitudinal changes in [18]F-RO6958948 Tau PET signal in four Alzheimer's subjects	Wong | Kuwabara | Comley | Klein | Vozzi | Honer | Roberts | Kitzmiller | Gapasin | Borroni	**Wong**
15	**37**	Algorithm for reference region delineation for amyloid imaging using pattern recognition scheme and kinetics of administered Aβ probe — considering the number of clusters	Yamada | Kimura | Nagaoka | Hosokawa | Murakami | Ishii	**Yamada**

THURSDAY

Abs. ID	Board #	Poster Title	Authors	Presenter
138	**1**	Tau PET in subjects at risk for chronic traumatic encephalopathy	Andrea | Alverio | Lee | Nowinski | Jacobs | McKee | Johnson | Jin	**Andrea**
131	**2**	Antemortem-postmortem correlation of florbeta-pir (18F) PET amyloid imaging with quantitative biochemical measures of Aβ40 and Aβ42	Beach | Maarouf | Intorcia | Sue | Serrano | Roher	**Beach**
54	**3**	Metabolic Syndrome and Amyloid Accumulation in the Aging Brain	Gomez | Beason-Held | Bilgel | An | Studenski | Resnick	**Beason-Held**
43	**4**	Measurement of pathological amyloid in routine clinical assessment: comparison of visual [18F]Flutemetamol PET and CSF	Bogdanovic | Fantoni | Farrar	**Bogdanovic**
29	**5**	Uncovering the local-to-distributed relationship between Î²-amyloid and glucose metabolism	Carbonell | Mclaren | Zijdenbos | Bedell	**Carbonell**
73	**6**	Microglial activation correlates in vivo with tau aggregation and amyloid deposition in mild cognitive impairment and Alzheimer's disease	Dani | Wood | Mizoguchi | Fan | Morgan | Walker | Calsolaro | Femminella | Hinz | Brooks | Edison	**Dani**
86	**7**	Tau PET imaging and atrophy in neurodegenerative dementias	Dickerson | McGinnis | Gomperts | Makaretz | Wolk | Schultz | Vasdev | Johnson	**Dickerson**
147	**8**	Greater regional cortical thickness is associated with selective vulnerability to atrophy in AD, independent of regional amyloid load	Li | Duara | Loewenstein | Cabrerizo | Barker | Adjouadi	**Duara**
89	**9**	Insulin resistance in midlife increases the risk for brain amyloid accumulation 15 years later	Ekblad | Johansson | Laine | Viitanen | Jula	**Ekblad**
185	**10**	Staging of amyloid-beta, tau, regional atrophy rates and cognitive change in a non-demented cohort	Fletcher | Renaud | Nandi | DeCarli	**DeCarli**
63	**11**	Detection of radiologic and laboratory features of cerebral amyloid angiopathy in patients with AD	Fotiadis | Becker | Schwab | Rosand | Viswanathan | Sperling | Johnson | Greenberg | Gurol | Neuroimaging Initiative	**Gurol**
57	**12**	Left frontal global connectivity is a substrate of cognitive reserve in mild cognitively impaired patients with a high amyloid burden	Franzmeier | Duering | Weiner | Dichgans | Ewers	**Franzmeier**
91	**13**	Imaging tau deposition in the Lewy body diseases	Gomperts | Locascio | Makaretz | Schultz | Caso | Neil | Sperling | Growdon | Dickerson | Johnson	**Gomperts**
142	**14**	PET staging of brain amyloidosis using striatum	Hanseeuw | Betensky | Mormino | Schultz | Papp | Buckley | Chhatwal | Marshall | Rentz | Sperling | Johnson	**Hanseeuw**
79	**15**	In vivo tau imaging in Parkinson's disease using 18F-AV-1451 PET	Hansen | Damholdt | Parbo | Brooks | Borghammer	**Hansen**
179	**16**	Contribution of neuritic and diffuse plaques to signal derived from CN-Flutemetamol: a preliminary study in AD autopsy brains	Ikonomovic | Abrahamson | Buckley | Mathis | Klunk | Farrar	**Ikonomovic**
166	**17**	Is tau accumulation detectable before neuronal injury markers? – Analysis from tau PET imaging with [C-11]PBB3 in clinical variants of Alzheimer's disease	Imai | Ishii | Tanaka | Ishibashi | Wagatsuma | Sakata | Tago | Toyohara | Murayama | Maruno | Shimada | Higuchi | Suhara	**Imai**
146	**18**	Hippocampal cingulum integrity predicts change in tau accumulation in a downstream-connected region in amyloid-positive normal older individuals	Jacobs | Schultz | Amariglio | Hedden | Papp | Perea | Rentz | Sepulcre | Sperling | Johnson	**Jacobs**
161	**19**	Distinctive clinical significance of hemorrhagic and amyloid imaging markers in patients with clinical-radiological cerebral amyloid angiopathy in memory clinic patients	Jang | Lee | Kim | Seo	**Jang**
186	**20**	Increased level of CSF neurofilament light chain is associated with amyloidosis in transgenic rat model of AD	Kang | Zimmer | Shin | Mathotaarachchi | Pascoal | Ng | Zetterberg | Soucy | Poirier | Gauthier | Cuello | Rosa-Neto | Blennow	**Kang**
171	**21**	Investigation of gait speed and β-amyloid in older adults from the Harvard Aging Brain Study	Kirn | Buckley | Hanseeuw | Amariglio | Sperling | Johnson	**Kirn**

Abs. ID	Board #	Poster Title	Authors	Presenter
1	**22**	Hippocampal activation is associated with longitudinal amyloid accumulation and cognitive decline	Leal | Landau | Bell | Jagust	**Leal**
69	**23**	18F-AV-1451 PET demonstrates Braak stage-specific associations with limbic white matter integrity in normal aging	Lockhart | Maass | Marks | Baker | Jagust	**Lockhart**
68	**24**	Elevated 18F-AV-1451 PET tracer uptake detected in incidental imaging findings	Lockhart | Ayakta | Winer | La Joie | Rabinovici | Jagust	**Lockhart**
34	**25**	[F-18]-AV-1451 binding correlates with neurofibrillary tangle Braak staging in postmortem brain tissue samples	Marquie-Sayagues | Anton-Fernandez | Siao Tick Chong | Meltzer | Saez-Calveras | Verwer | Ramanan | Normandin | Frosch | Gomez-Isla	**Marquie-Sayagues**
173	**26**	Greater [F-18]THK-5351 binding in medial and ventral temporal lobe is associated with altered microstructure and reduced myelin	Merluzzi | Adluru | Schoen | Dean | Singh | Christian | Betthauser | Lao | Barnhart | Dhanabalan | Asthana | Alexander | Johnson | Bendlin	**Merluzzi**
19	**27**	Lower white matter integrity is associated with higher amyloid deposition in older adults without dementia in two independent samples	Oh | Narkhede | Razlighi | Stern | Mayeux | Brickman	**Oh**
184	**28**	PET tau and amyloid synergy in default mode network determines the clinical status in predementia stages of Alzheimer's disease	A. Pascoal | Mathotaarachchi | Kang | Ng | Soucy | Gauthier | Rosa-Neto	**Pascoal**
97	**29**	Nonfluent variant of primary progressive aphasia: Tau deposition in the language network	Pascual | Zanotti-Fregonara | Funk | Rockers | Pal | Yu | Spann | Schulz | Masdeu	**Pascual**
123	**30**	Global white matter diffusion characteristics predict longitudinal cognitive change independent-ly from amyloid accumulation in older adults	Rabin | Perea | Rachel Buckley | Johnson | Sperling | Hedden	**Rabin**
130	**31**	[18F]AV1451 tau PET distinguishes PSP from controls and Parkinson's disease	Schonhaut | McMillan | Dickerson | Siderowf | Devous | Tsai | Winer | Russell | Litvan | Roberson | Kramer | Pressman | Nasrallah | Baker | Gomperts | Johnson | Grossman | Jagust | Boxer | Rabinovici	**Rabinovici**
144	**32**	Tau PET imaging tracks both pathology and brain perfusion in non-AD tauopathies: a multimodal study	Rodriguez-Vieitez | Leuzy | Chiotis | Saint-Aubert | Almkvist | Wall | Nordberg	**Rodriguez-Vieitez**
135	**33**	Proteomics Signatures of AD: gender differences and relationship to pathological markers	Srivatsa | Lucas | Doraiswamy	**Srivatsa**
98	**34**	Longitudinal decrease of white matter PiB uptake in aging and AD	Su | Chen | Reiman | Morris | Benzinger	**Su**
78	**35**	Correlation of regional amyloid load in cognitively healthy monozygotic twin pairs, measured using [18F]Flutemetamol	ten Kate | Konijnenberg | den Braber | Adriaanse | Yaqub | Boomsma | Scheltens | van Berckel | Visser	**ten Kate**
119	**36**	Improved estimation of gray matter volume in presence of white matter hyperintensities in AD and Down syndrome studies with amyloid burden	Tudorascu | Karim | Alhilali | Lao | Betthauser | Tamburo | Maccloud | James | Minhas | Cohen | Snitz | Price | Lopresti | Mathis | Lopez | Johnson | Crainiceanu | Handen | Christian | Aizenstein | Klunk	**Tudorascu**
5	**37**	Tau-PET imaging with [18F]AV-1451 in progressive apraxia of speech with and w/aphasia	Utianski | Whitwell | Schwarz | Senjem | Tosakulwong | Duffy | Clark | Machulda | Jack | Lowe | Josephs	**Utianski**
112	**38**	Longitudinal tau-PET imaging using [18F]AV-1451 in progressive supranuclear palsy	Whitwell | Lowe | Boeve | Kantarci | Senjem | Tosakulwong | Schwarz | Spychalla | Petersen | Jack | Josephs	**Whitwell**
111	**39**	18F-AV-1451 and 11C-PIB PET do not explain impairment in Parkinson's disease	Winer | Pressman | Stiver | Maass | Schonhaut | Kramer | Rabinovici | Jagust	**Winer**
116	**40**	Pittsburgh compound-B PET and MRI biomarkers of cognition in aging multiple sclerosis patients	Zeydan | Lowe | Przybelski | Schwarz | Tosakulwong | Zuk | Senjem | Gunter | Roberts | Mielke | Benarroch | Rodriguez | Machulda | Lesnick | Knopman | Petersen | Jack Jr | Kantarci | Kantarci	**Zeydan**

FRIDAY

Abs. ID	Board #	Poster Title	Authors	Presenter
83	**1**	Relationships between tau and glucose metabolism differ by amyloid status in aging	Adams | Lockhart | Jagust	**Adams**
153	**2**	Regional Uptake of FDDNP and Exposure to Professional Fighting	Banks | Kepe | DiFilippo | Lee | Barrio | Bernick	**Banks**
154	**3**	Tau Imaging in Professional Fighters	Banks | Sreenivisan | Bernick	**Banks**
46	**4**	Amyloid positivity is associated with steeper declines in prospective verbal episodic memory independent of neurodegeneration in cognitively normal older adults	Bilgel | An | Gomez | Helphrey | Elkins | Wong | Resnick	**Bilgel**
115	**5**	Functional network integrity predicts cognitive decline in preclinical Alzheimer's disease	Buckley | Schultz | Hedden | Papp | Hanseeuw | Marshall | Sepulcre | Smith | Rentz | Johnson | Sperling | Chhatwal	**Buckley**
100	**6**	Potential for Braak staging based on quantitative analysis of THK 5351 PET images'	Buckley | Lysvic | Dalsgaard | Okamura	**Buckley**
120	**7**	Subjective cognitive concerns exhibit region-specific relationships with tauopathy in the Harvard Aging Brain Study	Buckley | Hanseeuw | Vannini | Mormino | Rentz | Sperling | Johnson | Amariglio	**Buckley**
163	**8**	Relationships between [11C]PIB, [18F]AV1451 PET, and gray matter volumes within functional networks in Alzheimer's Disease	Cha | Benjanin | La Joie | Ayakta | L. Baker | Janabi | O'Neil | Miller | J. Jagust | D. Rabinovici	**Cha**
47	**9**	Tau burden localized in functional brain networks is associated with cognitive performance in beta amyloid positive subjects across the AD spectrum	Charil | Shcherbinin | Southekal | Joshi | Devous | Miller | Schwarz	**Charil**
136	**10**	Amyloid-beta associated cortical thinning of the lateral temporo-parietal cortex predicts symptom severity over time in amnestic MCI patients	d'Oleire Uquillas | Jacobs | Properzi | Schultz | LaPoint | Hanseeuw | Johnson | Sperling | Vannini	**d'Oleire Uquillas**
149	**11**	Memory Encoding and Recalling assessed by functional Near-Infrared Spectroscopy	Jahani | Harper | Ellison | Fantana | Boas | Yucel	**Fantana**
42	**12**	Regional Visual Read Inspection of [18F]Flutemetamol Brain Images from End-of-Life and amnestic MCI Subjects	Farrar | Zanette	**Farrar**
45	**13**	AMYPAD: A European public-private partnership to investigate the value of beta-amyloid brain scans as a diagnostic and therapeutic marker for AD	Barkhof | Farrar	**Farrar**
88	**14**	Is microglial activation protective in mild cognitive impairment?	Femminella | Dani | Wood | Fan | Calsolaro | Mizoguchi | Atkinson | Edginton | Waldman | Hinz | Brooks | Edison	**Femminella**
165	**15**	Genetic Drivers of Resilience in Asymptomatic AD	Hohman | Dumitrescu	**Hohman**
169	**16**	Predicting the Rate of Amyloid Accumulation Using Multimodal Data	Jin | Huang | ADNI	**Jin**
126	**17**	Determining smallest detectable difference from longitudinal data â€“ Application to hippocampal volume data from ADNI	Joshi | Feng | Baumgartner	**Joshi**
143	**18**	Amyloid-beta related memory decline is modified by years of school education in cognitively normal subjects: A study of PiB PET and cognitive reserve	Kato | Kaori | Kuratsubo | Inui | Fukaya | Ito | Nakamura | MULNIAD	**Kato**
160	**19**	Clinical Utility of Amyloid PET in amnestic mild cognitive impairment.	Kim | Lee | Jang | Seo	**Kim**
106	**20**	Both odor identification and amyloid status predict memory declineâ€¯in older adults	Kreisl | Jin | Lee | Dayan | Vallabhajosula | Pelton | Shaw | Devanand	**Kreisl**
81	**21**	Severity of lifetime trauma is related to hippocampal tau deposition in Vietnam war veterans with PTSD	Landau | Horng | Neylan | Jagust | Hayes | Aisen | Petersen | Veitch | Jack | DiCarli | Saykin | Grafman | Tosun | Weiner	**Landau**
164	**22**	Prevalence of amyloid PET positivity according to APOE genotype in subcortical vascular cognitive impairment	Lee | Kim | Yoo | Park | Choe | Jang | Ossenkoppele | Kim | Kim | Jang | Kim | Park | Na | Seo	**Lee**

Abs. ID	Board #	Poster Title	Authors	Presenter
152	**23**	Associations between regional amyloid load, cortical thickness, APOE genotype and cognition in ADNIGO/ADNI2 Participants	Li | Duara | Loewenstein | Cabrerizo | Barker | Adjouadi	**Li**
44	**24**	Tau mediates temporal lobe structure-function relationships and disrupts memory encoding in normal aging	Marks | Lockhart | Mellinger | Swinnerton | Horng | Baker | Jagust	**Marks**
180	**25**	Regional tau correlates of instrumental activities of daily living and apathy in mild cognitive impairment and Alzheimer's disease dementia	Marshall | Gatchel | Donovan | Schultz | Becker | Chhatwal | Hanseeuw | Papp | Amariglio | Rentz | Sperling | Johnson	**Marshall**
178	**26**	PET based network analysis reveals temporal lobe as a hub for tau propagation in MCI	Mathotaarachchi | Pascoal | Shin | Kang | Fonov | Benedet | Gauthier | Rosa-Neto	**Mathota-arachchi**
40	**27**	Concordance improves between amyloid-PET and CSF amyloid-β for diagnosing Alzheimer's disease in a clinical setting by applying Aβ1-42/Aβ1-40 ratio	Niemantsverdriet | Ottoy | Verhaeghe | Somers | De Roeck | Struyfs | Soetewey | Bjerke | Van den Bossche | Van Mossevelde | Goeman | De Deyn | Marien | Versijpt | Parizel | Sleegers | Van Broeckhoven | Wyffels | Albert | Ceyssens | Stroobants | Staelens | Engelborghs	**Niemants-verdriet**
77	**28**	Clinical significance of visually equivocal amyloid PET on ADNI cohort	Oh | Seo | Oh | Oh | Roh | Lee | Kim	**Oh**
167	**29**	Heterogeneity of amyloid-related cognitive decline in clinically normal older adults	Papp | Rentz | Amariglio | Schultz | Johnson | Sperling | Mormino	**Papp**
139	**30**	Does high baseline amyloid predict declines in activity participation and need for cognition over 4 years? Results from the Dallas Lifespan Brain Study	Parker | Festini | Farrell | Park	**Parker**
108	**31**	Relationship between neuroticism and biomarkers of AD pathology in familial Alzheimer's disease	Quiroz | Baena | Norton | Cosio | Schultz | Gatchel | Sperling | Johnson | Lopera	**Quiroz**
85	**32**	Relationships between NREM-sleep fragmentation and changes in brain structure, metabolism, amyloid burden and cognitive performance in healthy OA	Rauchs | Andre | Tomadesso | Mezenge | Branger | Fossey | De Flores | Laniepce | Eustache | Chetelat	**Rauchs**
124	**33**	Longitudinal Measures of Cognition and Clinical Status are Associated with Tau Deposition in Early Symptomatic Stages of AD	Risacher | Deters | Schwarz | Saykin	**Risacher**
92	**34**	Beta-Amyloid PET imaging of neurodegenerative disorders in a Chinese specialty hospital	Qiao | Seibyl | Han | Mao | Xu | Lu | Marek | Tamagnan | Chan	**Seibyl**
55	**35**	Does the tau signal increase over time differ across brain regions and stage of impairment in Alzheimer's disease?	Shcherbinin | Mintun | Brittain | Lu | Joshi | Southekal | Devous | Schwarz	**Shcherbinin**
52	**36**	Gait variability, an indicator of subclinical amyloid burden	Tian | Bair | Bilgel | Wong | Resnick | Studenski	**Tian**
62	**37**	Years to parental symptom onset predicts amyloid burden, neurodegeneration and resting state connectivity changes in healthy elderly with a parental history of Alzheimer's disease	Villeneuve | Vogel | Gonneaud | Poirier | Rosa-Neto | Fagan | Bateman | Morris | Pichet Binnette | Vachon-Presseau | Benzinger | Johnson | Breitner | .	**Villeneuve**
134	**38**	Additive effects of subjective cognitive decline and Amyloid-beta burden predict cognitive decline in healthy elderly individuals	Vogel | Varga Dolezalova | La Joie | Marks | Schwimmer | Landau | Jagust	**Vogel**
61	**39**	MRI-based amyloid imaging in Alzheimer's disease on clinical scanner	Yablonskiy | Zhao | Benzinger | Fagan | Hassenstab | Cairns | Wen | Vlassenko | Astafiev | Raichle | Morris	**Yablonskiy**

HAI 2017 PROGRAM

Wednesday, January 11, 2017		
11:30am	Check-in	
12:30pm	Welcome Notes	**Keith Johnson,** *Massachusetts General Hospital*
12:40	**SESSION 1** **Quantifying Tau and Amyloid PET Signal**	CHAIRS: **Chester Mathis,** *University of Pittsburgh*, and **Bradley Christian,** *University of Wisconsin*
12:40	**Evaluating different in vivo measures of tau pathology for use as biomarkers**	**Anne Maas**, *University of California, Berkeley*
12:55	**Tau Load: a novel method for quantifying subject-specific neuropathologic tau signal from Flortaucipir PET**	**Michael Navitsky**, *Avid Radiopharmaceuticals*
1:10	**Recovering signal from AV1451 in frontotemporal lobar degeneration with partial volume correction**	**Adam Martersteck**, *Northwestern University Feinberg School of Medicine*
1:25	**Unbiased clustering using entorhinal and neocortical tau-PET uptake on [18F]AV-1451 maps onto age and clinical presentation in Alzheimer's disease**	**Jennifer Whitwell**, *Mayo Clinic*
1:40	**Nonlinear alignment of multimodal empirical distributions for Level-2 Centiloid transformations**	**Michael Properzi**, *Massachusetts General Hospital, Harvard Medical School*
1:55	Discussion	
2:25	**Keynote Lecture:** **Tau Prion Strains: Implications for Imaging**	**Marc Diamond,** *University of Texas Southwestern*
2:55	Keynote Discussion	
3:10	**POSTER SESSION 1** and Coffee Break	
4:40	**SESSION 2** **Novel Tau Tracers**	CHAIRS: **Julie Price,** *Massachusetts General Hospital* and **Robert Koeppe,** *University of Michigan*
4:40	**Effects of [18F]AV-1451 binding in cerebellar gray and extra-cortical areas**	**Suzanne Baker**, *Lawrence Berkeley National Laboratory*
4:55	**[18F]MK-6240, a novel neurofibrillary tangles PET tracer: Evaluation in healthy subjects and Alzheimer's Disease patients**	**Cyrille Sur**, *Merck & Co., Inc.*
5:10	**Current efforts to overcome drawbacks of [11C]PBB3 by developing new PBB3 derivatives: first-in-human PET study with [18F]AM-PBB3**	**Hitoshi Shimada**, *National Institute of Radiological Sciences*
5:25	**Evaluation of baseline and longitudinal tau burden in Alzheimer's disease using [18F]GTP1 (Genentech tau probe 1) PET imaging**	**Robby Weimer**, *Genentech Inc.*
5:40	**Invited Lecture:** **Molecular Imaging Analysis for Tracer Validation and Clinical Trials**	**Roger Gunn**, *Imanova Ltd*
6:00	Discussion	
6:30-8:30	Welcome Reception	

Thursday, January 12, 2017

7:00am	Check-in and Breakfast	
8:00	**SESSION 3** **Neuropathology I: Tau PET Ligand Selectivity and Comparative Studies**	CHAIRS: **William Klunk,** *University of Pittsburgh* and **Milos Ikonomovic,** *University of Pittsburgh*
8:00	**Evaluation of the selectivity of Tau PET radioligand THK5351 in AD brain in vitro and nonhuman primate brain in vivo**	**Qi Guo**, *AbbVie Inc.*
8:15	**Characterizing the "off-target" binding of 18F-THK5351 in Alzheimer's disease: correlation between ante-mortem and post-mortem findings**	**Ryuichi Harada**, *Tohoku University Graduate School of Medicine*
8:30	**In vitro binding properties comparison of the tau PET tracers THK5117, THK5351, PBB3 and T807 in autopsy brain from Alzheimer diseases cases**	**Laetitia Lemoine**, *Karolinska Institute*
8:45	**An autoradiographic evaluation of THK-5351 compared to AV-1451**	**Melissa Murray**, *Mayo Clinic*
9:00	Discussion	
9:30	**POSTER SESSION 2A** and Coffee Break	
10:15	**SESSION 4** **Nauropathology II: PET to Autopsy Correlations**	CHAIRS: **Melissa Murray,** *Mayo Clinic* **Teresa Gomez-Isla,** *Massachusetts General Hospital*
10:15	**Neuropathology and biochemical correlations of [F-18]AV-1451 and [C-11]PiB PET imaging in a subject with Alzheimer's disease**	**Milos Ikonomovic**, University of Pittsburgh
10:30	**Neuroimaging-pathologic correlation of [F-18]-AV-1451 in an autopsy confirmed Parkinson's disease case**	**Marta Marquie-Sayagues**, *MassGeneral Institute for Neurodegenerative Disease*
10:45	**Multimodal evaluation of 18F-AV-1451 PET in an autopsy-confirmed corticobasal degeneration patient**	**Corey McMillan**, *Perelman School of Medicine at the University of Pennsylvania*
11:00	Discussion	
11:25	**Announcement: Alpha–synuclein Imaging Prize**	**Jamie Eberling**, *The Michael J. Fox Foundation for Parkinson's Research*
11:30	**Keynote Lecture**	**Thomas Beach,** *Banner Sunhealth Research Institute*
12:00pm	Keynote Discussion	
12:15	Lunch	
1:45	**SESSION 5** **Tau PET: Non-AD Targets**	CHAIRS: **Gil Rabinovici,** *University of California, San Francisco* and **Brad Dickerson,** *Massachusetts General Hospital*
1:45	**18F Flortaucipir binding in choroid plexus: association with race and hippocampus binding**	**Christopher Lee**, *Massachusetts General Hospital, Harvard Medical School*
2:00	**[18F]Flortaucipir, aka [18F]AV-1451, autoradiography matches immunofluorescent staining from AT8 tau antibody in Chronic Traumatic Encephalopathy (CTE) post-mortem brain tissue sections**	**Yin-Guo Lin**, *Avid Radiopharmaceuticals, Inc.*
2:15	**Microscopic neuropathological evaluation of the binding profile of tau selective PET ligands in AD and primary tauopathies**	**Melissa Wren**, *University College London*
2:30	**AV-1451 tau-PET uptake in MAPT mutation carriers varies by tau isoforms**	**David Jones**, *Mayo Clinic*
2:45	**18F-AV-1451 binding in familial frontotemporal lobar degeneration with tau pathology**	**William Kreisl**, *Columbia University*
3:00	Discussion	
3:30	**POSTER SESSION 2B** and Coffee Break	
4:15	**SESSION 6** **Thresholds and Centiloids**	CHAIRS: **Keith Johnson,** *Massachusetts General Hospital* and **Sylvia Villeneuve,** *McGill University*
4:15	**Defining cut-points for imaging biomarkers used in brain aging and Alzheimer's disease research**	**Clifford Jack**, *Mayo Clinic*
4:30	**Centiloids**	**Robert Koeppe**, *University of Michigan*
5:00	Discussion	
5:30-7:30	**Networking Reception**	

Friday, January 13, 2017

7:00am	Check-in and Breakfast	
8:00	**SESSION 7** **AMYLOID AND TAU PET IN CLINICAL TRIALS**	CHAIRS: **Bill Jagust,** *University of California, Berkeley* and **Susan Resnick,** *National Institutes of Health*
8:00	**The A4 Study: preliminary analyses of baseline tau PET imaging**	**Reisa Sperling**, *Harvard Medical School*
8:15	**Conversion of aMCI subjects to AD in relation to [18F]flutemetamol amyloid status, and hippocampal volume in a phase III longit. study**	**David Wolk**, *Perelman School of Medicine at the University of Pennsylvania*
8:30	**Baseline 18F Flortaucipir SUVR, but not amyloid or cognition, predicts cognitive decline over 18 months in Phase 2 trial subjects**	**Michael Devous, Sr.,** *Avid Radiopharmaceuticals*
8:45	**PET amyloid and tau imaging in a Phase 3 study of solanezumab**	**Mark Mintun**, *Avid Radiopharmaceuticals*
9:00	Discussion	
9:30	**POSTER SESSION 3A** and Coffee Break	
10:15	**SESSION 8** **PRECLINICAL AD**	CHAIRS: **Reisa Sperling** and **Beth Mormino,** *Harvard Medical School*
10:15	**Implementing and testing the new A/T/N classification in AIBL participants combining fluid (CSF) and different Aβ and tau imaging radiotracers**	**Victor Villemagne**, *University of Melbourne*
10:30	**The relationship of elevated medial temporal lobe and diffuse brain tau-PET signal in clinically normal participants**	**Val Lowe**, *Mayo Clinic*
10:45	**Prevalence and incidence of amyloid positivity in cognitively normal elderly individuals**	**Neelesh Nadkarni**, *University of Pittsburgh*
11:00	**Longitudinal tau accumulation is associated with cognitive decline in normal elderly**	**Bernard Hanseeuw**, *Harvard Medical School*
11:15	**Baseline amyloid burden predicts cognitive decline four years later in healthy adults: the value of a dose-response analysis**	**Michelle Farrell**, *University of Texas at Dallas*
11:30	Discussion	
12:00pm	**Keynote Lecture**	**Howard Feldman,** *Univ. of California, SD*
12:30	Keynote Discussion	
12:45	Lunch	
2:15	**SESSION 9** **AMYLOID, TAU, AND NEURODEGENERATION**	CHAIRS: **Clifford Jack,** *Mayo Clinic* and **Tammie Benzinger,** *Washington University at St Louis*
2:15	**Neocortical Tau and hippocampus volume reflect distinct processes in preclinical Alzheimer's disease**	**Elizabeth Mormino**, *Massachusetts General Hospital*
2:30	**Do neurodegeneration or amyloid pathology contribute to the relationship between AV-1451 and cognitive symptoms in AD?**	**Alexandre Bejanin**, *University of California, San Francisco*
2:45	**Comparing the contributions of tau and neurodegenerative biomarkers to cognitive decline**	**Susan Landau**, *University of California, Berkeley*
3:00	**Differential genotypic variance in PET and CSF measures of amyloid burden: Findings from the DIAN Study**	**Jasmeer Chhatwal**, *Massachusetts General Hospital*
3:15	**Relationships between AV1451-PET and CSF biomarkers in a heterogeneous clinical sample**	**Renaud La Joie**, *University of California, San Francisco*
3:30	Discussion	
4:00	**POSTER SESSION 3B** and Coffee Break	
4:45	Awards Ceremony	
4:50	**SESSION 10** **AMYLOID AND TAU PET IN DISTINCT POPULATIONS**	CHAIRS: **Trey Hedden,** *Massachusetts General Hospital* and **Charles de Carli,** *University of California, Davis*
4:50	**Association of regional FDG hypometabolism with age, amyloid, tau, and cardiac and metabolic conditions along the AD continuum**	**Prashanthi Vemuri**, *Mayo Clinic*
5:05	**18F-AV1451 PET in patients with subcortical vascular cognitive impairment**	**Sang Won Seo**, *Sungkyunkwan University School of Medicine*
5:20	**White matter hyperintensities and brain amyloid deposition: the ARIC-PET Study**	**Rebecca Gottesman**, *Johns Hopkins University*
5:35	**Association of amyloid-beta plaque accumulation and glucose hypo-metabolism in Down syndrome demonstrates pattern assoc. w/AD**	**Patrick Lao**, *University of Wisconsin*
5:50	Discussion	
6:20	Closing Notes	**Keith Johnson**, *Massachusetts Gen. Hospital*

HAI 2017 ABSTRACTS

WEDNESDAY

Wednesday, January 11, 2017 - 12:40 pm - 01:40 pm

SESSION 1: Quantifying Tau and Amyloid PET Signal

SESSION 1 **Quantifying Tau and Amyloid PET Signal**	**CHAIRS:** **Chester Mathis** ***University of Pittsburgh*** **Bradley Christian** ***University of Wisconsin***
Evaluating different in vivo measures of tau pathology for use as biomarkers	Anne Maas *University of California, Berkeley*
Tau Load: a novel method for quantifying subject-specific neuropathologic tau signal from Flortaucipir PET	Michael Navitsky *Avid Radiopharmaceuticals*
Recovering signal from AV1451 in frontotemporal lobar degeneration with partial volume correction	Adam Martersteck *Northwestern University Feinberg School of Medicine*
Unbiased clustering using entorhinal and neocortical tau-PET uptake on [18F]AV-1451 maps onto age and clinical presentation in Alzheimer's disease	Jennifer Whitwell *Mayo Clinic*
Nonlinear alignment of multimodal empirical distributions for Level-2 Centiloid transformations	Michael Properzi *Massachusetts General Hospital, Harvard Medical School*
Discussion	

Evaluating different in vivo measures of tau pathology for use as biomarkers

Anne Maass[1,2], Susan Landau[1,3], Andy Horng[1], Samuel N. Lockhart[1], Renaud La Joie[3], Suzanne L. Baker[4], Gil D. Rabinovici[1,3,4], William J. Jagust[1,3,4]

[1]*University of California, Berkeley, Berkeley, CA, USA*
[2]*German Center for Neurodegenerative Diseases, Magdeburg, Germany*
[3]*Memory and Aging Center, University of California San Francisco, San Francisco, CA, USA*
[4]*Lawrence Berkeley National Lab, Berkeley, CA, USA*

Objectives: To evaluate multiple whole-brain and region-specific approaches to quantify Alzheimer's Disease (AD)-related tau accumulation by AV-1451 tau PET, derive tau positivity cut-offs, and relate these measures to cognition, beta-amyloid (Aβ) and atrophy.
Methods: Two independent cohorts received AV-1451 PET, structural MRI, and Aβ PET (sample 1: PiB; sample 2: Florbetapir). Sample 1 comprised 11 young/middle-aged (YC/MAC: 39±17yrs), 66 older cognitively normal controls (OC: 78±6yrs) and 48 PiB^+ MCI/AD-dementia patients from UC Berkeley/UCSF. Sample 2 included 37 OC (73±6yrs) and 21 FBP^+ MCI/AD patients (80±6yrs) from ADNI. Tau PET measures were derived from native-space SUVR (80-100min post-injection, cerebellar gray reference) images after partial volume correction using Freesurfer-defined regions; for voxel-wise measures images were warped to MNI space. Several methods were used: (i) participants were categorized into Braak stages (Fig.1); (ii) SUVRs within the Braak ROIs were measured; (iii) tracer uptake was quantified by different whole-brain measures (e.g. number of supra-threshold voxels; Fig.2); (iv) AD-vulnerable voxels were identified to quantify tau (Fig.3); (v) a factor analysis defined key regions; and (vi) SUVR was derived from a previously-reported meta-ROI (Jack, et al., 2016). Receiver operating curves characterized accuracy in distinguishing $Aβ^-$ OC from AD/MCI patients. Each measure was regressed against clinical and other imaging variables.
Results: Braak staging, global and region-specific measures yielded similar diagnostic accuracy, which was higher in cohort 1 than cohort 2. All measures were strongly related to amyloid and global cognition (MMSE), but verbal memory and hippocampal/entorhinal volume/thickness were associated with tracer retention in more specific ROIs. Key regions contributing to high tau measures included medial temporal, inferior/middle temporal, retrosplenial, and inferior parietal cortex.

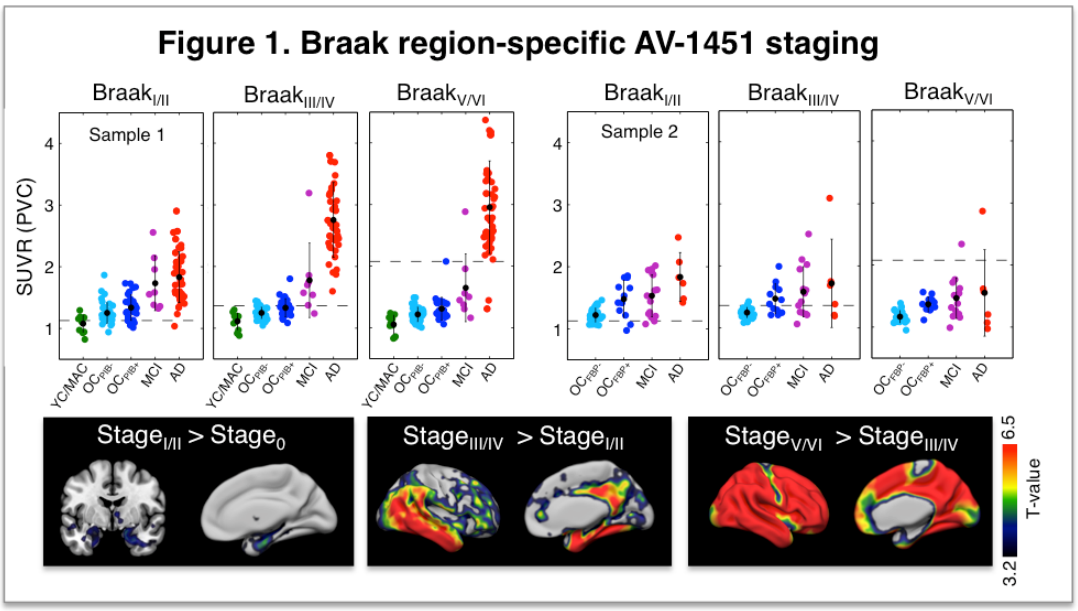

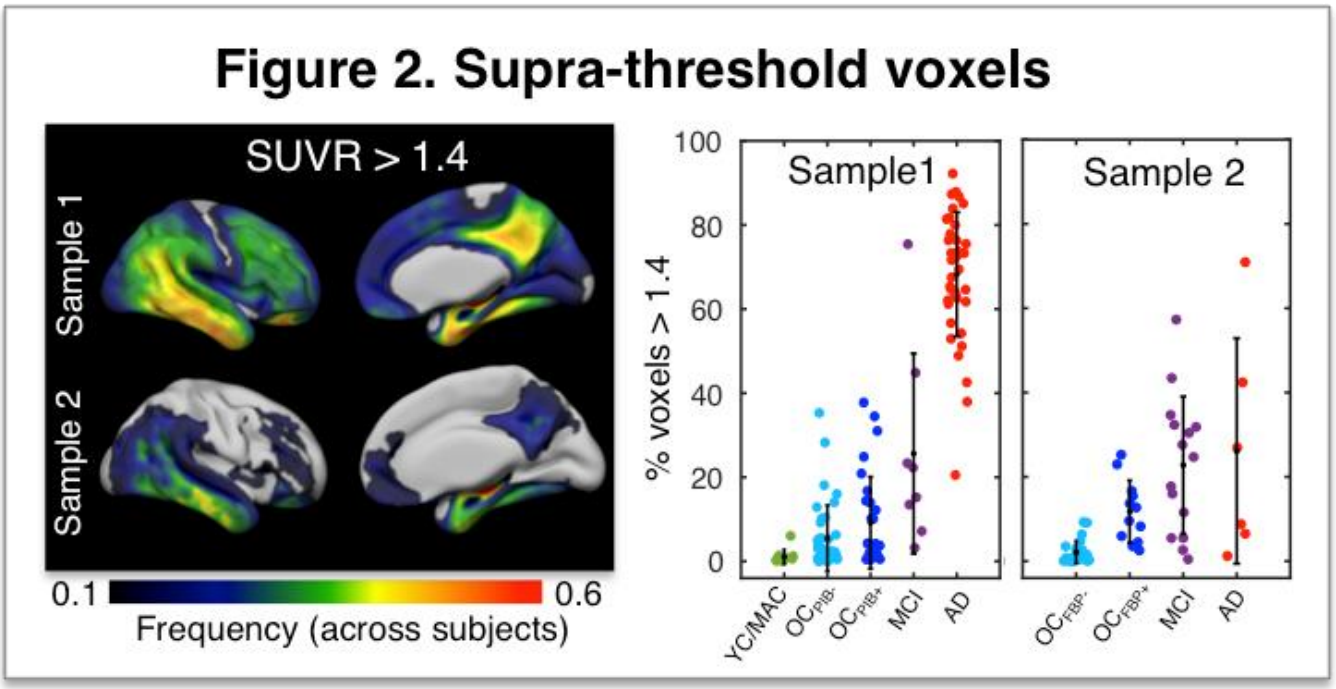

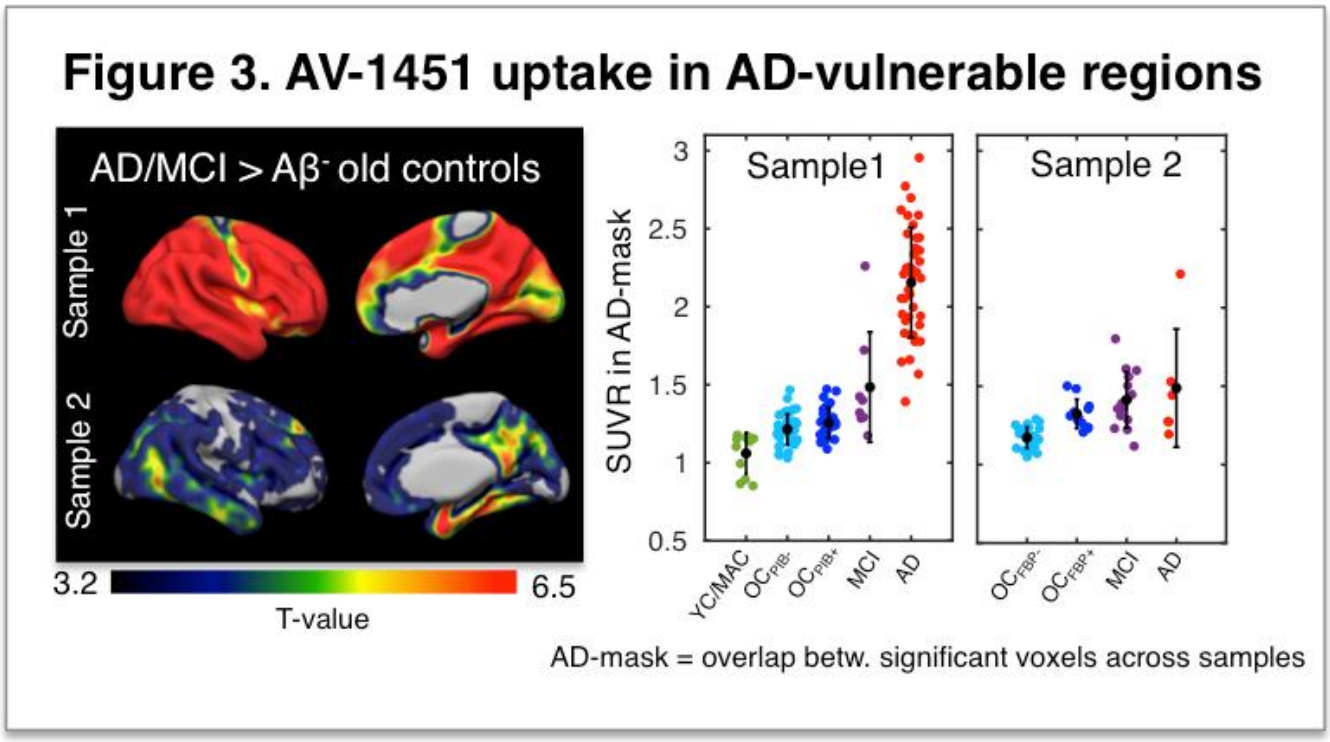

Conclusions: While whole-brain tau PET measures might be adequate biomarkers for capturing AD-related tau pathology, measures that assess AD-vulnerable regions may increase sensitivity to early tau accumulation and cognitive differences.

Keywords: tau, AV-1451, Braak staging, biomarker, cut points

Tau Load: a novel method for quantifying subject-specific neuropathologic tau signal from Flortaucipir PET

Michael Navitsky, Michael Devous, Abhinay Joshi, Ian Kennedy, Sudeepti Southekal, Michael Pontecorvo, Ming Lu, Mark Mintun

Avid Radiopharmaceuticals, Philadelphia, PA, USA

Background: Flortaucipir images generally demonstrate patterns of tau pathology predicted by the neuropathology literature. However, substantial heterogeneity in the image patterns has been observed that seems to relate to the character of cognitive impairment. Quantitating such heterogeneity poses challenges to the use of typical fixed anatomical VOIs. Herein we present a technique which incorporates both the density and distribution of the tau signal.

Methods: Flortaucipir scans from 52 amyloid negative (Aβ-) cognitively normal subjects (67.6±10.2 yr, MMSE 29.5±0.5) were used to create mean and standard deviation (SD) SUVr images (normalized to a parametrically derived white-matter reference region) in MNI space. Z-score images from control, MCI and AD subjects were then masked to include only voxels with Z≥3 (i.e., the pathologic volume PV) within subject-specific tissue segmentations obtained from co-registered T1 MRI scans (i.e., total tissue volume TV). Tau load was calculated as the average SUVr within the PV normalized by TV to account for differences in brain size (Fig. 1). Tau load was evaluated in test-retest, cross-sectional and longitudinal data in comparison to a weighted neocortical VOI (MUBADA).

Results: Tau load achieved high test-retest reproducibility (n=21, R^2=0.99), and distinguished groups based on Aβ status and diagnosis (Fig. 2). Both tau load and MUBADA demonstrated low uptake in young controls presumed to have no cortical tau. Similarly, among Aβ+ subjects, both measures detected longitudinal change and showed good correlation between baseline and Δtau (R^2 >0.5) at 18 months of follow up.

Conclusions: Tau load demonstrated equivalent performance on typical metrics to MUBADA while capturing characteristics of both the density and distribution of the tau signal. The subject-specific information captured by tau load by not being fixed to a given neuroanatomic brain region may be important in assessing natural disease progression or potential therapeutic response.

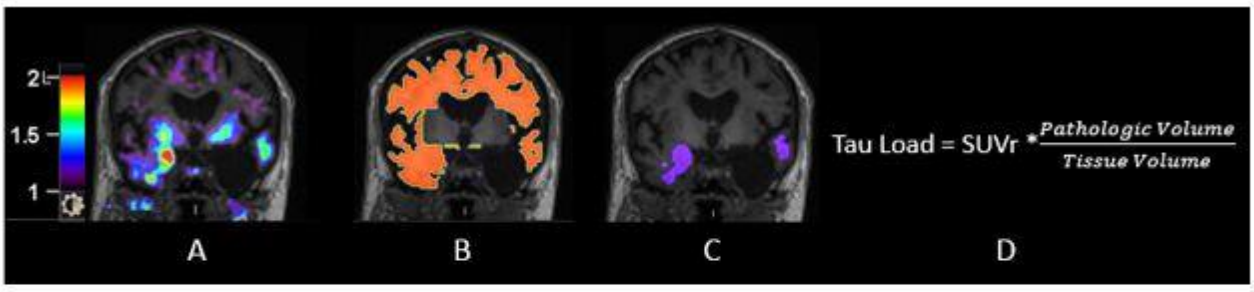

Figure 1. A) Flortaucipir SUVr image (normalized to a parametrically derived white-matter reference region). B) Tissue volume derived from subject-specific T1 MRI tissue segmentations. C) Pathologic volume defined as voxels with Z≥3 relative to a normal control data base. D) Tau load equation, where SUVr is the mean SUVr value from the masked pathologic tissue volume.

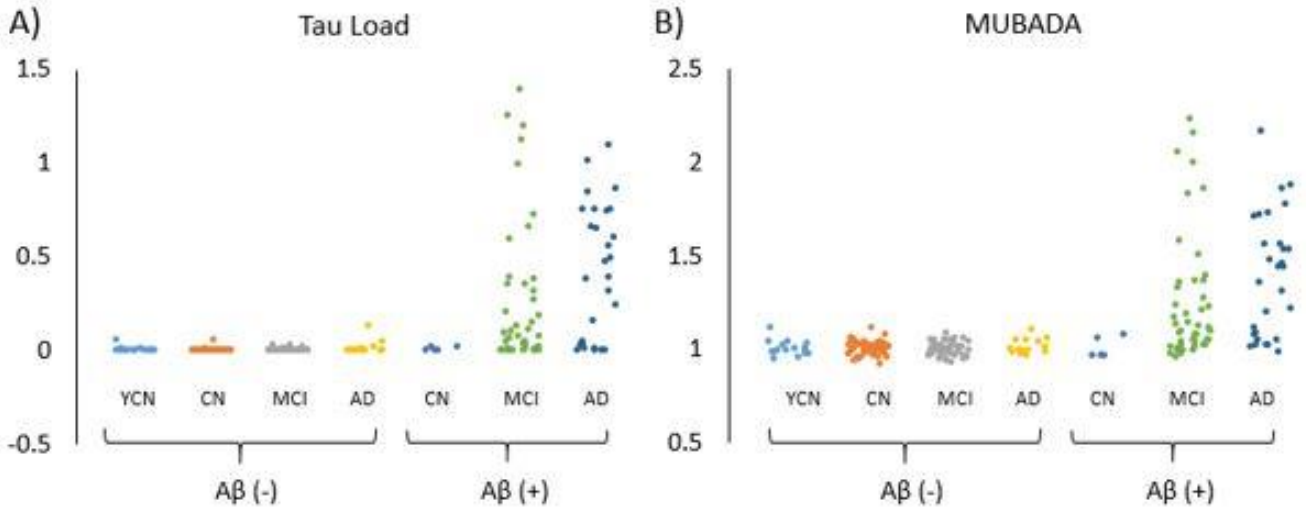

Figure 2. Cross-sectional (n=215) measures across groups defined by both clinical diagnosis and amyloid status for A) tau load and B) MUBADA SUVr. Both a tau load of 0 and SUVr of 1 are representative of no tau signal.

Keywords: Alzheimer's Disease, tau imaging, Flortaucipir, PET, quantification

Recovering signal from AV1451 in frontotemporal lobar degeneration with partial volume correction

Adam Martersteck[1,2], Jaiashre Sridhar[2], Allison Rainford[2], M.-Marsel Mesulam[2,3], Emily Rogalski[2]

[1]*Department of Radiology, Northwestern University Feinberg School of Medicine, Chicago, IL, USA*
[2]*Cognitive Neurology and Alzheimer's Disease Center, Northwestern University Feinberg School of Medicine, Chicago, IL, USA*
[3]*Department of Neurology, Northwestern University Feinberg School of Medicine, Chicago, IL, USA*

Background: Primary progressive aphasia (PPA) is a clinical dementia syndrome often characterized by asymmetric atrophy and proteinopathy of the language-dominant (usually left) hemisphere. Common neuropathologies reported for PPA include Alzheimer's disease (AD), frontotemporal lobar degeneration with tauopathy (FTLD-tau) or TDP43 (FTLD-TDP). PET imaging with ^{18}F-AV1451 has shown high binding to lesions of paired helical filament tau found in AD and there have been reports of clinically relevant signal found in FTLD-tau cases that match the expected straight filament tau deposition.
Objective: Determine if 1) the AV1451 binding found in PPA cases with suspected FTLD-tau pathology showed a clinically concordant distribution and 2) if using partial volume correction could improve our ability to detect a pattern of tau deposition above the grey cerebellar reference.
Methods:: Eight participants with PPA underwent T_1-weighted MRI, florbetapir amyloid PET, and AV1451 tau PET imaging. Freesurfer (FS) was used to reconstruct the T_1-weighted MRI scans (v5.1.0), generate atrophy maps (v5.1.0) and to complete partial volume correction (PVC; v6.0.0-beta). Partial volume correction was applied using the modified Müller-Gärtner (mMG) method, solving for white matter, ventricular CSF, and extracerebral segmentations by a symmetric geometric transfer matrix. Partial volume corrected and non-corrected AV1451 PET signal from the middle of the cortical ribbon were resampled to the FS pial surface and compared.
Results: Two agrammatic PPA participants showed a florbetapir mean cerebral-to-cerebellar SUVR < 1.10 (Aβ-negative) and were classified as "suspected FTLD-tau". In both PPA cases, there was no AV1451 tau signal above the 1.0 grey matter cerebellar SUVR before PVC (see figure). After applying mMG PVC, the regional distribution of AV1451 more closely aligned with patterns of neurodegeneration observed in PPA.
Conclusions: Using partial volume correction to recover signal in AV1451 PET may improve the detection of straight filament tau found in FTLD tauopathies.
Keywords: partial volume correction, frontotemporal lobar degeneration, primary progressive aphasia, freesurfer

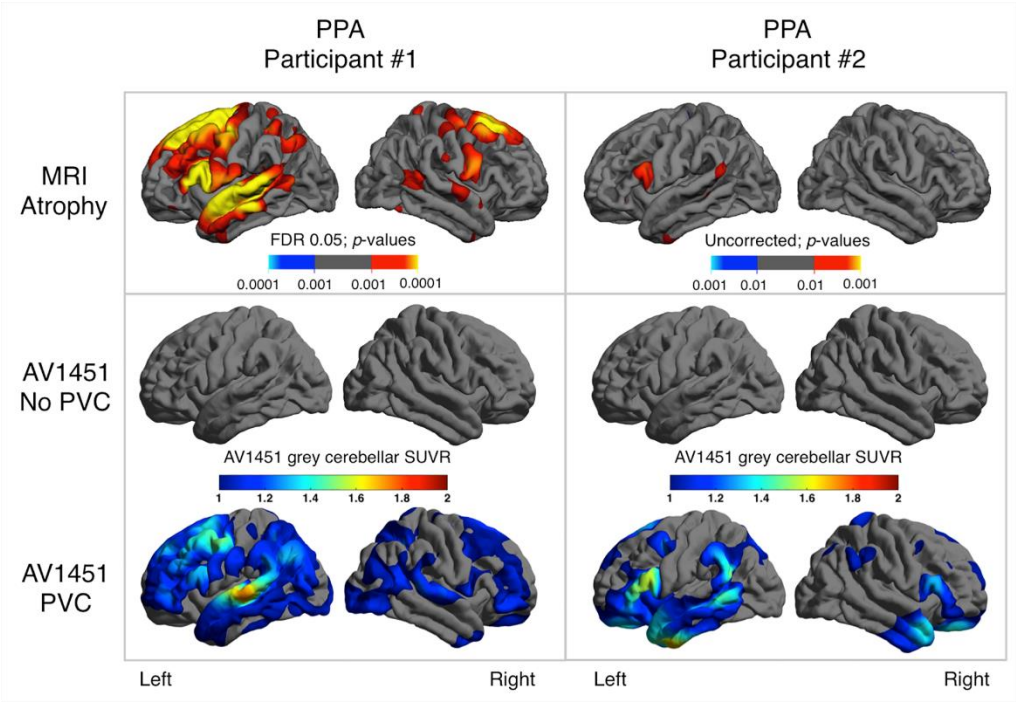

Unbiased clustering using entorhinal and neocortical tau-PET uptake on [18F]AV-1451 maps onto age and clinical presentation in Alzheimer's disease

Jennifer Whitwell[1], Jonathan Graff-radford[1], Nirubol Tosakulwong[1], Stephen Weigand[1], Matthew Senjem[1], Anthony Spychalla[1], David Jones[1], Daniel Drubach[1], Ronald Petersen[1], Val Lowe[1], Clifford Jack[1], Keith Josephs[1]

[1]*Mayo Clinic, Rochester, MN, USA*

Background: Alzheimer's disease (AD) is a heterogeneous disorder that often results in atypical clinical presentations, particularly in patients under the age of 65. We aimed to perform an unbiased assessment of tau uptake on AV-1451 tau-PET in AD and determine whether patterns of entorhinal cortex (allocortex) and neocortical tau uptake can help explain the emergence of atypical clinical presentations.

Methods: Seventeen patients with an atypical presentation of AD underwent AV-1451 PET. We also identified 47 typical dementia of the Alzheimer's type patients with tau-PET (20 under age 65 and 27 older than age 65). All patients showed amyloid deposition on Pittsburgh Compound B (PiB) PET. AV-1451 uptake was calculated in entorhinal cortex (ERC) and a neocortical region-of-interest (including temporal, parietal, frontal and occipital cortices). Values were normalized to the cerebellum to create SUVRs. Tau-PET SUVRs were log transformed and clustered unbiased to clinical diagnosis into three groups using K-mean cluster analysis.

Results: The cluster analysis identified a cluster with low cortical SUVRs (cortical sparing), one with high cortical SUVRs but relatively low ERC SUVRs (low ERC) and one with high cortical and ERC SUVRs (high ERC) (Figure). Clinical groups differed across clusters ($p<0.001$), with atypical AD associated with low ERC, young AD associated with high ERC and old AD associated with cortical sparing (Figure). Age differed across clusters, with older age observed in the cortical sparing cluster ($p<0.001$). Gender ratio, APOE genotype, global PiB ratio and mini-mental state examination score did not differ across clusters.

Conclusions: An unbiased clustering of tau-PET based on the ERC and neocortex maps well onto age and clinical presentation in AD. Atypical presentations tend to be associated with a pattern of high cortical tau similar to young-onset AD, but with relatively less involvement of the entorhinal cortex.

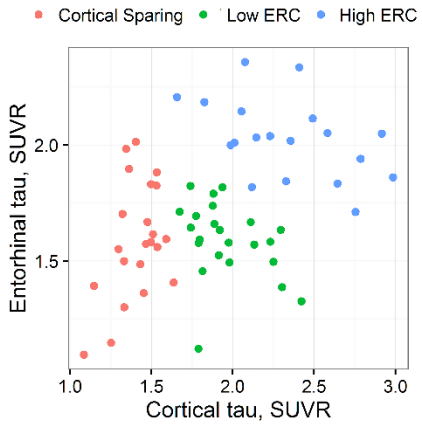

Tau cluster versus clinical group
P < 0.001

	Atypical AD	AD Young	AD Old
Cortical Sparing	4	1	17
Low ERC	11	7	5
High ERC	2	12	5

Keywords: tau, PET, AV-1451, Alzheimer's disease, atypical

Nonlinear alignment of multimodal empirical distributions for level-2 Centiloid transformations

Michael Properzi[1], Cristina Lois Gomez[2], Federico d'Oleire Uquillas[1], Reisa Sperling[1,3,4], Keith Johnson[2,3,4], Aaron Schultz [1,3]

[1]Department of Neurology, Massachusetts General Hospital, Harvard Medical School, Boston, MA, USA
[2]Department of Radiology, Massachusetts General Hospital, Harvard Medical School, Boston, MA, USA
[3]Athinoula A. Martinos Center for Biomedical Imaging, Massachusetts General Hospital, Harvard Medical School, Boston, MA, USA
[4]Department of Neurology, Brigham and Women's Hospital, Harvard Medical School, Boston, MA, USA

Introduction: The Centiloid project is intended to set a standard scale for reporting amyloid-PET measures. The current level-2 implementation relies on a strong linear assumption. We find alterations in processing methodology, target region, reference region, and partial volume correction (PVC) can all contribute to nonlinearities. We present a transformation that enables nonlinear mapping of a wider range of scale distributions onto the standard Centiloid scale (SCS).
Methods: The GAAIN Centiloid dataset was combined with baseline data from the Harvard Aging Brain Study (HABS) (278 Clinically normal older adults,74yrs SD=6.1). The combined PIB-PET dataset was processed with both the SCS and study specific HABS pipelines. The translation algorithm involved mapping between kernel-density smoothed empirical cumulative distribution functions from each pipeline. Centiloid values from the alternate pipelines were translated onto the SCS. Our method allows for mapping equivalent values between any two distributions where approximate rank-ordered matching can be assumed to hold.
Results: Figure 1 shows A) linearity between two SCS measures and B) greater variance between the SCS and Harvard/MGH pipelines for a cortical aggregate region (FLR), C) strong non-linearity within a focal region, and D) non-linearity with PVC. Discrepancies between linear and non-linear mapping to the SCS ranged as high as 19 Centiloids, with the location of strongest discrepancies dependent on the measure being mapped. For the regional measure shown in B), the max discrepancy occurs around 10 Centiloids, whereas PVC correction produced the strongest discrepancy at values exceeding 120.
Discussion: Our novel method has the advantage of accounting for realistic variation in measurement distributions, allowing for reporting of equivalent level-2 values that are more consistent with the SCS. Our approach offers an alternative for translating between any two empirical distributions, which has natural extension to combining data from multiple tracers. Future work will assess goodness-of-fit and distributions of errors.

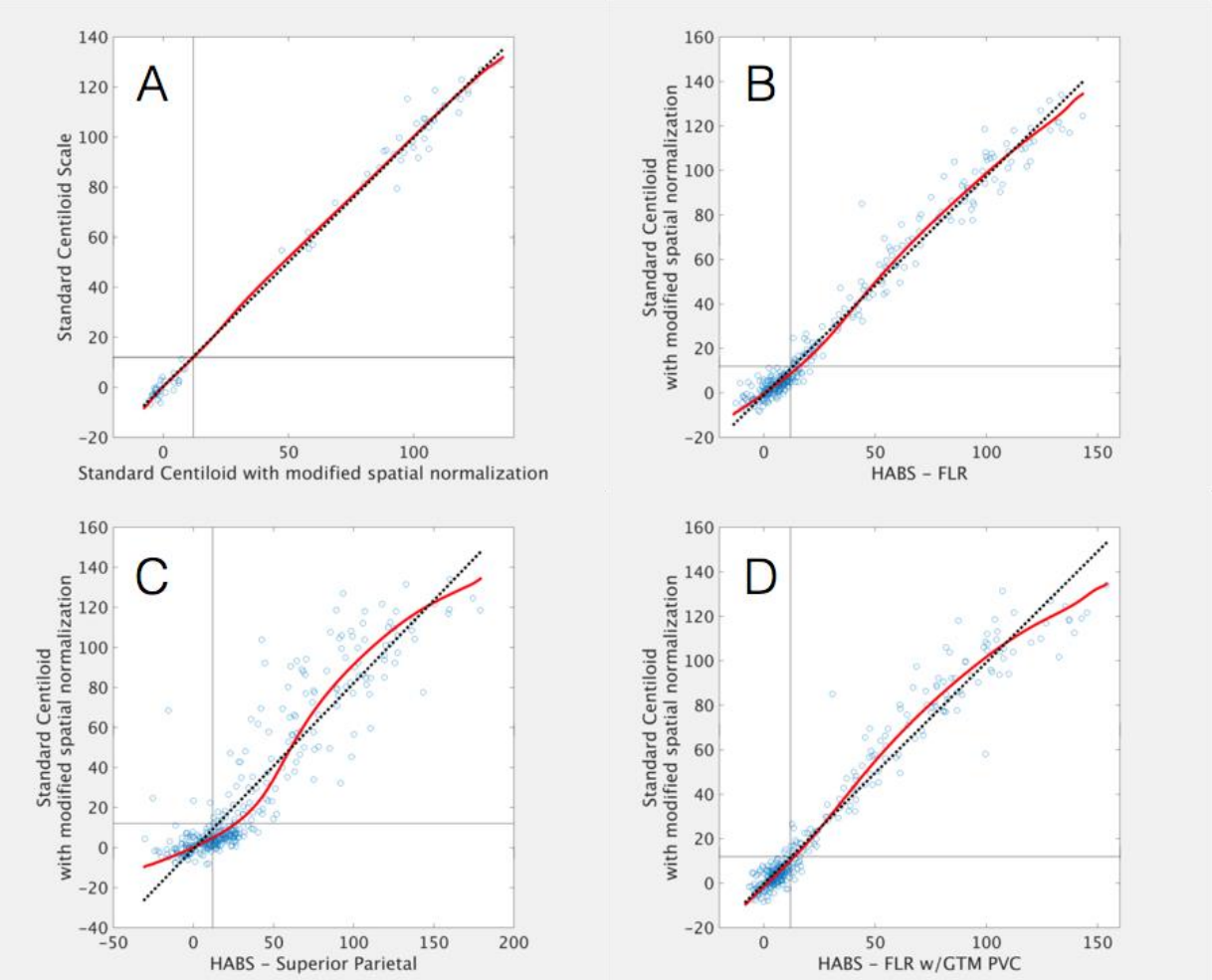

Keywords:

PIB,PET,Centiloid

Wednesday, January 11, 2017 - 02:25 pm - 03:10 pm

Keynote Lecture

Tau Prion Strains: Implications for Imaging

Marc Diamond

University of Texas Southwestern Medical Center, Dallas, TX, USA

Tauopathies are neurodegenerative disorders that affect distinct brain regions, progress at different rates, and exhibit specific patterns of tau accumulation. PET ligands cannot yet reliably identify and discriminate these conditions. Our lab has long studied the role transcellular propagation of protein aggregation in the pathogenesis and diversity of tauopathies. We have determined that tau shares essential biological properties with the prion protein. We have tested the idea that discrete tau aggregate conformers, or "strains" underlie unique patterns of progression and neuropathology. We previously characterized two tau prion strains that stably maintain unique conformations in vitro and in vivo, but did not determine the relationship of each strain to parameters that discriminate among tauopathies such as regional vulnerability or rate of spread. We have now isolated and characterized 18 tau strains in cells based on detailed biochemical and biological criteria.

Inoculation of transgenic tau P301S (PS19) mice with these strains causes strain-specific intracellular pathology in distinct cell types and brain regions, and induces different rates of network propagation. In this system, strains alone are sufficient to account for diverse neuropathological presentations, similar to those that define human tauopathies. Distinct conformations of tau aggregates could explain the failure of PET ligands to reliably distinguish the tauopathies. Detailed knowledge of strains could provide a rational approach both to understand the biological basis of tauopathies, and to design more effective imaging agents.

Sanabria, Sandra - 3

Kinetics of [18F]GTP1 (Genentech tau probe 1) in the basal ganglia of Alzheimer's patients and healthy controls

Sandra Sanabria Bohorquez[1], Thomas Bentsson[2], Olivier Barret[3], Gilles Tamagnan[3], David Alagille[3], Alex de Crespigny[1], Gai Ayalon[4], Michael Ward[5], Geoffrey Kerchner[5], Danna Jennings[3], John Seibyl[3], Ken Marek[3], Robby Weimer[6], Jan Marik[6]

[1]*Clinical Imaging Group, Genentech, Inc., South San Francisco, CA, USA*
[2]*Biostats, Genentech, Inc., South San Francisco, CA, USA*
[3]*Molecular NeuroImaging LLC, New Haven, CT, USA*
[4]*Department of Neuroscience, Genentech, Inc, South San Francisco, CA, USA*
[5]*Early Clinical Development, Genentech, Inc, South San Francisco, CA, USA*
[6]*Department of Biomedical Imaging, Genentech, Inc, South San Francisco, CA, USA*

Background: SUVR images from various tau ligands have shown increased retention in basal ganglia (BG). Here, we characterize the GTP1 kinetics and quantify the specific binding (C_S) and non-displaceable (C_{ND}) component in these regions.

Methods: GTP1 imaging with arterial input function (AIF) was performed in 5 healthy volunteers (HV) and 5 AD subjects. ROIs were defined in the cerebellum gray (CBL), cortex and BG. The AIF-2-tissue model (2TM) was applied to estimate $V_{ND} = K_1/k_2$ and $BP_{ND} = k_3/k_4$. CBL was used as reference to estimate SRTM BP_{ND} and the CBL k_2' as well as SUVR-CBL.

Results: V_{ND} values were larger in BG than in CBL and cortex whereas similar K_1 values were observed across regions (figure 1). The SRTM-CBL k_2' value obtained when fitting BG regions was higher than in cortex (figure 1) suggesting differences in V_{ND} across regions. These results show that while CBL is a good reference for estimating cortical V_{ND}, it is not an appropriate reference for BG resulting in specific binding overestimation: estimated BP_{ND}(BG) = P_{ND}*actual BP_{ND}(BG), $P_{ND} = V_{ND}(BG)/V_{ND}(CBL)$[1]. SUVR-CBL measurements will have a similar bias.

Figure 2 shows time activity curves in CBL, cortex and BG as well as SUVR-CBL in an AD patient (top); and the 2TM C_{ND} and C_S (bottom). Although the BG SUVR-CBL values can be similar to cortical SUVR-CBL, the specific binding is lower because of the larger C_{ND}. SUVR-CBL in cortex and BG do not reflect the same level of specific binding.

Conclusions: In cortex, GTP1 SUVR-CBL is a good surrogate of tau specific binding. In contrast, BG SUVR-CBL is strongly biased and may reflect age- and/or disease-related changes not directly related to tau accumulation. Although some specific binding may be present, BG SUVR-CBL values should be interpreted with caution.

1.Salinas et al.doi:10.1038/jcbfm.2014.202

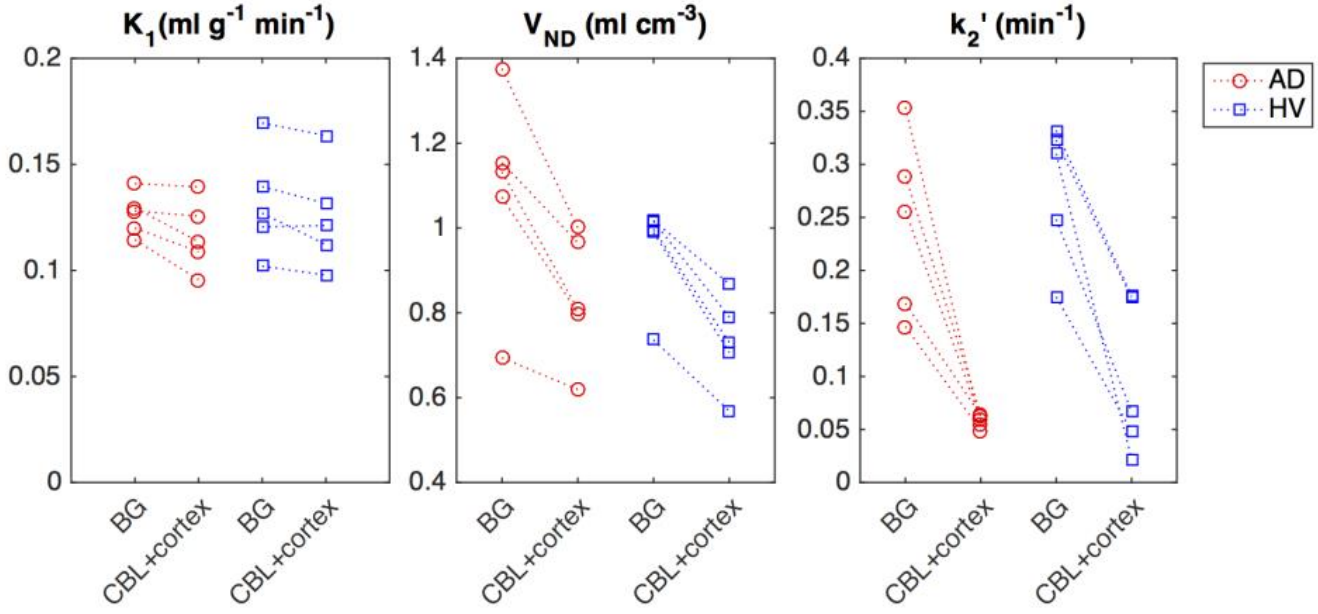

Figure 1

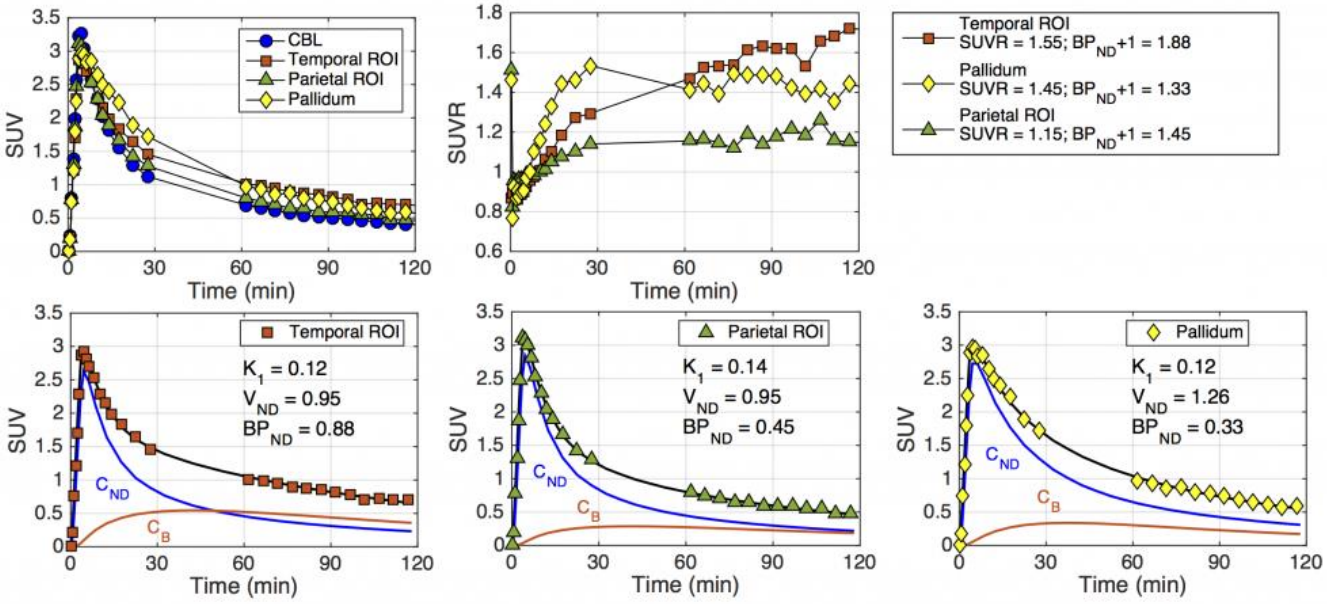

Figure 2

Keywords: Tau imaging, GTP1, basal ganglia, modeling, kinetics

Development of novel tau PET tracers, [18F]AM-PBB3 and [18F]PM-PBB3

Maiko Ono[1,2], Soichiro Kitamura[1], Hitoshi Shimada[1], Naruhiko Sahara[1], Hiroyuki Takuwa[1], Yasumasa Yoshiyama[3], John Trojanowski[4], Virginia Lee[4], Tetsuya Suhara[1], Ming-Rong Zhang[1], Ming-Kuei Jang[5], Gilles Tamagnan[6], Kenneth Marek[6], Makoto Higuchi[1]

[1]*National Institute of Radiological Sciences, National Institutes for Quantum and Radiological Science and Technology, Chiba, Japan*
[2]*Tohoku University, Sendai, Japan*
[3]*Chiba-East National Hospital, Chiba, Japan*
[4]*University of Pennsylvania, Philadelphia, PA, USA*
[5]*Aprinoia Therapeutics, Taipei, Taiwan*
[6]*MNI, New Haven, CT, USA*

PBB3 is a PET imaging agent for fibrillary tau lesions, and was shown to bind to tau inclusions in diverse neurodegenerative disorders, including Alzheimer's disease (AD) and 3-repeat and 4-repeat tauopathies, and in different tau transgenic mouse models. For the purpose of widely available and high-contrast tau PET scans, we have developed novel PET radioligands for tau aggregates, AM-PBB3 and PM-PBB3, which are ^{18}F-labeled analogs of PBB3, and characterized these compounds by in-vitro, ex-vivo and in-vivo assays. In-vitro fluorescence and autoraiographic labeling of brain sections demonstrated binding of AM-PBB3 and PM-PBB3 to various tau pathologies in AD, progressive supranuclear palsy (PSP), corticobasal degeneration, Pick's disease and tau transgenics (PS19 and rTg4510). High affinity binding of AM-PBB3 and PM-PBB3 to tau aggregates with Kd values < 10 nM was also observed in AD and PSP brain homogenates. In-vivo PET and ex-vivo autoradiography of rTg4510 tau transgenic mice supported the ability of AM-PBB3 and PM-PBB3 to capture tau deposits in living brains with a higher contrast than PBB3, primarily owing to their higher uptake into the brain. PM-PBB3 underwent faster clearance from the brain following peak uptake than AM-PBB3, and accordingly yielded the highest contrast of tau lesions among these three radioligands. Correspondingly, in-vivo two-photon fluorescence microscopy showed the most intense signals in individual tau inclusions of rTg4510 mice yielded by PM-PBB3. We also observed less radiometabolites of AM-PBB3 and PM-PBB3 in mouse plasma and brain than those of PBB3 along the course after intravenous injection. Our non-clinical findings support the utility of AM-PBB3 and PM-PBB3 as tau PET radioligands, and have finally been compared to results of pilot clinical PET with these compounds.
Keywords: Tau PET ligand, PBB3 derivative, Tau transgenic mouse, Alzheimer's disease, Progressive supranuclear palsy

Optimization of early phase [18F]flutemetamol scanning window as a proxy for relative tracer delivery

Kerstin Heurling[1,2], Koen Van Laere[3], Rik Vandenberghe[3], Christopher Buckley[4], Gill Farrar[4], Mark Lubberink[2,5]

[1]*Göteborgs Universitet, Göteborg, Sweden*
[2]*Uppsala Universitet, Uppsala, Sweden*
[3]*UZ Leuven, Leuven, Belgium*
[4]*GE Healthcare, Amersham, United Kingdom*
[5]*Uppsala Academic Hospital, Uppsala, Sweden*

Background: The "dual-phase" PET imaging concept, combining late-phase specific tracer binding with the early-phase influx aspect of tracer kinetics, has gained increasing attention for amyloid imaging due to its potential to replace a dedicated perfusion or metabolism scan. Our objective was to identify the optimal time window for capturing perfusion information from early-phase flutemetamol perfusion SUVR (p-SUVR) as compared to the delivery in target relative to reference region (R_1) estimated using kinetic modeling.

Methods: Six subjects (four amyloid-positive and two amyloid-negative) underwent dynamic flutemetamol PET scanning for 90 min post injection (p.i.). Parametric R_1 images were estimated using a basis function implementation of the simplified reference tissue model, and grey matter masked template regional values were extracted. p-SUVR was estimated over a range of scanning windows with start times 0-7 min and end times 1-11 min. Pearson's correlation coefficient and percentage bias were estimated for each time window.

Results: p-SUVR correlated best with R_1 for the time window 0.5-3 min p.i. (r=0.98) (Figure 1A). Correlations were, however, strong (r >0.95) over all combinations of scanning windows with start times between 0.5-2 min and end times up to 8 min. The lowest bias of p-SUVR compared to R_1 was found for the time window 1-2 min, (-0.7%) but bias was <2% for all time windows with start 0.5-2 min p.i. and end 1.5 to 6 min (Figure 1B). Average R_1 and p-$SUVR_{0.5\text{-}3\ min}$ images are shown in Figure 2, alongside a publicly available dementia-specific FDG template illustrating current practice.

Conclusion: Based on our findings, flutemetamol p-SUVR shows low sensitivity to the exact choice of start and end time within range 0-3 min. Future studies validating the use of early-phase flutemetamol imaging against perfusion imaging should collect data during a time window excluding the first 30 sec p.i., with a duration no longer than 6 min.

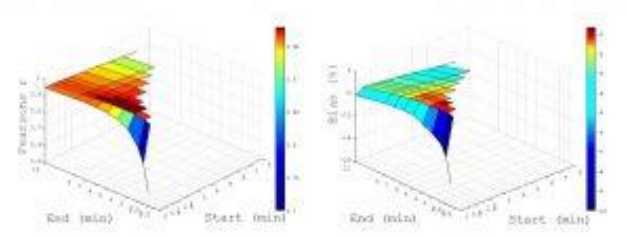

Figure 1. A) Visualization of Pearson's correlation coefficient r for the association of early-phase SUVR over different combinations of start and end times with R_1 across all six subjects. B) Bias of the different combinations of early phase SUVR compared to R_1 across all six subjects.

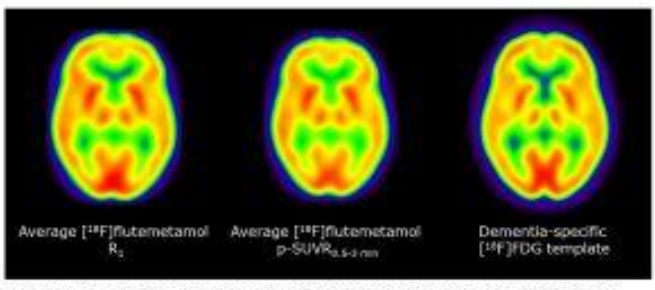

Figure 2. Spatially normalized average images for R_1 (left) and early-phase perfusion SUVR (p-SUVR) over the optimal time window 0.5-3 min post injection (middle) across all six subjects. Right hand image shows a dementia-specific [18F]FDG-template, based on 100 subjects, for comparison (Della Rosa et al., NeuroImage, 2014).

Keywords: [18F]flutemetamol, early-phase SUVR, perfusion, scanning window optimization

Algorithm for reference region delineation for amyloid imaging using pattern recognition scheme and kinetics of administered Aβ probe — considering the number of clusters

Takahiro Yamada[1], Yuichi Kimura[1], Takashi Nagaoka[1], Chisa Hosokawa[2], Takamichi Murakami[2], Kazunari Ishii[2]

[1]Graduate School of Biology-Oriented Science and Technology, Kindai University, Wakayama, Japan., Kinnokawa-shi, Japan
[2]Department of Diagnostic Radiology, Faculty of Medicine, Kindai University, Osaka, Japan., Osakasayama-shi, Japan

Introduction: For quantitative measurement of amyloid beta (Aβ) deposit, a kinetic analysis is applied to acquire binding potential () (Hosokawa, JNM, 56, 2015), and a reference region is placed on the cerebellar gray matter. Because it has a thin and complicated shape, an automated algorithm is required. The aim of this study is to propose a new automated algorithm (AutoRef) to delineate the reference region. AutoRef clusters voxels around the cerebellum into some clusters based on the shape of a tissue time activity curve (tTAC). The basic idea has been presented at SNM2016, and the number of the clusters is investigated.

Methods: tTACs have different shapes among different tissue groups. AutoRef detects the shape difference using a statistical clustering algorithm of Gaussian mixture model (GMM). The number of clusters should be given to GMM. The large number may capture the difference in tTACs, but it makes the estimation process astable. An appropriate number of clusters is thus investigated. AutoRef is evaluated using clinical 86 cases: 43 positive, 33 negative, and 10 equivocal cases.

Results: The typical result is demonstrated in Fig. 1 when 8-clusters clustering was conducted. If the case of 3-cluster clustering, the estimated reference region was located some voxels out from the manually defined reference region. All GMM were converged appropriately for 8-cluster clustering. No significant difference in was observed ($p<0.05$) between AutoRef and the manually defined reference region, and the difference was smaller than 0.46.

Conclusion: The difference is almost the same between the threshold of Aβ positive and negative, and we conclude that AutoRef is applicable.

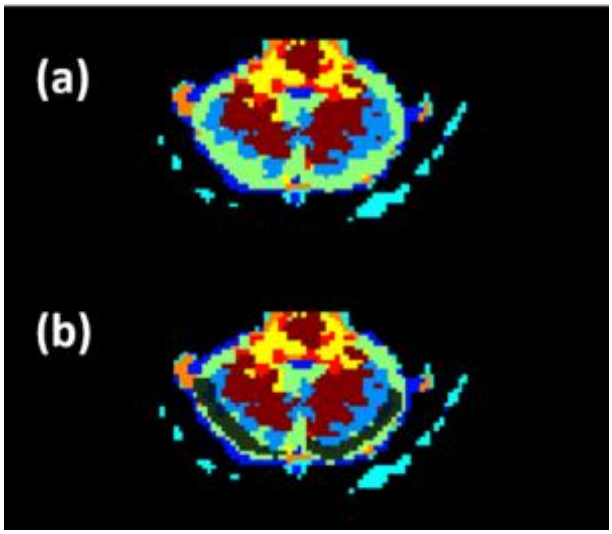

Fig. 1 (a) The result of 8-clusters clustering where a reference region is in yellow-green. (b) Manually defined reference region is superimposed.

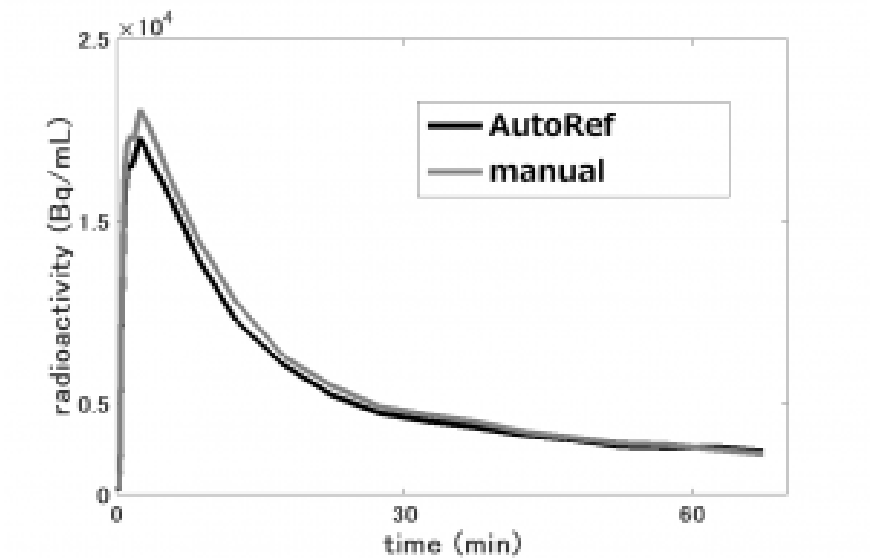

Fig. 2 The estimated and manually derived tTACs.

Keywords: PET, kinetic analysis, reference region

Rigid registration contributes significant imprecision to amyloid PET SUVR measurements

Christopher Schwarz[1], David Jones[1], Jeffrey Gunter[1], Val Lowe[1], Prashanthi Vemuri[1], Matthew Senjem[1], Ronald Petersen[1], David Knopman[1], Clifford Jack[1]

[1]*Mayo Clinic, Rochester, MN, USA*

Background: Quantitative measurements of amyloid PET scans typically use rigid registration to corresponding MRI scans for localizing atlas regions and applying partial volume correction (PVC). Although quality control (QC) is often performed to prevent gross failures, subtle variations within QC-acceptable registrations have not been studied as a source of imprecision in SUVR measurements.

Methods: We performed simulations using 598 Mayo PiB scans and 598 ADNI florbetapir scans, each matched by age, sex, and clinical status. For each PET scan, we applied 50 small random perturbations of starting location and orientation, then performed rigid registration between each perturbed PET scan and its corresponding MRI using *spm_coreg* in SPM12. SUVR measurements were calculated for each perturbed PET scan by using these registrations to localize MRI-based atlas regions. We examined effects of these perturbations upon registration parameters and their resulting SUVR measurements.

Conclusions: Registration parameters and SUVR values were significantly affected by registration starting position; they did not exhibit the ideal behavior of consistently reaching the same endpoint. Across perturbations, standard deviations of rotation parameters were ≈0.05 degrees about each axis, and those for translation were ≈0.025mm in each direction. Although this subtle variation was visible to human inspection, all registrations appeared equally valid. Imprecision in PET-MRI rigid registration: 1) contributes significant imprecision to SUVR measurements, on the order of ≈50% of the expected reference values for annual change in subjects with AD dementia; 2) increases with amyloid load, and thus indirectly with clinical severity; 3) differs with choice of reference region; 4) has a larger effect when using PVC. These findings were consistent across both datasets i.e. tracers, and also replicated using FreeSurfer's *mri_coreg*. Although PET-MRI registration imprecision does not account for all test-retest variability in amyloid PET SUVR values, processing pipelines that emphasize consistent registrations for serial scans could significantly reduce imprecision in change-over-time measures.

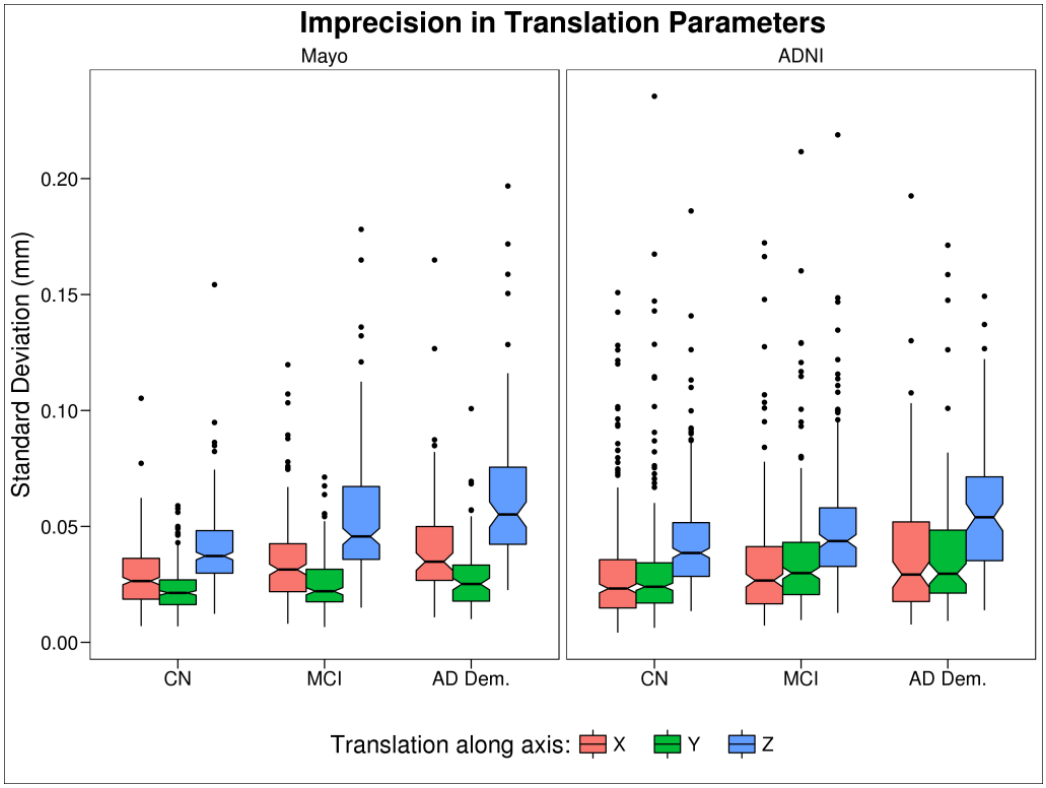

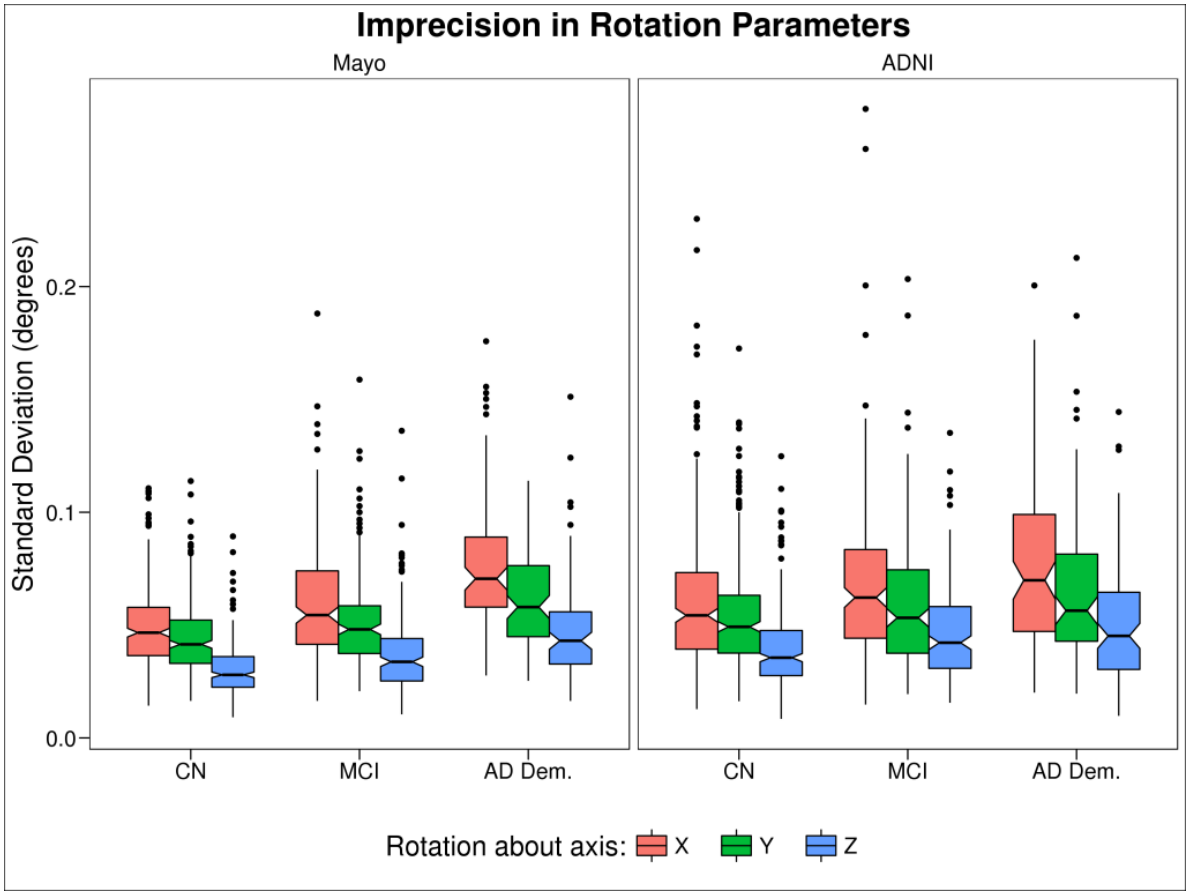

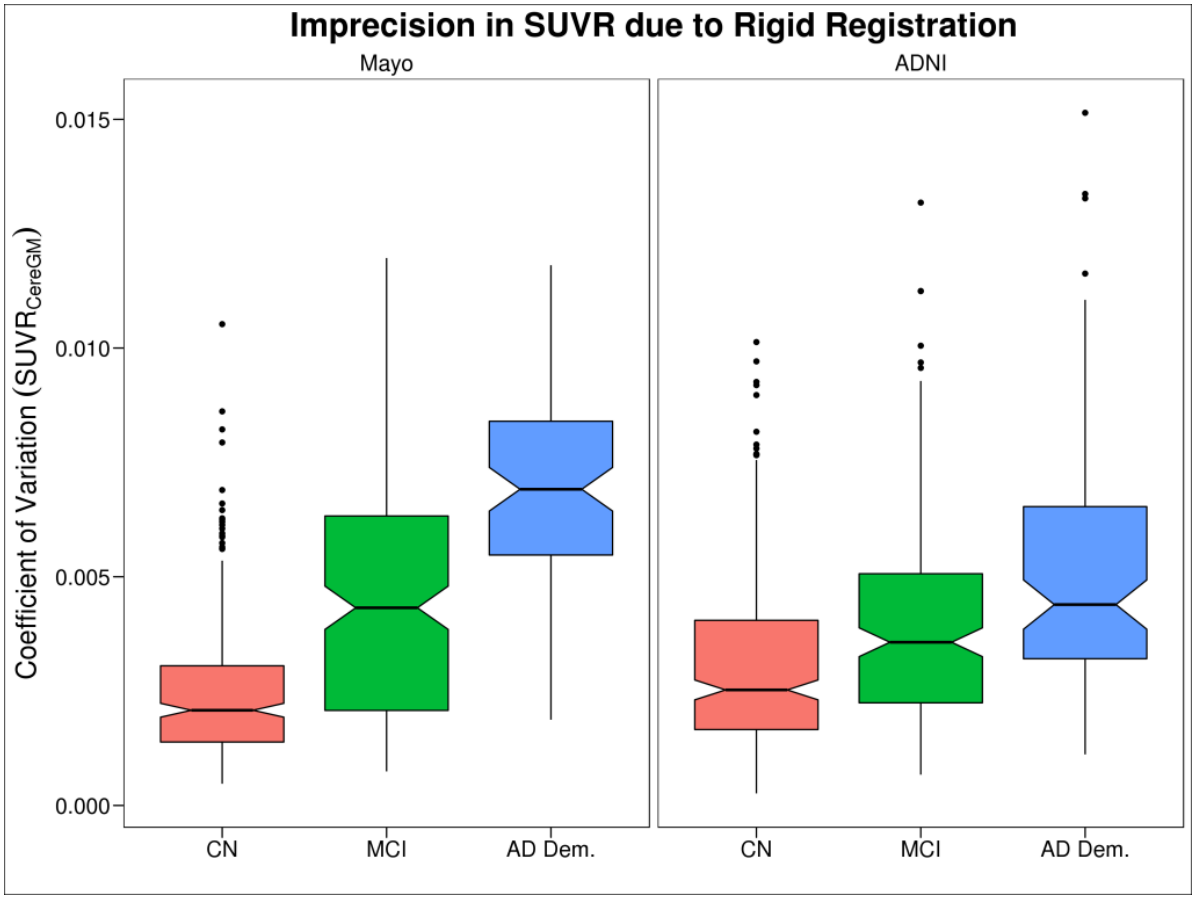

Keywords: registration, imprecision, SUVR, reliability, quantification

18F-Flortaucipir SUV normalization using a Parametric Estimate of Reference Signal Intensity (PERSI)

Sudeepti Southekal[1], Michael D. Devous Sr.[1], Ian Kennedy[1], Michael Navitsky[1], Ming Lu[1], Abhinay D. Joshi[1], Michael J. Pontecorvo[1], Mark A. Mintun[1]

[1]*Avid Radiopharmaceuticals, Inc, Philadelphia, PA, USA*

Background: White matter reference regions have shown reduced variability in longitudinal SUVr measurements for amyloid imaging agents (Landau et al. 2015). However, such regions are susceptible to partial volume contamination from the cortex. We present a new strategy (PERSI) to extract the white matter reference signal for ^{18}F-Flortaucipir SUV normalization.

Methods: Test-retest (n=21; 5-34 days between scans) and Phase 2 cross-sectional (n=215) and longitudinal (n=140/215; 18±2 months between scans) data comprising 3 clinical cohorts (AD, MCI, CN) were analyzed. Subjects underwent T1 MRI and Florbetapir imaging at screening, and Flortaucipir imaging at single or multiple time points. Baseline amyloid (Aβ) status was determined as described in Clark et al. 2012. Flortaucipir images acquired as 4x5 min frames, 80 min after a 370 MBq injection were motion corrected, averaged and transformed to MNI space. For each scan, the voxel intensity histogram within an atlas-based white matter mask was fit to a bimodal Gaussian distribution (Fig. 1). The center and width of the first peak were used to determine reference region voxels. A cerebellar gray matter reference region was also evaluated for comparison. SUVr values were calculated for a neocortical volume-of-interest. Test-retest reproducibility (SD of %difference between scans) and effect sizes for cross-sectional and longitudinal group differences (Cohen's d; Aβ+ impaired vs. Aβ- normal) were assessed.

Results: PERSI yielded >2-fold improvement in test-retest reproducibility (1.84% vs. 4.18%) and superior group separation (cross-sectional Cohen's d 9.54 vs 4.57; longitudinal Cohen's d 2.28 vs. 1.54) (Fig 2, Table 1) relative to cerebellar gray. Baseline variability in Aβ- CNs with no specific uptake was minimal (SUVr 1.0±0.04, ΔSUVr 0.0±0.02; Table 1).

Conclusions: PERSI reference regions reduced variability while enhancing discrimination between diagnostic cohorts. These improvements could lead to more accurate disease staging and robust measurements of changes in tau burden over time for evaluation of therapeutic response.

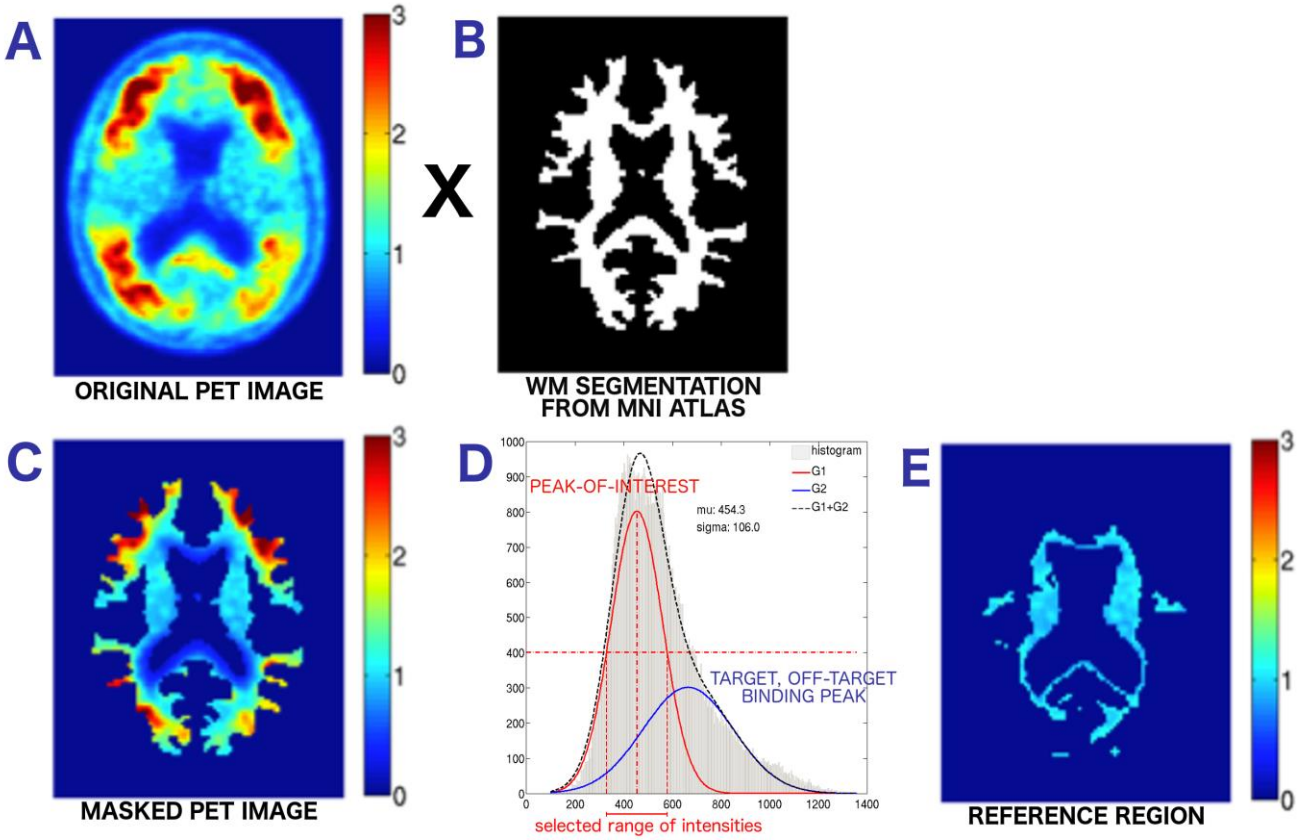

Figure 1. Graphical description of PERSI. The original PET image in A is masked by the atlas-based WM mask in B resulting in C (PET counts within the WM). These counts are then plotted as an intensity histogram (D) and fit to a bimodal Gaussian distribution. The parameters of the first Gaussian peak (mean ± FWHM) are used to identify the range of values selected as the reference region (E).

Measure	Reference Region	Aβ+ Impaired (MCI and AD)			Aβ- Cognitively Normal			Effect Size
		n	Mean	SD	n	Mean	SD	Cohen's d
SUVr	cerebellar gray	77	1.58	0.45	68	1.12	0.10	4.57
	PERSI	77	1.35	0.37	68	1.01	0.04	9.54
ΔSUVr 18-month	cerebellar gray	46	0.07	0.12	46	0.01	0.04	1.54
	PERSI	46	0.05	0.05	46	0.00	0.02	2.28

Table 1. Comparison of cross-sectional (SUVr) and longitudinal (ΔSUVr) values using PERSI and cerebellar gray matter, for impaired (Aβ+) and normal (Aβ-) subjects.

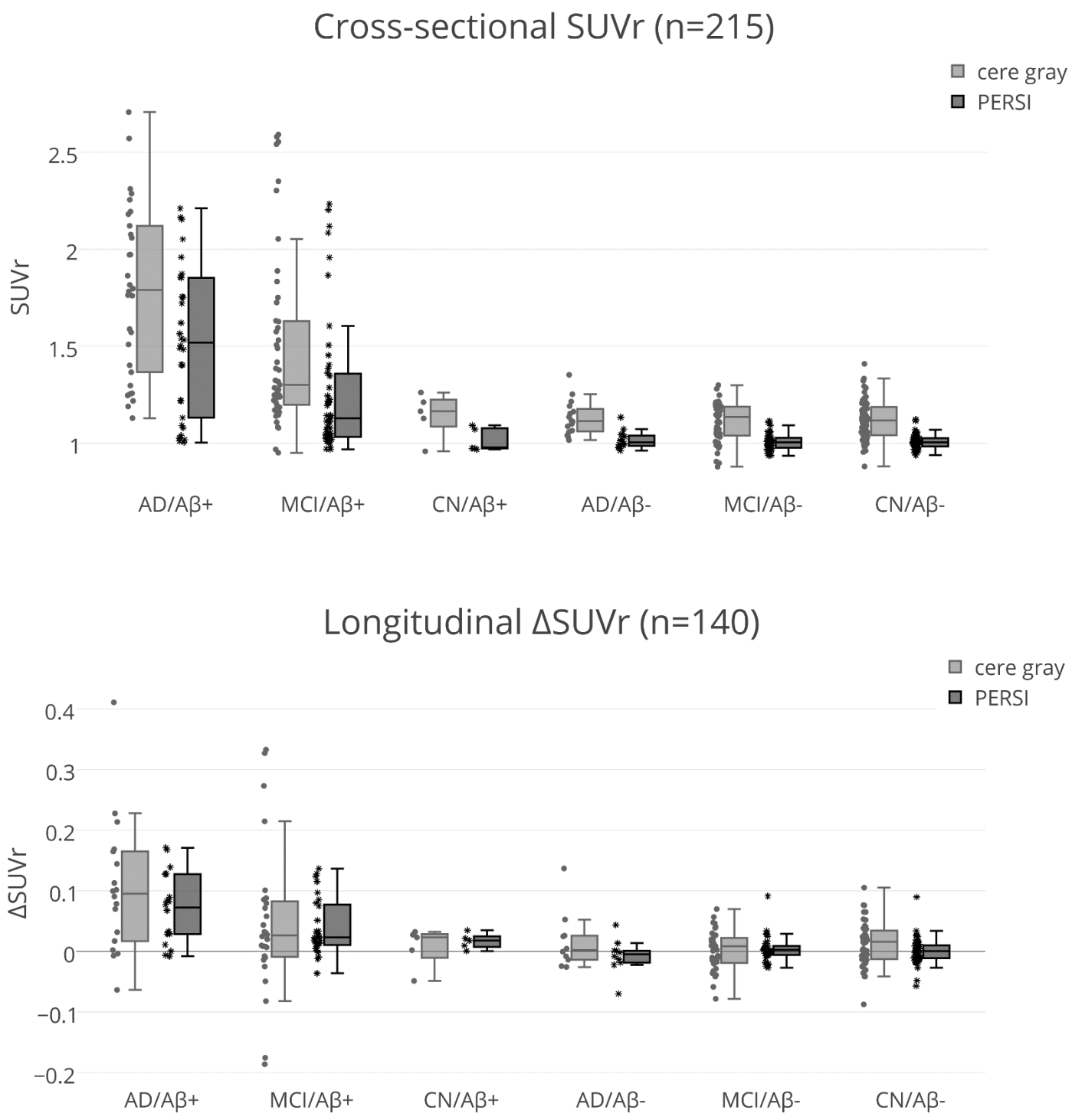

Figure 2. Comparison of reference regions for the measurement of cross-sectional SUVr (top) and longitudinal (18-month) change in SUVr (bottom) for 6 cohorts. PERSI reduces the range of SUVr values, but maintains group separation due to increased signal-to-noise.

Keywords: reference region, flortaucipir, AV1451, quantification

Validation of the semi-quantitative static SUVR method by pharmacokinetic modeling on dynamic cross-sectional [18F]-AV45 data

Julie Ottoy[1], Jeroen Verhaeghe[1], Ellis Niemantsverdriet[2], Leonie wyffels[3], Charisse Somers[2], Ellen De Roeck[2,4], Hanne Struyfs[2], Femke Soetewey[2], Steven Deleye[1], Tobi Van den Bossche[5,6,7], Sara Van Mossevelde[5,6,7], Sarah Ceyssens[3], Jan Versijpt[8], Sigrid Stroobants[3], Sebastiaan Engelborghs[2,7], Steven Staelens[1]

[1]*Molecular Imaging Center Antwerp (MICA), University of Antwerp, Antwerp, Belgium*
[2]*Reference Center for Biological Markers of Dementia (BIODEM), University of Antwerp, Antwerp, Belgium*
[3]*Department of Nuclear Medicine, Antwerp University Hospital, Edegem, Belgium*
[4]*Developmental and Lifespan Psychology, Vrije Universiteit Brussel, Brussels, Belgium*
[5]*Department of Molecular Genetics, VIB, University of Antwerp, Antwerp, Belgium*
[6]*Department of Neurology, Antwerp University Hospital, Edegem, Belgium*
[7]*Dept of Neurology and Memory Clinic, Hospital Network (ZNA) Antwerp Middelheim and Hoge Beuken, Antwerp, Belgium*
[8]*Department of Neurology, University Hospital Brussels, Brussels, Belgium*

Background Increased brain uptake of -AV45 (Florbetapir) visualized by PET is a key biomarker in Alzheimer's disease. The standardized uptake value ratio (SUVR) is widely used for quantification, but is subject to variability based on choice of reference region and changes in cerebral blood flow. Here we validated the SUVR method against the gold standard volume of distribution (V_T).

Methods Dynamic 60-min -AV45 (291±67 MBq) and 1-min -H_2O (370 MBq) scans were obtained in 10 probable AD dementia (AD), 15 amnestic MCI (aMCI) and 10 cognitively healthy control (HC) subjects. -AV45 V_T was determined from two-tissue compartment modeling using a metabolite-corrected plasma input function. Static SUVR was calculated from the 50-60 min p.i. data, using either cerebellar gray matter (CB) or whole subcortical white matter (WM) as the reference region. Blood flow was quantified by -H_2O SUV and the -AV45 delivery rate K1.

Results Compared to V_T, differences in Aβ-load between the aMCI and AD group were overestimated by $SUVR_{WM}$ (+4±2%) and underestimated by $SUVR_{CB}$ (-10±2%)

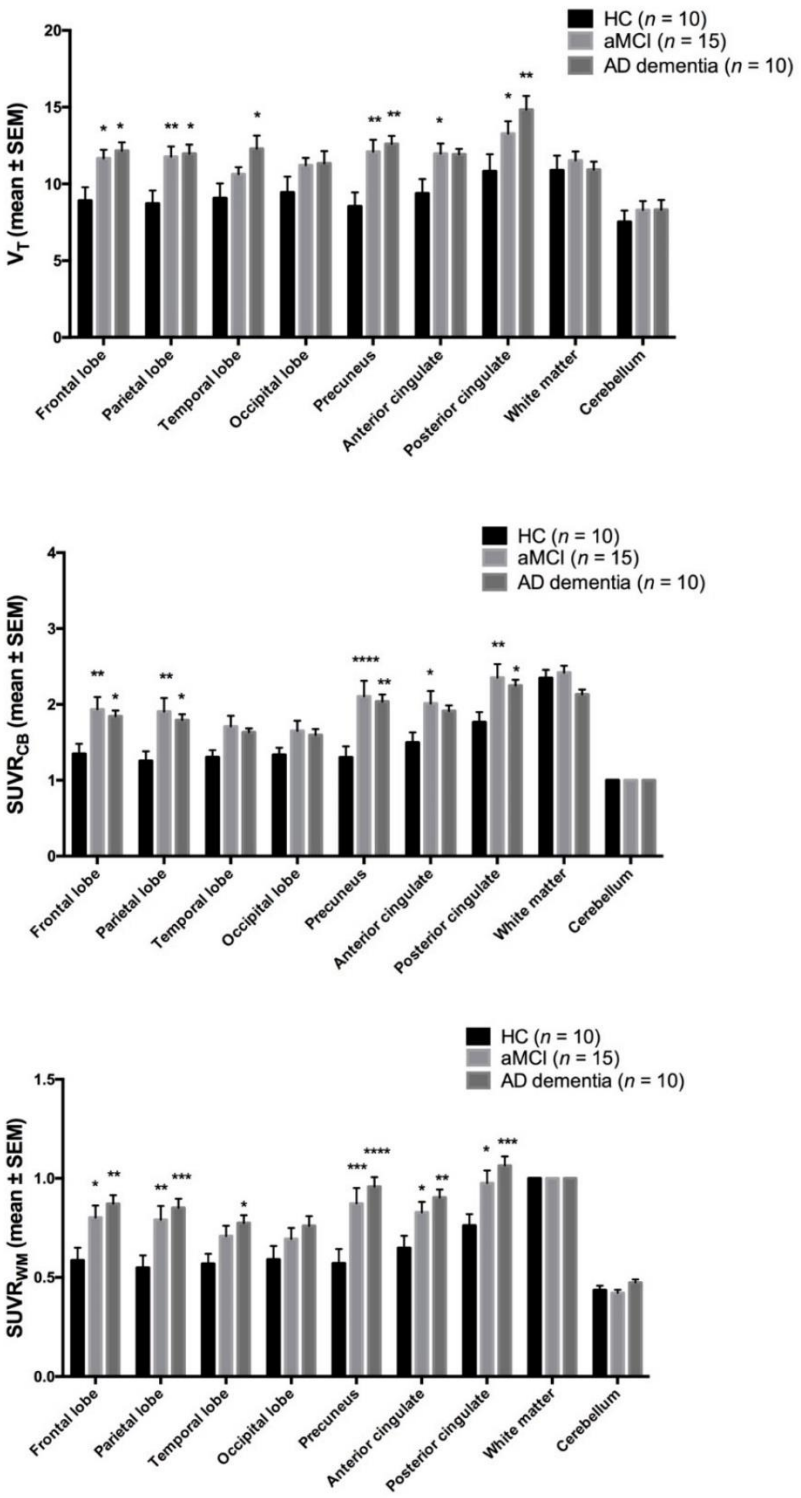

FIGURE 1. Regional [^{18}F]-AV45 V_T (top), $SUVR_{CB}$ (middle) and $SUVR_{WM}$ (bottom) (mean ± SEM) values for the three groups. Stars denote significant differences with the HC group (* $p<0.05$, ** $p<0.01$, *** $p<0.001$, **** $p<0.0001$). Abbreviations: V_T = volume of distribution; $SUVR_{CB}$ and $SUVR_{WM}$ = standardized uptake value ratio with resp. reference cerebellar gray matter and subcortical white matter.

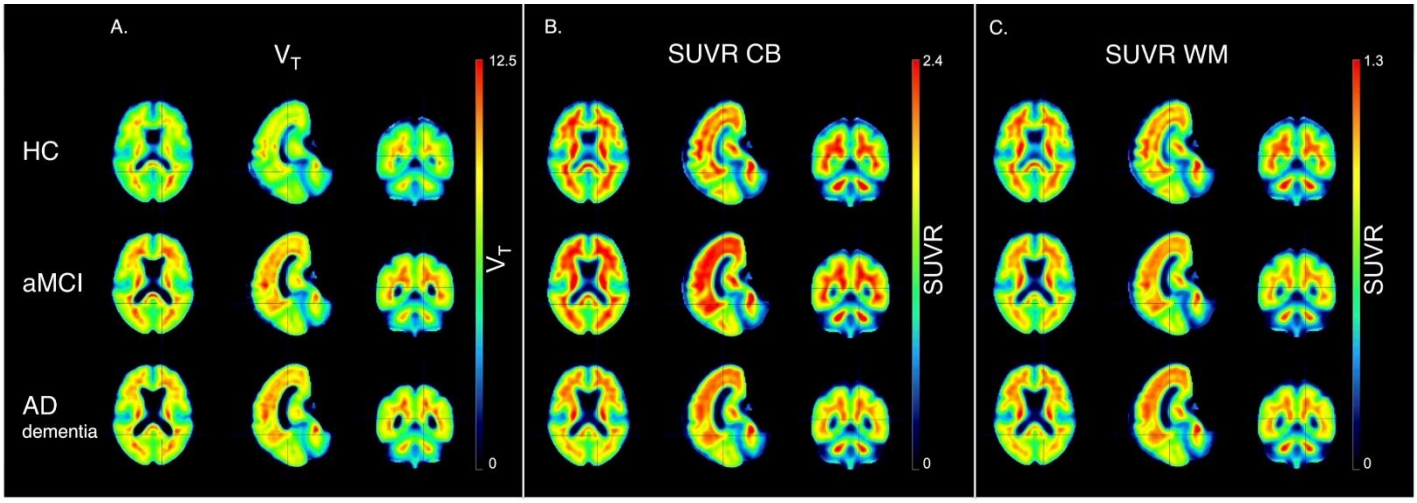

FIGURE 2. Average spatially normalized [^{18}F]-AV45 V_T (A), $SUVR_{CB}$ (B) and $SUVR_{WM}$ (C) images for the three groups. Abbreviations: V_T = volume of distribution; $SUVR_{CB}$ and $SUVR_{WM}$ = standardized uptake value ratio with resp. reference cerebellar gray matter and subcortical white matter.

(Figure 1 Figure 2). V_T correlated better with $SUVR_{WM}$ (Pearson r: 0.63 for posterior cingulate to 0.89 for precuneus, $p<0.0001$) than with $SUVR_{CB}$ (r: 0.51 for temporal lobe ($p=0.0023$) to 0.82 for precuneus ($p<0.0001$)). -AV45 K1 was decreased in AD compared to aMCI in cortical regions (-6±1%) and in the reference regions (CB: -10±6%, WM: -4±7%)

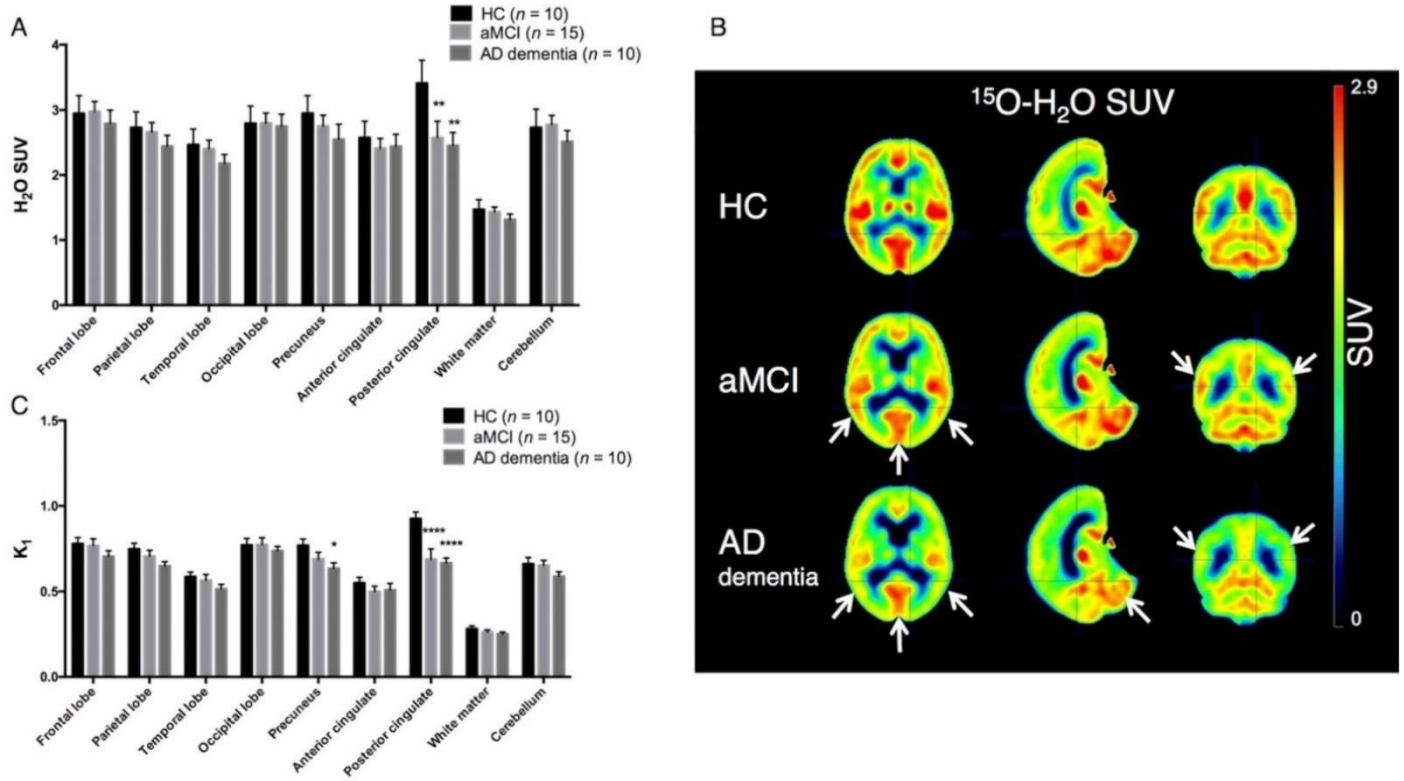

FIGURE 3. (A) Regional [^{15}O]-water SUV (mean ± SEM) values for the three groups. (B) Average spatially normalized [^{15}O]-water SUV images. White arrows indicate regions with reduced flow compared to controls (parieto-temporal cortex, posterior cingulate cortex, cerebellum). (C) [^{18}F]-AV45 delivery rate K1 (mean ± SEM). Stars denote significant differences with the HC group (*p < 0.05, ** p < 0.01, **** p < 0.0001). Abbreviations: SUV = standardized uptake value.

(Figure 3), and correlated well with -H_2O SUV to measure flow (Pearson's r: 0.50 for WM, temporal and frontal cortex ($p<0.01$) to 0.68 for posterior cingulate ($p<0.0001$).

Conclusion -AV45 assessed by the simplified static SUVR protocol does not truly reflect Aβ-load. However, $SUVR_{WM}$ is better correlated with V_T and more closely reflects V_T differences between the aMCI and AD group than $SUVR_{CB}$. This might be partly due to differential flow effects in the respective reference regions.

Keywords: Alzheimer's disease, [18F]-AV45, SUVR, reference region, validation

A simulation study on the quantification of the blood flow-dependent component in [18F]-AV45 SUVR differences between the MCI and AD stage

Julie Ottoy[1], Jeroen Verhaeghe[1], Sigrid Stroobants[3], Sebastiaan Engelborghs[2], Steven Staelens[1]

[1]Molecular Imaging Center Antwerp (MICA), University of Antwerp, Antwerp, Belgium
[2]Reference Center for Biological Markers of Dementia (BIODEM), University of Antwerp, Antwerp, Belgium
[3]Department of Nuclear Medicine, Antwerp University Hospital, Edegem, Belgium
[4]Dept of Neurology/Memory Clinic, Hospital Network Antwerp (ZNA) Hoge Beuken en Middelheim, Antwerp, Belgium

Background: The standardized uptake value ratio (SUVR) with respect to a reference region quantifies -AV45 brain uptake in Alzheimer's disease (AD) patients, but is subject to variability. Here we evaluate how SUVR in a cortical target region is affected by flow changes in both the target and reference.

Methods: Regional time-activity curves were simulated based on 2-tissue compartment modeling with a plasma input function, impulse response function (H(time;K1,k2,k3,k4)) and a contribution from whole blood. A change in flow was simulated as a change in K1 (and k2) in either the target region (precuneus) or reference region (cerebellar gray matter (CB) or subcortical white matter (WM)) to derive the corresponding change in $SUVR_{50\text{-}60min}$. Realistic parameters and input function were obtained from a aMCI and AD cohort. K1 was varied within the aMCI-AD range whereas other parameters were fixed at average aMCI values.

Results: Flow reduction in the target precuneus resulted in an increased SUVR (Figure 1, Figure 2).

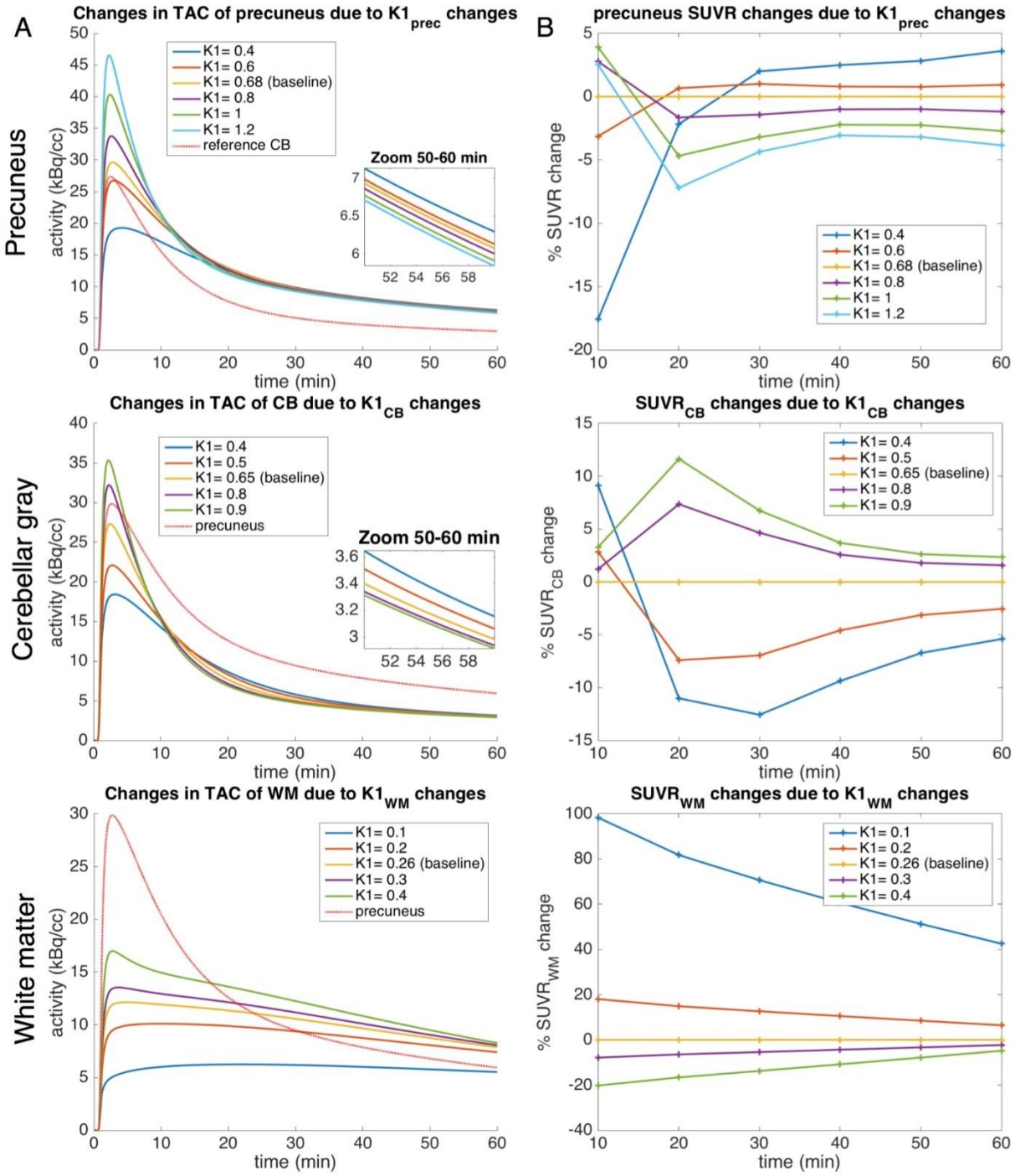

FIGURE 1. A) Changes in time-activity curves of the (from top to bottom) precuneus due to $K1_{prec}$ change, CB due to $K1_{CB}$ change, WM due to $K1_{WM}$ change. B) Percent change in (from top to bottom) precuneus SUVR due to $K1_{prec}$ change, $SUVR_{CB}$ due to $K1_{CB}$ change and $SUVR_{WM}$ due to $K1_{WM}$ change. Baseline was set as mean aMCI K1. Abbreviations: TAC= tissue time-activity curve; K1= tracer delivery rate; SUVR= standardized uptake value ratio; prec= precuneus; CB= cerebellar gray matter; WM= subcortical white matter.

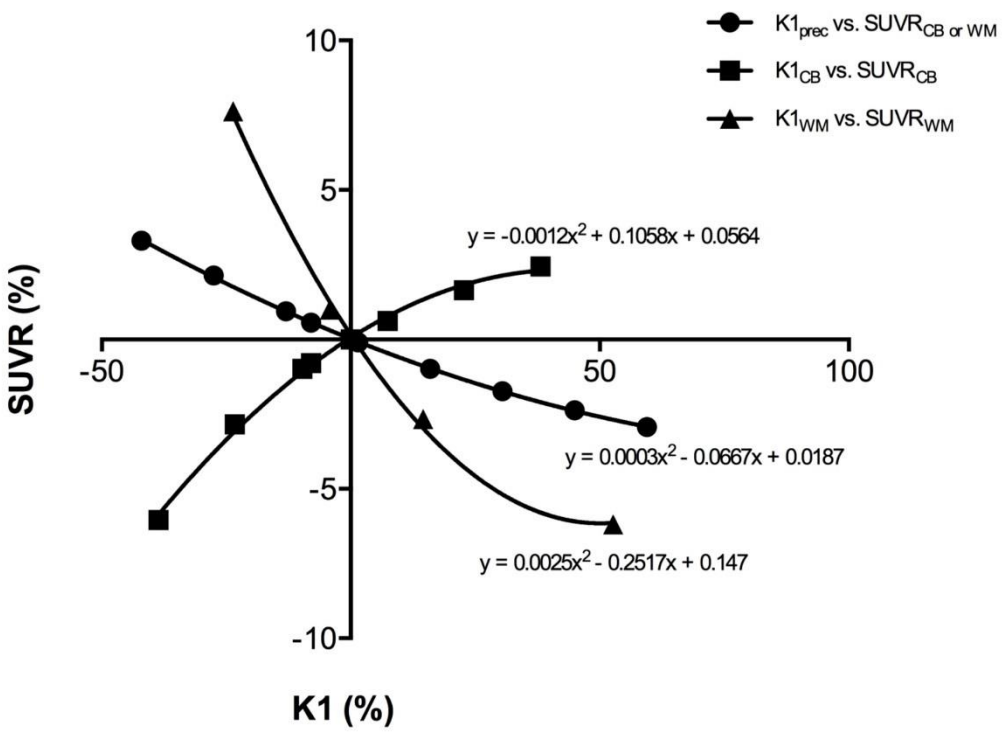

FIGURE 2. Changes in $K1_{prec}$ (circles) or $K1_{CB}$ (squares) versus changes in $SUVR_{CB}$ in the precuneus; changes in $K1_{prec}$ (circles) or $K1_{WM}$ (triangles) versus changes in $SUVR_{WM}$ in the precuneus Percent K1 changes are relative to mean K1 of the aMCI group. A second order polynomial function was fitted to the curves. Abbreviations: K1= tracer delivery rate; SUVR= standardized uptake value ratio; prec= precuneus; CB= cerebellar gray matter; WM= subcortical white matter.

Flow alterations in the two reference regions, WM and CB, exerted opposite effects on the respective SUVRs of the target: a flow reduction in WM caused an increase in $SUVR_{WM}$, whereas flow reduction in CB caused a decrease in $SUVR_{CB}$ (Figure 1, Figure 2).

On the individual level (Figure 3), the most extreme variations in $SUVR_{CB}$ and $SUVR_{WM}$ reached -4.4 and +9.3%. This was due to a combined flow decrease of -14 and -36% in the precuneus and CB, and -19 and -25% in the precuneus and WM, respectively.

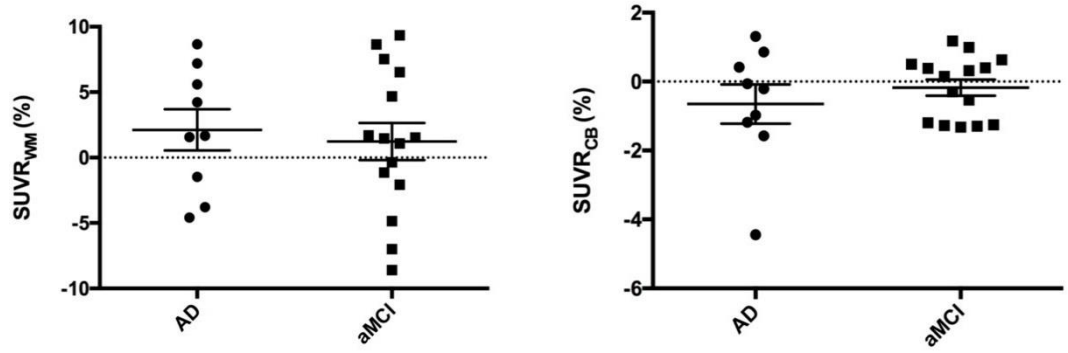

FIGURE 3. Flow-induced changes in $SUVR_{WM}$ (left) and $SUVR_{CB}$ (right) for all aMCI and AD subjects, compared to baseline mean aMCI values. Abbreviations: SUVR= standardized uptake value ratio; aMCI = amnestic mild cognitive impairment; AD= Alzheimer's disease.

Conclusion: Flow reductions in AD introduce a small bias in SUVR on group level (Figure 3), but have larger impact on the individual level. This is clinically relevant for reliable assessment of Aβ-modifying treatment in AD. Flow changes in the references CB and WM alter SUVR in opposing directions.

Keywords: Alzheimer's disease, [18F]-AV45, SUVR, blood flow, reference region

18F-PM-PBB3 a novel imaging tracer for visualization and quatification of TAU pathologies with Positron Emission Tomography

Paul Tempest[1], Ming-Kuei Jang[1], Gilles Tamagnan[2], Ken Marek[2], John Seibyl[2], David Alagille[2], Olivier Barret[2], Makoto Higuchi[3], Hitoshi Shimada[3], Maiko Ono[3], Tetsuya Suhara[3], Ming-Rong Zhang[3]

[1]*Aprinoia Therapeutics, Tapei, Taiwan*
[2]*MNI, New Haven, CT, USA*
[3]*National Institute for Quantum and Radiological Science and Technology, Chiba, Japan*

Non-invasive imaging diagnostics are critical in profiling and developing treatments for CNS diseases, including tracking disease progression, stratifying patients and monitoring efficacy for therapeutic interventions. A positron emission tomography (PET) tau tracer is desired for visualizing and quantifying neuronal and glial tau inclusions, a key pathological marker of tauopathies, including Alzheimer's Disease (AD) and progressive supranuclear palsy (PSP). 18F-PM-PBB3 is a novel PET imaging tau tracer under development for both preclinical and clinical utilities.

Here, we present data of in-vitro characterization and in-vivo imaging studies in animal models and humans. In PET imaging of normal mice and macaque monkeys, 18F-PM-PBB3 presented high brain uptake followed by rapid clearance from the brain. High-contrast 18F-PM-PBB3-PET signals corresponding to fibrillar tau deposition were also observed in the forebrain of a murine tauopathy model, rTg4510. Furthermore, kinetic and binding properties of 18F-PM-PBB3 have been clinically analyzed in normal controls and tauopathy patients.
Keywords: TAU, PET, imaging, PBB3, tauopathy

Quantitative analysis and correlation with clinical endpoints of [18F]MK6240 targeting neurofibrillary tangles (NFTs) in healthy volunteers and subjects with Alzheimer's disease

Cristian Salinas[1], Ping Chiao[1], Ajay Purohit[1], Karl Schmidt[1], John Beaver[1], Cyrille Sur[2], Arie Struyk[3], Idriss Bennacef[2], Talakad Lohith[2], Jeffrey Evelhoch[2], Rick Hiatt[4], Gilles Tamagnan[5], Danna Jennings[5], Ken Marek[5], Richard Hargreaves[1]

[1]*Biogen, Boston, MA, USA*
[2]*Translational Biomarkers, Merck & Co., West Point, PA, USA*
[3]*Translational Pharmacology, Merck & Co., West Point, PA, USA*
[4]*Enigma Biomedical Group Inc., Toronto, ON, Canada*
[5]*Invicro, New Haven, CT, USA*

Introduction: MK6240 is a sub-nanomolar affinity, highly selective NFT PET radiotracer and is not liable for off-target bindings as other tau radiotracers. It was developed as a biomarker for Alzheimer's (AD) pathology to support the development of novel therapies targeting NFTs. Herein the quantitative analysis of a Ph0 study in 3 healthy volunteers (HV) and 3 subjects with AD is presented.

Methods: Three HVs (amyloid negative, MMSE 30-28) and three AD subjects (amyloid positive, MMSE 26-18) were administered with ~10mCi MK6240 and dynamically scanned for up to 180 minutes. Biding potential (BP_{ND}) and SUVR were calculated in relevant brain regions using cerebellar grey matter as reference.

Results: In HVs MK6240 readily entered the brain and washed out fast and uniformly supporting the hypothesis of minimal in vivo off-target binding. In AD the tracer was selectively retained in regions prone to NFT deposition. A linear relationship was found between BP_{ND} and SUVR. Analytical analysis showed that SUVR measurements were robust against blood flow changes, an essenatial property supporting their usage to measure longitudinal changes in interventional studies. SUVR and BPnd measurements were highly correlated (R2>0.9) with MMSE in brain regions that are known to be affected in AD (hippocampus and enthorinal ctx).

Conclusion: MK6240 shows suitable kinetic properties and correlation between uptake and clinical endpoints. Although the results are encouraging, more data is needed to fully determine its utility as a AD biomarker.
Keywords: Tau, PET, MK6240, Alzheimer's

Implementation of the Centiloid transformation for 18F-florbetaben

Christopher C Rowe[1,2], Gareth Jones[1], Vincent Doré[1,3], David Baxendale[1], Rachel S Mulligan[1], Andrew Stephens[4], Susan De Santi[4], Colin L Masters[5], Ludger Dinkelborg[4], Victor L Villemagne[1,2,5]

[1]*Dept of Molecular Imaging & Therapy, Centre for PET, Austin Health, Melbourne, Australia*
[2]*Dept of Medicine, University of Melbourne, Melbourne, Australia*
[3]*eHealth, CSIRO Health and Biosecurity, Brisbane, Australia*
[4]*Piramal Imaging GmBH, Berlin, Germany*
[5]*The Florey Institute of Neuroscience and Mental Health, Melbourne, Australia*

Background: A common quantitative output value for Aβ imaging across tracers and methods will improve clinical and research use. A method has recently been developed for this purpose that produces a unit of measurement called the Centiloid (CL) (*Klunk et al, Alzheimers Dement, 2015*). This approach was implemented on Aβ imaging studies performed with ^{18}F-florbetaben (FBB) and ^{11}C-PiB (PiB).

Methods: All participants underwent PET imaging with both PiB and FBB, including 10 healthy young controls (32±9 yo) that were used to establish the "relative variance" ($^{FBB}CL_{Std}/^{PiB}CL_{Std}$) of FBB. Spatially normalized images were analyzed using the standard Centiloid regions (cortex and whole cerebellum reference region) downloaded from the Global Alzheimer's Association Investigators Network website (GAAIN; http://www.gaain.org). The non-standard reference regions, cerebellar cortex, pons, and whole cerebellum + pons were also investigated.

Results: FBB $SUVR_{WCb}$ had a smaller dynamic range in neocortex compared to PiB $SUVR_{WCb}$. Both tracers were highly correlated (R^2>0.93), irrespective of the reference region used for the scaling. The average Aβ burden for the young controls was -2.50±6.49 CL for FBB and -1.09±3.53 CL for PiB, yielding a FBB "relative variance" of 1.84.

Conclusions: ^{18}F-florbetaben results can soon be expressed in the common language of Centiloids by centers across the world using data that will be available through the GAAIN website. This is an important step towards better use of the clinical and research potential of Aβ imaging.
Keywords: Centiloid, florbetaben, PiB, Aβ imaging

Selection of reference region for 18F-THK-5351 PET imaging analysis

Po-Yen Chen[1], Ing-Tsung Hsiao[1,2], Kun-Ku Lin[1,2], Chin-Chang Huang[3]

[1]*Department of Medical Imaging and Radiological Sciences, Chang Gung University, Taoyuan, Taiwan*
[2]*Department of Nuclear Medicine, Chang Gung Memorial Hospital, Taoyuan, Taiwan*
[3]*Department of Neurology, Chang Gung Memorial Hospital, Taoyuan, Taiwan*

Introduction: The novel PET radiotracer ^{18}F-THK-5351 allows in vivo quantification of regional tau accumulation and monitoring the distribution of tau pathology. For semiquantitation using SUVR (standard uptake value ratios) in PET, the selection of reference region is important. The aim of this study is to explore the use of a proper reference region in ^{18}F-THK-5351 imaging based on group difference between Alzheimer's disease (AD) patients and normal controls (NC).

Methods: A total of 20 subjects included in this study were divided into two groups: one group with 10 NC, and another one with 10 AD. Each subject underwent MRI and PET scans. PET images were spatially normalized into MNI template aided from individual MRI. Total 19 VOIs merged from the AAL VOIs were applied for computing regional SUVR and effect size between AD and NC. Optimal reference regions were chosen based on larger effect size derived from SUVR normalized by the selected reference regions.

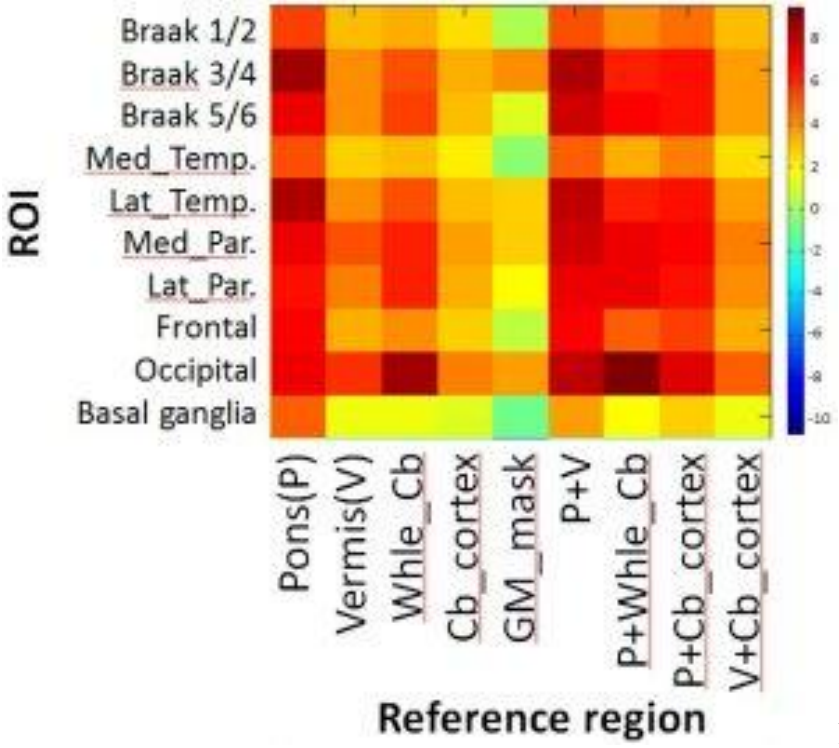

Fig.1 The heat map of effect size between AD and NC.

Results: The result indicates that both SUVR difference and effect size between AD and NC with intensity normalization from pons achieves stable and higher differentiation power than others (Fig.1). Moreover, larger effect size was observed when using the pons or the combination of pons and other regions as compared to those without pons. As compared to cerebellum cortex reference region, group SUVRs based on pons reference region are with less variation (Fig.2) but with smaller SUVRs.

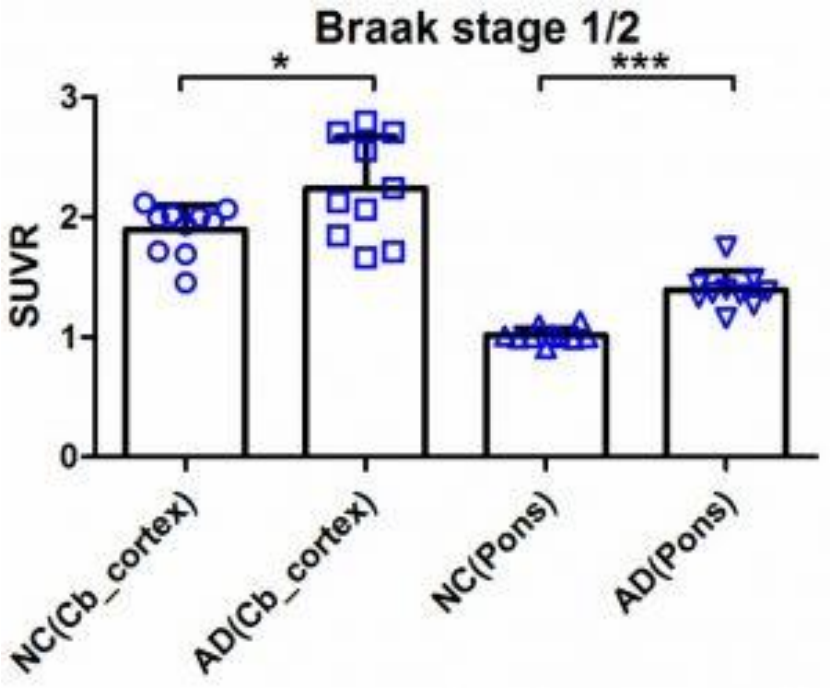

Fig.2 The group SUVRs differences between cerebellem cortex reference region and pons reference region in Braak stage 1/2.

Conclusions: Our results indicate that the regional ^{18}F-THK-5351 SUVR based on the selected pons reference region shows larger differentiation power than others, and thus is potentially useful for ^{18}F-THK-5351 imaging quantitation.

Keywords: 18F-THK-5351, PET, reference region

Noise reduction algorithm for amyloid imaging without loss of image resolution

Yuichi Kimura[1], Kohsuke Fujii[1], Takahiro Yamada[1], Chisa Hosokawa[2], Muneyuki Sakata[3], Takamichi Murakami[2], Kazunari Ishii[2]

[1]*Graduate School of Biology-Oriented Science and Technology, Kindai University, Kinokawa, Japan*
[2]*Department of Diagnostic Radiology, Faculty of Medicine, Kindai University, Osaka-Sayama, Japan*
[3]*Research Team of Neuroimaging, Tokyo Metropolitan Institute of Gerontology, Itabashi, Japan*

Introduction: This study aims at proposing a noise reduction algorithm for amyloid imaging without a loss of image resolution. In a reading of amyloid imaging, positiveness and negativeness to Aβ deposit is determined using an appearance of the white matter, and it has a thin and complicated structure. Such noise reduction algorithm is therefore expected that has small loss of spatial resolution. An ordinary noise reduction algorithm uses a spatial information of voxels; an averaging neighboring voxels, but another type of algorithm was proposed that utilize a kinetics of administered PET radiopharmaceutical, CAKS. CAKS was originally proposed for 1-tissue-2-compartment model, *e.g.* ^{15}O–H_2O, and its availability is investigated for ^{11}C–PiB whose kinetics is describes with 2-tissue-3-compartment model denoting a specific binding to Aβ in tissues.
Method: The ratio of is the function of a clearance rate from tissues to venous where is a tissue time activity curve (tTAC), T_E denotes the time of the last frame, and λ is a decay constant. R is computed for every voxels using tTAC. Voxels are then clustered based on R, and the tTACs are averaged to reduce the noise level. The performance is evaluated using a simulated PiB dynamic data, and CAKS is applied to a clinical data.
Results and Discussion: Estimated BP_{ND} were identical with the truth in a noise free simulation, and they were within 5% from the truth when a clinical level of noise was added. Fig. 1 demonstrates the results of CAKS. The white matter is well visualized. We can conclude that CAKS is applicable to an amyloid imaging.
Reference:

Yuichi Kimura, Hongbing Hsu, Hinako Toyama, and Nathaniel M. Alpert, "Improved Signal-To-Noise Ratio in Parametric Images by Cluster Analysis", *NeuroImage*, **9**, 554–561, 1999.

Keywords: PET, kinetic analysis, noise reduction, algorithm

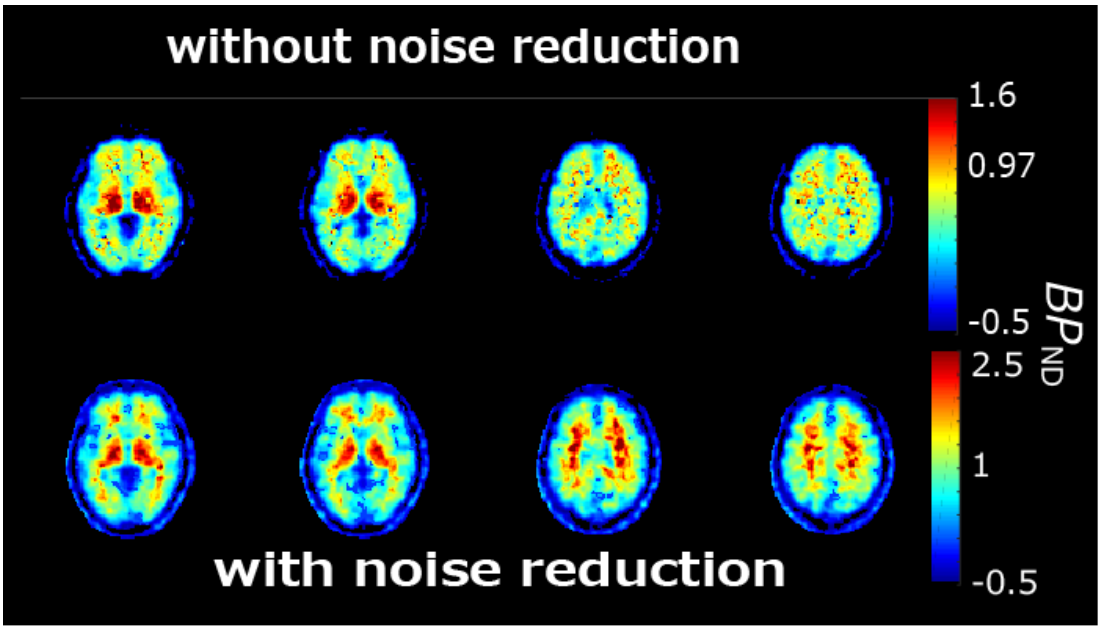

Fig. 1: BP_{ND} images of a typical Aβ negative case. The upper raw is the case of no noise reduction, and the lower raw is the results of CAKS.

Cerebral brain perfusion in cognitively normal elderly: measured with arterial spin labelling and [18F]Flutemetamol PET

Stephen Carter[1], Laura Parkes[2], Rainer Hinz[1], Neil Pendleton[2], Karl Herholz[1]

[1]University of Manchester, Wolfson Molecular Imaging Centre, Faculty of Biology Medicine and Health, Manchester, United Kingdom
[2]University of Manchester, Faculty of Biology Medicine and Health, Manchester, United Kingdom

Background: Amyloid PET and Arterial Spin Labelling (ASL) were acquired from elderly individuals to measure fibrillar amyloid-beta (Aβ) pathology and to compare perfusion measures from each modality.

Methods: 33 cognitively normal elderly (85.2±4.3 years; range 79-93; MMSE 28.9±1.3; delayed CERAD words 8.5±1.2; M/F = 8/25) were investigated. Participants underwent MRI at 3T (Philips Achieva), including T1 and ASL, and high-resolution PET (HRRT, Siemens); injected Flutemetamol dose = 187±3.2 MBq. ASL and PET data were coregistered to T1 MR and unique anatomical brain atlases for each participant, derived from T1 images, were used to extract grey matter (GM) perfusion data. Cerebral perfusion (ml/min/100ml) was calculated with ASL; summing PET data acquired 4-8 mins post-injection created a pseudo-perfusion image (SUVR with cerebellar GM reference).

Results: SUVR values were extracted from a global neocortical region of Flutemetamol images (90-110mins) revealing 20/33 (61%) Aβ positive individuals (Aβ+ = SUVR>1.5); 6 carried the ApoE4 gene. There was only a fair agreement between SUVR and visual assessment of PET images ($k = .38$, $p < .05$). Mean global perfusion in the GM with ASL was 21.8±5.4 ml/min/100ml. There was no correlation between perfusion measured with ASL and PET either globally or in composite frontal and posterior GM regions. Sub-dividing the population into Aβ+ and Aβ negative (Aβ-) groups revealed no significant difference in MMSE score or delayed CERAD words; the Aβ+ group was significantly younger (83.9 vs 87.2 years). Within the neocortex there was a significant difference in pseudo-perfusion between the Aβ+ and Aβ- groups; the Aβ+ participants displayed relative hyperperfusion (MannWhitney $U = 173$, $p < .05$).

Conclusions: The data revealed that 61% of cognitively normal elderly individuals (79-93 years) possessed pathological levels of brain Aβ. Perfusion (ASL) and pseudoperfusion (PET) were decoupled, suggesting global GM and anterior/posterior GM values of perfusion may not reliably compare between modalities.
Keywords: Preclinical AD, Amyloid PET, Arterial Spin Labelling

[18F]flutemetamol – quantification on the centiloid scale

Christopher Buckley[1], Mark Battle[1], Adrian Smith[1], Koen Van Laere[2], Rik Vandenberghe[2], Val Lowe[3]

[1]*GE Healthcare, Amersham, United Kingdom*
[2]*KU Leuven, Leuven, Belgium*
[3]*Mayo Clinic, Rochester, MN, USA*

Objectives

- To determine the flutemetamol centiloids equation.
- To compare the centiloid SPM8 & PMOD processing Pipelines
- To obtain the centiloid value for the CERAD[2] style division between sparse and moderate plaque assessments from autopsy data.

Methods: PiB data from HVs and ADs were processed by both by SPM8 and PMOD-PNEURO PET/MRI Centiloid VOI pipelines using whole cerebellum(wc), as a reference. The correlation metrics[1] were met for both processing pipelines. 23 HV and 17 AD subject flutemetamol PET & MRI images were both then processed by these two pipelines and the centiloids conversion equations obtained.

An autopsy determined sparse/moderate[2] boundary equivalent centiloid value was obtained. MRI data was not available in the majority of the end-of-life subjects in our autopsy studies. Therefore, we utilised the AD and HC subjects to obtain a linear relationship between SUVR obtained via a white-matter masked AAL atlas PET-only processing pipeline (Via Cortex ID^{TM}) and using the SPM8 Centiloids pipeline. This relationship was used to convert the PET-only SUVRs from the AAL analysis of the end of life subject to centiloid values. The autopsy pathology measures were then used in a ROC analysis to estimate the centiloid value corresponding to the boundary between none and sparse in the CERAD-style plaque scoring.

Results: The equation relating flutemetamol SUVR via the centiloid VOI atlas on the standard **SPM8 and PMOD** PET/MR pipeline to centiloid values were:

$$\text{Centiloid}_{\text{flutemetamol\_SPM8}} = 117.14 \times \text{SUVR}_{\text{flutemetamol}} - 116.57 \quad (1)$$

$$\text{Centiloid}_{\text{flutemetamol\_PMOD}} = 113.15 \times \text{SUVR}_{\text{flutemetamol}} - 105.90.57 \quad (2)$$

The boundary between sparse and moderate neuritic plaque density by CERAD scoring - i.e. the pathology boundary beyond which the majorityflutemetamol images are visually read as positive[3] was estimated via a PET-only analysis to be a value of 30 centiloids.

References

1 Klunk et. al. Alzheimer's & Dementia 2015 Jan;11(1):1-15.
2 Mirra et. al. Neurology. 1991 Apr;41(4):479-86.
3 Curtis et. al. JAMA Neurol. 2015 Mar;72(3):287-94

Keywords: Centioloid, [18F]flutemetamol, CERAD, autopsy, SUVR

Blood-brain barrier disruption in Alzheimer disease measured by PiB PET: a preliminary study

Yi Su, Andrei Vlassenko, Marcus Raichle, John Morris, Tammie Benzinger

[1]*Washington University in St. Louis School of Medicine, Saint Louis, MO, USA*

Background: Alzheimer disease (AD) is a disorder with complex etiology and multiple pathogenesis pathways. Recently, there is an increased interest in understanding the role of vascular factors in AD pathogenesis and progression. As a key component of the neurovascular system, the function of the blood-brain barrier (BBB) in aging and AD is an important area of research, and it is hypothesized that BBB disruption can contribute to subsequent neurodegeneration which in turn lead to AD and dementia. In this preliminary study, we used a recently developed imaging technique to quantify BBB permeability and examine its relationship to cognitive impairment

Methods: A total of 50 participants (43 asymptomatic, 6 CDR 0.5, and 1 CDR 1) from local memory and aging studies who had both dynamic PiB PET scans and ^{15}O-water scans were included in this study. A recently developed image-derived arterial input function (IDAIF) technique was adopted to quantify regional tracer influx rate (K1) and cerebral blood flow (CBF). The ratio of this two parameters (*E*=K1/CBF) is the single pass extraction fraction of the tracer and directly reflects the permeability of BBB.

Results: A significant positive correlation (p=0.001, r=0.32) was found between hippocampi single pass extraction fraction (*E*) of PiB tracer and the CDR rating of the participants. (Fig. 1). This finding suggests BBB permeability is increased in participants with cognitive impairment.

Conclusion: Disruption of BBB is observed in cognitively impaired participants using a novel imaging technique measuring BBB permeability based on PiB PET. The finding confirms recent report of BBB breakdown in AD using contrast enhanced MR. Further investigation is ongoing to examine BBB function in aging and AD.

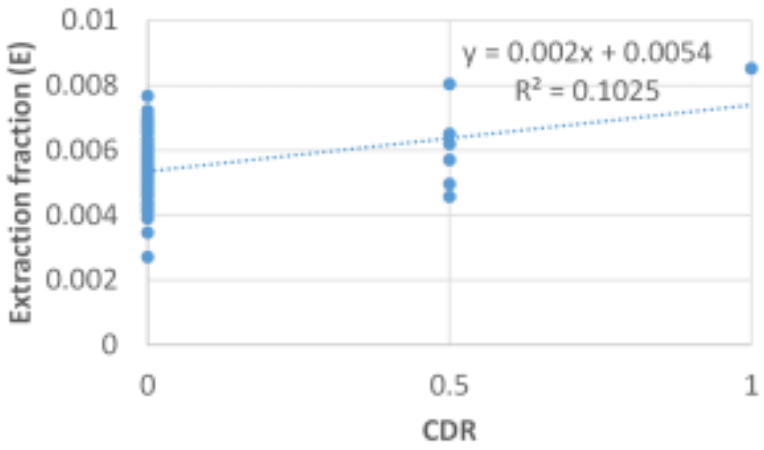

Figure 1. Positive correlation (p=0.001) between hippocampi single pass extraction fraction (*E*) and CDR score.

Keywords: blood-brain barrier, PiB, PET, Alzheimer disease,

Binding of a tau positron emission tomography ligand, PBB3, to α-synuclein pathology as assessed by fluorescence and autoradiographic labeling

Shunsuke Koga[1], Maiko Ono[2,3], Naruhiko Sahara[2], Makoto Higuchi[2], Dennis Dickson[1]

[1]*Department of Neuroscience, Mayo Clinic, Jacksonville, FL, USA*
[2]*National Institutes for Quantum and Radiological Science and Technology, National Institute of Radiological Sciences, Chiba, Japan*
[3]*Tohoku University Graduate School of Medicine, Department of Molecular Neuroimaging, Sendai, Japan*

Background: Tau positron emission tomography (PET) ligand, PBB3, binds to a wide range of tau pathology; however, binding property of PBB3 to non-tau inclusions remains unknown. Given that α-synucleinopathy is often clinically misdiagnosed as tauopathy, it is important to clarify whether PBB3 binds to α-synuclein pathology. To address this issue, reactivity of PBB3 was assessed by in vitro fluorescence and autoradiographic labeling of brain sections from patients with Lewy body disease (LBD) without Alzheimer-type pathology (pure form LBD, pLBD) and multiple system atrophy (MSA).

Method: Of 10 pLBD and 120 MSA in the Mayo Clinic brain bank, we selected 3 pLBD and 4 MSA cases with different severity of α-synuclein pathology, based on the quantitative analysis of α-synuclein burden performed in the amygdala of pLBD and in the striatopallidal fibers of MSA (Figure 1). PBB3 fluorescence labeling, double or single immunostaining for α-synuclein and phospho-tau, and in vitro autoradiography with PBB3 were performed for these selected samples.

Results: PBB3 fluorescence labeled various α-synuclein lesions including Lewy bodies, Lewy neurites, spheroids, glial cytoplasmic inclusions (GCIs) and neuronal cytoplasmic inclusions. Meanwhile, autoradiographic labeling with PBB3 at a 5,000-fold lower concentration (~10 nM) than fluorescence staining demonstrated no significant binding in pLBD cases. In contrast, significant autoradiographic binding of PBB3 to the striatopallidal fibers was found in two MSA cases (MSA-3 and MSA-4). This was in consistent with high density of GCIs in these cases (Figure 2). Furthermore, the absence of tau deposition in both cases was proven by immunohistochemistry.

Conclusions: Given that the maximum concentration of PBB3 in human PET scans is approximately 10 nM, the present data imply that α-synuclein pathology in pDLB is undetectable by PBB3-PET, while α-synuclein lesions in a considerable subset of MSA cases with high density of GCIs could be captured by this radioligand.

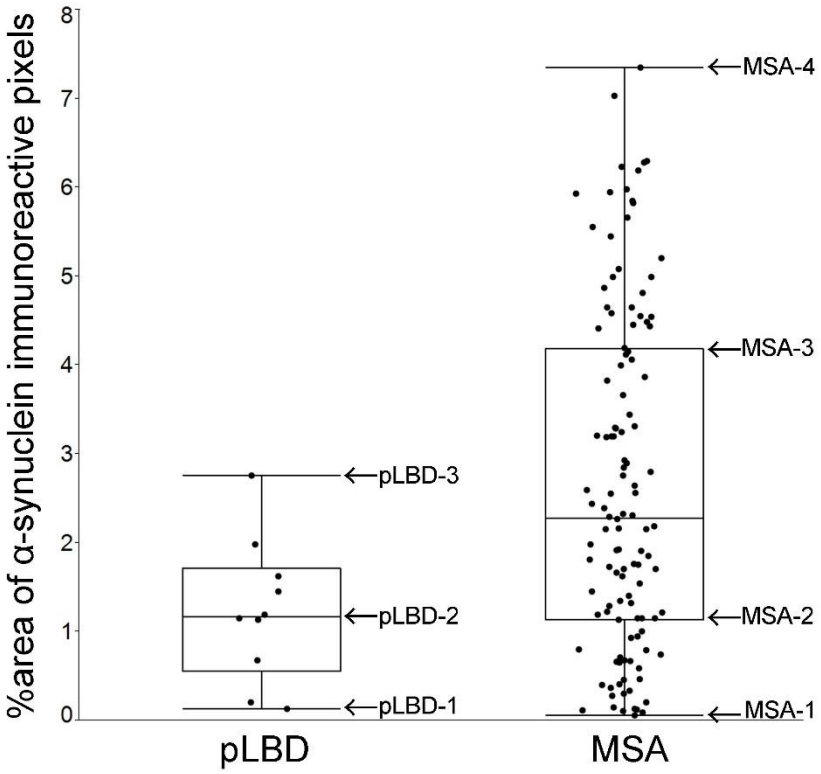

Figure 1. Cases with pLBD or MSA are selected based on the quantitative analysis of a-synuclein burden. LBD cases with minimum, median, and maximum burden are designated as pLBD-1, pLBD-2, and pLBD-3. MSA cases with minimum, 25th percentile, 75th percentile, and maximum burden are defined as MSA-1, MSA-2, MSA-3, and MSA-4.

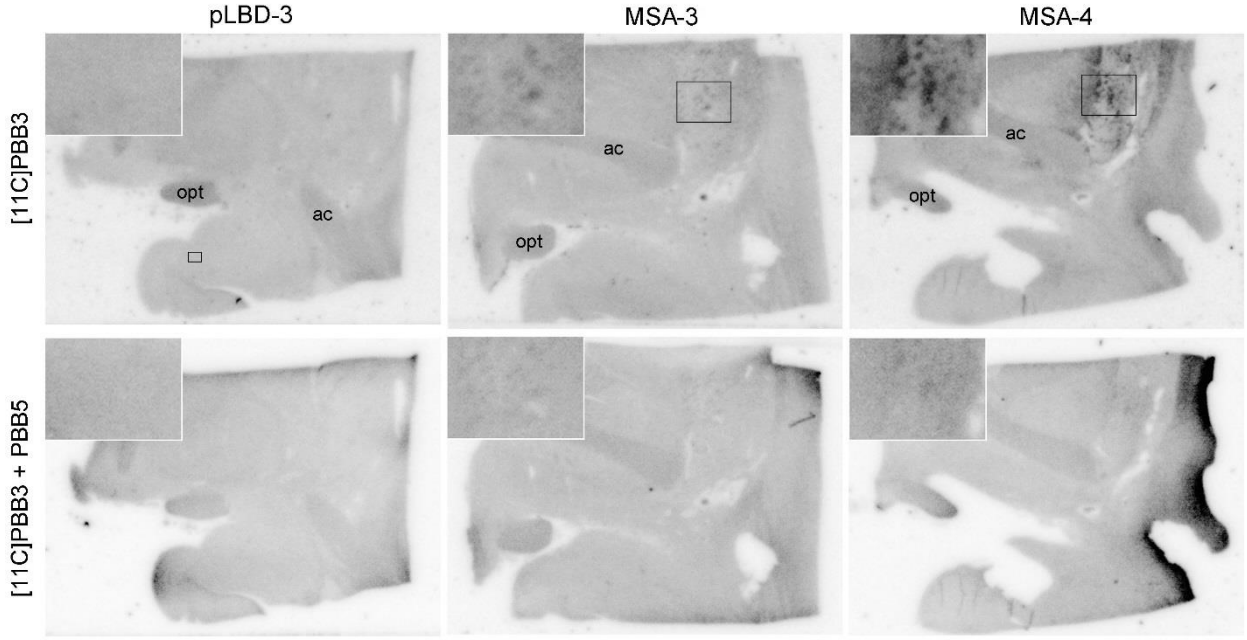

Figure 2. Representative images of Autoradiography. Even the most severe pLBD case (pLBD-3) shows no binding of [11]PBB3 to the amygdala, which have abundant Lewy bodies and Lewy neuites. In contrast, weak binding in MSA-3 and strong binding in MSA-4 to the striatopallidal fibers indicate the significant binding of [11]PBB3 to the glial cytoplasmic inclusions in this region. Less-intense signal is seen in the anterior commissure (ac) and optic tract (opt) due to nonspecific binding in all cases.

Keywords: Lewy body disease, multiple system atrophy, PBB3, autoradiography

A computationally efficient method for making PET measurements: the T1-GTM approach

Aaron Schultz, Reisa Sperling, Keith Johnson

Brigham and Women Hospital/Massachusetts General Hospital/Harvard Medical School, Boston, MA, USA

Background: It is often advantageous practices to use T1-MRI imaging to drive the regional measures in PET. Anatomical labeling to define grey matter regions of interest yield higher quality measures. The current standard is FreeSurfer(FS), however full FS recons are time and computation intensive. We present an alternative that utilizes a probabilistic version of the GTM atlas (FS-6; 100 ROIs covering the entire head), combined with automated tissue segmentation in SPM12 to create ROI that have 1) good overlap with the FS defined ROI, 2) high shared variance with the FS pipeline, and 3) greatly reduced processing time and effort.

Methods: 275 HABS subjects where processed with FS and SPM12-Segment. Normalizations computed by SPM12 were used to map the FS-gtmseg atlas to template space, where a winner-take-all approach was used to assign every voxel to one of the 100 ROI in the gtmseg atlas. This probabilistic template-space atlas is then reverse normalized to native T1 space where ROI are crossed with the applicable tissue classes, followed by iterative tissue-class based assignment of uncategorized voxels to existing labels. ROI measures are made in 100 ROI using co-registered PET data, including PVC with GTM method.

Results: Utilizing 353 AV1451-PET scans, comparison of FS-GTM ROI and T1-GTM ROI reveal good overlap with an average dice coefficient of 0.70±0.13, and an average correlation between suvr measurements of 0.97±0.06. In small ROI of interest such as entorhinal we observe a correlation of 0.99, and when excluding values greater than 1.2 the correlation is still 0.86. When examining GTM-PVC measures the average correlation across ROI is 0.94±0.10.

Conclusion: This approach allows for rapid processing of PET data (~45min.) that maintains high fidelity to a more fully optimized FS-based pipeline (14-30hrs), though without the benefit of detailed structural measures or the ability to create native surface maps.
Keywords: PET, PVC, GTM, T1, AV1451

Simplified reference tissue methods in [18F]AV1451 PET

Tessa Timmers[1,2], Sandeep Golla[1], Rik Ossenkoppele[1,2], Colin Groot[1,2], Sander Verfaillie[1], Philip Scheltens[1], Wiesje van der Flier[1,3], Lothar Schwarte[4], Mark Mintun[5], Michael Devous[5], Robert Schuit[1], Albert Windhorst[1], Adriaan Lammertsma[1], Ronald Boellaard[1,6], Maqsood Yaqub[1], Bart van Berckel[1]

[1]*Department of Radiology & Nuclear Medicine, VU University Medical Center, Amsterdam, Netherlands*
[2]*Alzheimer Center, Department of Neurology, VU University Medical Center, Amsterdam, Netherlands*
[3]*Department of Epidemiology & Biostatistics, VU University Medical Center, Amsterdam, Netherlands*
[4]*Department of Anaesthesiology, VU University Medical Center, Amsterdam, Netherlands*
[5]*Avid Radiopharmaceuticals, Philadelphia, PA, USA*
[6]*Department of Radiology & Molecular Imaging, University of Groningen, Groningen, Netherlands*

Background: Previous studies with AV1451 PET quantified tau load using the standardized uptake value ratio (SUVr) derived from a static scan. SUVr may, however, be flow dependent and should be validated against a fully quantitative approach. The objective of this study was to compare simplified reference tissue models to plasma input tracer kinetic models for AV1451.

Methods: Following intravenous injection of 225±16 MBq AV1451, 130 min dynamic PET scans were performed in 5 biomarker confirmed AD patients and 5 controls. Arterial blood sampling was performed to obtain a metabolite corrected plasma input function. Next, regional time-activity curves were generated using PVElab software. The optimal kinetic model for describing *in vivo* kinetics of AV1451 was selected based on the Akaike criteria. The simplified reference tissue model (SRTM) was performed with grey matter cerebellum as reference region. SRTM derived binding potential (BP_{ND}) was compared to distribution volume ratio (DVR) derived from the optimal plasma input tracer kinetic model. In addition, SUVr values were calculated using the time interval 80-100 minutes post injection.

Results: The reversible two tissue compartment model with blood volume parameter ($2T4k\_V_B$) best described the kinetics of AV1451 in AD and controls. The SRTM derived BP_{ND} showed good correlation (AD: $r^2 = 0.87$, slope = 1.06; controls: $r^2 = 0.87$, slope = 0.86) with indirect plasma input binding (DVR-1). SUVr (80-100 min) correlated well with DVR ($r^2 = 0.93$, slope = 1.07) and SRTM derived BP_{ND} ($r^2 = 0.84$, slope = 0.95).

Conclusion: SRTM derived BP_{ND} correlated well with DVR-1. High correlations obtained for SUVr (80-100 min) suggest that it might be an alternative for DVR and BP_{ND} (SRTM). However, since the present results are based on a small cohort and as SUVr values may be flow dependent, these results should be interpreted with caution, especially when used longitudinally.
Keywords: AV1451, tau, PET, kinetic modelling, simplified reference tissue models

In vitro binding of [3H]RO6958948, [3H]AV-1451, [3H]THK5351 and [3H]T808 to tau aggregates in non-AD tauopathies

Michael Honer[1], Luca Gobbi[1], Dieter Muri[1], Edilio Borroni[1]

[1]Roche Pharmaceutical Research and Early Development, Roche Innovation Center Basel, Basel, Switzerland

Objectives: Aggregation of tau is a hallmark of many neurodegenerative diseases, and tau imaging with PET tracers would allow early diagnosis and efficacy monitoring of a therapeutic intervention. Recently, AV-1451, THK5351 and RO6958948 have been described as promising PET tracers to visualize and quantify aggregated tau in AD patients. This study presents a detailed comparison of in vitro binding of RO6958948, AV-1451, THK5351 and T808 to tau aggregates in non-AD tauopathies such as PSP, FTLD-tau, CBD and Pick's disease.

Methods: Binding of tritiated tracers to fresh frozen tissue sections from patients with different, histopathologically confirmed tauopathies was analyzed under physiological conditions without tissue fixation or stringent washing conditions to reflect the in vivo situation of a PET scan. Tracer binding was visualized by high-resolution phosphor screen autoradiography, followed by co-localization studies with tau mAb immunohistochemistry on the same tissue section. Binding specificity was also analyzed by tracer displacement studies using co-incubation with cold variants of the different tracers.

Results: All tracers showed a similar binding profile to tau aggregates in AD and non-AD tauopathy tissue. Radioligand binding to tau aggregates in AD brain sections was confirmed by macroscopic and microscopic co-localization of radioligand binding and tau mAb staining. In vitro displacement studies suggested that all four tracers bind to an overlapping binding site on the AD-type of tau aggregates. None of the tracers displayed a significant binding to tau pathology in PSP, CBD and Pick’s disease. Only in brain tissue samples from certain FTLD-tau MAPT mutation carriers some tau tracer binding to tau aggregates could be identified.

Conclusions: The results highlight the importance of characterizing the in vitro binding of tau PET tracer candidates to different species of tau aggregates to guide the clinical application of these tracers for the detection and quantification of tau aggregates in non-AD tauopathies.
Keywords: tau, autoradiography, RO6958948, PSP, AV-1451

Evaluation of Caspase-3 activation in Alzheimer's disease using [18F]ICMT-11 PET/CT

Valeria Calsolaro, Grazia Daniela Femminella, Zhen Fan, Melanie Dani, Kasia Kozlowski, Eric Aboagye, Paul Edison

[1]*Faculty of Medicine, Imperial College London, London, United Kingdom*

Introduction. Caspase 3 belongs to the family of cysteine aspartate-specific proteases involved in apoptosis, but it also exerts different functions in the central nervous system. Caspase 3 is involved in several neurodegenerative diseases, like Alzheimer's disease (AD), and increased Caspase 3 immunoreactivity in has been shown in AD patient's hippocampus. Moreover, activated Caspase 3 seems to co-localize with neurofibrillary tangles (NFT) and amyloid plaques in AD brains. ICMT-11 has been characterized as a caspase-3/7 specific positron emission tomography (PET) imaging radiotracer for the assessment of apoptosis. In this study we examine for the first time the brain uptake and kinetics of ICMT-11 in healthy volunteers and in patients diagnosed with AD.

Methods. Seven subjects (four AD and three HC) underwent ICMT-11 PET with arterial input and structural MRI. Arterial input data was analysed using two tissue compartmental model, and region of interest (ROI) analysis was performed. Object map was created in PET space, and distribution volumes (V_T) were calculated for each brain region.

Results. We detected statistically significant increase in the uptake of ICMT-11 in medial temporal lobe (MTL) ($p=0.036$) and fusiform gyrus ($p=0.002$) in the Alzheimer's group compared to controls, with at least two fold increase. The AD group also showed a significant smaller hippocampal volume compared to HC ($p=0.047$).

Conclusions. This pilot study evaluated ICMT-11 in an AD population, and demonstrated that there is increased ICMT-11 uptake in a cohort of Alzheimer's disease subjects. This is in line with ex vivo demonstration of Caspase 3 activity in different aspects of Alzheimer's disease. While larger studies necessary to validate the finding, these preliminary data suggest that ICMT-11 has the potential to detect apoptosis in Alzheimer's disease.
Keywords: Alzheimer's disease, Caspase 3, positron emission tomography, [18F]ICMT-11

Considerations for defining a striatal region of interest in amyloid PET studies within the Down syndrome population

Patrick Lao[1], Tobey Betthauser[1], Julie Price[2], William Klunk[2], Peter Bulova[2], Sigan Hartley[1], Regina Hardison[2], Rameshwari Tumuluru[2], Dhanabalan Murali[1], Chester Mathis[2], Annie Cohen[2], Todd Barnhart[1], Dana Tudorascu[3], Darlynne Devenny[2], Charles Laymon[1], Sterling Johnson[2], Ben Handen[1], Bradley Christian

[1]*University of Wisconsin-Madison, Madison, WI, USA*
[2]*University of Pittsburgh, Pittsburgh, PA, USA*
[3]*New York State Institute for Basic Research in Developmental Disabilities, New York City, NY, USA*

Background: Amyloid PET studies in the Down syndrome(DS) population, or in autosomal dominant Alzheimer's disease(AD), demonstrate elevated striatal amyloid in nearly all amyloid-positive subjects, often appearing before elevated cortical amyloid. Therefore, special attention should be placed on the analysis of early elevated striatal amyloid, in these conditions characterized by amyloid-β overproduction.

Methods::Eighty-one non-demented adults with DS (37.2±7.0yrs;44M,37F) underwent up to 3 cycles of PiB scans for a total of 80 cycle1, 54 cycle2, and 11 cycle3 scans. Standard uptake value ratio (SUVR;50-70min;cerebellar gray matter reference region) images were normalized to MNI space via a DS-specific PiB template and mean SUVRs were extracted from hand-drawn (on T1 MRIs;nucleus accumbens 2328mm^3) or atlas-based masks (WakeForestUniversity pickatlas, SPM8;caudate 8240mm^3, putamen 13752mm^3, globus pallidus 4928mm^3). Region of interest(ROI) dilation was accomplished by smoothing with an 8mm Gaussian kernel and thresholding at various cutoffs to investigate the effects of ROI size on mean SUVR.

Results: Distributions of PiB SUVR in the caudate (overall mean±SD;1.16±0.41), putamen (1.52±0.42), nucleus accumbens (1.26±0.29), and globus pallidus (1.04±0.11) are shown in Figure1. The change in PiB SUVR between cycles (3.0±0.7years apart) were 0.07±0.15, 0.10±15, 0.06±0.13, -0.01±0.09 for the caudate, putamen, nucleus accumbens, and globus pallidus, respectively. Mean SUVR was stable after ROI dilation (|ΔSUVR| at 0.1 threshold: caudate 0.02;putamen 0.01;nucleus accumbens 0.01;globus pallidus 0.06), despite the widening of voxel-wise distributions due to inclusion of adjacent ventricle space or white matter.

Conclusion: Combinations of caudate, putamen, or nucleus accumbens provide meaningful information about early amyloidogenesis in the DS population, but the degree of inclusion for each subregion affects the mean SUVR. ROI size has minimal impact on ROIs that fully encompass a striatal subregion, but inclusion of adjacent ventricle space or white matter introduces extreme values that will have a greater influence on the mean SUVR in partial ROIs, e.g., just a few axial slices.

Research Support:R01AG031110, U54HD090256, U01AG051406

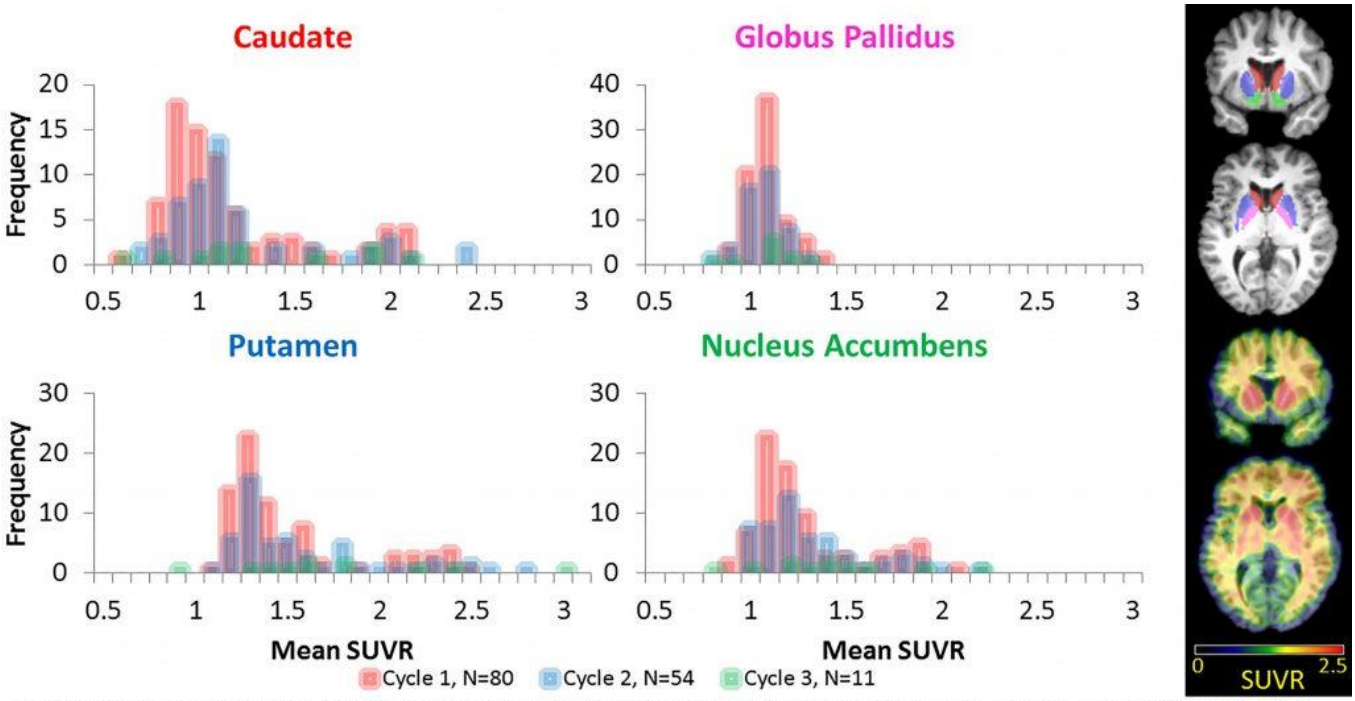

Frequency histograms of mean [^{11}C]PiB standard uptake value ratios (SUVRs) for four striatal subregions: the caudate, putamen, globus pallidus, and nucleus accumbens. While the caudate, putamen, and nucleus accumbens demonstrate a similar distribution across subjects, the globus pallidus does not show elevated binding. The panel on the right shows the regions of interest color coded to match the histogram title, and a representative [^{11}C]PiB SUVR image.

Keywords: Down syndrome, preclinical Alzheimer's disease, PiB, amyloid, striatum

Head-to-head comparison of tau-specific tracers in Alzheimer's disease: [11C]THK5351 vs [11C]PBB3 PET imaging

Konstantinos Chiotis[1], Per Stenkrona[2], Ove Almkvist[1,3], Ryosuke Arakawa[2], Akihiro Takano[2], Vladimir Stepanov[2], Andrea Varrone[2], Makoto Higuchi[4], Christer Halldin[2], Agneta Nordberg[1,5]

[1]*Dept NVS, Center for Alzheimer Research, Translational Alzheimer Neurobiology, Karolinska Institutet, Stockholm, Sweden*
[2]*Department of Clinical Neuroscience, Center for Psychiatric Research, Karolinska Institutet, Stockholm, Sweden*
[3]*Department of Psychology, Stockholm University, Stockholm, Sweden*
[4]*Molecular Imaging Center, National Institute of Radiological Sciences, 4-9-1 Anagawa, Inage-ku, Chiba, Japan*
[5]*Department of Geriatric Medicine, Karolinska University Hospital Huddinge, Stockholm, Sweden*

Objective: During the past five years, the development of different tau-specific PET tracers has enabled the visualization of tau deposits in Alzheimer's disease (AD) as well as other tauopathies. In this study we evaluated *in vivo* THK5351 and PBB3, two tau-specific PET tracers that belong to different chemical families, in the same patients with AD.

Materials & Methods: A group of patients with clinical diagnoses of mild cognitive impairment and probable AD were recruited after thorough clinical assessment. All patients underwent multimodal imaging with the tau-specific tracers THK5351 and PBB3, the amyloid-specific tracer AZD2184 as well as a 3D T1 MRI sequence. In addition to the clinical assessment, all patients were evaluated for the purposes of the project with a detailed neuropsychological battery.

Results: All patients showed high widespread cortical binding of AZD2184. Binding of THK5351 and PBB3 was observed in the temporal lobes as well as other isocortical areas, however, distinct from the distribution pattern of AZD2184 binding. Compared to PBB3, THK5351 showed greater grey matter binding. Distinct areas showing off-target binding for every tracer were identified.

Significance: To date, this is the first study to investigate *in vivo* the comparability of two different tau-specific PET tracers in the same patients with AD. This study will shed new light into the regional binding properties of the tracers as well as the underlying interrelationship between the tau tracers' binding with markers of cognitive decline and amyloid burden in the AD brain.
Keywords: tau, amyloid, THK5351, PBB3

Flow changes affect SUVr but not binding potential in an AD clinical trial

Colin Groot[1,2], Tessa Timmers[1,2], Rik Ossenkoppele[1,2], Maqsood Yaqub[1], Niels D Prins[2,3], Adriaan A Lammertsma[1], Philip Scheltens[2], Bart NM van Berckel[1]

[1]Department of Radiology & Nuclear Medicine, VU University Medical Center, Amsterdam, Netherlands
[2]Alzheimer Center & Department of Neurology, VU University Medical Center, Amsterdam, Netherlands
[3]Alzheimer Research Center, Amsterdam, Netherlands

Background: Clinical trials investigating changes in amyloid load in patients with Alzheimer's disease (AD) following treatment routinely make use of the semi-quantitative measure standardized uptake value ratio (SUVr). It has been shown, however, that PiB SUVr is sensitive to changes in blood flow, potentially leading to misinterpretation of therapy effects. The objective of the present study was to assess if blood flow changes during a clinical trial affect SUVr compared with the fully quantitative measure of amyloid load, which is binding potential (BP_{ND}).

Methods: 14 amyloid-positive patients with mild cognitive impairment (MCI) or AD (age 67±5) underwent 90-minute dynamic PiB PET scans before and after a 12-week treatment period. A global cortical ROI was defined on (individual) structural MRI images using a probability map based template. BP_{ND} and SUVr (60-90 min post-injection) were calculated using cerebellar grey matter as reference region. In addition, an index of flow was obtained from the ratio of tracer deliveries to cortical and cerebellar regions (R_1). Changes between baseline and follow-up (Δ) were calculated for R_1, BP_{ND} and SUVr.

Results: Paired T-tests revealed no significant differences between baseline and follow-up values for any of the parameters (Table, Figure 1). ΔBP_{ND} showed good correlation with ΔSUVr (Spearman's $\rho=0.76$, $p<0.01$). ΔBP_{ND} did not correlate with ΔR_1 (Spearman's $\rho=0.37$, $p=0.20$), whilst ΔSUVr did (Spearman's $\rho=0.65$, $p=0.01$).

Conclusion: These results indicate that changes in SUVr, but not BP_{ND}, are affected by changes in blood flow. Although this had no effect on the interpretation of SUVr in the present study, the sensitivity of SUVr to changes in perfusion indicates that treatment effects in AD should preferably be assessed using fully quantitative methods such as BP_{ND}, especially if the interval between baseline and follow-up scans is longer and for drugs that have a direct effect on perfusion.

	Baseline	Follow-up
SUVr (60-90 min)	1.98 (0.36)	2.01 (0.41)
BP_{ND}	0.74 (0.24)	0.76 (0.27)
R_1	0.85 (0.06)	0.85 (0.05)

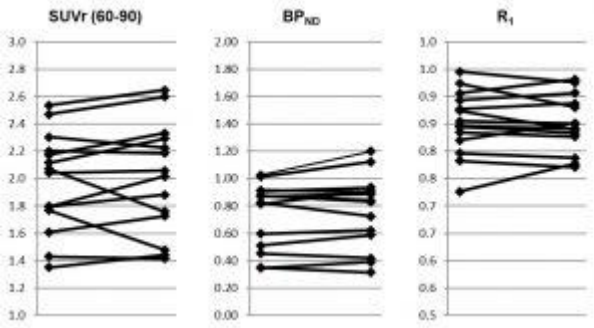

Values are displayed as mean (standard deviation)

Keywords: SUVr, binding potential, flow, PiB, PET

Developing a tracer agnostic pipeline for amyloid and tau PET data

Zachary Hobel[1], Suzanne Baker[2], Matthew Ellis[1], Judy Pa

[1]*Stevens Neuroimaging and Informatics Institute, University of Southern California, Los Angeles, CA, USA*
[2]*Life Sciences Division, Lawrence Berkeley National Laboratory, Berkeley, CA, USA*

Background: With the availability of sensitive and specific PET radioligands for beta-amyloid and tau aggregates, many studies are incorporating both markers in large-scale, within-subject designs. Thus, there is an increasing need to harmonize the analysis approach for amyloid and tau PET data to maximize biologically-relevant signals and minimize methodological noise. The goal of this project was to develop a tracer-agnostic analysis pipeline for amyloid and tau PET.

Methods: We utilized publicly available data from the Alzheimer's Disease Neuroimaging Initiative (ADNI). As of June 2016, there were 53 cognitively normal or mild cognitive impairment participants who had both amyloid and tau PET data available (24 women, age: 76.4$\pm$7.5 years). We first constructed an amyloid PET analysis pipeline based by published studies from the ADNI PET Core, tested our pipeline on raw data downloaded from ADNI, and then developed a complementary tau PET pipeline.

Results: We produced an analysis pipeline with key features, including image realignment, coregistration, averaging, reslicing, and smoothing. Smoothing parameters were dependent on each scanner's resolution and performed to bring images acquired at different scanners to a common resolution. The reference regions were a composite of the whole cerebellum, brainstem/pons, and white matter for AV-45 and the whole cerebellum for AV-1451. Using our harmonized pipeline, we replicated the AV-45 SUVR composite scores processed by the ADNI PET Core with 10^{-3} accuracy. In proof of principal analyses, we found that 1) AV-1451 SUVR values in the right inferior temporal cortex were negatively associated with long-delay memory, and 2) APOE-e4 carriers had higher AV-45 SUVR values when compared to APOE-e4 non-carriers (all p's<0.01).

Conclusions: A flexible analysis pipeline for processing amyloid and tau PET data is feasible and enables combining datasets from different sources for large-scale analyses. Future work will include optimizing this pipeline for clinical trials, integrating other tracers, and standardizing to centiloids.
Keywords: Alzheimer's disease, AV-45, AV-1451, clinical trials, harmonization

Kinetic modeling of the tau PET tracer [18F](S)THK-5351 in healthy controls and Alzheimer's disease subjects

Olivier Barret[1], Cristian Constantinescu[1], Christopher Buckley[3], Grethe Dalsgaard[3], Alex Gibson[3], Ajay Purohit[2], John Beaver[2], John Seibyl[1], Gilles Tamagnan[1], Ken Marek[1], Danna Jennings[1], Cristian Salinas-Valenzuela[2]

[1]*Molecular NeuroImaging, LLC, New Haven, CT, USA*
[2]*Biogen Inc, Boston, MA, USA*
[3]*GE Healthcare, Amersham, United Kingdom*

Objective: To perform kinetic analysis of (S)THK-5351 with arterial input function in healthy controls (HC) and Alzheimer's disease (AD) subjects, and assess test/retest variability of different measures.

Methods: PET brain imaging was completed in five HC (age 51-69), five mild AD (age 64-71, MMSE 21-26) and five moderate AD (age 54-75, MMSE 8-19). Subjects were administered 9.0 ± 0.7 mCi (S)THK-5351 and imaged twice for 3.0 hours with arterial blood sampling. PET data were analyzed with Logan graphical analysis (invasive (LGA) and non-invasive (NI-LGA)) to estimate the distribution volume ratio (DVR). SUVR curves were calculated over 180 min and compared to DVR for different time windows. The cerebellar cortex was used as reference region. DVR and SUVR were compared between the three groups.

Results: (S)THK-5351 is rapidly metabolized, with ~15-20% of parent remaining at 30 min. There was very good agreement between LGA and NI-LGA DVR estimates. SUVR curves plateaued around 40 min post injection. SUVR measurements correlated with DVR (R^2>0.9) but overestimated DVR by ~50-100%, with SUVR (40-60 min) showing highest correlation with DVR. DVR estimates were robust, with <5% change when truncating data from 180 to 90 min. NI-LGA DVR (90 min) test/retest variability was 3.4±2.8% across regions and subjects. Variability of SUVR was lower for 40-60 min (3.6±2.8%) compared to 60-90 min (4.7±4.0%). NI-LGA DVR (90 min) for HC, mild AD and moderate AD was 1.32±0.03, 1.49±0.05 and 1.55±0.06 in inferior lateral temporal cortex and 1.66±0.04, 1.79±0.05 and 1.75±0.06 in hippocampus.

Conclusions: SUVR curves rapidly reach a plateau and SUVR at 40-60 min highly correlate with DVR while providing lower test/retest variability compared to later imaging windows. Small signal increase was measured in AD compared to HC in regions expected to exhibit tau pathology, while high signal was measured in HC in subcortical regions and hippocampus.
Keywords: PET, Tau, Kinetic analysis, Test/Retest, THK-5351

Longitudinal changes in [18]F-RO6958948 Tau PET signal in four Alzheimer's subjects

Dean Wong[1,2,3], Hiroto Kuwabara[1], Robert Comley[5], Gregory Klein[4], Christina Vozzi[4], Michael Honer[4], Joshua Roberts[1], Kelly Kitzmiller[1], Lorena Gapasin[1], Edilio Borroni[4]

[1]Johns Hopkins University Department of Radiology and Radiological Sciences, Baltimore, MD, USA
[2]Johns Hopkins University Department of Psychiatry and Behavioral Sciences, Baltimore, MD, USA
[3]Johns Hopkins University Department of Neurology, Baltimore, MD, USA
[4]Roche Pharmaceutical Research and Early Development, Roche Innovation Center, Basel, Switzerland
[5]AbbVie (former employee of Roche Pharmaceutical Research and Early Development), North Chicago, USA

Objective: RO6958948, a novel radiopharmaceutical for imaging of tau deposits, has previously been evaluated in 11 AD, 5 YHC, and 6 OHC in PET imaging studies, determining kinetic and test-retest properties. Here we report preliminary longitudinal data from 4 AD subjects imaged at a second time point ranging from 8 to 22 months.

Methods: Four AD subjects (Age: 70 – 86; Baseline MMSE: 22 - 24) had baseline and follow up dynamic scans on a HRRT for 90 minutes after a bolus injection of RO6958948. Data were analyzed using the reference tissue graphical analysis and SUVR 60-90 minutes post-injection (reference region: cerebellum). Changes in DVR and SUVR between baseline and follow-up were examined in eleven brain regions (a total of 22 left and right regions) that showed higher binding in the 11 AD subjects (Age: 55 – 86; MMSE: 16 – 25), and/or are typically used for Braak staging of tau pathology. Paired t-test was used to examine whether DVR or SUVR increased in individual subjects.

Results: AD subjects showed changes of MMSE scores (baseline and follow-up MMSE / scan intervals in months) as: Subject A1: 24 → 25 / 18 months; A2: 20 → 19 / 8 months; A3: 23 → 19 / 22 months and A4: 22 → 18 / 21 months). Increase in DVR values of the 22 regions were observed in: A1 (up to 12%) and A4 (up to 23%), uncorrected p values: $p>10^{-3}$ and $p<10^{-4}$. SUVR values increased in subject A1 (up to 27%), A3 (up to 14%) and A4 (up to 27%) uncorrected p values: A1 $p<10^{-5}$, A3 $p<0.01$ and A4 $p<10^{-4}$. Data evaluation using other reference regions is ongoing.

Conclusions: Substantial increases between baseline and greater than one year follow-up PET scans were seen in 3 AD subjects suggesting that RO6958948 can detect Tau pathology progression.

Keywords: Tau, novel, radiopharmaceutical, Alzheimer's, longitudinal

Longitudinal Centiloid change in ADNI [18F]Florbetapir PET data: implications for clinical trials

Donald McLaren[1], Felix Carbonell[1], Vincent Auclair[1], Alex Zijdenbos[1], Abhinay Joshi[2], Micheal Navitsky[2], Mark Mintun[2], Ping Chiao[3], Barry Bedell[1,4]

[1]*Biospective, Inc., Montreal, QC, Canada*
[2]*Avid Radiopharmaceuticals, Inc., Philadelphia, PA, USA*
[3]*Biogen, Inc., Cambridge, MA, USA*
[4]*McGill University, Montreal, QC, Canada*

Introduction: Alzheimer's Disease clinical trials routinely use Florbetapir positron emission tomography (PET) scans as imaging endpoints. However, it is important to understand the changes observed in response to therapeutic interventions relative to natural history data and to other clinical trials. To this end, we have determined the annual change in Amyloid PET, in both SUVR and Centiloids, in ADNI to provide context for clinical trials.

Methods: Data from 188 ADNI subjects with repeated Amyloid PET scans were utilized. Florbetapir PET and 3D T1-weighted MRI scans were processed through Biospective's PIANO^{TM} pipeline. SUVR values were calculated using the whole cerebellum as a reference region and converted to Centiloids. The Centiloid conversion equation (Klunk, 2015) was generated using data from 43 subjects across the AD spectrum (provided by Avid Radiopharmaceuticals) with PiB PET, Florbetapir PET, and 3D T1-weighted MRI scans. Only subjects with an amyloid-positive Florbetapir baseline PET scan, based on visual reads, were used for longitudinal analysis.

Results: The annual SUVR changes (±s.d.) were 0.039±0.065 and 0.014±0.055 for cognitively normal and cognitively impaired groups, respectively (80% power). The corresponding annual Centiloid changes were 7.96±13.42 and 2.85±11.38. The sample sizes per arm needed to detect a halt in SUVR or Centiloid change over one year were 45 and 244 for cognitively normal and cognitively impaired groups, respectively. The sample size per arm needed to detect a 10 Centiloid (0.049 SUVR) reduction in annual change was ≤30 subjects per group (80% power).

Discussion: Based on this analysis, the detection of significant effects of anti-amyloid therapies that only halt the accumulation of β-amyloid will be limited by the statistical power. However, if an anti-amyloid therapy results in a substantial reduction of β-amyloid burden, then the required sample sizes would be drastically reduced, thereby facilitating the use of Amyloid PET in early-phase, disease-modifying clinical trials.
Keywords: amyloid, longitudinal, ADNI, Centiloid, sample size

FreeSurfer approach to the Centiloid standardization method: Evaluation of alternative cortical target regions and partial volume correction

Davneet Minhas[1], Brian Lopresti[1], Howard Aizenstein[2,3], Charles Laymon[1,3], Elizabeth Campbell[1], Zheming Yu[1], Dana Tudorascu[4], Chester Mathis[1], William Klunk[2,5]

[1]*University of Pittsburgh, Radiology, Pittsburgh, PA, USA*
[2]*University of Pittsburgh, Psychiatry, Pittsburgh, PA, USA*
[3]*University of Pittsburgh, Bioengineering, Pittsburgh, PA, USA*
[4]*Univeristy of Pittsburgh, Biostatistics, Pittsburgh, PA, USA*
[5]*University of Pittsburgh, Neurology, Pittsburgh, PA, USA*

Background: Central to the Centiloid standardization process is the cortical target region (SPM-CTX), derived by warping the CTX subject set (19 Alzheimer's disease and 25 older-control subjects) to MNI space using the Unified method within SPM and identifying the region of maximum difference between groups. However, the warping may be susceptible to differences in cortical grey matter (GM) atrophy. Further, the method does not account for the partial volume effect (PVE). This work evaluates alternative methods for generating a standard cortical region using FreeSurfer.
Methods: An initial alternative cortical region was generated by warping the Centiloid CTX subjects to a common space using FreeSurfer's Talairach transform and identifying the region of maximum difference (FS-CTX). A second GM-only cortical region was generated that follows the pial surface and GM-WM tissue boundaries by combining FreeSurfer GM parcellation regions that best match the FS-CTX region (FS-GM-CTX).
18 subjects independent of the Centiloid CTX set with PiB and MRI acquisitions were selected having either high (SUVR > 2.50; n=11) or low (SUVR < 1.20; n=7) amyloid load based on hand-drawn ROIs. Cortical SUVR values were determined using 4 methods: SPM-CTX, FS-CTX, FS-GM-CTX, and FS-GM-CTX with geometric transform matrix (GTM) partial volume correction (+PVC). Effect sizes (Cohen's d) were evaluated for distinguishing high vs. low amyloid load.
Results: SPM-CTX, FS-CTX, and FS-GM-CTX VOIs are overlaid on a native-space MRI in FIGURE. Average high-amyloid SUVRs (Cohen's d) were: SPM-CTX=2.82±0.24 (9.62); FS-CTX=2.59±0.17 (11.14); FS-GM-CTX=2.28±0.17 (9.86); FS-GM-CTX+PVC=3.73±0.31 (11.18).
Conclusions: The FS-GM-CTX method generated the lowest average high-amyloid SUVR and lower effect size than FS-CTX, likely due to its increased susceptibility to PVEs at the pial surface. However, FS-GM-CTX+PVC resulted in a similar effect size to FS-CTX despite a significantly larger standard deviation in the high-amyloid group. These results suggest PVC should be explored as part of a standardized amyloid methodology.

Keywords: amyloid, PET, partial volume, Centiloid, FreeSurfer

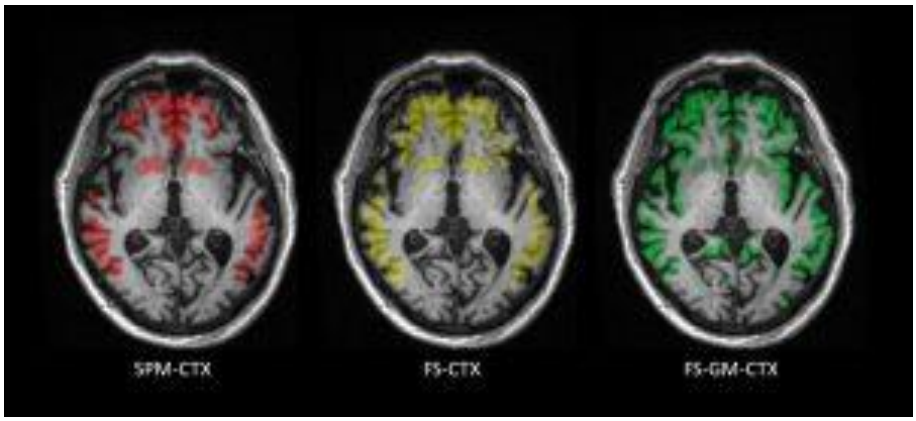

The quantitative impact of emission-transmission scan misalignment and region selection upon amyloid measurement accuracy

Randolph Andrews[1], Dawn Matthews[1], Anne Smith[2]

[1]*ADM Diagnostics LLC, Northbrook, IL, USA*
[2]*Siemens Healthcare, Knoxville, TN, USA*

Background: Statistically powered measurement of amyloid accumulation and removal is challenged by low biological accumulation rates and potentially subtle treatment reduction values. Several technical factors can overwhelm detection of these changes, including attenuation correction error due to misalignment between transmission scan and emission scan, but this has not been quantified. We systematically quantified emission-transmission misalignment impact upon Standardized Uptake Value Ratio, and the role of reference and target region selection.

Methods: Florbetapir PET-CT scans with negligible subject motion were obtained from three subjects with a range of clinical diagnoses, morphologies, and amyloid: Healthy Control amyloid negative (Am-), amnestic MCI Am+ threshold, and early AD Am+. The CT (mu-map) and emission scans of each were systematically misaligned and reconstructed using 56 different permutations including translational motion in each of x, y, and z directions of 0 to 10mm, and rotational motion relative to each axis of 0 to 10 degrees, and combined translation and rotation in all directions. Versions were also constructed that required realignment of the emission scans during processing vs. no realignment, to segregate realignment error from embedded attenuation correction error. Differences in measured regional values relative to the correctly aligned case were calculated and compared for different target regions of interest and reference region definitions, including regions based upon the AAL atlas and regions comprised of the Freesurfer segments applied in ADNI (Landau). Impact was compared across misalignment permutations, regions, and subjects.

Results: SUVR percent error ranged from 1% to over 50% depending upon motion and regions measured. Error increased notably after 4mm or 4 degrees. Subcortical white matter showed less error than gray cerebellum and pons in most cases, and certain cortical regions showed greatest change.

Conclusions: Emission-transmission scan misalignment must be minimized to assure accurate amyloid measurement. Reference and target regions can be selected to minimize misalignment related error.

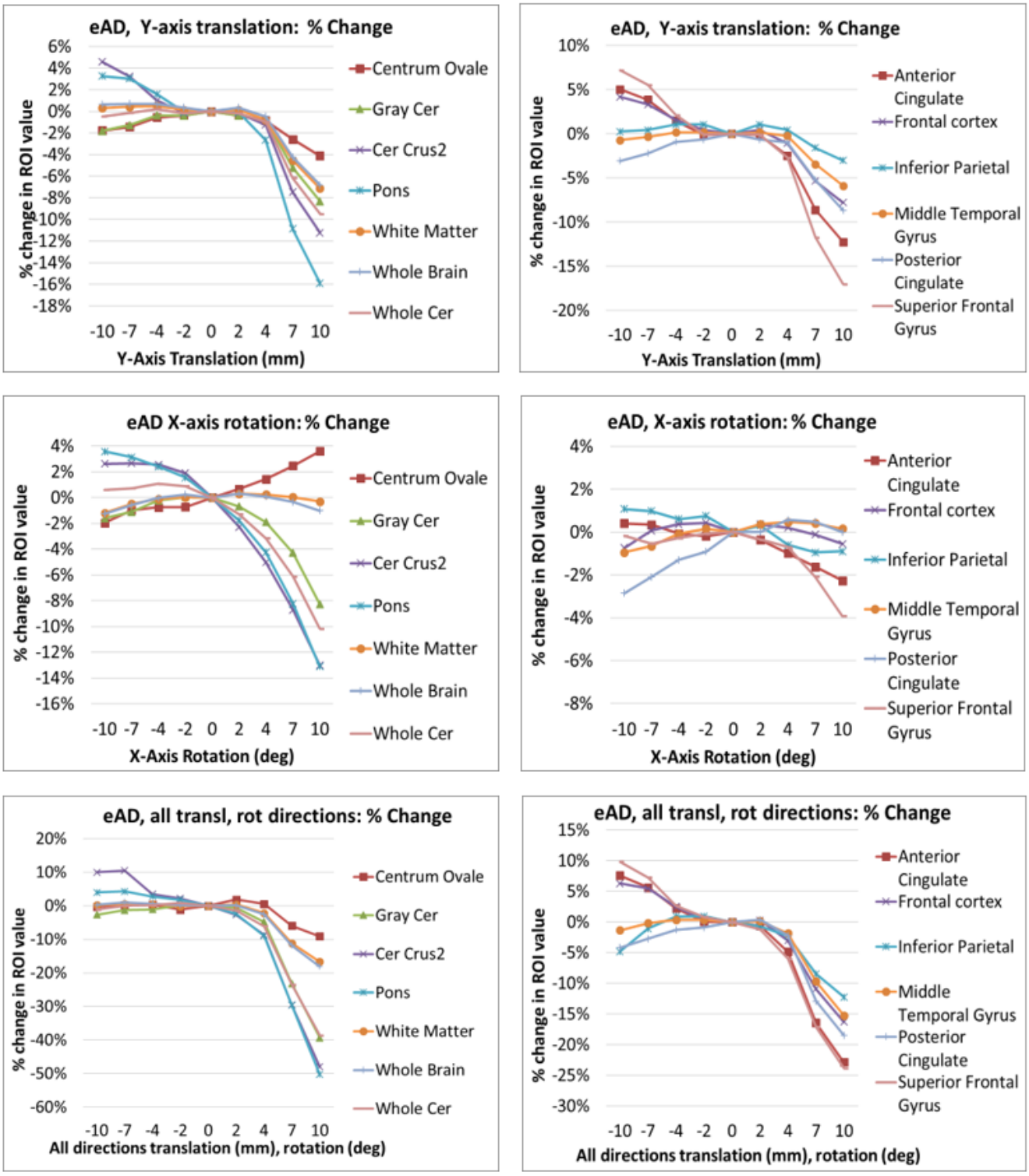

Figure 1. Percent change in regional amyloid PET values associated with y-axis translation, x-axis rotation, and combined translation and rotation across all axes. Reference regions shown on left, and example target AAL-based regions on right.

Keywords: amyloid, attenuation, quantitation, SUVR, rates

High quantitative accuracy amyloid PET imaging with precision estimation

Pawel Markiewicz[1,2], Kjell Erlandsson[2], Jonathan Schott[3], Catherine Scott[1], David Cash[3], Frederik Barkhof[1], Nick Fox[3], Sebastien Ourselin[1,3]

[1]Translational Imaging Group, CMIC, University College London, London, United Kingdom
[2]Institute of Nuclear Medicine, University College London, London, United Kingdom
[3]Dementia Research Centre, University College London, London, United Kingdom

We present an advanced infrastructure dedicated to quantification of amyloid imaging using PET/MR. The proposed software provides full control of list-mode data processing, image reconstruction and analysis leading to precise quantitative estimates of regional or voxel-level SUVr, and includes:

(1) generation of an atlas-based pseudo-CT (pCT) μ-map for attenuation correction which can be coregistered to any time frame of PET data to account for head motion;

(2) 3D scatter correction for long axial FOV scanners;

(3) voxel-based partial volume correction (PVC, iterative Yang) using T1w brain parcellations and up-sampled PET image;

(4) full detector normalisation and reduced noise randoms correction.

The entire processing chain is implemented on high-throughput graphical processing units (GPU). This enables comprehensive investigation of the sources of uncertainty through 100-times bootstrap resampling of the list-mode data and consequent multiple image reconstructions and analyses.

This methodology allows for a critical evaluation of the impact of PET count statistics; different methods for attenuation correction (UTE, pCT), scatter correction, PVC, registration and interpolation; choice of reference region; and size and position of the region-of-interest relative to the scanner's field-of-view. We show that partial volume effects and attenuation correction inaccuracies are the biggest sources of error (accounting for up to 10% each) followed by the limited count statistics (error of up to 8%). The type of interpolation used in image up-sampling for PVC and ROI analysis may cause changes of up to 4% in SUVr. Coregistration of the mu-map to any given time frame PET image increases accuracy due to misalignment correction but is a source of additional uncertainty.

The proposed infrastructure enables very accurate estimates of amyloid deposition using static and dynamic PET imaging. Estimates of uncertainty estimated at voxel and ROI levels aid in the interpretation of cross-sectional data, and are likely to allow for increased precision in longitudinal analyses.

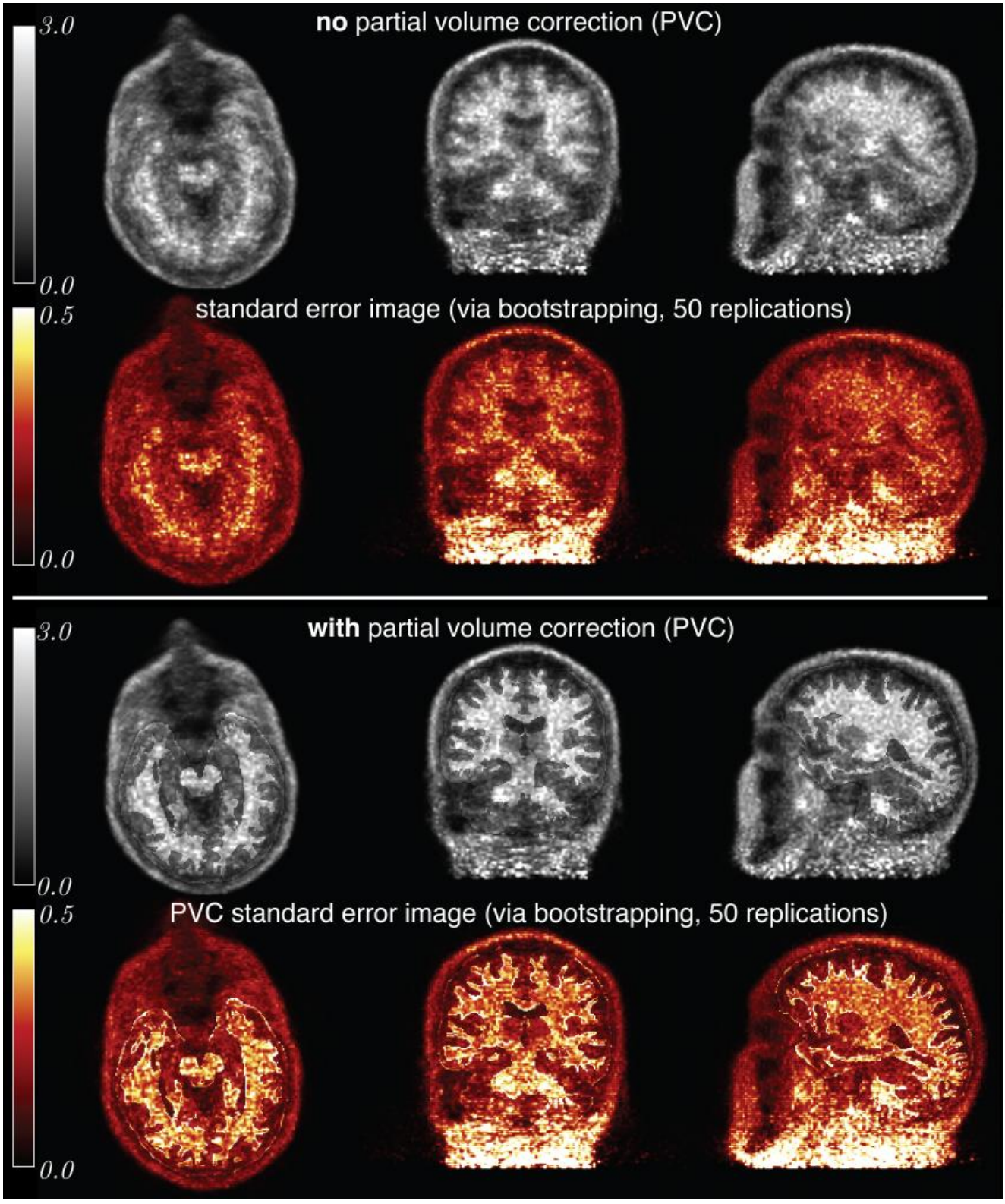
3.0
0.0
no partial volume correction (PVC)
0.5
0.0
standard error image (via bootstrapping, 50 replications)
3.0
0.0
with partial volume correction (PVC)
0.5
0.0
PVC standard error image (via bootstrapping, 50 replications)

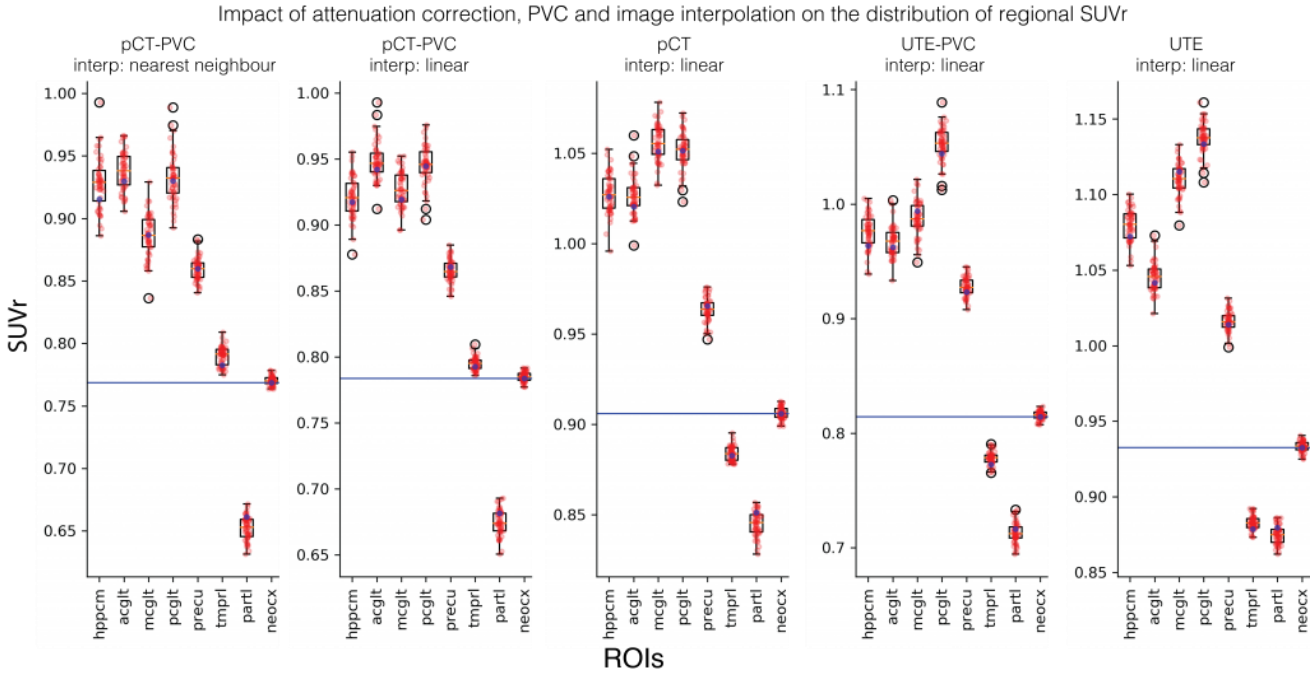

blue horizontal lines: standard global neocortex SUVr
blue dots: standard regional SUVr
red dots/box plots: bootstrapped distributions of SUVr (uncertainties)

hppcm: hippocampus
acglt, **mcglt**, **pcglt**: anterior, middle, posterior cingulate
precu: precuneus
tmprl: temporal, partl: parietal, **neocx**: neocortex

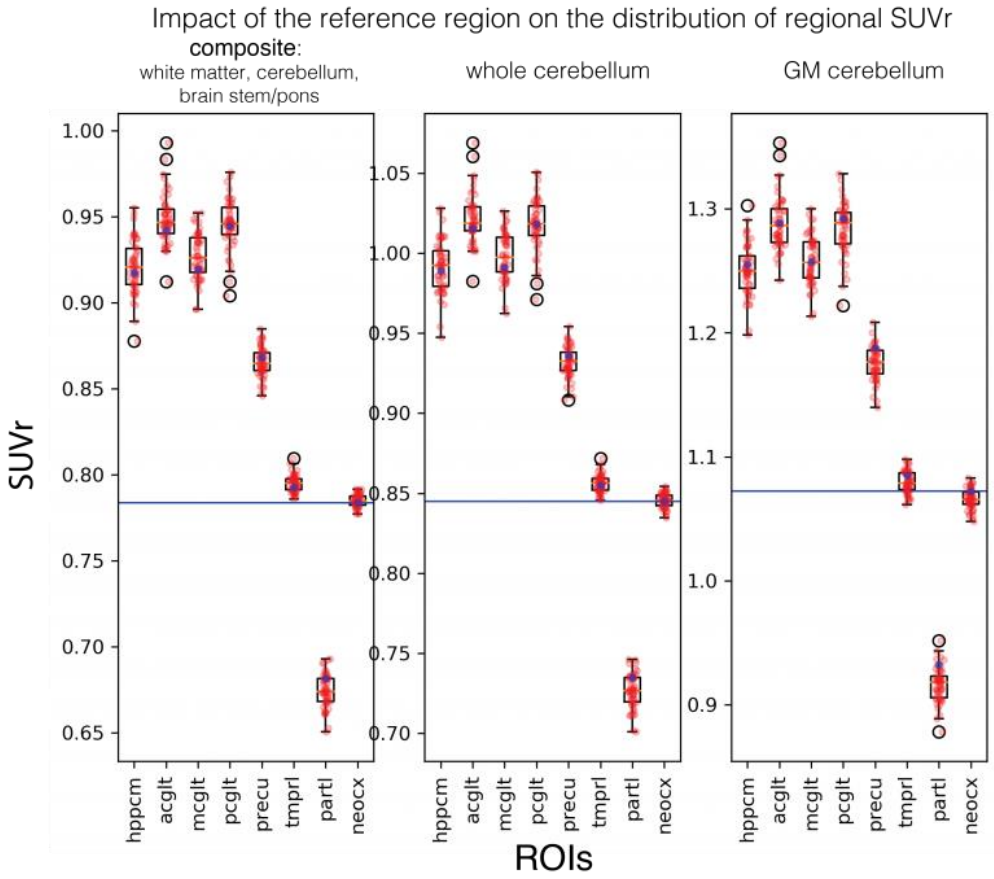

blue horizontal lines: standard global neocortex SUVr
blue dots: standard regional SUVr
red dots/box plots: bootstrapped distributions of SUVr (uncertainties)

hppcm: hippocampus
acglt, **mcglt**, **pcglt**: anterior, middle, posterior cingulate
precu: precuneus
tmprl: temporal, **partl**: parietal, **neocx**: neocortex

Keywords: amyloid quantification, PET, bootstrap resampling, uncertainty estimation, partial volume correction, scatter correction, attenuation correction

Comparison of region of interest segmentation methods for extraction of 11C-PiB SUVR in the Down syndrome population

Tobey Betthauser[1], Patrick Lao[1], Dana Tudorascu[2], Julie Price[2], Peter Bulova[2], Sigan Hartley[1], Regina Hardison[2], Rameshwari Tumuluru[2], Davneet Minhas[3], Charles Laymon[2], Dhanabalan Murali[1], Chester Mathis[2], Annie Cohen[2], Todd Barnhart[1], Darlynne Devenny[3], William Klunk[2], Sterling Johnson[1], Ben Handen[2], Bradley Christian[1]

[1]*University of Wisconsin - Madison, Madison, WI, USA*
[2]*University of Pittsburgh, Pittsburgh, PA, USA*
[3]*Institute for Basic Research in Developmental Disabilities, New York, NY, USA*

Introduction: Region of interest (ROI) segmentation can be problematic in populations with brain structure abnormalities, particularly for automated processing routines. Differences in ROI delineation could affect statistical outcomes when extracting PET binding measures. This work compares three methods of ROI delineation for ^{11}C-PiB SUVR extraction in the Down syndrome population.

Methods: Fifty-four individuals, selected from a larger cohort, with Down syndrome underwent ^{11}C-PiB PET (50-70 min) and T1-weighted MRI scans. Parametric SUVR images were generated (GM cerebellum reference) and coregistered to MRI (SPM8). Mean SUVRs were extracted from hand-drawn (HD) (Rasario2011), FreeSurfer 5.1.0 (FS), and Wake Forest University Pick Atlas (WFU) derived ROIs. HD and FS ROIs were defined in native MRI space. WFU ROIs were defined in MNI space. WFU SUVRs were extracted from SUVR images that were normalized from native MRI space (SPM8) to a study-specific PET template in MNI space. Between-method differences in mean SUVR were determined using a repeated measures analysis with a fixed method factor and a random subject effect (to account for within subject correlation). HD ROIs were the standard for comparison. Intra-class correlation coefficients (ICCs) were calculated using a one-way random effects model to assess agreement of the FS and WFU methods with the HD method.

Results: Compared to HD SUVRs, both WFU and FS SUVRs were significantly lower for all ROIs (Tables 1 and 2). ICCs indicated reasonable agreement with HD SUVRs for FS (except temporal cortex) and WFU methods, with WFU generally having slightly higher ICC's with HD (Table 3).

Conclusions: The use of a study-specific PET template in combination with the WFU PickAtlas improves agreement with hand drawn ROIs compared to using FreeSurfer and is a viable method for ROI delineation in the Down syndrome population. Normalizing to a PET template allows for regional SUVR extraction without requiring MRI data.

Region	Hand Drawn (n=54)	Pick Atlas (n=54)	Freesurfer (n=54)
Anterior Cingulate	1.44 (0.32)	1.28 (0.26)	1.29 (0.25)
Frontal Cortex	1.38 (0.32)	1.17 (0.27)	1.12 (0.23)
Parietal Cortex	1.30 (0.24)	1.20 (0.28)	1.22 (0.20)
Precuneus	1.35 (0.31)	1.27 (0.29)	1.25 (0.26)
Temporal Cortex	1.34 (0.24)	1.18 (0.20)	1.08 (0.19)
Striatum	1.42 (0.50)*	1.32(0.37)	1.35 (0.34)

Table 1 Descriptive statistics for computed SUVRs for each method and region. Values are presented as mean and standard deviation across all subjects. (*n=53)

Region	Pick Atlas vs Hand Drawn	Freesurfer vs Hand Drawn
Anterior Cingulate	-0.166 (-0.195, -0.136)	-0.158 (-0.187, -0.129)
Frontal Cortex	-0.209 (-0.243, -0.175)	-0.266 (-0.299, -0.232)
Parietal Cortex	-0.097 (-0.130, -0.065)	-0.176 (-0.208, -0.144)
Precuneus	-0.083 (-0.105, -0.060)	-0.095 (-0.118, -0.073)
Temporal Cortex	-0.158 (-0.184, -0.132)	-0.263 (-0.289, -0.236)
Striatum	-0.095 (-0.139, -0.051)	-0.063 (-0.106, -0.019)

Table 2 Results from the repeated measures model represented as the mean estimated differences and 95% confidence interval using hand-drawn values as the reference method.

Region	Hand Drawn and Pick Atlas ICC (Agreement)	Hand Drawn and Free Surfer ICC (Agreement)
Anterior Cingulate	0.785 (0.658, 0.869)	0.762 (0.623, 0.854)
Frontal Cortex	0.683 (0.512, 0.803)	0.526 (0.304, 0.694)
Parietal Cortex	0.806 (0.689, 0.883)	0.629 (0.437, 0.766)
Precuneus	0.925 (0.875, 0.956)	0.889 (0.817, 0.934)
Temporal Cortex	0.673 (0.497, 0.796)	0.369 (0.116, 0.577)
Striatum	0.925 (0.875, 0.956)	0.909 (0.848, 0.946)

Table 3 Intra-class correlation coefficients with 95% confidence intervals comparing agreement of FreeSurfer and WFU Pick Atlas SUVRs with hand-drawn SUVRs.

Keywords: Down Syndrome, Beta-amyloid, PET, PiB, SUVR

Comparison of tau distribution according to tau tracers in various neurodegenerative diseases: Using [18F]AV1451 and [18F]THK-5351

Young Koung Jang[1], Gil Rabinovich[2], Heejin Kim[1], Jin San Lee[1], Ko Woon Kim[1], Sang Won Seo

[1]Samsung Medical Center, Seoul, Korea
[2]University of California, San Francisco, San Francisco, CA, USA

Tau accumulation is known to be core pathologic change in various neurodegenerative diseases including AD. Several tau tracers have been developed to detect tau deposition in vivo. Recently, AV1451 and THK-5351 are widespread tau tracers among many tau tracers. We evaluated how each tau tracer reflected tau distribution and weather there were some differences between two tracers or not in various neurodegenerative diseases including AD-spectrum tauopathies and non-AD neurodegenerative diseases.

Six participants performed Tau-PET using two tracers, FBB-PET, and MRI. The participants consisted of two bvFTD, one svPPA, one AD, one LPA, and one SMI patients. To compare regional tau tacers uptake, we used the standardized uptake value ratios (SUVR) which is uptake ratio of automated volume of interest to reference region.

We found that THK-5351showed higher amount and larger area of retention than AV1451 in non-AD neurodegenerative diseases. Conversely, in AD spectrum diseases, higher amount and larger area of uptake were shown in AV1451, compared to THK. We also found that off target binding in midbrain and basal ganglia was prominent in THK-5351 than AV1451.

This study revealed that AV1451 was more specific to AD tauopathies and less likely to present off target binding, while THK-5351 was more likely to reflect non-specific neurodegeneration. These results would provide better understanding to clinical application of AV1451 and THK-5351.
Keywords: tau, PET, tracer

A comparison of DVR and SUVR methods for THK5317 and THK5351

Tobey Betthauser[1], Patrick Lao[1], Dhanabalan Murali[1], Todd Barnhart[1], Shozo Furumoto[2], Nobuyuki Okamura[2], Charles Stone[1], Sterling Johnson[1], Bradley Christian[1]

[1]*University of Wisconsin - Madison, Madison, WI, USA*
[2]*Tohoku University, Sendai, WI, USA*

Objectives: This work compared quantification strategies for estimating specific binding with dynamic and static imaging of PET tau radioligands ^{18}F-THK-5351 and ^{18}F-THK-5317.

Methods: Twenty-eight participants (mean=71±7 yrs) underwent 90-minute dynamic ^{18}F-THK-5351 or ^{18}F-THK-5317 PET scans and T1-w MRI. Ten participants were scanned with both tracers (321±46 days between PET scans). Participants included individuals at-risk for Alzheimer's disease (AD) (15 parental history, 18 APOE-ε4 carriers) and included probable AD (n=6), amnestic MCI (n=3), cognitively declining (n=10), and cognitively stable (n=9) individuals. Regression and Bland-Altman analyses were carried out to compare SUVR and DVR estimates determined derived from Logan graphical analysis, MRTM2, and basis function SRTM. The effects of t* (and k_2 for Logan) were investigated for MRTM2 and Logan. Effects of scan duration and scanning window were determined for DVR and SUVR, respectively. Regressions analyses were performed to compare within-subject DVR and SUVR estimates for the ten participants that received both THK scans.

Results: MRTM2 and Logan DVR estimates were stable for t*=30 min and t*=40 min, respectively. The Logan method was sensitive to combinations of t* and k_2. Between-method DVR estimates were generally in agreement for 90-minute dynamic scans for both tracers, with the exception of SRTM, which failed to converge in some ROIs for THK-5317. Sixty-minute scan durations using MRTM2 and 70-minutes using Logan produced DVR estimates consistent with 90-minute derived estimates. SUVR became temporally stable 50-70 minutes post-injection and SUVR from 30-50 minutes post-injection had the highest correlation with DVR. Agreement was observed between THK-5351 and THK-5317 DVR and SUVR estimates for individuals scanned with both tracers with THK-5351 having higher binding estimates.

Conclusions: THK-5351 has more favorable imaging characteristics for tau imaging compared to THK-5317. Shortened 60-minute dynamic scans are suitable for DVR estimation using MRTM2 for both THK-5351 and THK-5317 in this subject population.

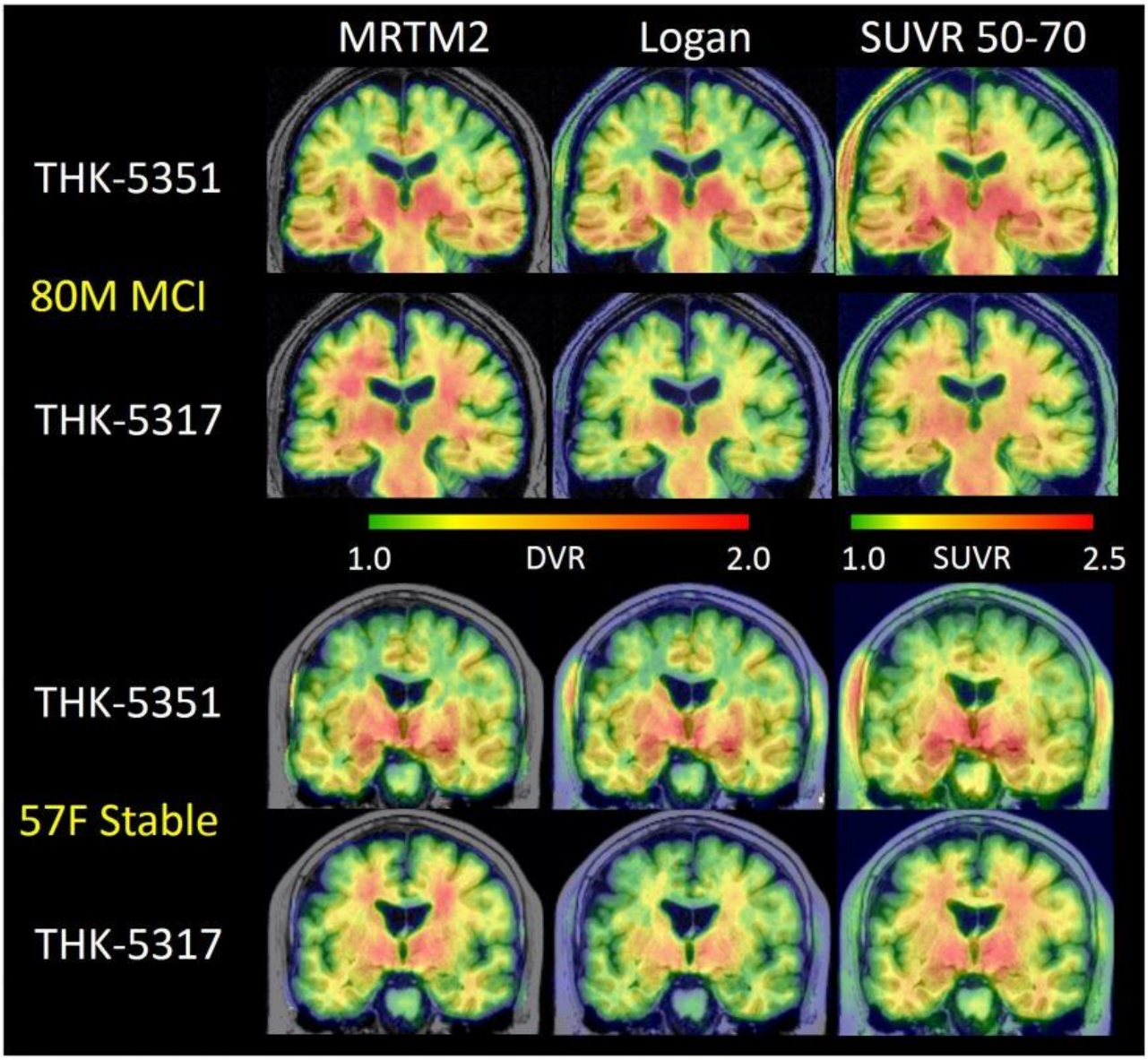

Figure 1: Comparison of parametric THK-5351 and THK-5317 DVR and SUVR images. Differences were most predominant in WM for THK-5317 where MRTM2 and SUVR methods showed higher signal compared to Logan. DVR and SUVR methods for THK-5351 were generally in agreement. THK-5351 had higher binding estimates in gray matter regions associated with tau pathology compared to THK-5317.

Keywords: THK, Tau, Quantification, DVR, SUVR

A cortical cluster-based measure of change in longitudinal 18F-T807 FTP PET

J. Alex Becker[1], Danielle Cosio[1,3], Chris Lee[1], Nick Andrea[1], Reisa Sperling[2], Keith Johnson[1,2]

[1]*Massachusetts General Hospital, Boston, MA, USA*
[2]*Brigham and Women's Hospital, Boston, MA, USA*
[3]*Massachusetts Institute of Technology, Cambridge, MA, USA*

Introduction: Post-mortem studies have shown that tau deposition in early Alzheimer's Disease occurs predominantly in inferior and middle temporal cortex, and in subject-specific patterns which do not respect anatomical boundaries. PET ligand 18F-T807 (FTP) allows measurement of intra-subject change in tau binding. We investigated rate of change of tau binding in cognitively-normal (CN) subjects using a surface-based cluster approach.

Methods: Two time-points of FTP PET (10mCi, 80-100min) were acquired in each of 31 CN subjects (baseline age 76.2±6yr, interval 20.2±5 months). Time-points were registered to a subject-specific FTP template that was registered to baseline MPRAGE. FTP data was sampled at midpoint vertices of the Freesurfer-calculated grey-matter-ribbon, surface-smoothed at 10mm FWHM, and expressed as SUVR (cerebral white-matter reference). Clusters in the lateral and medial temporal lobes and spanning both time-points were formed from vertices with FTP SUVR>=1.0 sharing a segment of the triangular surface mesh in each time-point, or occupying congruent positions across time-points. An FTP uptake measure (ClustSUVR) for each subject was computed as the average SUVR across all clusters with overlap between time-points of at least 20% of the number of cluster vertices in each time-point, to minimize error due to misregistration. Mixed-effect models were used to determine rate of change of ClustSUVR in CN subjects.

Results: The 31 CN subjects had average rate of change of ClustSUVR of 0.009 SUVR/yr (0.00012,0.015) (1st,3rd quartiles), with minimum/maximum -0.013/0.063 SUVR/yr. Modeled ClustSUVR rate of change was 0.007±0.0021 SUVR/yr ($p<0.003$).

Conclusions: Our initial findings with FTP Tau-PET a group of normal subjects suggest that most showed evidence of increases in tau binding over time in spatially associated temporal lobe clusters of vertices with FTP SUVR>=1.0.

Keywords: Clusters, T807, Tau

Selegiline reduces brain [18F]THK5351 binding

Kok Pin Ng[1,3], Gassan Massarweh[2], Jean-Paul Soucy[2], Paul Gravel[2], Tharick A. Pascoal[1], Sulantha Mathotaarachchi[1], Min Su Kang[1], Monica Shin[1], Joseph Therriault[1], Sophie Levasseurr[1], Kayla Horowitz[1], Serge Gauthier[1], Pedro Rosa-Neto[1]

[1]*Translational Neuroimaging Laboratory - McGill University, Montreal, QC, Canada*
[2]*McConell Brain Imaging Center - McGill University, Montreal, QC, Canada*
[3]*National Neuroscience Institute, Singapore, Singapore*

Introduction: Interactions between molecular imaging agents and their respective targets might be affected by the chronic or acute use of certain pharmacological interventions. Here we described changes in THK5351 binding elicited by a single dose of a widely used MAO-B inhibitor, selegiline.

Methods: Patients with mild cognitive impairment (MCI; N=3; 72±5.2 y.o; MMSE) and a progressive supranuclear palsy patient (PSP; 68 y.o; MMSE=29) had a baseline THK5351 scan (6.8±0.1 mCi). All participants had two days later, a second THK5351 scan (6.6±0.5mCi) conducted 1h following an oral dose of 10mg of selegiline. Dynamic images were obtained using the ECAT HRRT (High Resolution Research Tomograph). A six-minute transmission acquisition was obtained for each scan. The primary outcome measure was the standardized uptake value (SUV). SUVs were obtained using tissue radioactivity concentration obtained 50 to 70 minutes following THK5351 injection, normalized by body weight and injected tracer dose.

Results: On baseline scans, all individuals showed high uptake in the frontal, temporal lobes, basal ganglia and thalamus (see Figure 1). These regions of uptakes were reduced in a range of 36.2% - 51.3% in the follow up scans, presumably due to the blocking of MAO-B binding sites by selegiline (Figure 2).

Conclusion: Quantification of THK5351 binding is affected by concomitant use of selegiline. These results merit careful studies focusing on the underlying basis of this phenomenon, particularly interactions between THK5351 and MAO-B binding sites.

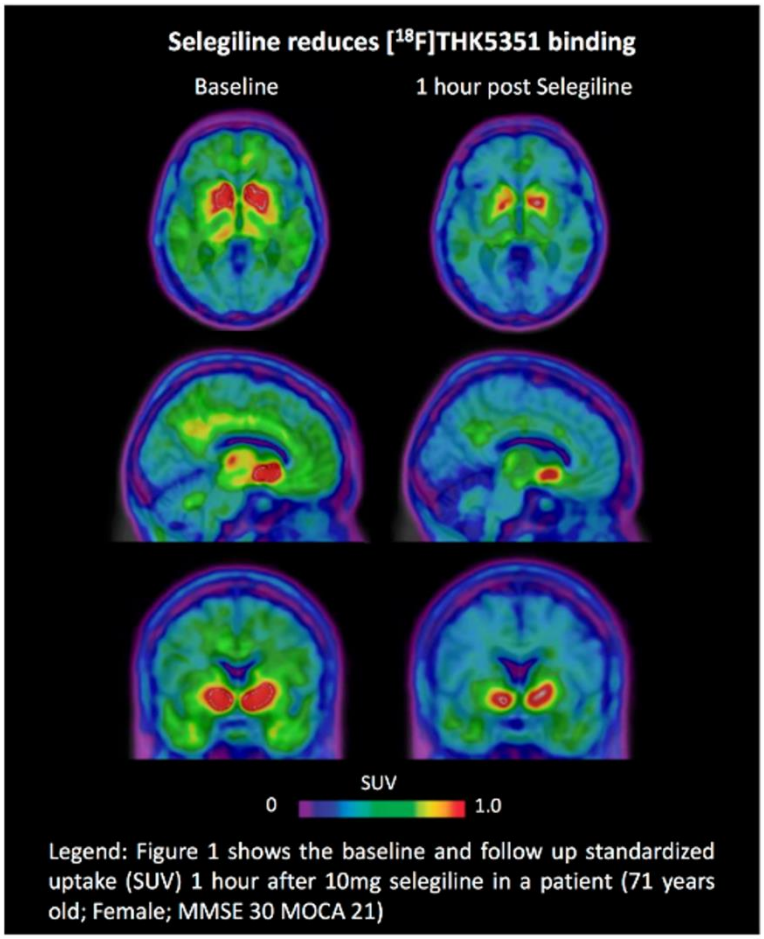

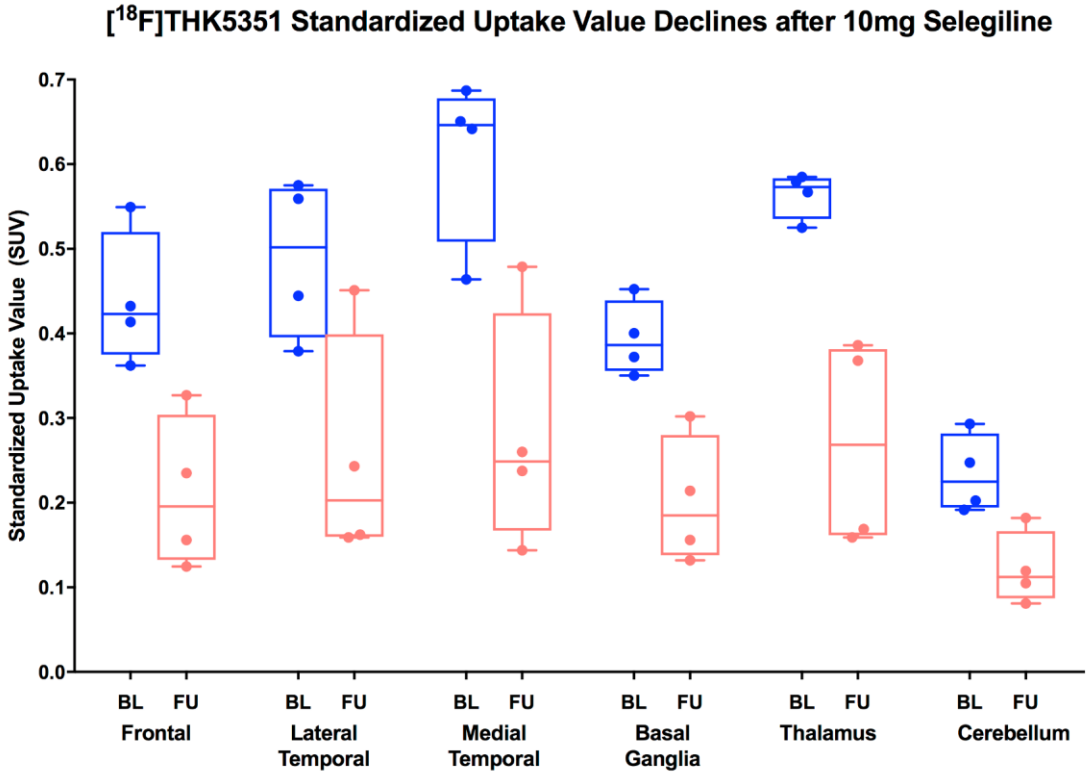

Figure 2: Plot shows the baseline (BL) and follow up (FU) SUVs 1 hour post 10mg selegiline of the 4 study individuals

Keywords: [18F]THK5351, PET, selegiline, MAO-B

Wednesday, January 11, 2017 - 04:40 pm - 05:25 pm

SESSION 2: Novel Tau Tracers

SESSION 2 **Novel Tau Tracers**	**CHAIRS:** **Julie Price** ***Massachusetts General Hospital*** **Robert Koeppe** ***University of Michigan***
Effects of [18F]AV-1451 binding in cerebellar gray and extra-cortical areas	Suzanne Baker *Lawrence Berkeley National Laboratory*
[18F]MK-6240, a novel neurofibrillary tangles PET tracer: Evaluation in healthy subjects and Alzheimer's Disease patients	Cyrille Sur *Merck & Co., Inc.*
Current efforts to overcome drawbacks of [11C]PBB3 by developing new PBB3 derivatives: first-in-human PET study with [18F]AM-PBB3	Hitoshi Shimada *National Institute of Radiological Sciences*
Evaluation of baseline and longitudinal tau burden in Alzheimer’s disease using [18F]GTP1 (Genentech tau probe 1) PET imaging	Robby Weimer *Genentech Inc.*
Invited Lecture: **Molecular imaging analysis for tracer validation and clinical trials**	Roger Gunn *Imanova Ltd*
Discussion	

Effects of [18F]AV-1451 binding in cerebellar gray and extra-cortical areas

Suzanne Baker[1], Anne Maass[2,3], Susan Landau[2], Samuel Lockhart[2], William Jagust[1,2]

[1]*Lawrence Berkeley National Laboratory, Berkeley, CA, USA*
[2]*University of California, Berkeley, Berkeley, CA, USA*
[3]*German Center for Neurodegenerative Diseases, Magdeburg, Germany*

Objectives: Evaluate high AV-1451 uptake in cerebellar gray subregions and extra-cortical regions.

Methods: Subjects (Table) received AV-1451 scans from 80-100 min and structural MRIs. MRIs were segmented using FreeSurfer5.3 and SPM12. SUVR80-100 was calculated using cerebellar gray as the reference region and coregistered to the MRI. Seven controls received a second scan 1.9±0.5 years later. SUIT cerebellum atlas was reverse-normalized to native space and masked by FreeSurfer cerebellar gray for gray matter subregions. Extra-cortical high-uptake (ECHU) regions (SUVR80-100>1.3 and k > 500 voxels) were created in soft tissue and bone masks from SPM12. Cerebellar gray subregions and ECHUs were smoothed by the scanner resolution to quantify their partial volume effects (PVE) on cortical ROIs.

Table: Subjects

	Age	f/m	# Subjects	2nd scan
Young Healthy Controls (yHC)	39.5±16.8	2/9	11	0
Healthy Controls (HC)	78.3±5.8	42/27	69	7
Mild Cognitive Impairment (MCI)	62.9±10.5	4/10	14	0
Alzheimer's Disease (AD)	66.9±8.9	14/13	27	0

Results: Figure 1 shows SUVR80-100 for cerebellar gray subregions by diagnosis. Superior subregions showed higher AV-1451 uptake, with no differences observed across diagnosis within subregion. Superior subregions showed PVEs from 1-3% on parahippocampal, fusiform, and lingual gyri. For the 7 HCs with longitudinal data, the superior portions of cerebellar gray (relative to inferior cerebellar gray) changed a small amount (0±2%). Figure 2 shows the mean ECHU across subjects and a modest partial volume effect on cortical regions. Of the voxels classified as ECHU regions in scan 1, 31±14% were classified as ECHU in scan 2, while number of ECHU voxels increased by 63±81% from scan 1 to scan 2.

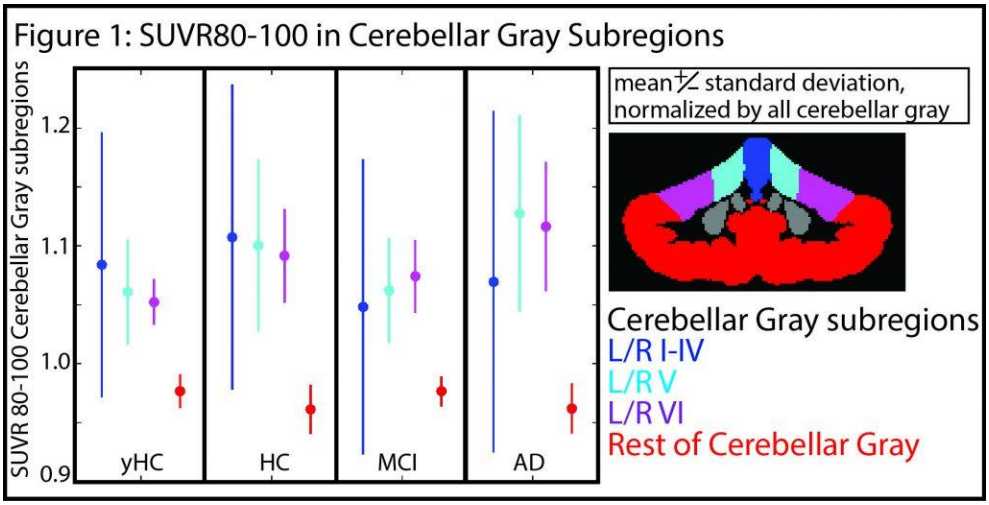

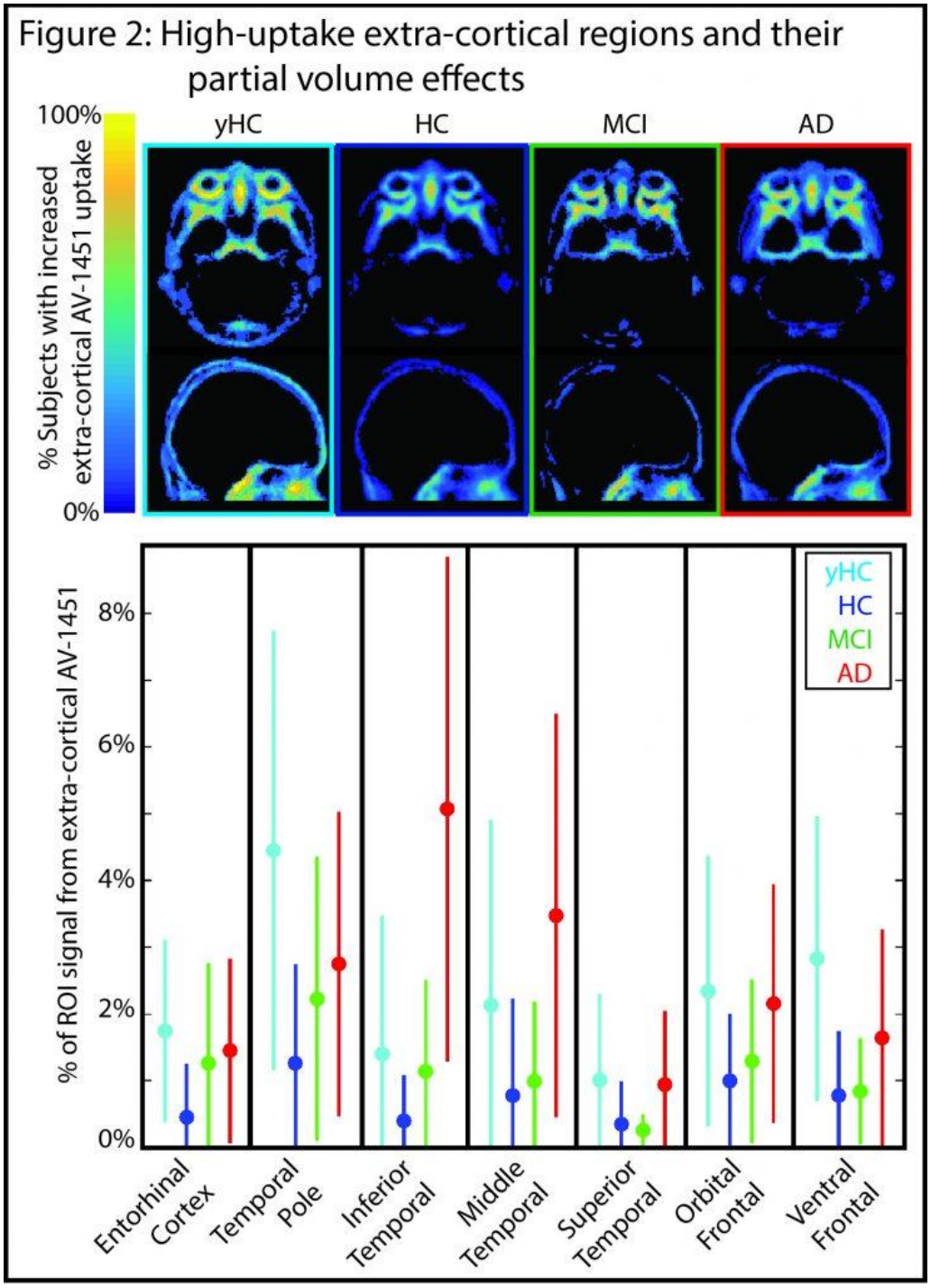

Conclusion: AV-1451 uptake varies in cerebellar gray subregions, showing increased uptake in superior regions. Although this has minimal PVE on ROIs and is stable over time, the inclusion of superior portions of cerebellar gray in the reference region could add noise to cross-sectional analyses. ECHU has a moderate effect on regional SUVRs and is not stable over time, resulting in noise in analyses across diagnosis and longitudinal studies.

Keywords: [18F]AV-1451, tau, non-specific binding

[18F]MK-6240, a novel neurofibrillary tangles PET tracer: evaluation in healthy subjects and Alzheimer's disease patients

Cyrille Sur[1], Arie Struyk[2], Idriss Bennacef[1], Talakad Lohith[1], Cristian A Salinas[5], Florestina Telan-Choing[2], Ruben Declercq[4], Tom Reynders[4], Sofie Celen[8], Kim Serdons[8], Guy Bormans[8], Mathieu Vandenbulcke[8,10], Rik Vandenberghe[9,10], Jan de Hoon[8], Corinne Vandermeulen[8], Michel Koole[8], Koen Van Laere[8,10], Gilles Tamagnan[7], Danna Jennings[7], Ken Marek[7], Olivier Barret[7], John Seibyl[7], Ping Chiao[5], Zhizhen Zeng[1], Abbas Walji[3], Eric Hostetler[1], Richard J Hargreaves[5], Rick Hiatt[6], Mark Forman[2], Jeffrey Evelhoch[1]

[1]*Translational Biomarkers, Merck & Co., Inc., West Point, PA, USA*
[2]*Translational Pharmacology, Merck & Co., Inc., North Wales, PA, USA*
[3]*Discovery Chemistry, Merck & Co., Inc., West Point, PA, USA*
[4]*Translational Pharmacology, MSD, Brussels, Belgium*
[5]*Biogen, Boston, MA, USA*
[6]*Enigma Biomedical Group Inc., Toronto, ON, Canada*
[7]*Invicro, New Haven, CT, USA*
[8]*KU Leuven, Leuven, Belgium*
[9]*Neurology department, University Hospitals Leuven, Leuven, Belgium*
[10]*Alzheimer Research Centre KU Leuven, research Institute for Neuroscience and Disease, Leuven, Belgium*

Background: MK-6240 is a novel PET tracer for the detection of neurofibrillary tangles (NFT) in Alzheimer's Disease (AD) patients. Here, we present the pharmacological profile of MK-6240 and preliminary characterization in healthy elderly (HE) and AD subjects.

Methods: The pharmacological profile of MK-6240 was established and compared to AV-1451 in various preclinical models. Whole body images were collected over 5 hours in healthy volunteers to estimate biodistribution and effective dose (ED). HE and AD patients received a MK-6240 scan to determine tracer kinetics. After bolus injection of MK-6240 (153-349 MBq) dynamic scans were acquired for up to 180 minutes. Some of the dynamic scans were acquired with arterial input to perform tissue compartmental modeling.

Results:In vitro experiments using AD tissue homogenates showed that MK-6240 is a potent (K_D:0.3 nM) and selective NFT ligand. In contrast to AV-1451 no saturable MK-6240 in vitro binding was observed in control tissue sections. In vivo, self-block studies in rhesus showed no off-target binding for MK-6240. Dosimetry evaluation in human resulted in an effective dose of 29.4+/-0.6 µSv/MBq allowing several scans per year. MK-6240 showed high peak brain uptake of ~ 5 SUV followed by quick washout from all brain regions in HE but retention in medial temporal lobe and neocortical regions in AD. Tracer kinetics were best fitted by a 2-tissue-compartment model and a linear relationship was found between DVR and SUVR(60-90 min) using cerebellum as a reference region. In AD patients the distribution of MK-6240 signal was consistent with post-mortem pattern of NFT deposition with SUVR >3-4 in patients exhibiting neocortical signal.

Conclusion: MK-6240 is a novel selective and specific NFT PET tracer with a favorable radiation profile and a large dynamic range. These characteristics are promising for characterizing the pathological burden of low and high NFT expressing brain regions.
Keywords: Tau, PET, Alzheimer, clinical

Current efforts to overcome drawbacks of [11C]PBB3 by developing new PBB3 derivatives: first-in-human PET study with [18F]AM-PBB3

Hitoshi Shimada[1], Soichiro Kitamura[1], Yasuyuki Kimura[1,2], Masanori Ichise[1], Maiko Ono[1], Hitoshi Shinotoh[1,3], Manabu Kubota[1], Keisuke Takahata[1], Sho Moriguchi[1], Tetsuya Ishii[1], Chie Seki[1], Ming-Rong Zhang[4], Tetsuya Suhara[1], Makoto Higuchi[1]

[1]*Department of Functional Brain Imaging Research, National Institute of Radiological Sciences, National Institutes for Quantum and Radiological Science and Technology, Chiba, Japan*
[2]*Department of Clinical and Experimental Neuroimaging, Center for Development of Advanced Medicine for Dementia, National Center for Geriatrics and Gerontology, Aichi, Japan*
[3]*Neurology Chiba clinic, Chiba, Japan*
[4]*Department of Radiopharmaceutics Development, National Institute of Radiological Sciences, National Institutes for Quantum and Radiological Science and Technology, Chiba, Japan*

Background and aims: Accumulating evidence indicates that PBB3 can bind diverse tau conformations, such as Alzheimer's disease (AD), progressive nuclear palsy (PSP), corticobasal syndrome, Pick's disease, and transgenic mouse models. Meanwhile, it is gradually revealed that PBB3 have several issues including the short half-life of ^{11}C, limited dynamic range and off-target binding around basal ganglia and thalamus, leading to difficulty in wide use and early detection of tau pathology. Then, we have developed novel PBB3 derivatives, AM-PBB3 and PM-PBB3, to overcome such drawbacks. Here we present preliminary data of PET imaging with fluorinated PBB3 derivatives.

Methods: Four patients with AD and four age-matched cognitive healthy control (HC) subjects underwent a dynamic PET scan, arterial blood sampling, and free fraction measurements after injection of AM-PBB3. PBB3 and PiB PET scans were also performed within a month. Parametric AM-PBB3, PBB3- and PiB-images were generated by voxel-based calculation of standard standardized uptake value ratio (SUVR) to the cerebellum. Furthermore, one- and two-tissue compartment analyses (1TCM, 2TCM) and a reference tissue model ($MRTM_O$) were also applied to estimate binding potential (BP_{ND}).

Results: Since plasma parent free fractions decreased over time, we analyzed kinetics of ^{18}F-AM-PBB3 using corrected plasma input functions with sequentially measured parent free fractions. 2TCM produced a better fit to tissue TACs than did 1TCM with corrected input functions, and was in good agreement with $MRTM_O$. AM-PBB3 yields a 1.5 – 2 fold higher dynamic range than PBB3 in visualizing AD tau lesions. Off-target binding of PBB3 is noticeable in the basal ganglia and thalamus, while AM-PBB3 does not produce prominent off-target signals in these areas.

Conclusions: Fluorinated PBB3 derivatives were promising novel tau PET ligands, which showed similar characteristics to PBB3 with long half-life, broad dynamic range and less off-target binding around the basal ganglia and thalamus.
Keywords: tau, PET, [11C]PBB3, [18]AM-PBB3, [18F]PM-PBB3

Evaluation of baseline and longitudinal tau burden in Alzheimer's disease using [18F]GTP1 (Genentech Tau Probe 1) PET imaging

Robby Weimer[1,2], Olivier Barret[3], Gilles Tamagnan[3], David Alagille[3], Jan Marik[1], Gai Ayalon[2], Thomas Bengtsson[4], Mike Ward[5], Geoffrey Kerchner[5], Danna Jennings[5], John P. Seibyl[3], Ken Marek[3], Sandra Sanabria[6]

[1]*Department of Biomedical Imaging, Genentech Inc., South San Francisco, CA, USA*
[2]*Department of Neuroscience, Genentech Inc., South San Francisco, CA, USA*
[3]*Molecular NeuroImaging LLC, New Haven, CT, USA*
[4]*Biostats, Genentech Inc., South San Francisco, CA, USA*
[5]*Early Clinical Development, Genentech Inc, South San Francisco, CA, USA*
[6]*Clinical Imaging Group, South San Francisco, CA, USA*

Objectives: In Alzheimer's disease (AD), the density and anatomical distribution of tau pathology in the brain correlates with cognitive dysfunction. GTP1 is a tau PET tracer that exhibits desirable pharmacokinetics, enabling the use of $SUVR_{60\text{-}90min}$ as a surrogate measure of specific binding, and robust test-retest reliability. We report preliminary results on the burden of tau pathology detected by GTP1 PET imaging in an AD cross-sectional cohort, and changes observed at 6 and 12 months in participants of a longitudinal 18-month natural history study.

Methods: Subjects (age 50 to 85, inclusive) were enrolled in an ongoing study; inclusion criteria: cognitively normal (MMSE 28-30, CDR 0), prodromal AD (amyloid(+), MMSE 24-30, CDR = 0.5), mild AD (amyloid(+), MMSE 22-30, CDR 0.5 or 1) and moderate AD (amyloid(+), MMSE 16-21, CDR 0.5 or 1 or 2). GTP1 images are acquired over 30 minutes starting 60 minutes post injection. The cerebellar gray reference tissue is used to calculate SUVR, and tau burden was assessed by exploratory metrics: a *density* metric (average SUVR) and an *extent* metric (% of voxels above a SUVR threshold).

Results: Baseline tau burden in gray matter, using both *density* and *extent*, generally increased as a function of disease state (prodromal, mild, moderate), yet varied in distribution between subjects and across cohorts, with *extent* providing greater dynamic range. Preliminary longitudinal data show that increases in tau burden could be detected in mild and moderate subjects within 6-9 months. In contrast, healthy controls show low baseline gray matter tau burden and no longitudinal change.

Conclusion: Preliminary analysis suggests that GTP1 imaging can detect baseline tau pathology and progression. Additional interim analysis from this ongoing study will be presented.
Keywords: Tau PET, Alzheimer's disease, longitudinal

Wednesday, January 11, 2017 - 05:40 pm - 06:00 pm

Invited Lecture:

Molecular Imaging Analysis for Tracer Validation and Clinical Trials

Roger N Gunn

Imanova & Imperial College London, UK

PET molecular imaging data, using tracers that bind to misfolded proteins, can be acquired as dynamic or static data, with or without associated blood data. The analysis of these data aims to derive an outcome measure that is proportional to the density of the misfolded protein, however the quantitative accuracy of the outcome measure derived is dependent on both the chosen acquisition and analysis method.

There are three types of approach: 1) Full tracer kinetic analysis of dynamic tissue data using an arterial input function and an appropriate tracer kinetic model to derive VT and DVR outcome measures, 2) Reference tissue analysis of dynamic tissue data using a reference tissue input function to derive a DVR outcome measure and 3) Tissue ratio analysis from static data at a particular time point to derive an SUVR outcome measure.

The utility of the different analytical approaches will be explored in the context of tracer validation studies and clinical trials of novel therapeutics. For validation of novel tracers the goal is to understand the tracers key characteristics, which includes an assessment of BBB penetration, target binding, selectivity and any metabolite liabilities. For clinical trials the goal is to select an approach that balances quantitative accuracy with an experimental design that is practical for phase II/III trials.

THURSDAY

Thursday, January 12, 2017 - 08:00 am - 08:45 am

SESSION 3: Neuropathology I: Tau PET Ligand Selectivity and Comparative Studies

SESSION 3 **Neuropathology I: Tau PET Ligand Selectivity and Comparative Studies**	**CHAIRS:** **William Klunk** ***University of Pittsburgh*** **Milos Ikonomovic** ***University of Pittsburgh***
Evaluation of the selectivity of Tau PET radioligand THK5351 in AD brain in vitro and nonhuman primate brain in vivo	Qi Guo *AbbVie Inc.*
Characterizing the "off-target" binding of 18F-THK5351 in Alzheimer's disease: correlation between ante-mortem and post-mortem findings	Ryuichi Harada *Tohoku University Graduate School of Medicine*
In vitro binding properties comparison of the tau PET tracers THK5117, THK5351, PBB3 and T807 in autopsy brain from Alzheimer diseases cases	Laetitia Lemoine *Karolinska Institute*
An autoradiographic evaluation of THK-5351 compared to AV-1451	Melissa Murray *Mayo Clinic*
Discussion	

Evaluation of the selectivity of Tau PET radioligand THK5351 in AD brain in vitro and nonhuman primate brain in vivo

Qi Guo[1], Bernd Otterstätter[2], Simone Benninghoff[2], David Reuter[1], Jiquan Wang[1], Marc Skaddan[1], Ann Tovcimak[1], Cecelia Schroeder[1], Gokul Krishnan[1], Kyle Wilcox[1], Robert Comley[1], Paul Makidon[1], Martin Voorbach[1], Andreas Haupt[2], Manolo Mugnaini[2], Laurent Martarello[1]

[1]*AbbVie Inc., North Chicago, IL, USA*
[2]*AbbVie Deutschland GmbH & Co. KG, Ludwigshafen, Germany*

Objectives: Tau deposition has been shown to be highly associated with cognitive impairment. Furthermore tau deregulation is a key mediator of neurodegeneration. Positron emission tomography (PET) with a selective tau radioligand allows disease progression monitoring as well as direct demonstration of the mechanism of action of new therapies. Multiple tau radioligands have been developed; however the question about their selectivity in vivo remains. Here, we evaluate the off-target binding of THK5351 in Alzheimer's Disease (AD) brain tissue in vitro and in cynomolgus macaques (cynos) in vivo.

Methods: Competitive binding assays were performed in homogenate from entorhinal cortex of an AD donor with THK5351 in the presence of various concentrations of THK5351 as well as clorgyline and selegiline, in order to evaluate the total specific binding and binding to monoamine oxidase A and B (MAO-A and MAO-B) respectively.

Ten young (8-10yrs) and four geriatric (24-26yrs) cynos went through 120 min dynamic THK5351 PET scan with arterial sampling. Three old cynos had a second scan post i.v. administration of 1mg/kg selegiline. The total volume of distribution (V_T) was estimated using kinetic modeling.

Results: The in vitro binding assay demonstrated strong specific binding of THK5351. 100nM selegiline blocked 70% of the total binding whilst clorgyline showed no blocking effect at that concentration(Figure 1). The V_T in aged cynos was 20% higher than in the young (Figure 2) in globus pallidus ($p=0.02$) and striatum ($p=0.06$). Following selegiline pretreatment, there was 20-60% reduction in V_T across brain regions in aged cynos (Figure 3), suggesting MAO-B binding.

Conclusion: A sizable fraction of total THK5351 binding in the brain is attributable to MAO-B, the level of which is reported to increase with age. To our knowledge this dataset provides the first in vivo evidence of THK5351 binding to MAO-B. This off target (non-tau) binding should be considered as a confounding effect in longitudinal clinical trials using THK5351.

Figure 1. In vitro competitive binding assay with [^{3}H]THK5351 in AD brain

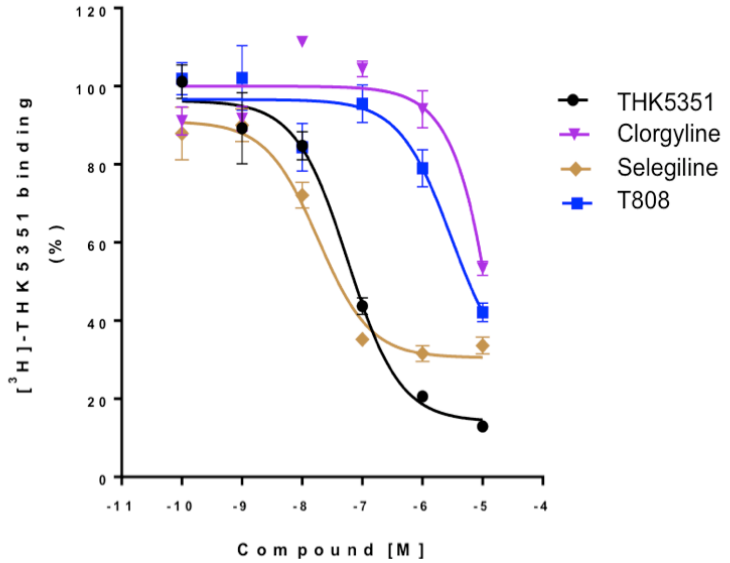

Figure 2. Comparison of [^{18}F]THK5351 V_T in young and aged cynos

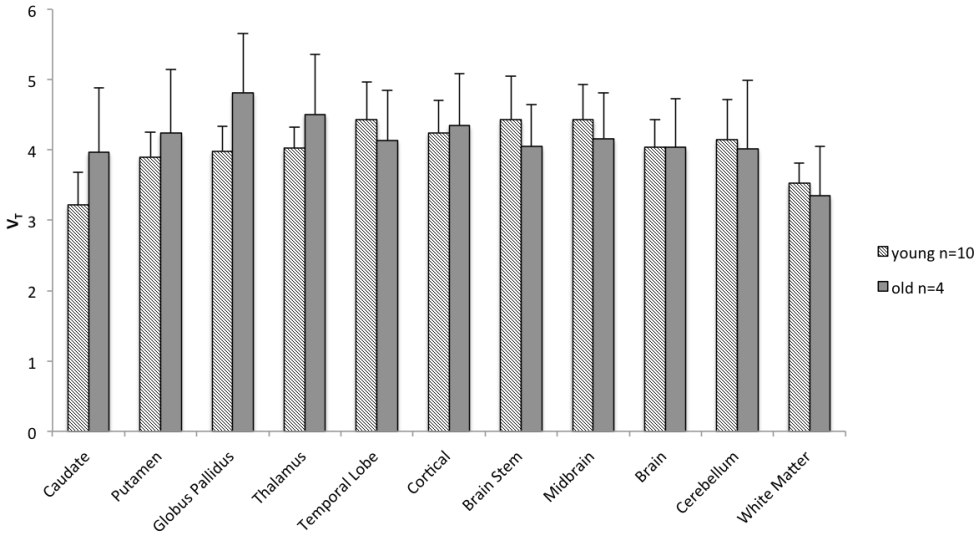

Figure 3. V_T parametric maps of [^{18}F]THK5351 in aged cyno brain with and without selegiline blockade

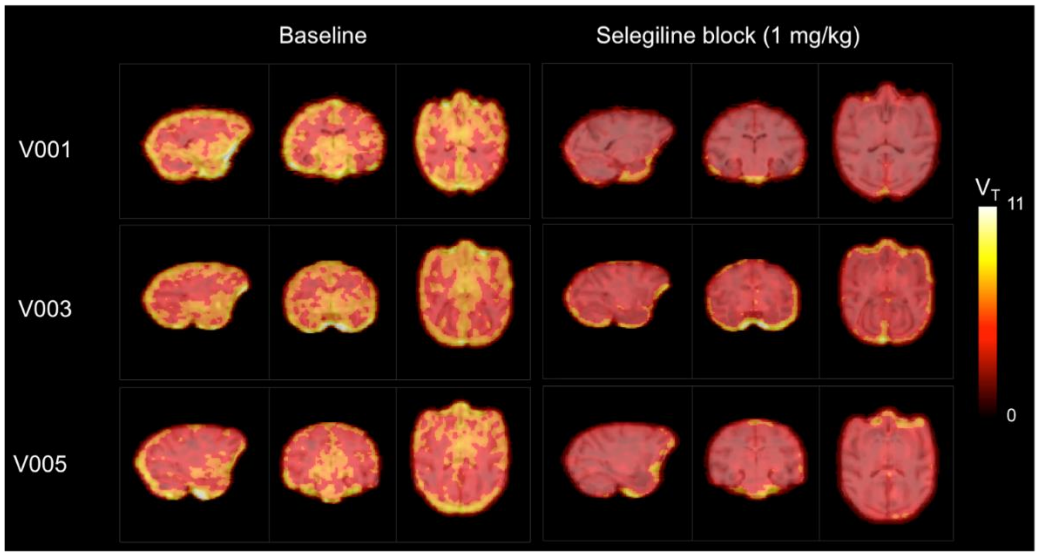

Keywords: PET, Tau, THK5351, MAO-B, Selegiline

Characterizing the "off-target" binding of 18F-THK5351 in Alzheimer's disease: correlation between ante-mortem and post-mortem findings.

Ryuichi Harada[1,2], Aiko Ishiki[3], Shozo Furumoto[4], Katsutoshi Furukawa[4,5], Manabu Tashiro[4], Hiroyuki Arai[3], Kazuhiko Yanai[1,4], Yukitsuka Kudo[2], Nobuyuki Okamura[4,5]

[1]*Department of Pharmacology, Tohoku University Graduate School of Medicine, Sendai, Japan*
[2]*Division of neuro-imaging, Institute of Development, Aging and Cancer, Tohoku University, Sendai, Japan*
[3]*Department of Geriatrics and gerontology, Institute of Development, Aging and Cancer, Tohoku University, Sendai, Japan*
[4]*Cyclotron and Radioisotope Center, Tohoku University, Sendai, Japan*
[5]*Tohoku Medical and Pharmaceutical University, Sendai, Japan*

Objectives: ^{18}F-THK5351 has been widely used for the *in vivo* detection of tau pathology in the Alzheimer's brain. In spite of this, "off-target" binding has not been characterized, nor has ante to post-mortem validation been reported. The aim of study was to examine the on- and off-target binding of ^{18}F-THK5351 using postmortem brain sections.

Methods: We performed postmortem examination of brain samples from an autopsy-confirmed Alzheimer's disease case (81-yo male, MMSE 16) who underwent ^{18}F-THK5351 PET 7 months before death. *In vitro* autoradiography (ARG) of ^{3}H-THK5351 was performed using frozen brain sections. *In vitro* binding assay was also performed using the brain homogenates from the corresponding regions. We quantitatively measured tau aggregates in the brain tissue from autopsy and examined the correlation with regional tracer retention in ^{18}F-THK5351 PET image.

Results: We observed a significant correlation between cortical ^{18}F-THK5351 SUVR in ante-mortem PET image with tau pathology at postmortem examination. We also observed ^{18}F-THK5351 retention in the basal ganglia that contained no remarkable tau pathology in this case. To identify off-target tracer retention, competitive screening was performed using ARG with several compounds. Although no remarkable competition was observed with dopamine transporter inhibitor, μ-opioid receptor agonist, and monoamine oxidase-A (MAO-A) inhibitors, MAO-B inhibitor completely displaced ^{3}H-THK5351 binding in the basal ganglia. *In vitro* binding assay also indicated that ^{3}H-THK5351 binds with high affinity to recombinant MAO-B.

Conclusions: These results suggest that cortical ^{18}F-THK5351 signal reflects tau pathology in the brain. MAO-B seems to explain ^{18}F-THK5351 off-target retention in basal ganglia. A human study to confirm the *in vitro* findings is currently ongoing.
Keywords: tau PET, Alzheimer's disease, imaging-autopsy, off-target binding

In vitro binding properties comparison of the tau PET tracers THK5117, THK5351, PBB3 and T807 in autopsy brain from Alzheimer's diseases cases

Laetitia Lemoine[1], Per-göran Gillberg[1], Marie Svedberg[2], Vladimir Stepanov[2], He Tian[3], Makoto Higuchi[3], Christer Halldin[2], Agneta Nordberg[1,4]

[1]Karolinska Institute, Department of neurobiology, Care sciences and society, Center for Alzheimer Research, Division of Translational Alzheimer Neurobiology, Stockholm, Sweden
[2]Karolinska Institute, Department of Clinical Neuroscience, Center for Psychiatric Research, Stockholm, Sweden
[3]Molecular Imaging Center, National Institute of Radiological Sciences, Chiba, Japan
[4]Karolinska University Hospital, Department of Geriatrics, Stockholm, Sweden

During the past years, there has been a rapid development of radiotracers for visualizing tau deposition in human brain. Three families of tau ligands have been studied in patients after having shown good *in vitro* binding-properties. Due to the presence of different tau isomers in Alzheimer´s disease and other tauopathies it is important to further characterize and compare the binding properties between different Tau PET tracers. In this study we aimed at comparing the two THK compounds, THK5117 and THK5351 with T807 and PBB3, head to head in the same human brain tissue, using both autoradiography and binding assay studies. We are reporting for the first time the binding in large frozen autoradiography of ^{11}C-THK5351.

Methods: Regional distribution comparison between ^{3}H-THK5117 and ^{3}H-THK5351 were performed in brain homogenate from 3 AD cases. Autoradiographies on large frozen section were done using ^{3}H-THK5351, ^{3}H-THK5117, ^{11}C-THK5351 and ^{11}C-PBB3. T807 was used as cold compound for the ^{11}C compound autoradiography. *In vitro* binding assay competition using ^{3}H-THK5351 with THK5351, THK5117 and T807 respectively were performed in hippocampus homogenate.

Results: Binding studies with ^{3}H-THK5117 and ^{3}H-THK5351 showed similar regional distribution in AD brain. The autoradiography with ^{11}C-THK5351 showed similar binding distribution in brain compared to ^{3}H-THK5351. *In vitro* binding assay using ^{3}H-THK5351 in competition with THK5351, THK5117 and T807, respectively, showed two binding sites that were similar for the two THK compound and different for T807. Those results were also confirmed by inhibition experiment in autoradiography.^{11}C-PPB3 showed in comparison to ^{11}C-THK5351 autoradiographies corresponding binding pattern with lower binding in most brain areas.

Conclusion: Tau tracers from three different families showed different binding properties probably reflecting different binding site on tau. These results may have an influence on the outcome of the clinical use of *in vivo* PET study targeting different form of tauopathies.
Keywords: tau pathology, autoradiography, biomarker imaging, autopsy brain

An autoradiographic evaluation of THK-5351 compared to AV-1451

Val Lowe[1], Melissa Murray[2], Vidur Sarma[1], Geoffry Curran[1], Ping Fang[1], Mukesh Pandey[1], Tyler Bruinsma[1], David Jones[1], Casey Cook[2], Keith Josephs[1], Joseph Parisi[1], David Knopman[1], Bradley Boeve[1], Kejal Kantarci[1], Leonard Petrucelli[2], Clifford Jack[1], Dennis Dickson[2], Ronald Petersen[1]

[1]Mayo Clinic, Rochester, MN, USA
[2]Mayo Clinic, Jacksonville, FL, USA

Background: Several tau-PET imaging agents have been developed. Comparing the characteristics of these different agents is important to better understand future applications. We therefore compared the binding of THK-5351 to AV-1451 PET in the same brain tissue samples in a wide range of pathologies.

Methods: Serial sections were obtained from our research brain bank from multiple different pathologies (normal, n=2; pathologic aging (PA, Braak $\leq$3), n=1; AD, n=4; FTD-TDP, n=2; AGD, n=1; CBD, n=1; PSP n=1, PART, n=1; MAPT N297K, n=2; MAPT R406W, n=1; and MAPT 301L, n=1). Adjacent sections were incubated with AV-1451 and THK-5351 using identical methods. Self-blocking with each respective cold tau-PET agent was performed. Adjacent sections were also stained with PHF-1 and CP-13 for comparison. Visual comparison of the autoradiography results with the immunohistochemistry findings was performed.

Results: Both AV-1451 and THK-5351 show binding to AD-tau (3R+4R) with THK-5351 showing less intense binding in some sections and similar binding in others (Figure 1). The binding of THK-5351 was similar to AV-1451 in the remaining sections except for discordant uptake in the case of PA, some of which may be "off-target" binding (see Figure 2), less uptake in the MAPT 406W case, and discordant uptake in the CBD case. Similar binding between the two agents was seen in common "off-target" sites such as neuromelanin.

Conclusions: Reduced binding of THK-5351 vs. AV-1451 in some AD cases may result in lower THK-5351 signal in AD dementia clinical imaging. Mild THK-5351 binding in non-AD tau cases, similar to AV-1451, was generally seen and argues for similar clinical imaging characteristics. While some "off-target" sites had similar appearances between the two agents, additional suspicious "off-target" binding by THK-5351 needs to be better characterized and, at least in some cases tested, has incremental potential over AV-1451 to falsely mimic tau pathology.

Figure 1. Autoradiography findings of THK-5351 (left) and AV-1451 (right) in a posterior hippocampal section of a case with AD-type tau (respective blocking studies are shown below each). Reduced binding is seen with THK-5351 in PHF-1 positive regions (red arrows) as compared to AV-1451.

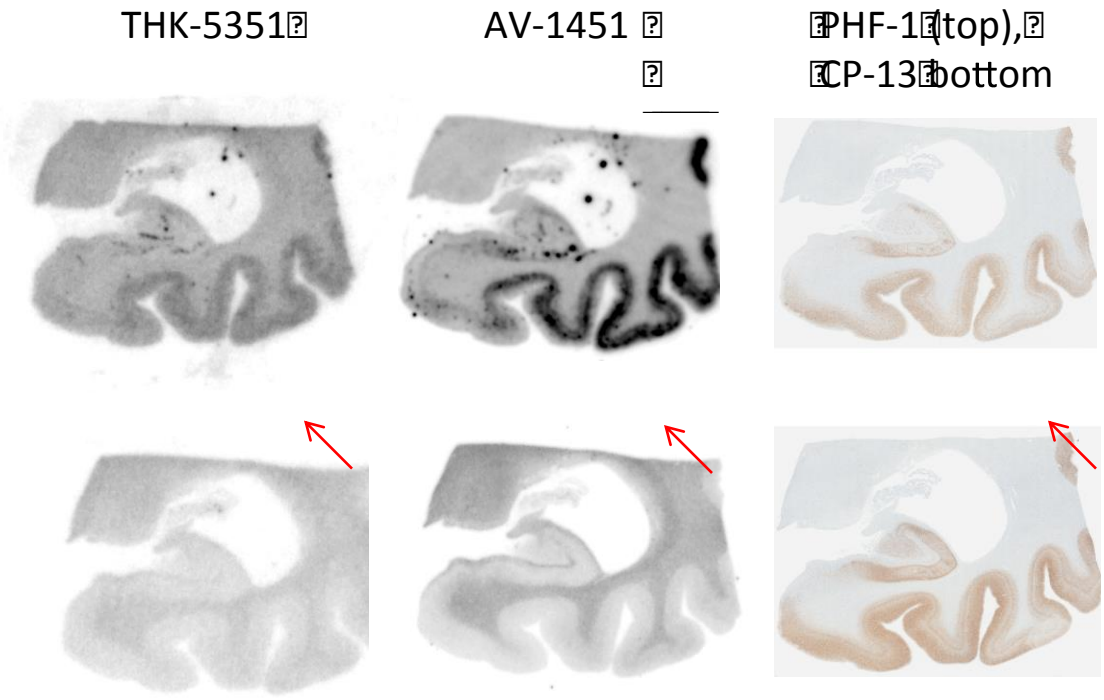

Figure 2. Autoradiography findings of THK-5351 (left) and AV-1451 (right) in a posterior hippocampal section (respective blocking studies are shown below each) of a case staged as Braak ≤ 3 with no more than sparse plaques (sometimes referred to as pathologic aging (PA)). Discordant binding is seen with THK-5351 in PHF-1 negative regions (red arrows) unlike AV-1451. In addition, focal sites of "off-target" binding are more prevalent on THK-5351.

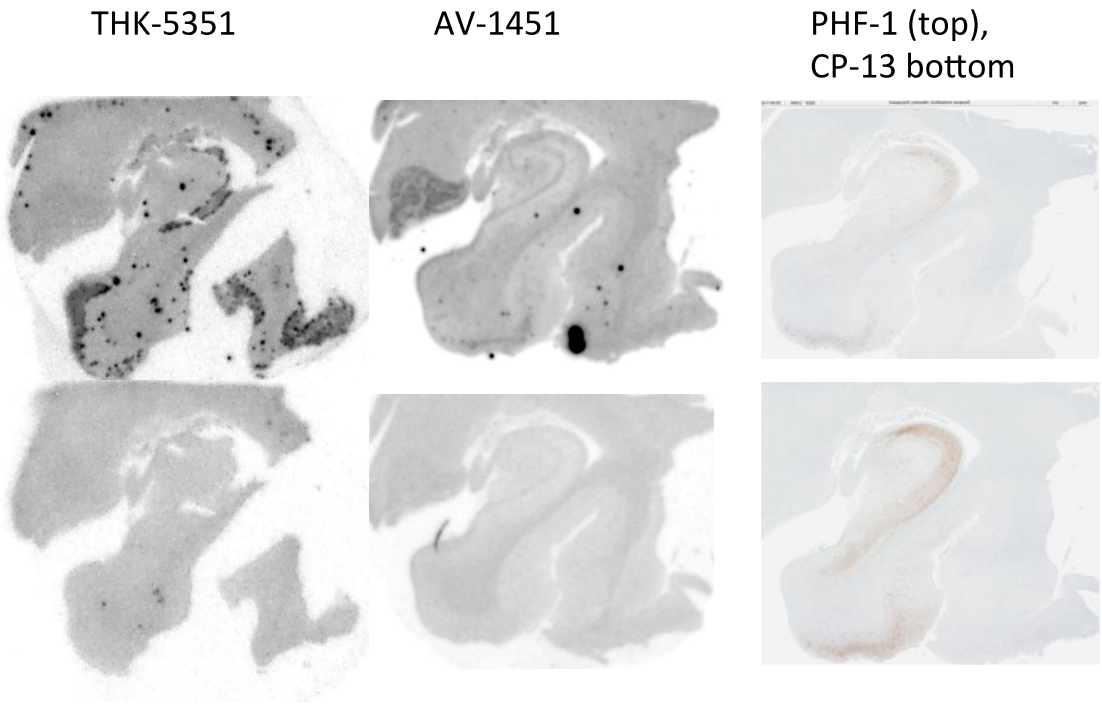

Keywords: Tau, PET, Tauopathy, AD

Leal, Stephanie - 1

Hippocampal activation is associated with longitudinal amyloid accumulation and cognitive decline

Stephanie Leal[1], Susan Landau[1], Rachel Bell[1], William Jagust[1]

[1]*Helen Wills Neuroscience Institute, Berkeley, CA, USA*

The amyloid hypothesis suggests that beta-amyloid deposition leads to alterations in neural function and ultimate cognitive decline, however, why beta-amyloid deposition occurs to begin with remains unclear. One proposed model suggests that patterns of neural activity, namely increased brain activity, may lead to beta-amyloid deposition. More specifically, hyperactivity in the hippocampus may be detrimental and could be one factor that drives beta-amyloid deposition. We were interested in examining the relationship between hippocampal activity during a memory task using fMRI and change in beta-amyloid using longitudinal PIB-PET imaging in humans. We found that greater hippocampal activation at baseline was associated with increased beta-amyloid over time. Furthermore, greater change in beta-amyloid was associated with worse memory performance over time, suggesting that increased levels of beta-amyloid mediate the relationship between hippocampal activation and memory decline. These findings support the model linking increased hippocampal activation to beta-amyloid deposition.
Keywords: hippocampus, PIB, hyperactivity, memory, longitudinal

Tau-PET imaging with [18F]AV-1451 in progressive apraxia of speech with and without aphasia

Rene Utianski[1], Jennifer Whitwell[1], Christopher Schwarz[1], Matthew Senjem[1], Nirubol Tosakulwong[1], Joseph Duffy[1], Heather Clark[1], Mary Machulda[1], Clifford Jack[1], Val Lowe[1], Keith Josephs[1]

[1]*Mayo Clinic, Rochester, MN, USA*

Background: Apraxia of speech (AOS) is a motor speech disorder characterized by combinations of a slowed speaking rate, abnormal prosody, distorted sound substitutions, and trial-and-error articulatory movements. AOS is due to the abnormal planning and/or programming of speech production. When AOS is a presenting symptom of a neurodegenerative condition in the presence of aphasia (a disorder of language), it is referred to as progressive apraxia of speech (PAOS); when AOS is the only symptom, it is referred to as primary progressive apraxia of speech (PPAOS). Past reports suggest associations with a primary tau (e.g. progressive supranuclear palsy, corticobasal degeneration), rather than amyloid pathology.
Aim: The goal of the current study was to investigate tau-PET imaging in patients with progressive AOS.
Methods: Five patients with PPAOS and four patients with PAOS underwent tau-PET imaging using the AV-1451 ligand and amyloid-PET imaging using Pittsburgh Compound B (PiB). Uptake of AV-1451 was assessed as cortical to cerebellar crus grey matter ratios (SUVr) in cortical regions of interest, measured using the automated anatomical labeling atlas. A global PiB ratio of 1.5 was used to define positivity on amyloid-PET.
Results: Regions of abnormal AV-1451 binding differed between patients with PAOS and PPAOS. While both groups demonstrated increased binding in the supplementary motor areas, there was increased uptake in the language network in patients with PAOS (e.g. left greater than right supramarginal gyrus and inferior frontal operculum). Data revealed 3/5 patients with PPAOS and 2/4 patients with PAOS were negative on amyloid-PET, with positive AV-1451 binding.
Conclusions: The study demonstrated AV-1451 PET uptake in PPAOS and PAOS patients, with no discernible relationship between PiB positivity and tau deposition. Results provide support that PPAOS is a distinct entity from PAOS and support the notion that PPAOS and PAOS are primary tauopathies.

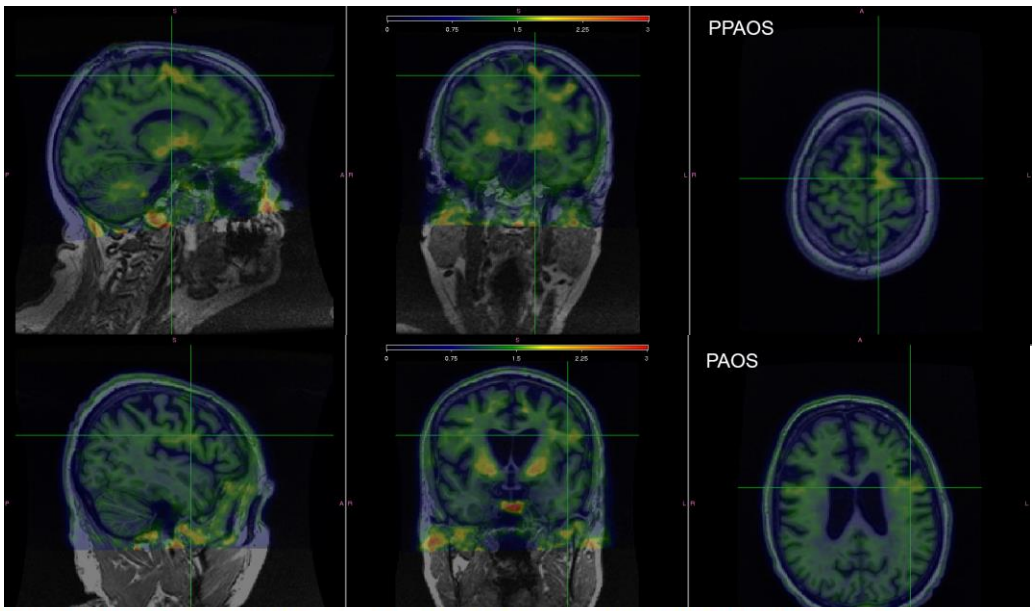

Top Panel: PPAOS patient (female, 77 years old), demonstrating focal tau binding in the supplementary motor area.
Bottom Panel: PAOS patient (male, 58 years old), demonstrating diffuse tau binding in regions associated with the language network.

Keywords: [18F]AV-1451, PiB, apraxia of speech, aphasia

Lower white matter integrity is associated with higher amyloid deposition in older adults without dementia in two independent samples

Hwamee Oh[1], Atul Narkhede[1], Qolamreza R. Razlighi[1], Yaakov Stern[1], Richard P. Mayeux[1], Adam M. Brickman[1]

[1]*Department of Neurology and the Taub Institute for Research on Alzheimer's disease and the Aging Brain, Columbia University, New York, NY, USA*

The accumulation of beta-amyloid (Aβ), a pathological hallmark of Alzheimer's disease (AD), is highly age-related and regionally selective. Abnormality of white matter (WM) tracts is very common in clinically normal older adults and has been associated with a higher risk of developing AD. Furthermore, the regional variability in age-related deterioration in WM tracts has been noted, showing that long-range cortico-cortical connections undergo deterioration with aging more steeply than WM tracts constrained within lobes. Using two independent samples of older adults without dementia, we examined a relationship between long-range WM tract integrity and amyloid deposition. One hundred twenty-six nondemented, ethnically diverse, and community-dwelling older adults from the Washington Heights-Inwood Columbia Aging Project (WHICAP) underwent ^{18}F-Florbetaben amyloid PET and diffusion-weighted scans that quantify brain amyloid burden and WM tract integrity, respectively. A global amyloid index was calculated by standardized uptake value ratio (SUVR) with a cerebellar gray matter reference region and Aβ positivity cutoff was determined using a K-means clustering method, which classified 89 subjects as "Amyloid-negative (Aβ− O)" and 37 as "Amyloid-positive (Aβ+ O)". Figure 1A shows significant interactions between axial diffusivity of superior longitudinal fasciculus and the body of corpus callosum (higher values indicating lower WM integrity) and amyloid group predicting the level of global Aβ deposition, accounting for age and sex ($ps < 0.05$). The relationship between WM integrity and amyloid deposition was further confirmed in an independent sample of cognitively normal older adults (N=44) obtained from Alzheimer's Disease Neuroimaging Initiative (ADNI) II, as shown in Figure 1B. The consistent results from two independent samples suggest a strong relationship between long-range WM tract integrity and amyloid deposition in older adults without dementia. Future studies are warranted to determine a directionality of this relationship using longitudinal assessments.

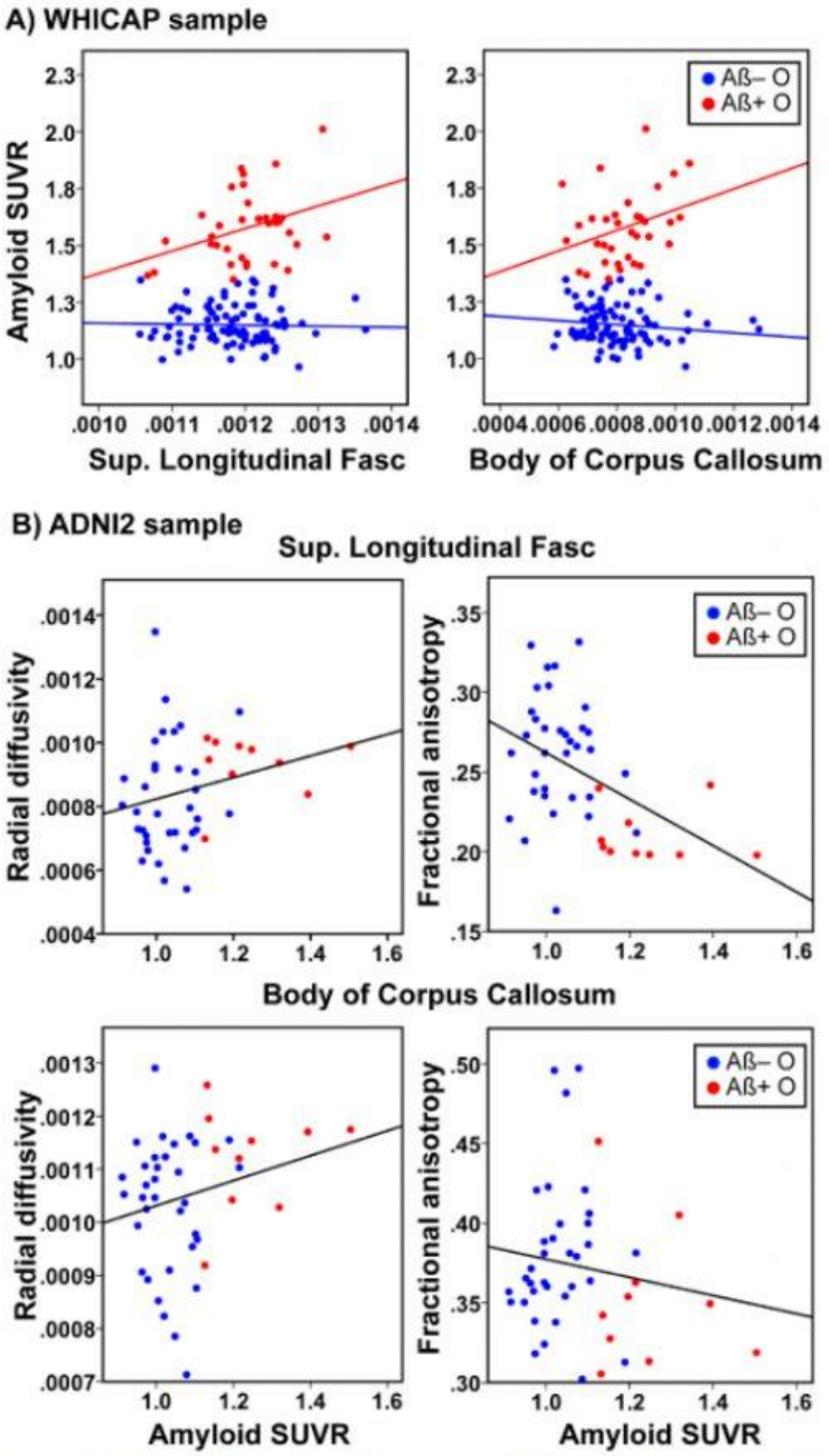

Figure 1. Relationship between white matter integrity and global amyloid index from two independent samples (WHICAP [A] and ADNI2 [B]). WM measures of radial/axial diffusivity and fractional anisotropy assessed in superior longitudinal fasciculus and body of corpus callosum

Keywords: beta-amyloid deposition, white matter tract integrity, amyloid PET, Diffusion Tensor Imaging, non-demented older adults

Uncovering the local-to-distributed relationship between β-amyloid and glucose metabolism

Felix Carbonell[1], Donald G. Mclaren[1], Alex P. Zijdenbos[1], Barry J. Bedell[1,2]

[1]*Biospective Inc., Montreal, QC, Canada*
[2]*McGill University, Montreal, QC, Canada*

Background: Several PET studies have explored the relationship between β-amyloid burden and glucose metabolism. It has been reported that **global** cortical β-amyloid burden has little contribution to glucose hypometabolism in cognitively normal (NC) and mild cognitive impairment (MCI) subjects. It has been also reported that **regional** hypometabolism is unrelated to **regional** β-amyloid burden in NC and MCI subjects. We hypothesize that these measurements of β-amyloid burden do not provide the complete relationship with glucose metabolism. As such, we have sought to determine if **local** β-amyloid burden measures are related to a **distributed** pattern of glucose metabolism.

Methods: We utilized a voxel-wise correlation analysis (VCA) to assess patterns of cross-correlation structure between glucose metabolism, as measured by FDG PET, and β-amyloid, as measured by florbetapir PET, in 607 NC/MCI subjects from the ADNI study. VCA yields a set of regions where **local** β-amyloid burden is statistically related to **local** glucose metabolism. We then regressed the mean β-amyloid burden in local seeds against glucose metabolism data while controlling for age, gender, MMSE, and APOE ε4 status.

Results: Significant negative relationships of β-amyloid burden with glucose metabolism in temporal-parietal regions and posterior cingulate cortex (**Figure 1**) in the VCA revealed localized cross-modality relationships.

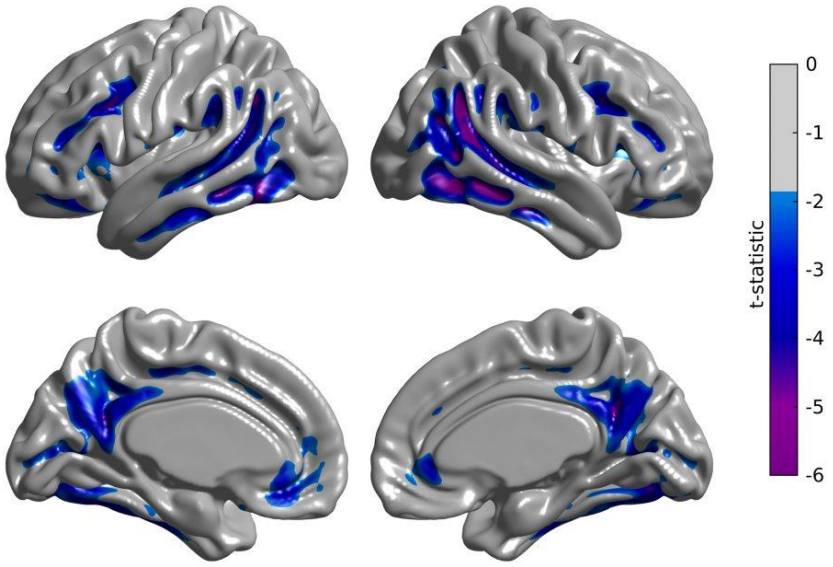

Figure 1. False Discovery Rate (FDR)-thresholded t-statistic map associated with negative local-to-local correlations between β-amyloid burden and glucose metabolism.

Local measures of β-amyloid burden in the left inferior temporal sulcus (ITS) and the right angular gyrus (ANG) showed distinct distributed relationships with glucose metabolism (**Figure 2A, B**).

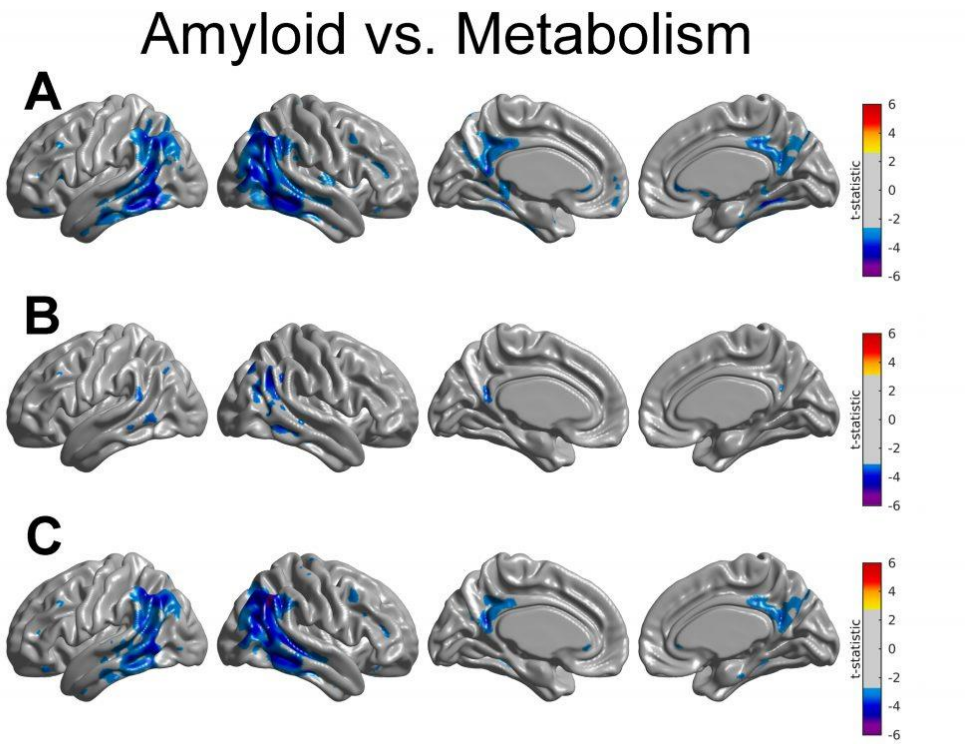

Figure 2. FDR-thresholded t-statistic maps of glucose metabolism corresponding to (A) left ITS amyloid seed, (B) right ANG amyloid seed, and C) global cortical amyloid burden. Pearson's correlations between local β-amyloid and local glucose metabolism in the left ITS and right ANG were r=-0.23 (p<0.001) and r=-0.25 (p<0.001), respectively.

The statistically significant pattern observed with ANG β-amyloid burden did not resemble the pattern found when using global β-amyloid burden (**Figure 2C**). These distributed negative patterns did not appear to be driven by the strength or spatial extent of the corresponding β-amyloid pattern of spread or "network" (**Figure 3**).

Conclusions: The β-amyloid network has hubs that contribute to distributed metabolic decreases, which, in turn, are not necessarily foci for β-amyloid deposition.

Keywords: β-amyloid, glucose metabolism, mild cognitive impairment, Alzheimer's Disease

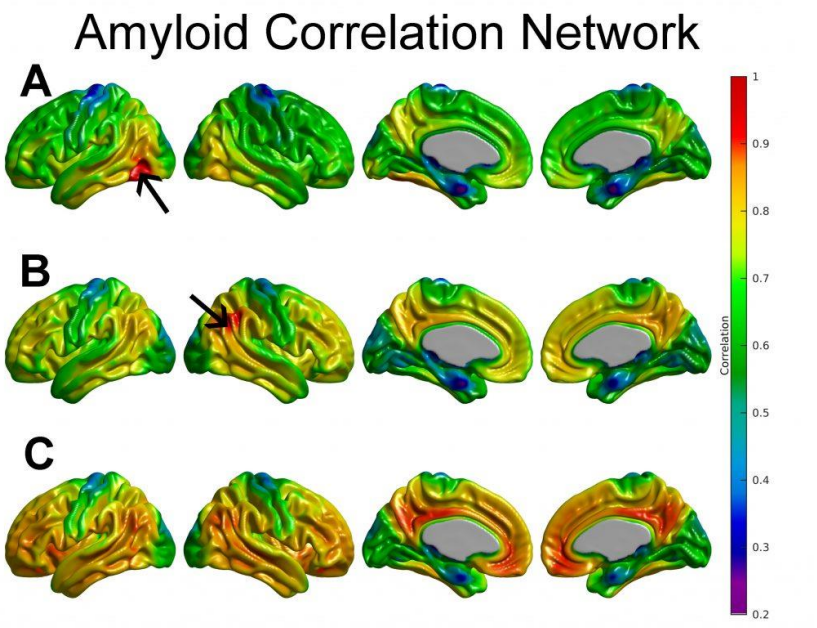

Figure 3. The β-amyloid network corresponding to (A) left ITS β-amyloid seed, (B) right ANG β-amyloid seed, and (C) global cortical β-amyloid burden. Black arrows correspond to the left ITS and right ANG seed locations. Pearson's correlations between local β-amyloid in the left ITS/right ANG seeds and global β-amyloid burden were r=0.89 and r=0.93, respectively.

[F-18]-AV-1451 binding correlates with neurofibrillary tangle Braak staging in postmortem brain tissue samples

Marta Marquié-Sayagués[1,2], Alejandro Antón-Fernández[1,2], Michael Siao Tick Chong[1,2], Avery C. Meltzer[1,2], Nil Sáez-Calveras[1,2], Eline Verwer[3], Prianca Ramanan[1,2], Marc D. Normandin[3], Matthew P. Frosch[4], Teresa Gómez-Isla[1,2]

[1]MassGeneral Institute for NeuroDegenerative Disease, Charlestown, MA, USA
[2]Massachusetts General Hospital, Department of Neurology, Boston, MA, USA
[3]Massachusetts General Hospital, Department of Radiology, Boston, MA, USA
[4]Massachusetts General Hospital,, C.S. Kubik Neuropathology Center, MA, USA

Introduction: -AV-1451, a PET tracer specifically developed to detect brain tau neurofibrillary pathology, has the potential to improve diagnostic accuracy for Alzheimer's disease (AD) and to allow reliable quantification of brain tau burden; something that may prove essential for evaluating disease progression and for assessing response to tau-targeted therapies. Recent PET studies show that patients with mild cognitive impairment and AD dementia exhibit significantly higher *in vivo* -AV-1451 retention than cognitively normal controls. Importantly, PET patterns of -AV-1451 correlate well with disease severity and seem to match the predicted topographic Braak staging of neurofibrillary tangles (NFTs) in AD, although this awaits confirmation.

Objectives: We studied the correlation of autoradiographic binding patterns of -AV-1451 and the stereotypical spatiotemporal pattern of progression of NFTs using legacy postmortem brain samples representing different Braak NFT stages (I-VI) (Braak and Braak, 1991).

Methods: We performed -AV-1451 phosphor-screen autoradiography and quantitative tau measurements (stereologically-based NFT counts and biochemical analysis of tau pathology) in four brain regions (entorhinal cortex, superior and inferior banks of the superior temporal sulcus and occipital cortex) in a total of 22 cases: low Braak (I-II, n=6), intermediate Braak (III-IV, n=7) and high Braak (V-VI, n=9).

Results: Strong and selective -AV-1451 binding was detected in all tangle-containing regions matching precisely the observed pattern of PHF-tau immunostaining across the different Braak stages. As expected, no signal was detected in the white matter or other non-tangle containing regions. Quantification of -AV-1451 binding was very significantly correlated with the number of NFTs present in each brain region and with the total tau and phospho-tau content as reported by Western blotting. Conclusion: AV-1451 is a promising biomarker for *in vivo* detection and quantification of brain tau burden in AD. Neuroimaging–pathologic studies conducted on postmortem material from individuals imaged while alive are now needed to confirm these observations.
Keywords: [F-18]-AV-1451, PET, postmortem, Braak, neurofibrillary tangles, tau

Measurement of pathological amyloid in routine clinical assessment: comparison of visual [18F]Flutemetamol PET and CSF

Nenad Bogdanovic[1], Enrico Fantoni[2], Gill Farrar[2]

[1]*University Hospital Oslo, Oslo, Norway*
[2]*GE Healthcare, Amersham, United Kingdom*

Introduction: Amyloid PET and CSF beta-amyloid (Aβ42) are valid alternatives for determining pathological load. Accuracy of the two methods was found by Palmqvist *et al.,* 2015 to be comparable. However, the CSF Aβ42 threshold required to establish a "positive" diagnosis of β-amyloid plaque accumulation varies between sites. Assessment of a cohort from routine clinical practice compared CSF Aβ42 with flutemetamol PET reads to assess the concordance between PET and CSF measures.
Methods: 60 patients referred by their general practitioner to the Oslo University Memory Clinic with cognitive complaints (mean age 69; range 49 to 81 years) underwent lumbar CSF fluid sampling and PET scanning of approximately 185 MBq flutemetamol. CSF measures were determined in Akerhus University Hospital, Oslo using INNOTEST enzyme-linked immunosorbent assays (Fujirebio, Ghent, Belgium). flutemetamol images were classified by readers trained per the manufacturer's instructions as either positive or negative.
Results: Flutemetamol PET scanning identified 38 subjects as being amyloid-positive, 15 of whom had CSF Aβ42 below 550 pg/mL (Figure 1). Of the 22 patients with negative amyloid scans, 17 had CSF Aβ42 values above 770pg/mL. The remainder of the 28 cases had Aβ42 CSF measures between 550-770 pg/ml with 23 evaluated as amyloid positive in the PET image read and only 5 as amyloid negative.
Conclusion: A review of the ranked data suggests a threshold > 720pg/mL for CSF Aβ42 captures 78% of PET negatives, whilst below a PET positivity rate of 89% is observed. This threshold is higher than previously observed (550 pg/mL), suggesting that the PET read is sensitive to the presence of early pathological amyloid observed when CSF Aβ42 is starting to trend down. Further work will examine any centre dependent bias in the CSF analysis as well as a second PET scan read of the discordant cases. Clinical diagnosis of these cases will also be examined.

Ref: Palmqvist et al (2015) Neurology; 85: 1-10

Keywords: [18F]flutemetamol, CSF Aβ42, routine clinical assessment, threshold

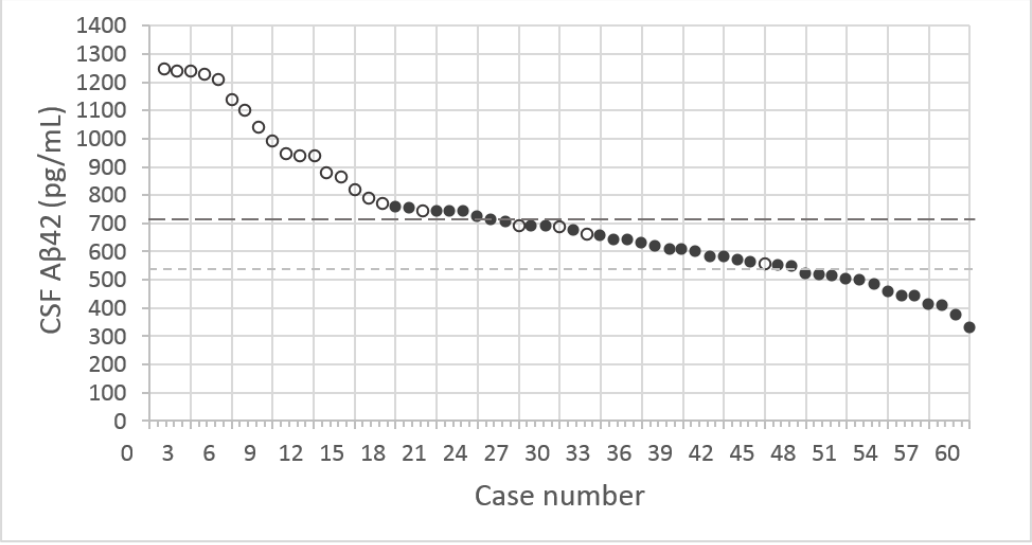

Figure 1 CSF Aβ42 levels and [18F]flutemetamol PET visual read result for each of the 60 participants to this study. *Cases were re-ordered for this analysis by descending CSF Aβ assay value.*
○ Negative (normal) amyloid PET scan; ● Positive (abnormal) amyloid PET scan;
- - - Current CSF Aβ42 threshold; — — Revised CSF Aβ42 threshold.

Metabolic syndrome and amyloid accumulation in the aging brain

Gabriela Gomez[1], Lori Beason-Held[1], Murat Bilgel[1], Yang An[1], Stephanie Studenski[1], Susan Resnick[1]

[1]*Intramural Research Program, NIA, NIH, Baltimore, MD, USA*

Introduction: Metabolic Syndrome (MetS) affects 35% of all adults and 50% of adults over 60yr. A growing body of evidence supports a link between MetS and the neuropathology of Alzheimer's disease (AD), yet key components of the relationship between MetS and AD remain unexplored. In this study of older adults, we investigated the association between MetS and global cerebral amyloid status (positivity) and longitudinal regional change of amyloid accumulation.

Methods: We followed 170 participants enrolled in the Baltimore Longitudinal Study of Aging Neuroimaging substudy (BLSA-NI) over a mean interval of 2.7 years (mean baseline age=76.7yr). Cerebral amyloid was measured using 11C-Pittsburgh compound B (PiB) dynamic positron emission tomography (PET). Participants were then separated into PiB+/- groups based on mean cortical distribution volume ratios (DVR). Fisher's exact test was conducted to assess whether PiB status differed by concurrent MetS diagnosis. A linear mixed effects model was then used in the PiB+ group (N=56, mean age at baseline=80.07, mean interval=2.3yr) to assess the cross-sectional and longitudinal relationship between baseline MetS and regional DVR in areas derived from the Desikan-Killiany atlas ($p<0.05$, FDR-corrected).

Results: We found that PiB positivity did not significantly differ by concurrent MetS diagnosis (odds ratio 0.93, $p=0.87$). Within the PiB+ group, a linear mixed model revealed no significant association between MetS diagnosis and concurrent regional DVR levels at baseline. However, diagnosis of MetS was associated with increased rates of Aβ accumulation in several regions over time, including the superior parietal lobe, precuneus, medial frontal cortex, and insula.

Conclusion: Although MetS was not associated with overall amyloid positivity, the disorder was associated with accelerated Aβ accumulation in individuals with preexisting cerebral amyloid levels. These findings suggest that MetS may be an important factor in the progression of AD, and highlight the importance of health-related preventative strategies for dementia.
Keywords: health, obesity, hypertension, diabetes, dementia

Left frontal global connectivity is a substrate of cognitive reserve in mild cognitively impaired patients with a high amyloid burden

Nicolai Franzmeier[1], Marco Duering[1], Michael Weiner[2], Martin Dichgans[1,3,4], Michael Ewers[1]

[1]*Institute for Stroke and Dementia Research, Klinikum der Universität München, Munich, Germany*
[2]*University of California at San Francisco, San Francisco, CA, USA*
[3]*Munich Cluster for Systems Neurology, Munich, Germany*
[4]*German Center for Neurodegenerative Diseases, Munich, Germany*

Background: Previous studies in Alzheimer's disease (AD) suggest, that higher cognitive reserve (CR) allows maintaining memory performance relatively well when facing AD pathology. However, the neural mechanisms underlying CR remai n unknown. We assessed the lateral frontal cortex (LFC) - a hub region supporting cognitive control - as a potential substrate of CR in mild cognitively impaired subjects with increased levels of amyloid-PET uptake (MCI-Ab+). We hypothesized firstly, that higher global LFC functional connectivity (gLFC-connectivity) is associated with higher CR (i.e. years of education). Secondly, we hypothesized that greater gLFC-connectivity is associated with reduced effects of FDG-PET hypometabolism onto memory performance in MCI-Ab+.

Methods: We included 44 MCI-Ab+ and 24 amyloid-PET negative healthy controls (HC-Ab-). We assessed seed-based functional connectivity between an 8mm spherical LFC ROI (BA6/44) and each grey matter voxel. To yield gLFC-connectivity, all positive correlations were averaged across voxels. Using voxel-wise regression, we tested whether in MCI-Ab+ greater education was predicted stronger FDG-PET hypometabolism, controlling for memory performance. In further regression analyses, we tested whether higher gLFC-connectivity was associated with greater education and reduced effects of FDG-PET hypometabolism onto episodic memory (interaction FDG-PET metabolism x gLFC-connectivity).

Results: We found precuneus FDG-PET metabolism to be reduced in MCI-Ab+ compared to HC-Ab- ($p=0.028$), with stronger reductions observed in MCI-Ab+ with greater education ($p=0.006$), when controlling for memory performance. This suggests that MCI-Ab+ with greater education can better tolerate FDG-PET hypometabolism. In MCI-Ab+, greater education predicted higher gLFC-connectivity (Fig.1A). The interaction gLFC-connectivity x precuneus FDG-PET on memory was significant in MCI-Ab+ ($p=0.027$), such that at higher levels of gLFC-connectivity the association between precuneus hypometabolism and memory impairment was attenuated, suggesting a compensatory LFC effect (see Fig.1B).

Conclusion: Higher gLFC-connectivity is a functional substrate of CR that helps maintaining memory performance relatively well in the face of high Ab-deposition and emerging FDG-PET hypometabolism.

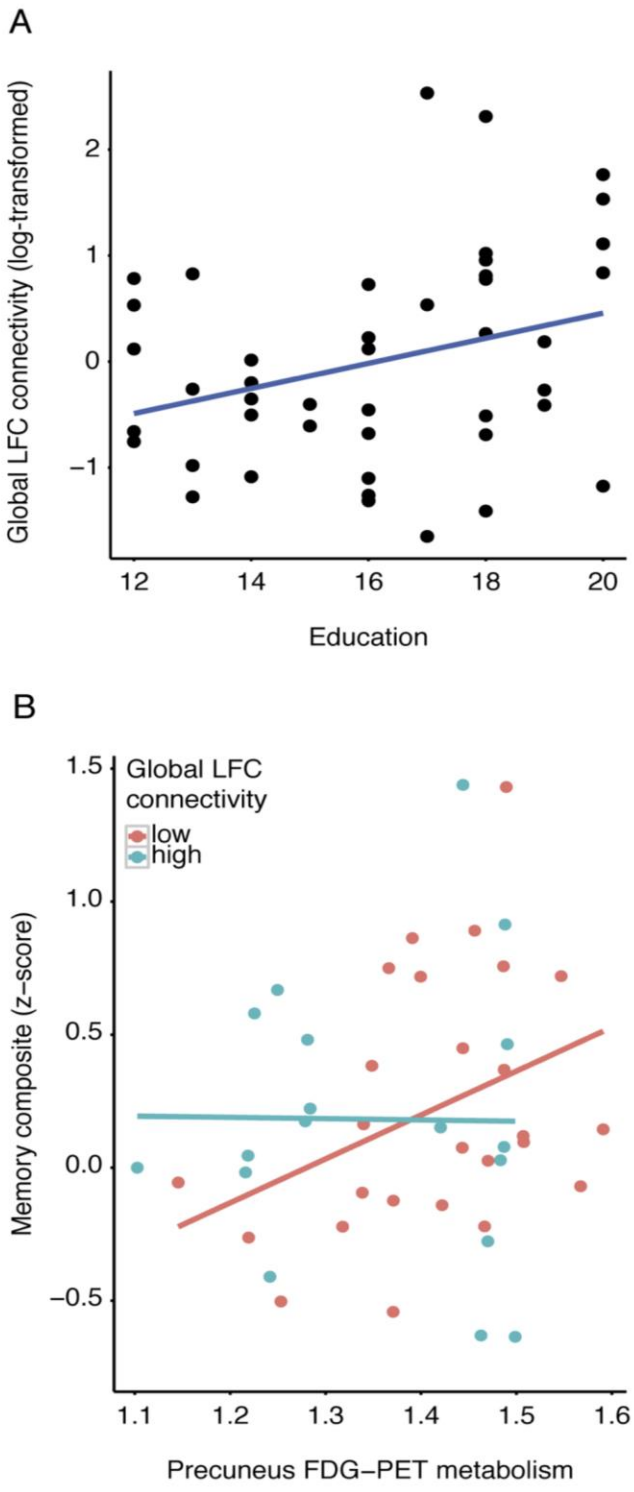

Association between education, gLFC-connectivity and precuneus FDG-PET metabolism in MCI-Aβ+. (A) Scatterplot of the association between years of education and gLFC-connectivity. (B) Scatterplot for the interaction gLFC-connectivity × precuneus FDG- PET metabolism on memory performance in MCI-Aβ+. Precuneus FDG-PET metabolism is plotted against the memory composite score for participants with high and low gLFC-connectivity. Groups of high and low gLFC-connectivity (defined via median split) are plotted separately for illustrational purposes.

Keywords: Alzheimer's disease, fMRI connectivity, Cognitive reserve, memory

Detection of radiologic and laboratory features of cerebral amyloid angiopathy in patients with Alzheimer's disease

Panagiotis Fotiadis[1], John Becker[2], Kristin Schwab[1], Jonathan Rosand[1], Anand Viswanathan[1], Reisa Sperling[2], Keith Johnson[2], Steven Greenberg[1], Edip Gurol[1], Alzheimer's Disease Neuroimaging Initiative[3]

[1]J. P. Kistler Stroke Research Center, Department of Neurology, Massachusetts General Hospital, Boston, MA, USA
[2]Department of Radiology, Athinoula Martinos Center for Biomedical Imaging, Massachusetts General Hospital, Charlestown, MA, USA
[3]Alzheimer's Disease Neuroimaging Initiative, Los Angeles, CA, USA

Background Patients with Cerebral Amyloid Angiopathy (CAA) have posterior vascular amyloid deposition and lower Amyloid Beta (Aβ) levels when compared to patients with Alzheimer's Disease (AD). We hypothesized that similar findings would be observed in AD patients with strictly lobar microbleeds (LMB) and/or cortical superficial siderosis (cSS) attributable to CAA , when compared to AD patients with no hemorrhagic lesion(s) .

Methods We reviewed MRIs of AD patients with T2*-, FLAIR and 3D T1-weighted MRI as well as Florbetapir PET, CSF Aβ-42 and tau levels, and APOE status within the Alzheimer's Disease Neuroimaging Initiative (ADNI) database.

Results The CAA-AD (n=51) and NH-AD (n=85) groups were balanced for age, gender and history of hypertension (all p>0.2). The APOE4 was more frequently present in the CAA-AD group (78% vs 60%, p=0.038). Patients with CAA-AD had higher White Matter Hyperintensity (WMH) volumes (0.73 vs 0.49 % intracranial volume , p=0.035) and higher occipital-to-global Florbetapir ratio (0.98 vs 0.94, p=0.02) but similar mean cortical Florbetapir uptake (1.38 vs 1.36, p=0.57), cortical thickness (2.22 vs 2.20 mm, p=0.38), and hippocampal volume (0.37 vs 0.38 % of ICV, p=0.24) when compared to NH-AD. In multivariable regression models, higher occipital-to-global Florbetapir ratio (p=0.009) and presence of APOE4 (p=0.002) were associated with CAA-AD. In 117 patients with CSF data, CAA-AD (n=46) had lower Aβ-42 (127 vs 140 pg/ml, p=0.038) but similar tau levels (131 vs 136 pg/ml, p=0.68) when compared to NH-AD. Lower Aβ-42 was also associated with CAA-AD (p=0.024) in multivariable regression models.

Conclusions Over one-third of AD patients displayed CAA-induced hemorrhagic lesion(s). When compared to NH-AD, they presented higher occipital-to-global Florbetapir uptake, suggesting vascular amyloid binding, and lower CSF Aβ-42 levels potentially related to amyloid sequestering in cortical vessel walls. These results support the possibility that advanced CAA commonly accompanies clinically diagnosed AD, contributing to dementia pathogenesis, and potentially affecting clinical treatment decisions.
Keywords: Cerebral Amyloid Angiopathy, Alzheimer's Disease, Hemorrhagic Lesions, Beta Amyloid, CSF

Elevated 18F-AV-1451 PET tracer uptake detected in incidental imaging findings

Samuel Lockhart[1], Nagehan Ayakta[2], Joseph Winer[3], Renaud La Joie[2], Gil Rabinovici[2], William Jagust[1]

[1]Helen Wills Neuroscience Institute, University of California, Berkeley, CA, USA
[2]Department of Neurology, Memory and Aging Center, University of California, San Francisco, San Francisco, CA, USA
[3]Department of Psychology, University of California, Berkeley, Berkeley, CA, USA

Objective: To assess elevations in AV-1451 (tau) PET tracer uptake colocalized with incidental imaging findings.

Methods: We discovered 5 cases (2 normal controls, 3 patients: 1 Alzheimer's Disease , 1 mild cognitive impairment, 1 Parkinson's disease) with surprising increases in AV-1451 uptake in regions of incidental neuroimaging findings. In each participant, we collected T1 and FLAIR MRI, 80-100 min 18F-AV-1451 PET SUVR images, and generated a global cortical average from 11C-PiB DVR images for amyloid positivity classification. PET images used a cerebellar grey matter reference region. AV-1451 and FLAIR were linearly aligned to T1 images and resliced. Target ROIs (9x9x9 mm cubes) were drawn on T1 images over the observed imaging findings, as were ROIs in the hemisphere contralateral to the findings.

Results: Participant A (Table) has T1 images (Figure) revealing right temporal hypointensity surrounded by hyperintensity on FLAIR images, consistent with chronic infarction. Participant B's MRI sequences reveal the characteristic appearance of a right cerebellar cavernous malformation. Participant C has imaging also consistent with a remote infarct, located in the right frontal lobe. Participant D's imaging reveals a right medial frontal meningioma, while participant E exhibits a left superior frontal meningioma. We found elevated AV-1451 signal associated with the chronic infarcts, cavernous malformation, and meningiomas. For all participants, AV-1451 signal is markedly increased in the location of the target ROI covering each incidental imaging finding, particularly compared to the contralateral ROI.

Conclusions: In certain conditions, tracer binding might complicate image interpretation. Here, we demonstrated tracer uptake in meningiomas, vascular malformations and remote infarcts. In studies using AV-1451 and other tau tracers to study aging and disease, researchers must carefully examine PET images for focal tracer accumulation and MRI images for incidental findings; these may produce spurious signal elevations not reflective of the presence of age or AD-related pathology.

Table. Participant demographics.

	A	B	C	D	E
Age (y)	80	80	67	77	80
Sex	M	F	F	F	F
Diagnosis	Normal	Normal	PD	AD	aMCI
PiB+/-	-	+ (borderline)	+ (borderline)	+	+

PD = Parkinson's Disease, AD = Alzheimer's Disease, aMCI = Amnestic MCI.

Figure. Elevated AV-1451 tracer uptake seen in incidental neuroimaging findings. *Axial images for participants A-E (columns). Images (radiological convention) are 18F-AV-1451 SUVR (1st row), FLAIR (2nd row), T1 (3rd row), and target and contralateral ROIs (red and blue masks in 4th row) on T1. Voxel histograms from target and contralateral ROIs are in 5th and 6th rows (dashed line = mean). Participant D exhibits strong cortical tracer retention, consistent with AD diagnosis. Participant E inset shows close-up of meningioma on T1.*

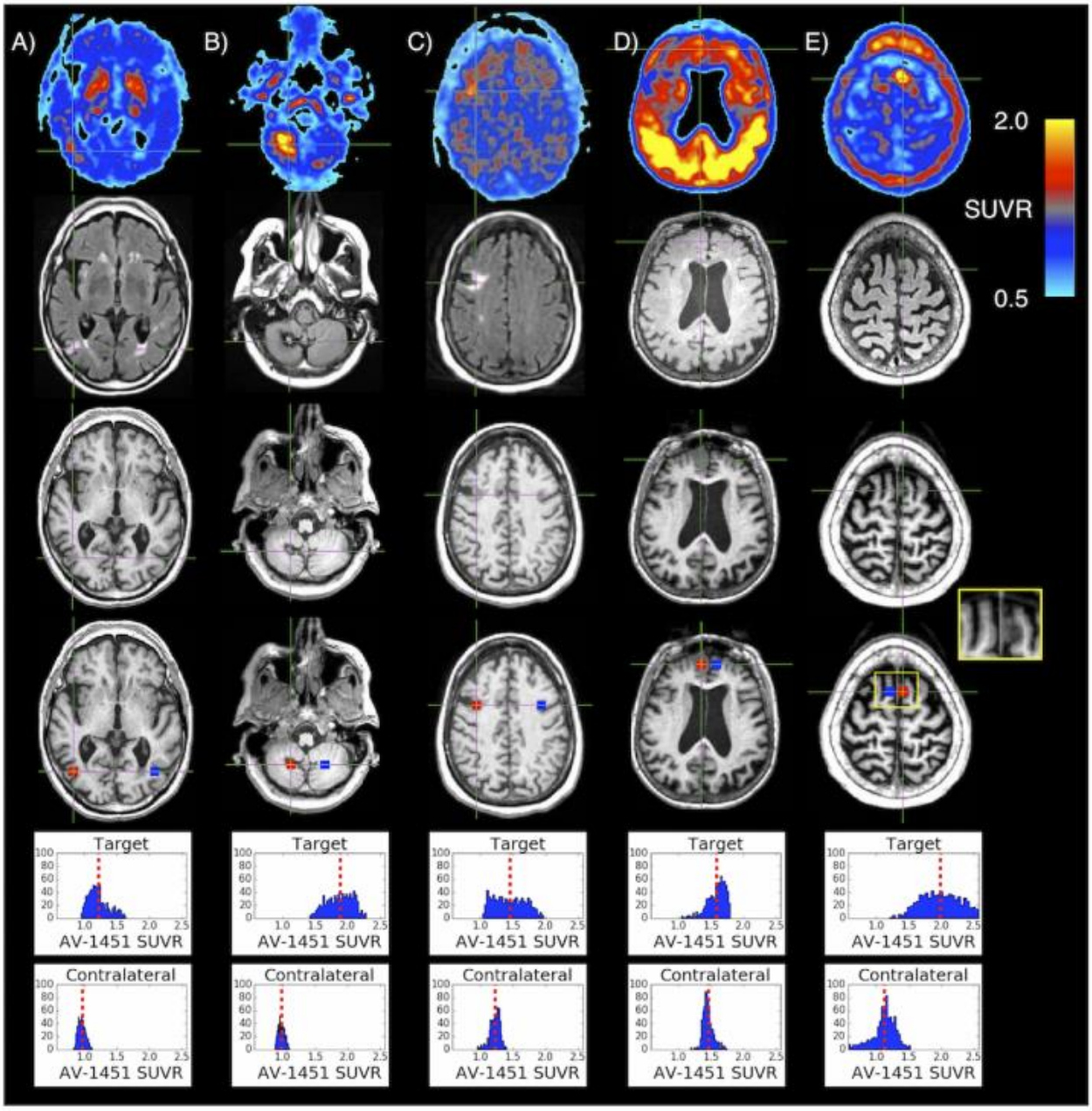

Keywords: AV-1451, Imaging, Binding, Infarction, Meningioma

18F-AV-1451 PET demonstrates Braak stage-specific associations with limbic white matter integrity in normal aging

Samuel Lockhart[1], Anne Maass[1], Shawn Marks[1], Suzanne Baker[2], William Jagust[1]

[1]Helen Wills Neuroscience Institute, University of California, Berkeley, Berkeley, CA, USA
[2]Molecular Biophysics and Integrated Bioimaging, Lawrence Berkeley National Laboratory, Berkeley, CA, USA

Objectives: To evaluate associations of age, beta-amyloid (Aβ), and tau with white matter (WM) microstructure in cognitively normal older adults (OA).

Methods: 47 OA (Table) received 18F-AV-1451 (tau) PET, 11C-PiB (Aβ) PET, and T1 and diffusion-weighted MRI. For each subject we calculated a global cortical PiB average. We segmented T1 MRIs using FreeSurfer v5.3, coregistered 18F-AV-1451 (80-100 min SUVR, cerebellar grey reference) scans to T1, partial volume corrected 18F-AV-1451 images (including a correction for choroid plexus), and calculated 18F-AV-1451 in ROIs that reflect Braak stages. Diffusion data were processed using FSL to generate native-space fractional anisotropy (FA) and mean diffusivity (MD) images, and warped to MNI space using ANTS. Images were smoothed, and means for select limbic WM tracts (Hopkins atlas) calculated. We assessed statistical relations using non-parametric bivariate and partial Spearman correlation analyses.

Results: 18F-AV-1451 retention demonstrated a specific pattern of associations with limbic WM integrity. Mean 18F-AV-1451 retention in Braak stage 2 ROIs (bilateral hippocampus) showed negative associations with ventral cingulum bundle and fornix column/body FA (Figure), and positive associations with MD in the same tracts ($|.30| < rho < |.37|$). Age showed negative associations with limbic tract FA ($-.34 > rho > -.44$), and positive MD associations in all tracts ($.43 < rho < .57$). In a model controlling for age and global PiB, Braak 2 18F-AV-1451 significantly predicted reduced ventral cingulum FA (rho = -.30, $p = .043$). Controlling for age and ventral cingulum FA, Braak 2 18F-AV-1451 predicted reduced memory performance (CVLT long delay free recall; rho = -.30, $p = .045$).

Conclusions: Although the mechanisms by which late-life tau and amyloid accumulation influence brain structural connectivity and cognition are not well understood, these results suggest that early medial temporal tau accumulation is associated with reduced limbic tract integrity.

Table. Participant Demographics.

	Braak Stage		
	0	**1/2**	**3/4**
n	6	31	10
Age, y	80.7 (8.3)	78.1 (5.5)	79.3 (2.4)
Global PiB DVR	1.08 (0.1)	1.07 (0.1)	1.35 (0.3)
CVLT Long delay free recall	13 (2.1)	11 (3.1)	8.6 (5)

Figure. Spearman rho values for bivariate relations of AV-1451, PiB, and age with tract white matter microstructure. (a) Correlation matrix for associations between white matter tract FA (y-axis) and other measures (x-axis), with color indicating negative (red) and positive (blue) monotonic associations; (b) values for FA of rho > ±0.3. (c) Correlation matrix for similar MD associations and (d) values for MD of rho > ±0.3.

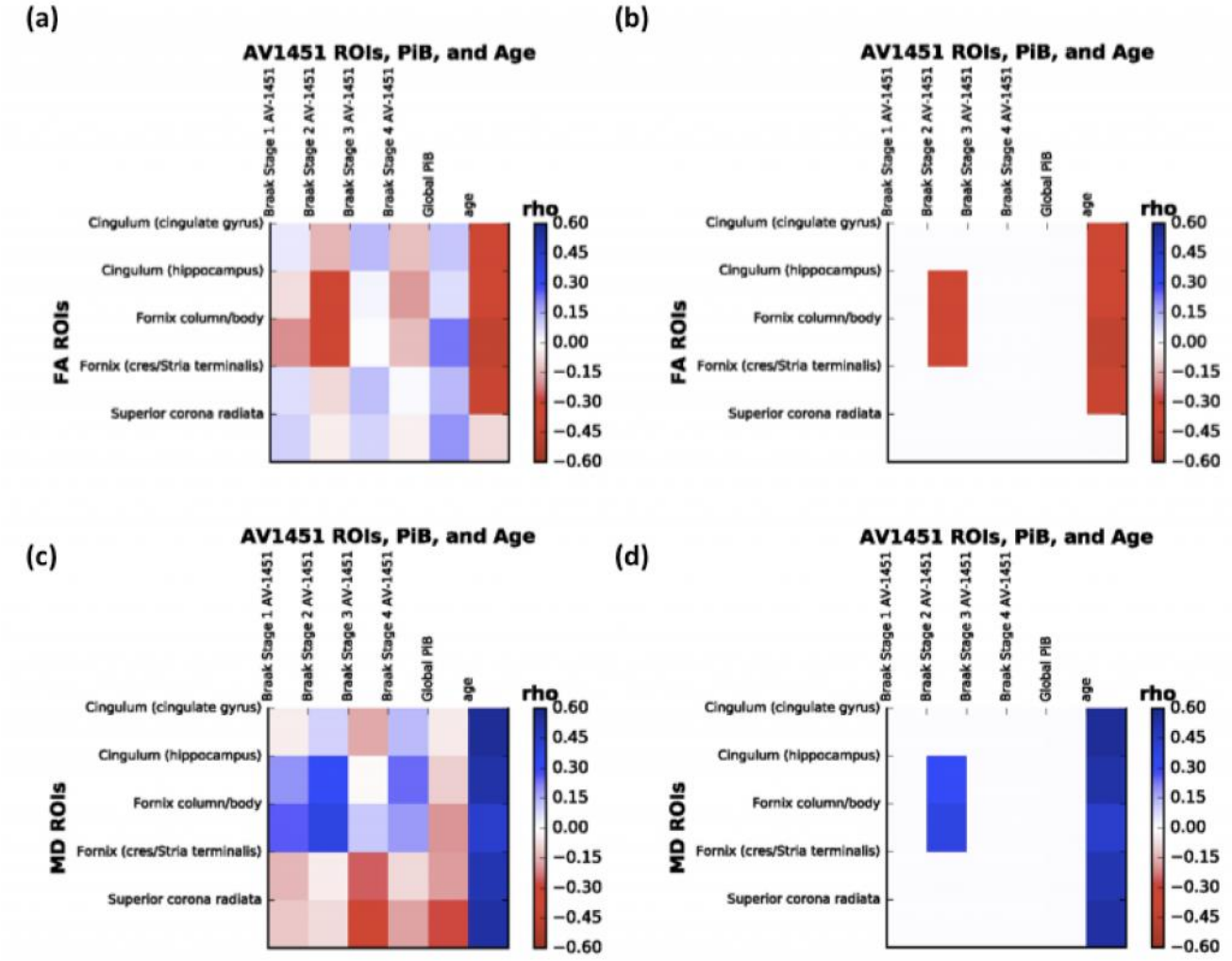

Keywords: AV-1451, DTI, Tau, Amyloid, Cingulum

Microglial activation correlates in vivo with tau aggregation and amyloid deposition in mild cognitive impairment and Alzheimer's disease

Melanie Dani[1], Melanie Wood[1], Ruth Mizoguchi[1], Zhen Fan[1], Richard Morgan[2], Zuzana Walker[3,4], Valeria Calsolaro[1], Grazia Femminella[1], Rainer Hinz[5], David Brooks[6], Paul Edison[1]

[1]Neurology Imaging Unit, Imperial College London, London, United Kingdom
[2]Chelsea and Westminster Hospital, London, United Kingdom
[3]Division of Psychiatry, University College London, London, United Kingdom
[4]North Essex Partnership University NHS Foundation Trust, London, United Kingdom
[5]Wolfson Molecular Imaging Centre, University of Manchester, Manchester, United Kingdom
[6]Department of Nuclear Medicine, Aarhus University, Aarhus, Denmark

Introduction: In addition to amyloid deposition and neurofibrillary tangle deposition, microglial activation plays a key role in the pathophysiological processes in Alzheimer's disease (AD) and Mild Cognitive Impairment (MCI). However, the exact relationship between microglial activation and protein aggregation is still debated. In this study, we examined voxel-level correlations between microglial activation, amyloid, and tau aggregation using ^{11C}-PBR28, ^{18}F-flutemetamol, and ^{18}F-AV1451 PET, respectively.

Methods: 20 AD, 23 MCI subjects and 21 healthy controls were included. Subsets of this group had ^{11}C-PBR28, ^{18}F-flutemetamol, and ^{18}F-AV1451 PET scans.
Biological parametric mapping in SPM was used to interrogate the voxel-level correlation between the pathologies. SPM t-maps were generated to localise differences between the MCI and AD patients with controls for each tracer. Correlations were performed at a voxel-level with a statistical threshold of significance set at $P<0.01$ and an extent threshold of 25 voxels. All clusters identified with a corrected $p<0.05$ were deemed significant.

Results:

MCI

There were clusters of positive correlations across the cortex between

- Microglial activation and amyloid deposition
- Microglial activation and tau aggregation
- Amyloid deposition and tau aggregation

AD

There were clusters of positive correlations across the cortex between

- Microglial activation and tau aggregation
- Amyloid deposition and tau aggregation

Interestingly, there were clusters of negative correlations across the cortex between microglial activation and amyloid deposition.

Discussion: Microglial activation is associated with protein aggregations in MCI and AD. The distribution patterns differ between the pathologies, and also between the MCI and AD groups, indicating that the distribution of microglial activation may change later in the disease. These findings are compatible with all three pathologies playing a significant role in progressive neuronal damage, and a multi-targeted intervention may be necessary for effective disease prevention and cure.
Keywords: amyloid, tau, microglial activation, Alzheimer's

Correlation of regional amyloid load in cognitively healthy monozygotic twin pairs, measured using [18F]Flutemetamol

Mara ten Kate[1], Elles Konijnenberg[1], Anouk den Braber[1,2], Sofie Adriaanse[3], Maqsood Yaqub[3], Dorret Boomsma[2], Philip Scheltens[1], Bart van Berckel[3], Pieter Jelle Visser[1,4]

[1]Alzheimer Center, Department of Neurology, VU University Medical Center, Amsterdam, Netherlands
[2]Department of Biological Psychology, VU University Amsterdam, Amsterdam, Netherlands
[3]Department of Radiology & Nuclear Medicine, VU University Medical Center, Amsterdam, Netherlands
[4]Department of Psychiatry and Neuropsychology, School for Mental Health and Neuroscience, Alzheimer Centre Limburg, Maastricht, Netherlands

Background: Amyloid pathology precedes clinical dementia by decades. So far it remains unclear to what extent genetic and environmental influences play a role in amyloid pathology. Studies in monozygotic twins are useful to estimate the upper-limit of genetic contribution to a disease. The aim of this study is to estimate the concordance of regional amyloid load between cognitively healthy elderly monozygotic twin pairs.

Methods: We included 93 monozygotic twin pairs from the NTR-EMIF-AD PreclinAD study. Inclusion criteria were age ≥60 years and delayed recall score above -1.5 SD of normative data. Dynamic flutemetamol (FMM) scans were performed with combined data from two scans (30 minutes starting directly after FMM injection and 90-110 minutes post injection). Non-displaceable binding potential (BP_{ND}) with cerebellar grey matter as reference region was calculated for whole brain and various regions using the basis function implementation of the simplified reference tissue model (RPM1). Twin correlations for amyloid pathology were estimated with and without correcting for age and gender.

Results: Subjects were on average 70±7 years old and 57% were female. They had 15±5 years of education and an MMSE score of 29.0±1.1. Correlation of global BP_{ND} was 0.47 (p <0.001). Regional correlations were 0.47 for parietal, 0.47 for frontal, 0.43 for temporal and 0.49 for posterior cingulate (all $p < 0.001$). When correcting for age and gender all correlations dropped by 0.05 on average. All remained significant.

Conclusion: We found a significant correlation between cognitively healthy monozygotic twins for global and regional amyloid pathology. These data suggest that in addition to a moderately-strong genetic background for amyloid pathology, also non-genetic factors substantially influence the occurrence of amyloid. Future studies on the causes of identical twin discordance may provide novel insights into the pathophysiology of amyloid depositions, thereby providing new treatment targets for AD.
Keywords: amyloid, Flutemetamol, twins, genetic

In vivo tau imaging in Parkinson's disease using 18F-AV-1451 PET

Allan Hansen[1], Malene Damholdt[2], Peter Parbo[1], David Brooks[1,3], Per Borghammer[1]

[1]Dept of Nuclear Medicine, Institute of Clinical Medicine, Aarhus University, Aarhus, Denmark
[2]Department of Psychology and Behavioural Sciences, Aarhus University, Aarhus, Denmark
[3]Division of Neuroscience, Newcastle University, Newcastle, United Kingdom

Background: Alzheimer disease (AD) co-pathology is common in Parkinson's disease (PD) at autopsy, particularly in PD dementia, which 80% of patients develop. In non-PD subjects diagnosed with mild cognitive impairment (MCI), increased tau deposition in neurofibrillary tangles (NFT) can be detected using the NFT tracer AV-1451. We hypothesized that AV-1451 PET would show tau aggregation in patients with early stage PD-MCI and that the signal would correlate with cognitive dysfunction.

Methods: 23 PD patients and 25 healthy age-matched controls had 18F-AV-1451 PET and comprehensive neuropsychometric assessment of memory, working memory, language, executive and visuospatial domains to detect the presence of MCI. Between-group comparisons of cortical AV1451 binding at a voxel level and correlations with cognitive domain z-scores were interrogated with SPM12. VOI-based analysis for group comparison and estimation of Braak tau stages (EBS) was performed using PMOD and Stata.

Results: 7 PD patients were identified as PD-MCI and 16 as PD-nonMCI. Voxel-wise analysis showed no significant group differences that survived a family wise error correction. No domain z-score was found to correlate with cortical 18F-AV-1451 signal. One PD-MCI patient was EBS 5, two healthy controls EBS 1, all other test subjects were EBS 0. No group differences were seen in VOIs used for Braak staging, including entorhinal cortex, middle and inferior temporal gyrus and visual cortical areas. Further, there were no group differences between PD and controls in pallidum, putamen or caudate nucleus, VOIs often examined for the differential diagnosis of progressive supranuclear paresis (PSP). PD patients had decreased signal in the midbrain compared to controls in contrast to the reported increases in PSP.

Conclusion: Our results indicate that tau pathology as detected by the 18F-AV-1451 tracer is uncommon in both PD-nonMCI and PD-MCI and show no significant correlation with cognitive function at this stage.
Keywords: AV-1451, tau, Parkinson, PD-MCI

Tau PET imaging and atrophy in neurodegenerative dementias

Brad Dickerson[1], Scott McGinnis[1], Stephen Gomperts[1], Sara Makaretz[1], David Wolk[2], Aaron Schultz[1], Neil Vasdev[1], Keith Johnson[1]

[1]*Massachusetts General Hospital/Harvard Medical School, Charlestown, MA, USA*
[2]*University of Pennsylvania, Philadelphia, PA, USA*

Background: Using tau PET imaging, investigators have begun to demonstrate relationships between the magnitude of tau PET signal and the magnitude of FDG PET hypometabolism or MRI-derived atrophy. Here we investigate the relationship between atrophy and T807 signal in patients with MCI or dementia.

Methods: We have used T807 to scan a series of patients with MCI (PPA, PCA, amnesic MCI), AD dementia, FTLD dementia, and DLB dementia. We have compared them with cognitively intact controls, analyzing SUVR (cerebellum reference) data in comparison to % atrophy derived from quantitative analysis of MRI scans relative to controls.

Results: In areas of elevated T807 signal, atrophy is typically present when T807 SUVR is greater than 2.2. Areas with T807 SUVR between 1.8 and 2.2 may demonstrate atrophy. Areas with T807 SUVR below 1.8 usually do not demonstrate atrophy. Within each patient, the magnitude of T807 SUVR correlates with the magnitude of atrophy relative to controls.

Conclusions: In patients with neurodegenerative dementias, T807 signal is co-localized with atrophy and its magnitude correlates with the magnitude of atrophy.

Funding: R21 AG051987, R01 DC014296, P50 AG005134, R01 AG046396
Keywords: tau PET, atrophy, AD, FTD

Insulin resistance in midlife increases the risk for brain amyloid accumulation 15 years later

Laura Ekblad[1], Jarkko Johansson[1], Hanna Laine[2,3], Matti Viitanen[2,4], Antti Jula[5], Juha Rinne [1,6]

[1]*Turku PET Centre, University of Turku, Turku, Finland*
[2]*Turku City Hospital, University of Turku, Turku, Finland*
[3]*Department of Medicine, Turku University Hospital, Turku, Finland*
[4]*Clinical Geriatrics, Karolinska Institutet, Karolinska University Hospital, Huddinge, Sweden*
[5]*National Institute for Health and Welfare, Turku, Finland*
[6]*Division of Clinical Neurosciences, Turku University Hospital, Turku, Finland*

Background: Diabetes is an acknowledged risk factor for Alzheimer´s disease. Insulin resistance (IR) seems to be the key link between type 2 diabetes and the risk for Alzheimer´s disease. Insulin resistance contributes to the neuropathological changes of Alzheimer´s disease through multiple pathways. We hypothesized that midlife insulin resistance, estimated by the Homeostatic Model Assessment of Insulin Resistance (HOMA-IR) would increase the risk for brain amyloid accumulation 15 years later, and that this risk might be modulated by APOEε4 genotype.

Methods:: We studied the possible presence of brain beta-amyloid accumulation in 60 cognitively healthy elderly individuals (mean age 70.4 years, 53.3 % women) from the Finnish, population based, nationwide Health 2000 study (n=5935) using -PIB-positron emission tomography (PET) imaging during 2015–2016. The study volunteers had been measured for fasting insulin and glucose values15–16 years before the PET scans. 30 individuals (IR+ group) belonged to the highest tertile of HOMA-IR in the Health 2000 study (HOMA-IR>2.16). The control group consisted of those belonging to the lowest tertile of HOMA-IR (IR- group, HOMA-IR<1.24). 50 % of participants in both groups were APOEε4 genotype carriers (ε4/ε4 or ε3/ε4). None of the participants had diabetes at baseline. The -PIB-PET scans were analyzed visually and rated as PIB+/PIB-.

Results: As expected, APOEε4 genotype was a greater risk factor for amyloid accumulation than insulin resistance. Insulin resistance in midlife increased the risk for amyloid accumulation both in APOEε4 carriers and non-carriers. In the IR-/APOEε4- group 2/15 (13.3 %) were PIB positive; in the IR+/APOEε4- 3/15 (20.0 %); in the IR-/APOEε4+ 10/15 (66.7 %), and in the IR+/APOEε4+ 12/15 (86.7 %).

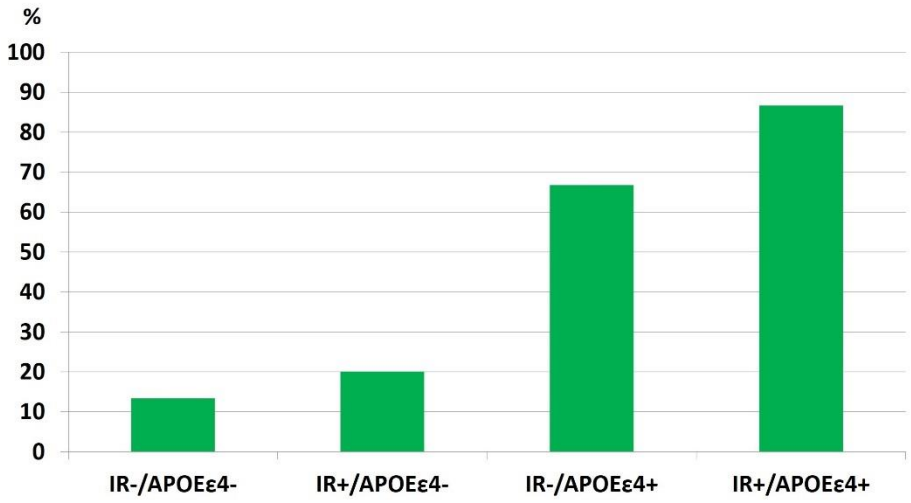

Conclusions: The preliminary analysis of our PET data shows that insulin resistance in midlife is an additive risk factor for brain amyloid accumulation later in life both in non-carriers and carriers of APOEε4 genotype.

Keywords: Alzheimer´s disease, insulin resistance, PIB-PET imaging, beta-amyloid, APOE-epsilon4 genotype

Imaging tau deposition in the Lewy body diseases

Stephen Gomperts[1], Joseph Locascio[1], Sara Makaretz[1], Aaron Schultz[2], Christina Caso[4], Vasdev Neil[2], Reisa Sperling[1,3], John Growdon[1], Brad Dickerson[1], Keith Johnson[1,2]

[1]Department of Neurology, Massachusetts General Hospital, Harvard Medical School, Boston, MA, USA
[2]Department of Radiology, Massachusetts General Hospital, Harvard Medical School, Boston, MA, USA
[3]Center for Alzheimer Research and Treatment, Brigham and Women's Hospital, Harvard Medical School, Boston, MA, USA
[4]Department of Radiology, University of Washington, Seattle, WA, USA

Background: Although Lewy body inclusions define the Lewy body diseases - dementia with Lewy bodies (DLB), Parkinson disease (PD), and Parkinson disease dementia (PDD), Alzheimer's disease (AD) pathological changes of intracellular tau and extracellular amyloid deposition are also commonly observed. Neuropathological studies have implicated tau pathology in cognitive impairment in both DLB and PD. We set out to evaluate the contribution of tau pathologic changes to these diseases during life using Flortaucipir (FTP) PET and to relate FTP retention to PiB binding and cognitive function.

Methods: Twenty-four patients with Lewy body disease - 7 DLB (age 68±2 years), 8 PD with cognitive impairment (PD-impaired, age 72±2 years), and 9 PD without cognitive impairment (PD-normal, age 67±3 years) - underwent FTP PET, PiB PET, and MRI, along with neurologic and neuropsychological evaluation, and were contrasted with an independently acquired group of 29 normal control subjects with minimal amyloid burden (age 69±2 years) . FTP retention was expressed as the SUVR using a cerebellar gray reference. PiB retention was expressed as the DVR using a cerebellar reference.

Results: FTP cortical uptake in DLB subjects exceeded NC, particularly in the inferior temporal gyrus and precuneus. Foci of elevated FTP binding were also observed in PD-impaired subjects, in a similar distribution, but not in PD-normal subjects. Four of seventeen Lewy body disease subjects had elevated FTP binding despite low cortical PiB uptake. FTP binding in the inferior temporal gyrus and precuneus correlated with MMSE and Clinical Dementia Rating scale sum-of-boxes-scores.

Conclusion: Cortical tau deposits are common in DLB and PD-impaired subjects, in an anatomical distribution reminiscent of AD, and contribute to cognitive impairment. In contrast with AD, it appears that high levels of amyloid burden are not necessary for tau deposition in the Lewy body diseases.
Keywords: Lewy, DLB, tau, Flortaucipir, amyloid

Nonfluent variant of primary progressive aphasia: Tau deposition in the language network

Belen Pascual[1], Paolo Zanotti-Fregonara[1], Quentin Funk[1], Elijah Rockers[1], Neha Pal[1], Meixiang Yu[2], Bryan Spann[1], Paul Schulz[3], Joseph C Masdeu[1]

[1]Department of Neurology, Houston Methodist Research Institute, Weill Cornell Medical College, Houston, TX, USA
[2]PET Core, Houston Methodist Research Institute, Weill Cornell Medical College, Houston, TX, USA
[3]Department of Neurology, UT Physicians, Houston, TX, USA

Background: The sporadic nonfluent/agrammatic variant of primary progressive aphasia (nfvPPA) is characterized by impaired speech sound production and distorted grammar. The core of the initial damage is localized to Broca's area. Tau imaging using ^{18}F-AV-1451 PET provides a unique opportunity to determine the brain distribution of tau deposition in this syndrome.

Methods: We evaluated with ^{18}F-AV-1451 PET six patients with nfvPPA and six normal controls. Both patients and controls were amyloid-negative, and they did not differ significantly in age and sex (nfvFTD: n = 6, 3 women, mean age = 64.2 ± 5.9; controls: n = 6, 3 women, mean age = 68.8 ± 7.6). ^{18}F-AV-1451 images from 80 to 100 min were averaged, and standardized uptake value ratios were calculated using the mean activity in the cerebellar gray matter as the reference region. Additionally we determined functional connectivity with BOLD MRI in a group of 35 healthy volunteers group-matched to the patients, using as seed the volume of the largest tau cluster in the nfvPPA group.

Results: On voxel-wise analysis and compared to controls, patients with nfvPPA had increased tau uptake ($p < 0.001$ uncorrected) in two major clusters. The larger cluster was in Broca's area. The smaller cluster was located in the planum temporale of the superior temporal gyrus, extending to the supramarginal gyrus (Wernicke's area). As expected, on the MRI functional connectivity study, the seed in the location of the larger tau cluster showed the most significant connectivity with a region located in the same area as the smaller tau cluster.

Conclusions: In nfvPPA, ^{18}F-AV-1451 PET showed abnormal tau deposition not only in Broca's area, but also, and separately, in Wernicke's area. This study provides direct *in vivo* evidence of network tau propagation in humans, postulated to occur in these neurodegenerative disorders and already documented in animal models.
Keywords: Primary Progressive Aphasia, Language, 18F-AV-1451, Frontotemporal Dementia

Longitudinal decrease of white matter PiB uptake in aging and Alzheimer's disease

Yi Su[1], Kewei Chen[2], Eric Reiman[2], John Morris[1], Tammie Benzinger[1]

[1]*Washington University in St. Louis School of Medicine, St. Louis, MO, USA*
[2]*Banner Alzheimer's Institute, Phoenix, AZ, USA*

Background: A number of recent studies reported that when WM as by itself, or part of, the reference region to quantify cerebral amyloid burden, improved sensitivity to longitudinal changes can be achieved. Hence, using WM as the reference region to quantify amyloid PET data is gaining popularity in aging and Alzheimer disease (AD) research community. On the other hand, lower white matter PiB binding is reported in regions with myelin damage in the context of multiple sclerosis. In this study we examine the longitudinal amyloid tracer binding in white matter regions.

Methods: A total of 183 participants (112 female; 64 APOE4 carriers; age 45~86; 137 amyloid negative and CDR=0 ; 36 amyloid positive and CDR=0 ; 10 CDR>0) from our local memory and aging studies who had longitudinal PiB imaging data were included in this preliminary analysis. Quantification of PiB PET imaging data was performed using standard procedure based on region of interest defined using T1-weighted MR scan during the same period and with cerebellar cortex as the reference region.

Results: Significant longitudinal decreases ($p<0.05$) in white matter SUVR was observed for the whole group ($p=1.34\times10^{-6}$), normal control ($p=1.09\times10^{-4}$), preclinical AD ($p=0.029$), and the cognitively impaired group ($p=4.35\times10^{-3}$) (Figure 1). The results hold with or without partial volume correction.

Conclusion: Longitudinal decreases in white matter PiB binding is observed in our memory and aging study cohorts, suggesting possible gradual white matter demyelination due to aging and AD pathology. White matter signal in amyloid imaging may serve as a biomarker for white matter integrity and the validity of using white matter as the reference region needs further investigation.

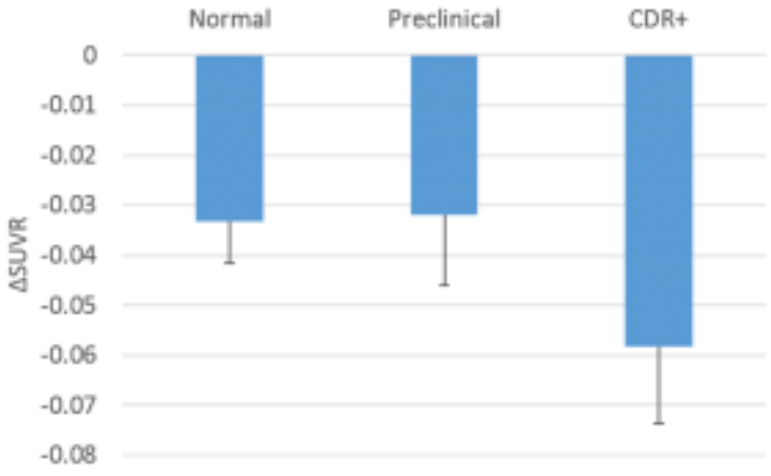

Figure 1. Longitudinal white matter SUVR changes in normal control, preclinical AD, and CDR+ groups.

Keywords: Amyloid imaging, PET, white matter

18F-AV-1451 and 11C-PIB PET do not explain impairment in Parkinson's disease

Joseph Winer[1], Peter Pressman[2], Jordan Stiver[2], Anne Maass[3], Daniel Schonhaut[2], Joel Kramer[2], Gil Rabinovici[2], William Jagust[3]

[1]*Department of Psychology, University of California, Berkeley, Berkeley, CA, USA*
[2]*Department of Neurology, Memory and Aging Center, University of California, San Francisco, San Francisco, CA, USA*
[3]*Helen Wills Neuroscience Institute, University of California, Berkeley, Berkeley, CA, USA*

Background: Multiple pathologies contribute to impairment in Parkinson's disease (PD), including Lewy bodies, cerebrovascular disease, and Alzheimer's disease (AD). Emerging studies have reported increased tau deposition in PD dementia, but tau has not been characterized in cognitively normal PD and PD with mild cognitive impairment.

Methods: Here we compared *in vivo* AV-1451 and PIB retention in cognitively normal patients with PD (PD-CN, N=15, age 67 ± 6.6), PD patients with mild cognitive impairment (PD-MCI, N=14, age 67 ± 4.9), and PIB positive and negative normal controls (NC-PIB+, N=29, age 75 ± 4.7; NC-PIB-, N=29, age 77 ± 3.86). ^{18}F-AV-1451 SUVRs (80-100 min, cerebellar gray reference) were normalized to template space for voxel-wise group contrasts, and regions of interest (ROIs) that paralleled AD Braak stages were created in native space using FreeSurfer. A global cortical ^{11}C-PIB DVR index was calculated for each subject.

Results: Six PD patients (21%, 1 PD-MCI, 5 PD-CN) were PIB positive and 23 PIB negative. Voxel-wise contrasts between PD-CN and PD-MCI, and additionally between PD and PIB- controls, did not reveal significant differences. AV-1451 binding did not differ between PD-MCI and PD-CN in AD Braak stages I/II, III/IV, or V/VI, and did not differ from PIB- healthy older adults (**Figure 1**). PD PIB+ and PD PIB- AV-1451 binding differed significantly in Braak stages III/IV and V/VI (**Figure 2**). PD PIB+ binding was similar to PIB+ controls, while PD PIB- binding was similar to PIB- controls.

Conclusions: These findings suggest that patterns of cortical Aβ and tau do not differ in PD-CN, PD-MCI, and healthy older adults. Age, Aβ, and tau do not differentiate PD-CN and PD-MCI. Tau deposition is related to Aβ status and age in both PD and healthy older adults. Cognitive deficits in PD-MCI do not appear to reflect AD pathology.

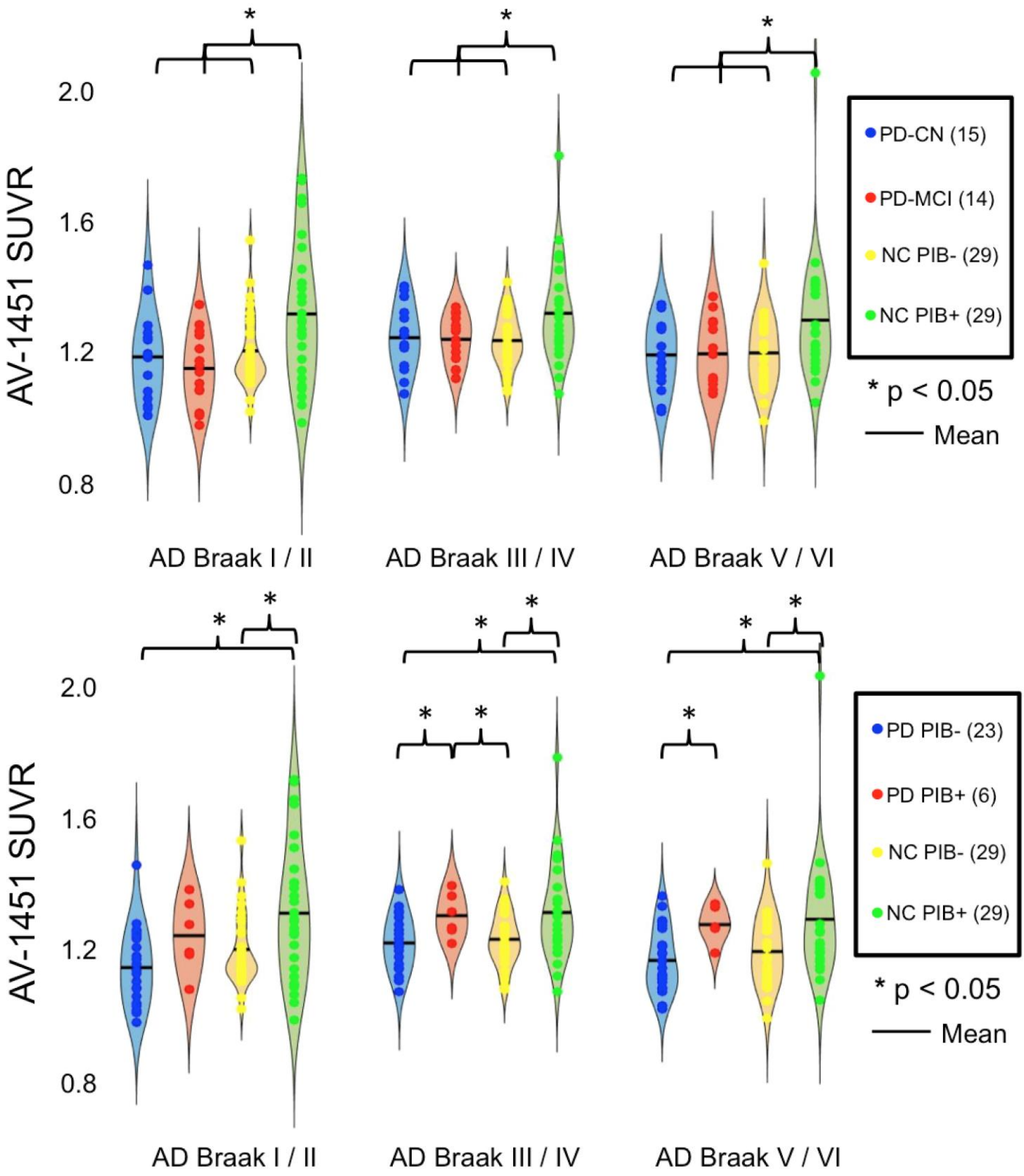

Keywords: Parkinson's disease, PD-MCI, tau, AV-1451, PIB

Longitudinal tau-PET imaging using [18F]AV-1451 in progressive supranuclear palsy

Jennifer Whitwell[1], Val Lowe[1], Bradley Boeve[1], Kejal Kantarci[1], Matthew Senjem[1], Nirubol Tosakulwong[1], Christopher Schwarz[1], Anthony Spychalla[1], Ronald Petersen[1], Clifford Jack[1], Keith Josephs[1]

[1]*Mayo Clinic, Rochester, MN, USA*

Background: Positron emission tomography (PET) imaging using a tau ligand could be a valuable biomarker of disease progression in a primary tauopathy like progressive supranuclear palsy (PSP), although it is unknown whether longitudinal change in tau-PET signal can be detected in PSP.
Methods: We performed serial tau-PET imaging using the AV-1451 ligand in two patients with PSP. Median AV-1451 uptake was calculated for six subcortical and brainstem regions (midbrain, dentate nucleus of the cerebellum, thalamus, pallidum, putamen, and caudate nucleus) and four cortical regions (supplementary motor cortex, precentral cortex, postcentral cortex and superior frontal cortex) that are typically involved pathologically in PSP. To account for age-associated confounds, regional values were converted into age-corrected z-scores representing difference from 71 healthy controls. The PSP patients were also compared to four reference subjects who had a non-PSP clinical diagnosis and had also undergone serial tau-PET scans at our institution.
Results: An increase in tau-PET signal over time was observed in all the subcortical and brainstem structures, except for the caudate nucleus, in PSP. Both PSP subjects showed an increased tau-PET signal over time in midbrain, dentate nucleus of the cerebellum, and thalamus, with one of the PSP subjects also showing an increase in signal over time in the pallidum and putamen (Figure). The PSP patients also showed greater involvement of the subcortical and brainstem structures than the four reference subjects. In contrast, no consistent increase over time in tau-PET signal was observed in the four cortical regions in PSP.
Conclusions: This data provides evidence that tau-PET measurements of subcortical and brainstem structures could prove to be useful longitudinal biomarkers in PSP.

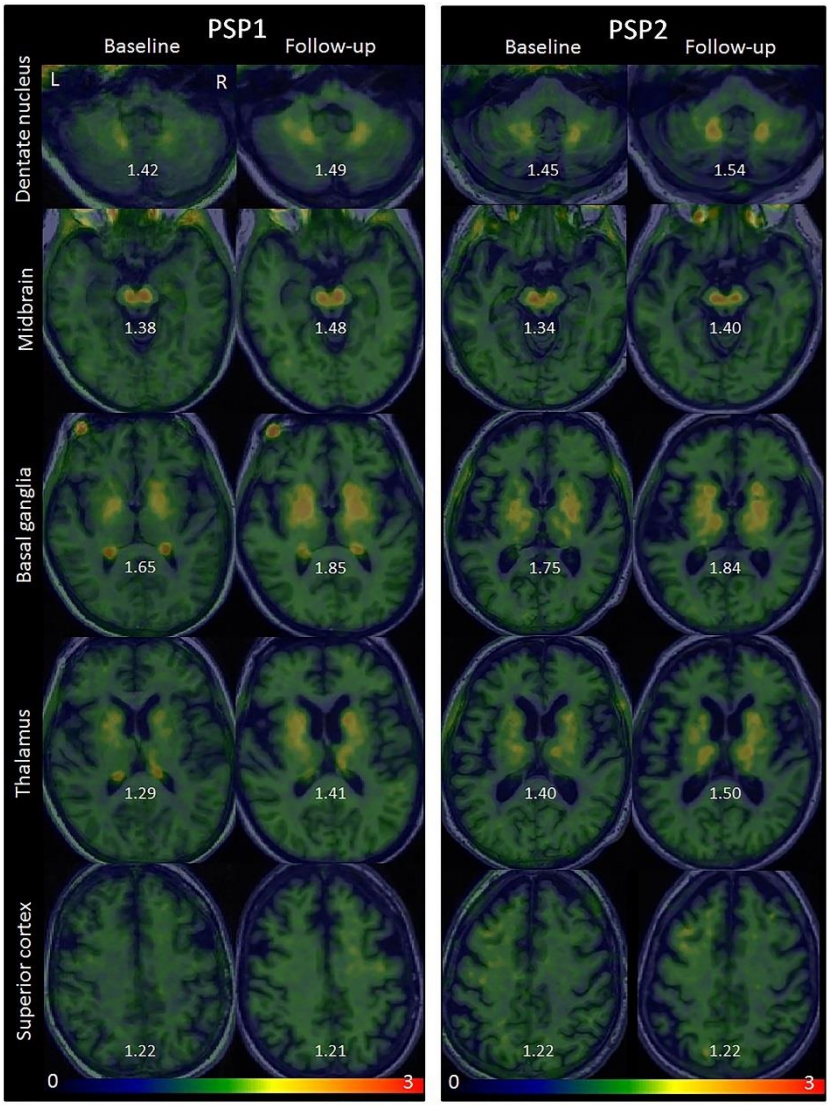

Longitudinal tau-PET scans in two patients with PSP

Keywords: tau, PET, progressive supranuclear palsy, serial

Pittsburgh compound-B PET and MRI biomarkers of cognition in aging multiple sclerosis patients

Burcu Zeydan[1,2], Val J. Lowe[1], Scott A. Przybelski[3], Christopher G. Schwarz[1], Nirubol Tosakulwong[3], Samantha M. Zuk[1], Matthew L. Senjem[4], Jeffrey L. Gunter[4], Rosebud O. Roberts[2], Michelle M. Mielke[2], Eduardo E. Benarroch[2], Moses Rodriguez[2], Mary M. Machulda[5], Timothy G. Lesnick[3], David S. Knopman[2], Ronald C. Petersen[2], Clifford R. Jack Jr[1], Kejal Kantarci[1], Orhun H. Kantarci[2]

[1]*Mayo Clinic College of Medicine, Department of Radiology, Rochester, MN, USA*
[2]*Mayo Clinic College of Medicine, Department of Neurology, Rochester, MN, USA*
[3]*Mayo Clinic College of Medicine, Department of Health Sciences Research, Rochester, MN, USA*
[4]*Mayo Clinic College of Medicine, Department of Information Technology, Rochester, MN, USA*
[5]*Mayo Clinic College of Medicine, Department of Psychiatry and Psychology, Rochester, MN, USA*

Background/Objective: Advanced MRI techniques used in imaging myelin of brain parenchyma are not myelin-specific. In contrast, amyloid tracers such as cortical Pittsburgh compound-B (PiB) are recently shown to target myelin. We studied the association of cognitive function with thalamic volume, lobar cortical thickness PIB positron emission tomography (PET) and white matter (WM) PiB binding as a potential myelin marker in an aging MS population.

Design/Methods: In the population-based Mayo Clinic Study of Aging, 24 of 4869 participants had MS, with a subset who underwent brain MRI (n=16) and PiB-PET (n=12). One MS patient fulfilled criteria for mild cognitive impairment while another fulfilled criteria for dementia and neither had PiB-PET. Controls from the same cohort were age- and sex-matched (5:1) to MS patients. Quantitative image analyses were performed using automated or semi-automated image processing pipelines.

Results: MS patients had lower cognitive z-scores for memory (p=0.03) and language (p=0.02) than controls. MS patients had smaller thalamic volumes (p=0.003), thinner temporal cortices (p=0.001) and thinner frontal cortices (p=0.045) than controls. Thalamic volume loss was associated with decreased attention-executive performance (p=0.02). PiB uptake was reduced in areas of WM hyperintensities compared to normal appearing WM in MS (p=0.0002) and controls (p<0.0001). Reduced PiB uptake in areas of WM hyperintensities was associated with decreased visuospatial performance in MS (p=0.02). There was no difference in global cortical PiB standardized uptake value ratios between MS and controls (p=0.39).

Conclusions: Late MS is characterized by reduced cognitive performance, cortical and thalamic atrophy, but normal PiB uptake in the cortex. The frontal and temporal multimodal association areas interconnected via a large number of WM tracts are prone to damage in MS. The correlation between thalamic atrophy and lower attention-executive function likely reflects WM injury in thalamo-cortical projections. The correlation between PiB-PET and visuospatial processing may reflect injury to association area connectivity.
Keywords: Pittsburgh compound-B, PET, multiple sclerosis, myelin, cognition

Improved estimation of gray matter volume in presence of white matter hyperintensities in Alzheimer's and Down syndrome studies with amyloid burden

Dana Tudorascu[1], Helmet Karim[1], Lea Alhilali[2], Patrick Lao[3], Tobey Betthauser[3], Erica Tamburo[1], Rebecca Maccloud[1], Jeffrey James[1], Davneet Minhas[1], Annie Cohen[1], Beth Snitz[1], Julie Price[4], Brian Lopresti[1], Chet Mathis[1], Oscar Lopez[1], Sterling Johnson[3], Ciprian Crainiceanu[5], Ben Handen[1], Brad Christian[3], Howard Aizenstein[1], William Klunk[1]

[1]*University of Pittsburgh, Pittsburgh, PA, USA*
[2]*Barrow Neurological Institute, Phoenix, AZ, USA*
[3]*University of Wisconsin, Madison, WI, USA*
[4]*Athinoula A. Martinos Center, Harvard Medical School, Charlestown, MA, USA*
[5]*Johns Hopkins University, Baltimore, MD, USA*

Introduction: White matter hyperintensities (WMHs) appear as hyperintense areas in magnetic resonance imaging (MRI). WMHs present a challenge for standard segmentation algorithms that misclassify WMHs as gray matter (GM). Our objective was to investigate tissue class segmentation in two longitudinal samples: Down syndrome (DS, 3 years) and Alzheimer's disease (AD, 6 years).
Methods: Gray matter volume (GMV) was obtained in 39 ADs (14 PiB+) and 28 DS (13 PiB+) with three methods: *1) Standard*: MPRAGES are segmented into six tissue types: GM, white matter (WM), cerebrospinal fluid, and 3 non-brain tissues (SPM12); *2) Multi-spectral*: MPRAGE and FLAIR are used in the segmentation for more accurate classification; *3) Fill*: A WMH mask is obtained from FLAIR (Wu et. Al, 2006), MPRAGEs are filled with normal appearing WM, which are then segmented. GMV is computed (max of probabilities among tissue maps) for each subject, within each method. The GMV is compared using a repeated measures model with a fixed effect of method, time, PiB status and a random subject effect. To assess accuracy between methods, a neuroradiologist case investigation is presented in Figure1.
Results: AD Study: Statistically significant differences were detected in GMV between the segmentation methods ($p<0.0001$), time ($p<0.0001$), and PiB status ($p=0.0002$) (Tables1.1, 1.2) with higher mean GMV for standard and fill method and lower for multi-spectral. DS study: Statistically significant differences were detected between GMV from different methods ($p<0.0001$) (Tables2.1, 2.2) with higher mean GMV for standard and fill method and lower for multi-spectral.
Conclusion: Our results suggest that GMV is more precisely estimated in the presence of WMH using fill or multispectral techniques. Without correctly accounting for WMH, GMV could be overestimated, thus affecting the analysis and conclusions. Moreover, in studies with heavy amyloid burden, additional caution should be taken due to differences between PiB

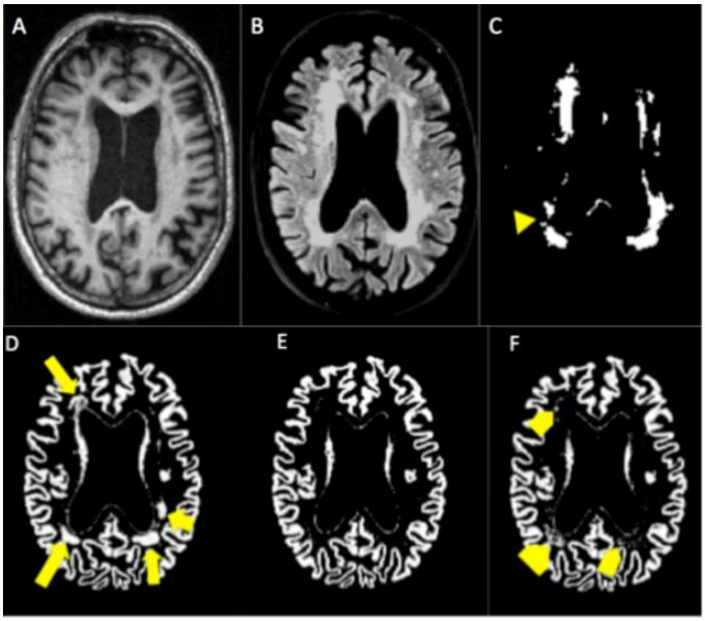

Figure 1. (A) MPRAGE at the level of the a lateral ventricle. (B) FLAIR image demonstrating WMH predominantly in the periventricular and deep white matter.(C) WMH map demonstrates excellent concordance with the FLAIR WMH, with the small exception of slight underestimation in the right posterior periventricular region (yellow arrowhead). (D)Standard segmentation, demonstrating large regions of periventricular WMH classified as gray matter around the frontal horn of the right lateral ventricle and in the posterior periventricular regions bilaterally (yellow arrow). (E) Multispectral: no misclassification of WMH as GM. (F) Fill: demonstrating small areas of WMH misclassified as GM, predominantly in the right posterior periventricular white matter, but also punctate regions in the left posterior periventricular white matter and around the right frontal horn (square yellow arrowheads). Segmentations were all performed using SPM12.

groups in GMV.

Table 1.1. AD study results (Descriptive statistics):

PiB status/Method	PiB (+)		PiB (-)	
	GMV Time 1 (n=15)	GMV Time 2 (n=4)	GMV Time 1 (n=25)	GMV Time 2 (n=9)
Standard	488.83 (88.80)	472.70 (45.30)	483.01 (54.05)	457.14 (39.08)
Multispectral	478.93 (82.73)	459.30 (46.02)	470.72 (49.77)	445.37 (32.87)
Fill	491.47 (90.51)	480.16 (42.70)	481.63 (55.51)	454.55 (34.54)

Results are in mL and presented as mean (sd).

Table 1.2. AD study results (Model estimates):

Effect	β (SE)	T (df)	p-value	95% CI for β
Intercept	580.73 (11.41)	42.13 (46.8)	<0.0001	(457.77, 503.69)
Fill (Standard=ref)	0.22 (1.66)	0.13 (115)	0.78	(-3.07, 3.52)
Multispectral (Standard=ref)	-11.61 (1.66)	-6.98 (115)	<0.0001	(-14.90, -8.31)
PiB Status (PiB (-)=ref)	-27.04 (9.75)	-3.88 (136)	0.0002	(-40.80, -13.27)
Time (Time 2=ref)	14.65 (2.00)	7.29 (117)	<0.0001	(14.83, 25.77)

β coefficient for the method represents the difference in GMV mean between standard segmentation (reference method) and each other method when time and PiB status are fixed; β coefficient for the PiB status represents the difference in GMV mean between PiB (+) and PiB (-) when time and volume are fixed; β coefficient for time represents the difference in GMV mean between Time 1 and Time 2 when method and PiB status is fixed. GMV were computed by counting the number of voxels in which the GM tissue class was the highest (compared to other tissue), multiplying by their dimension and dividing by 1000 to represent it in mL.

Table 2.1. DS study results (Descriptive statistics):

PiB status/Method	PiB (+)		PiB (-)	
	GMV Time 1 (n=15)	GMV Time 2 (n=7)	GMV Time 1 (n =13)	GMV Time 2 (n=8)
Standard	524.03 (41.73)	459.28 (67.44)	499.92 (62.67)	523.11 (49.28)
Multispectral	417.30 (119.36)	416.29 (59.19)	446.74 (41.35)	439.83 (66.92)
Fill	511.24 (46.41)	458.81 (67.74)	499.77 (62.87)	523.11 (49.18)

Results are in mL and presented as mean (sd).

Table 2.2. DS study results (Model estimates):

Effect	β (SE)	T (df)	p-value	95% CI for β
Intercept	505.16 (16.25)	31.08 (60.6)	<0.0001	(472.66, 537.67)
Fill (Standard=ref)	-3.99 (9.66)	-0.41 (96.7)	0.68	(-23.18, 15.19)
Multispectral (Standard =ref)	-73.25 (9.66)	-7.58 (96.7)	<0.0001	(-92.44, -54.06)
PiB Status (PiB (-)=ref)	-6.44 (16.81)	-0.38 (59.9)	0.70	(-40.06, 27.17)
Time (Time 2=ref)	5.61 (9.66)	0.58 (115)	0.56	(-13.54, 24.74)

β coefficient for the method represents the difference in GMV mean between standard segmentation (reference method) and each other method when time and PiB status are fixed; β coefficient for the PiB status represents the difference in GMV mean between PiB (+) and PiB (-) when time and volume are fixed; β coefficient for time represents the difference in GMV mean between Time 1 and Time 2 when method and PiB status is fixed. GMV were computed by counting the number of voxels in which the GM tissue class was the highest (compared to other tissue), multiplying by their dimension and dividing by 1000 to represent it in mL.

Keywords: improved segmentations in amyloid (+), GM overestimation in presence of WMH,

Global white matter diffusion characteristics predict longitudinal cognitive change independently from amyloid accumulation in older adults

Jennifer S. Rabin[1], Rodrigo Perea[4], Rachel Rachel Buckley[3,5,6], Keith A. Johnson[3,4], Reisa A. Sperling[3,4,5], Trey Hedden[2,4]

[1]*Department of Psychiatry, Massachusetts General Hospital, Boston, MA, USA*
[2]*Department of Radiology, Massachusetts General Hospital, Boston, MA, USA*
[3]*Department of Neurology, Massachusetts General Hospital, Boston, MA, USA*
[4]*Athinoula A. Martinos Center for Biomedical Imaging, Department of Radiology, Massachusetts General Hospital, Charlestown, MA, USA*
[5]*Florey Institute of Neuroscience and Mental Health, University of Melbourne, Melbourne, Australia*
[6]*Melbourne School of Psychological Sciences, University of Melbourne, Melbourne, Australia*
[7]*Center for Alzheimer Research and Treatment, Department of Neurology, Brigham and Women's Hospital, Harvard Medical School, Boston, MA, USA*

Objective: Reduced white matter integrity has been proposed as one explanation for age-related cognitive decline. Here, we examined (1) whether diffusion characteristics of global versus tract-specific white matter predicted longitudinal cognitive decline in healthy older adults and (2) whether white matter diffusion characteristics affected cognition independently from amyloid accumulation or white matter hyperintensities (WMH).

Methods:: Pittsburgh Compound B–positron emission tomography and diffusion tensor imaging (DTI) were performed at baseline in 259 clinically normal older adults (aged 63 – 89) from the Harvard Aging Brain Study. DTI data were processed with Tract-Based Spatial Statistics. Global white matter diffusion was measured as mean fractional anisotropy (FA) across the whole white matter skeleton. Tract-specific diffusion was measured as mean FA for 8 major white matter tracts. Factor scores derived from neuropsychological tests represented processing speed, executive function, and episodic memory. Baseline age, gender and education and their interactions with time were controlled in each model.

Results: Linear mixed models found that global white matter FA at baseline predicted longitudinal changes in processing speed and episodic memory but not executive function. After accounting for global white matter FA, no individual tracts significantly predicted a change in any cognitive domain. Next, we investigated whether the relationship between global white matter FA and cognitive change (for processing speed and memory) was independent of amyloid and WMH. In these models, global white matter FA remained a significant predictor of episodic memory and processing speed over time; amyloid significantly predicted a change in episodic memory, but not processing speed; and WMH did not predict a change in either domain.

Conclusion: These findings suggest that longitudinal changes in episodic memory and processing speed are associated with global, rather than tract-specific, white matter diffusion characteristics and that white matter FA and amyloid accumulation independently predict cognitive change.
Keywords: white matter, DTI, amyloid, cognition, white matter hyperintensities

[18F]AV1451 tau PET distinguishes PSP from controls and Parkinson's disease

Daniel Schonhaut[1], Corey McMillan[2], Brad Dickerson[3], Andrew Siderowf[4], Michael Devous[4], Richard Tsai[1], Joe Winer[5], David Russell[6], Irene Litvan[7], Erik Roberson[8], Joel Kramer[1], Peter Pressman[1], Ilya Nasrallah[2], Suzanne Baker[9], Stephen Gomperts[3], Keith Johnson[3], Murray Grossman[2], William Jagust[9], Adam Boxer[1], Gil Rabinovici[1]

[1]*University of California San Francisco Memory & Aging Center, San Franscisco, CA, USA*
[2]*Dept. of Neurology, University of Pennsylvania Perelman School of Medicine, Philadelphia, PA, USA*
[3]*Dept. of Neurology, Harvard Medical School, Boston, MA, USA*
[4]*Avid Radiopharmaceuticals, Philadelphia, PA, USA*
[5]*Helen Wills Neuroscience Institute, University of California Berkeley, Berkeley, CA, USA*
[6]*Institute for Neurodegenerative Disorders, New Haven, CT, USA*
[7]*Dept. of Neurology, University of California San Diego, San Diego, CA, USA*
[8]*Dept. of Neurology, University of Alabama Birmingham, Birmingham, AL, USA*
[9]*Lawrence Berkeley National Laboratory, Berkeley, CA, USA*

Background: AV1451 binds selectively to neurofibrillary tangles in Alzheimer's disease, but studies assessing post-mortem binding to tau aggregates in progressive supranuclear palsy (PSP) have yielded mixed results. We compared *in vivo* AV1451 retention in patients with PSP (N=33, 12% Aβ PET+) compared to normal controls (NC, N=46, all Aβ PET-) and patients with Parkinson's disease (PD, N=26, 19% Aβ PET+).
Design/methods: Participants were recruited in Avid-sponsored multi-site imaging trials (NCT #02167594 and #02016560) and independent studies at UCSF/LBNL and MGH **(Figure 1)**. 80-100 mean AV1451 images were co-registered to subject-specific T1-weighted MRI, and SUVR images were derived referencing cerebellar gray matter (excluding dentate nucleus, DN). Voxel-wise and region-of-interest group comparisons were performed in template space (SPM12), covarying for age. Receiver Operator Characteristic (ROC) analyses were performed to assess single-subject discrimination.
Results: On voxel-wise analysis, PSP showed elevated binding compared to NC and PD in bilateral globus pallidus (GP), dorsal midbrain, subthalamic nucleus (STN), and DN (p(FWE)<0.05, **Figure 2**). Mean SUVR were increased in PSP vs. NC and PD in GP, STN and DN (p<0.001), and in PSP vs. PD in substantia nigra (SN, p<0.001) **(Figure 3)**. There were no differences in AV1451 retention between PD and NC. On ROC analyses, Areas Under the Curve were 0.862 for PSP vs. NC (sensitivity 84.8% specificity 78.3%) and 0.879 for PSP vs. PD (sensitivity 90.9%, specificity 80.8%). Regional and voxel-wise AV1451 SUVR did not correlate with disease severity as measured by PSP Rating Scale.

Figure 1

	N	Site	Age	Sex	PSPRS
PSP	33	10 UCSF/LBL 19 Avid A09 study 4 MGH	69.6 ± 5.7	23 Male 10 Female	34.7 ± 11.6
PD	26	26 UCSF/LBL	67.1 ± 5.4	14 Male 12 Female	
NC	46	20 UCSF/LBL 17 Avid A05/A09 studies 9 MGH	69.6 ± 5.4	25 Male 21 Female	

PSP-RS: PSP Rating scale (0-100, higher scores relate to worsening disease)

Conclusions: AV1451 uptake is elevated in PSP compared to NC and PD in a pattern that matches the expected distribution of tau aggregates. Longitudinal studies with autopsy confirmation are needed to further assess the utility of AV1451 as a biomarker of tau pathology in PSP and other non-AD tauopathies.

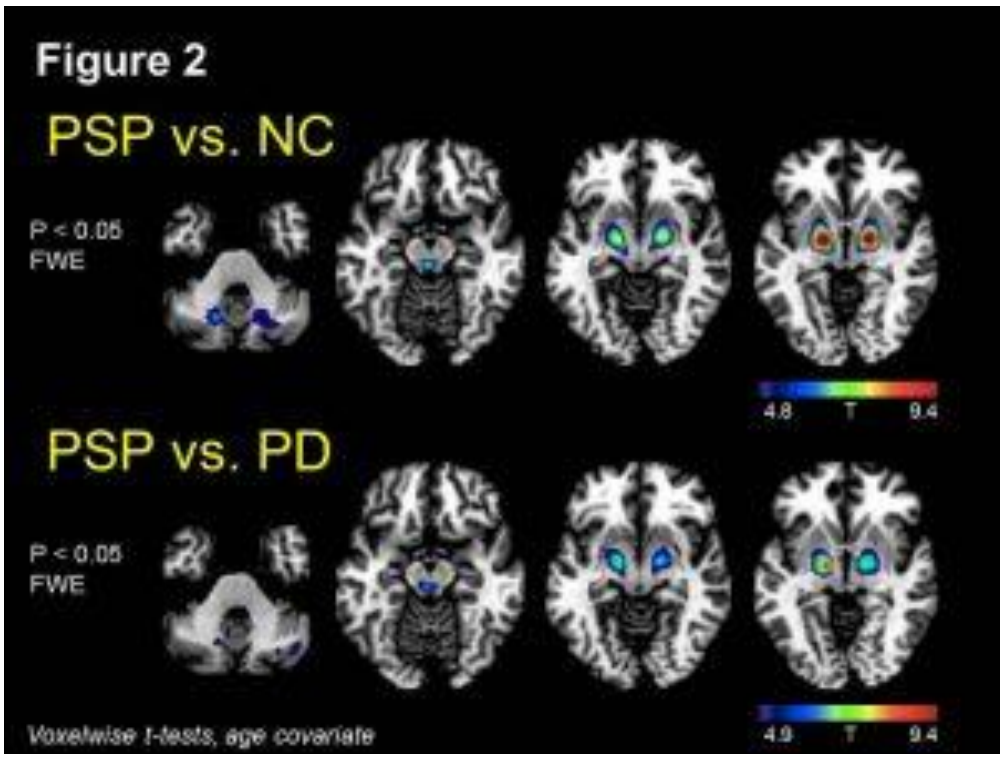

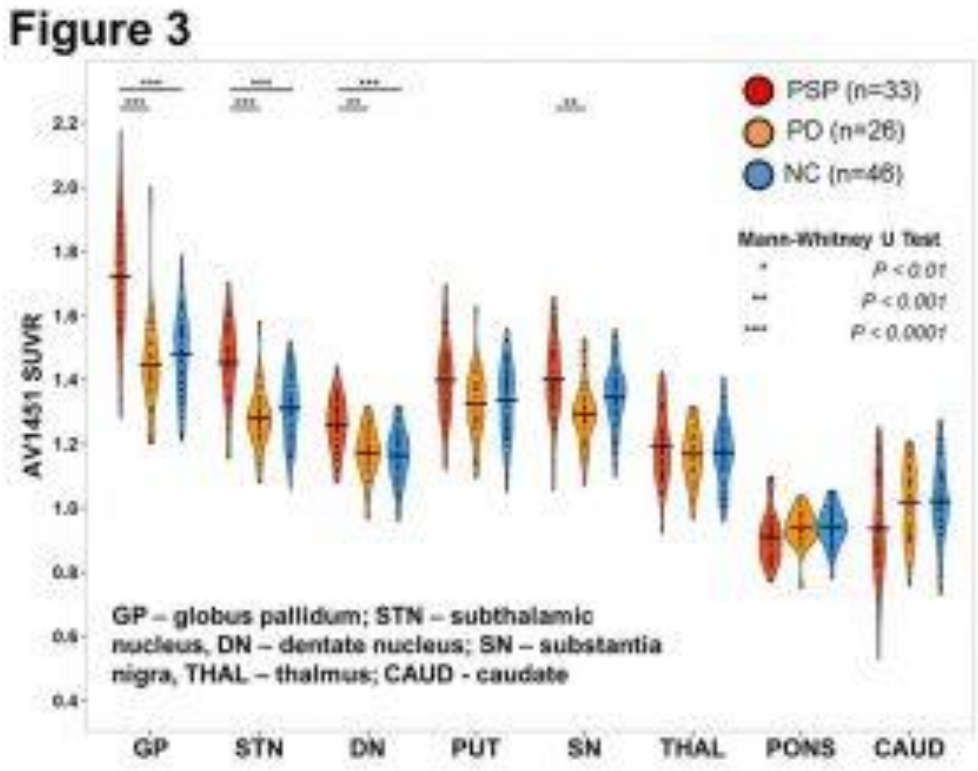

Sponsors: Avid Radiopharmaceuticals, Tau Consortium, Michael J. Fox Foundation.

Keywords: AV1451, PSP, non-AD tauopathies, Parkinson's disease

Antemortem-postmortem correlation of florbetapir (18F) PET amyloid imaging with quantitative biochemical measures of Aβ40 and Aβ42

Thomas Beach, Chera Maarouf, Anthony Intorcia, Lucia Sue, Geidy Serrano, Alex Roher

[1]*Banner Sun Health Research Institute, Sun City, AZ, USA*

Amyloid imaging effectively demonstrates the *in vivo* presence of amyloid-beta (Aß) deposits in the aging human brain but it is still unknown which of the many structural forms and modifications of Aß are detected. In Alzheimer's disease, most amyloid deposits are predominantly composed of Aß ending at amino acid residues Val40 or Ala42. The relative abundance of these two major forms differs between individuals but in general it has been reported that Aß40 is largely restricted to neuritic plaques and larger blood vessels while Aß42 may be deposited in senile plaques and vascular amyloid of all types, and is often the sole component of diffuse plaques. The distinction is important as it is mainly the neuritic plaques that correlate with cognitive impairment while diffuse plaques may be the initial type of Aß deposited. Whether PET amyloid ligands such as florbetapir-^{18}F (Amyvid) are partially or wholly selective for brain deposits of Aß40 or Aß42 is currently unknown. We compared antemortem florbetapir PET cortical/cerebellar signal intensity (SUVr) of 55 subjects with postmortem biochemical (ELISA) measurements employing specific antibodies against Aß1-40 and Aß1-42. Correlation analyses were significant for both Aß40 and Aß42, but were much stronger for Aß42. Despite this, SUVr in these 55 individuals was not dependent on the Aß40/42 concentration ratio. These results suggest that, while florbetapir binds to both species in the human brain, the interaction with Aß42 dominates over that with Aß40. This may be in large part due to the generally higher Aß42 concentrations, but may be partially due to preferential Aß42 binding, possibly due to its higher likelihood to be present in a ß-pleated sheet tertiary structure, or to differences in ß-pleated sheet tertiary or quaternary structure.

Keywords: Alzheimer's disease, autopsy, diagnosis, neuritic plaque, diffuse plaque

Proteomics signatures of Alzheimer's disease: gender differences and relationship to pathological markers

Shantanu Srivatsa[1], Joseph Lucas[1], Murali Doraiswamy[1]

[1]*Duke University, Durham, NC, USA*

Background: Women may have a greater risk for Alzheimer's disease (AD) and there is interest in examining potential gender differences in AD biomarkers. While prior studies have focused on brain imaging or cerebrospinal fluid, there is also a need to validate personalized blood biomarkers.

Methods and results: We analyzed baseline clinical and cognitive data from the Alzheimer's Disease Neuroimaging Initiative (ADNI-1) as well as baseline proteomics data in individuals with MCI, AD or normal cognition. The Biomarkers Consortium Plasma Proteomics Project RBM multiplex data, referred to as the human discovery map, was developed on the Luminex xMAP platform by Rules-Based Medicine (RBM) to contain proteins previously reported in the literature to be altered as a result of cancer, cardiovascular disease, metabolic disorders and inflammation. Details of the assay technology and validation has been described elsewhere. We conducted statistical analyses to examine if there were gender differences in plasma protein signatures and whether such signatures were related to diagnosis and pathological markers.

Conclusions: In initial analyses, a number of protein markers differed by diagnosis and gender. Full results of our analyses and analyses will be presented. Discovering gender specific biomarkers may provide novel mechanistic insights into disease modification in subjects at risk.
Keywords: Proteomics, amyloid, tau, sex differences

Tau PET in subjects at risk for chronic traumatic encephalopathy

Nicolas Andrea[1], Jonathan Alverio[1], Christopher Lee[1], Christopher Nowinski[2], Heidi Jacobs[1], Ann McKee[2], Keith Johnson[1], David Jin[1]

[1]*Departments of Radiology and Neurology, Massachusetts General Hospital, Boston, MA, USA*
[2]*Center for the Study of Traumatic Encephalopathy, Boston University School of Medicine, Boston, MA, USA*

Background: Chronic traumatic encephalopathy (CTE) is a progressive tauopathy resulting from repetitive brain trauma. Tau deposition is widely scattered in neocortical sulci, but by Stage III, medial temporal lobe (MTL) is typically involved. We tested whether MTL tau PET measures were elevated in 10 former american football players with histories of multiple trauma exposure (TE) compared to non-exposed control subjects (CS).

Methods: TE (n=10, aged 45.2 ± 8.7y; 10.4 ± 2.8 football seasons played) and CS (n=10, aged 49.4 ± 7.1y) participants underwent clinical evaluations, MRI, 18F Flortaucipir (FTP)-PET, and PiB-PET. Group differences in FTP SUVR (80-100min) defined individually in 4 MTL ROIs (Freesurfer) were assessed with robust linear regression, adjusting for age.

Results: TE and CS groups were similar in age, education, MMSE, ICV-adjusted total hippocampal volume, and amyloid burden assessed with PiB FLR (all p >0.2), but differed in Ohio State Traumatic Brain Injury score (p<0.05). FTP SUVR was greater in TE compared to CS in parahippocampal gyrus and hippocampus (p<0.05) and at trend level in entorhinal cortex and amygdala (p<0.07) (Figure 1). Age by group interaction was seen in parahippocampal gyrus (p<0.01, CTE>CS), and trending in entorhinal cortex (p<0.1).

Conclusions: These preliminary data suggest that PET measures of tau deposition in MTL may be elevated in individuals with a history of repeated brain trauma, consistent with postmortem observations. While the binding properties of FTP to cortical CTE lesions are at present incompletely understood, our data are consistent with autopsy data in CTE that indicate greater MTL tauopathy than expected for age. While these trauma-exposed participants were non-demented, further evaluations of tau PET in relation to features of putative CTE clinical phenotypes may yield important insights.

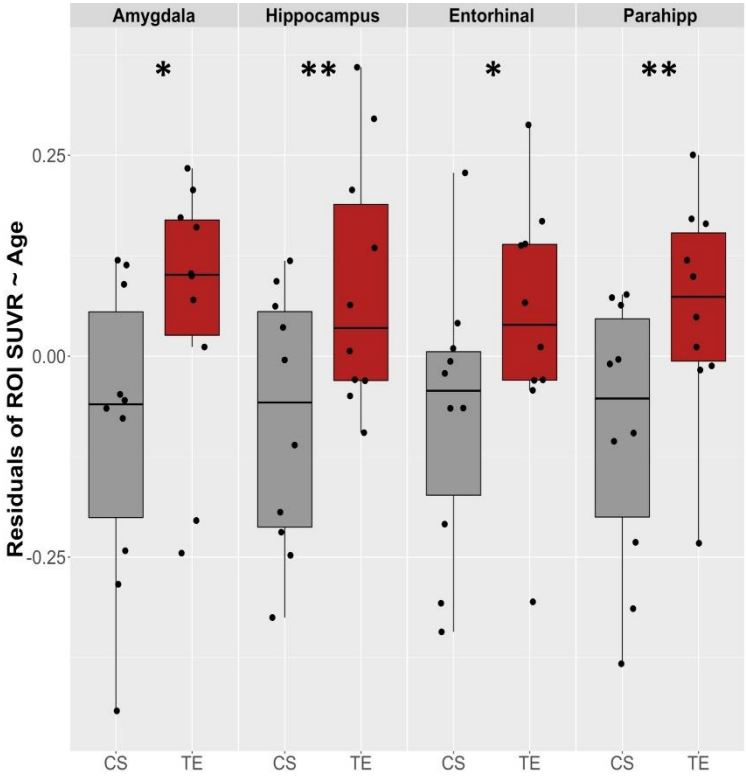

Figure 1: Residuals of MTL ROI SUVR vs age linear regression, plotted against subject group.
* $p < 0.075$
** $p < 0.05$

Keywords: PET, CTE, Tau

PET staging of brain amyloidosis using striatum

Bernard Hanseeuw[1], Rebecca Betensky[2], Beth Mormino[1], Aaron Schultz[1], Kate Papp[1,3], Rachel Buckley[1], Jasmeer Chhatwal[1], Gad Marshall[1,3], Dorene Rentz[1,3], Reisa Sperling[1,3], Keith Johnson[1,3]

[1]*Massachusetts General Hospital, Boston, MA, USA*
[2]*Harvard School of Public Health, Boston, MA, USA*
[3]*Brigham and Women's Hospital, Boston, MA, USA*

Objective: To disentangle neocortical and striatal Aβ contributions to cognitive decline in CN and MCI from HABS and ADNI, and evaluate how much power clinical trials would gain by selectively enrolling participants with striatal amyloidosis.

Methods: We included 643CN and 573MCI with baseline Aβ-PET and longitudinal MMSE over an average 3.3-year follow-up. We classified subjects in three Aβ-Stages. Stage 0: Low-Aβ; Stage1: High-neocortical, low-striatal Aβ; and Stage2: High-neocortical, high-striatal Aβ. We used mixed-models to assess the association between Aβ-Stages and subsequent MMSE decline, adjusting for demographics and cohort. We also tested whether use of a PET staging system including striatal Aβ would improve power in a clinical therapeutic trial.

Results: MMSE declined faster in Stage2-CN (0.28points/y) than in Stage1-CN (0.16points/y; p=0.026) and faster in Stage1-CN than in Stage0-CN (0.04points/y; p=0.002). MMSE declined faster in Stage2-MCI (1.2points/y) than in Stage1-MCI (0.25points/y; p<0.00001) and faster in Stage1-MCI than in Stage0-MCI (0.07points/y; p=0.003). To compare striatal- and neocortical-Aβ contributions within the high-Aβ group, we used a 2-by-2design based on striatum (Stage1/Stage2) and neocortex (high/very high: +/++). Decline rates were 0.17 (Stage1+), 0.43 (Stage1++), 0.65 (Stage2+), and 0.95 (Stage2++) MMSE-points/y. All pairwise comparisons were significant (p<0.050), indicating faster progression associated with high-striatal Aβ (Stage2+) than very high neocortical Aβ (Stage1++). A 300-CN trial (2 arms over 3-year duration; 80% power; alpha=0.05) would detect a drug effect on MMSE (PACC) of 52.8% (30.5%) or greater in Stage2-CN compared to 93.8% (45.9%) in unselected Aβ+. A 300-MCI trial would detect a drug effect on MMSE of 24.7% or greater in Stage2 compared to 51.3% in unselected Aβ+.

Conclusions: Striatal Aβ-PET signal indicates increased risk of subsequent decline amongst high-Aβ non-demented individuals. PET staging including both striatal and neocortical Aβ measures may be useful in the context of anti-Aβ trials as a biomarker of progression, and potentially as an endpoint for assessing drug efficacy.

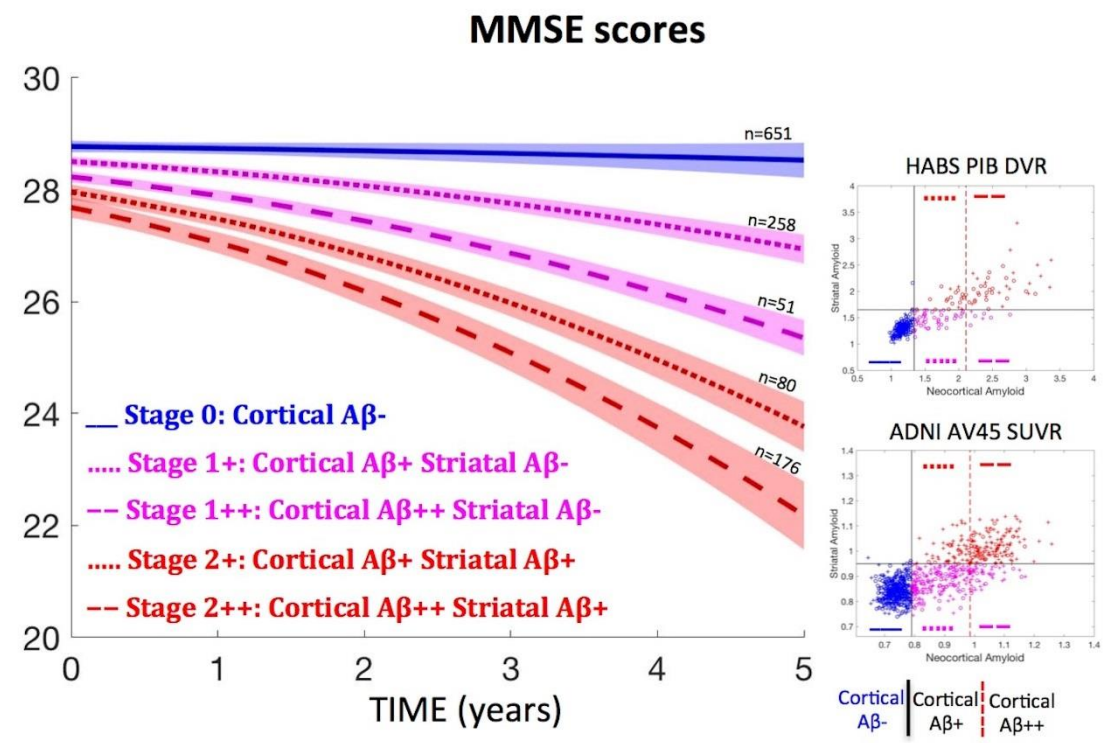

HABS and ADNI, CN and MCI pooled: Total n=1216

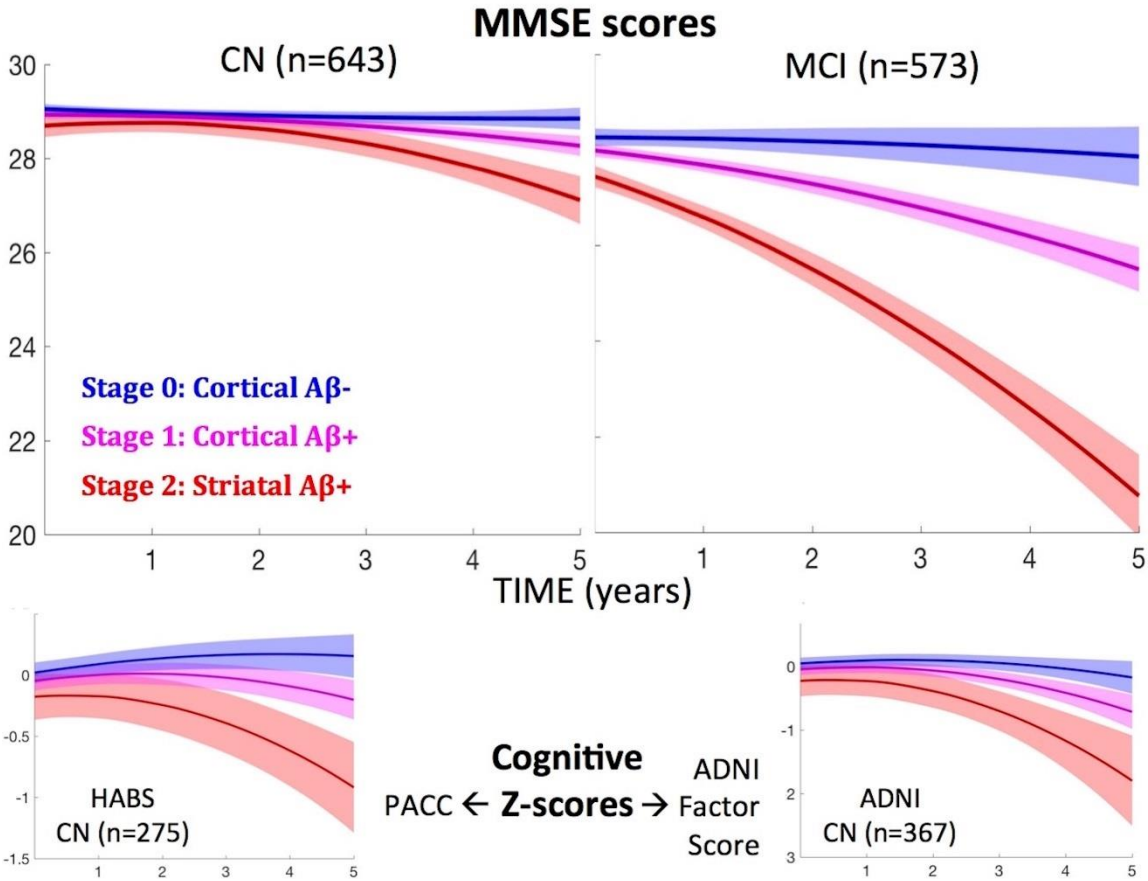

Keywords: Amyloid-PET, Striatum, Clinically normal, Mild Cognitive Impairment, Anti-amyloid therapeutic trial

Tau PET imaging tracks both pathology and brain perfusion in non-AD tauopathies: a multimodal study

Elena Rodriguez-Vieitez[1], Antoine Leuzy[1], Konstantinos Chiotis[1], Laure Saint-Aubert[1], Ove Almkvist[1], Anders Wall[2], Agneta Nordberg[1,3]

[1]Translational Alzheimer Neurobiology, Center for Alzheimer Research, Dept. NVS, Karolinska Institute, Stockholm, Sweden
[2]Section of Nuclear Medicine and PET, Department of Surgical Sciences, Uppsala University, Uppsala, Sweden
[3]Department of Geriatric Medicine, Karolinska University Hospital Huddinge, Stockholm, Sweden

Objectives: We have recently shown that THK5317 tau PET may prove a potential dual biomarker, describing both molecular pathology and brain perfusion in Alzheimer's disease (AD). The aim of this study was to illustrate the dual-use of THK5317 in non-AD tauopathy cases, in relation to biomarkers including glucose metabolism, amyloid and cognition.

Methods: Non-AD patients were recruited, including three patients with clinical diagnoses of frontotemporal dementia, one with semantic dementia, one with corticobasal syndrome (CBS), and two amyloid-negative mild cognitive impairment (MCI) patients. All patients underwent T1 MRI, PET imaging with THK5317, PIB and FDG, and comprehensive neuropsychological assessments. The CBS patient, and one of the amyloid-negative MCIs, were longitudinally followed-up (at 23 and 17 months, respectively) with the same multimodal protocol (except PIB); both were diagnosed as CBS at follow-up. Brain perfusion was estimated using the simplified reference tissue model R_1 and the early-phase (0-3 min) standardized uptake value ratio (SUVR), with cerebellum grey matter (GM) as reference. PET quantification (THK5317 Logan DVR, PIB SUVR, FDG SUVR and perfusion parameters) was performed using the cerebellum GM as reference. Regional and voxel-wise comparisons were performed with respect to groups of young (n=5; 22-28 years) and elderly healthy volunteers (n=4; 60-65 years), and of AD patients (n=20, 60-74 years).

Results: All non-AD patients were amyloid negative (<1.40 SUVR cortical composite PIB PET) and showed heterogeneous brain distributions of THK5317 retention, with significantly greater retention than in young healthy controls. Heterogeneous regional patterns of both hypometabolism and hypoperfusion were observed in these patients, corresponding to their diverse clinical phenotypes.

Conclusion: The findings suggest the usefulness of THK5317 as a dual biomarker, capable of tracking the different pathology and brain perfusion patterns in non-AD patients, and supporting its potential applicability to help discriminate between AD and non-AD tauopathies using a single PET scan.
Keywords: tau; perfusion; tauopathies; corticobasal syndrome; frontotemporal dementia

Hippocampal cingulum integrity predicts change in tau accumulation in a downstream-connected region in amyloid-positive normal older individuals

Heidi Jacobs[1,3], Aaron Schultz[3], Rebecca Amariglio[4], Trey Hedden[3], Kathryn Papp[4], Rodrigo Perea[3], Dorene Rentz[4], Jorge Sepulcre[3], Reisa Sperling[2,3,4], Keith Johnson[1,2,3]

[1]Department of Radiology, Massachusetts General Hospital, Harvard Medical School, Boston, MA, USA
[2]Department of Neurology, Massachusetts General Hospital, Harvard Medical School, Boston, MA, USA
[3]Athinoula A. Martinos Center for Biomedical Imaging, Massachusetts General Hospital, Harvard Medical School, Boston, MA, USA
[4]Center for Alzheimer Research and Treatment, Department of Neurology, Brigham and Women's Hospital, Harvard Medical School, Boston, MA, USA

Introduction: Neuropathology studies suggest that tau pathology propagates via connections in a process potentiated by amyloid pathology. We examined longitudinally whether hippocampal volume (HV) predicts tau accumulation in a connected area, the isthmus, via its anatomic connection, the hippocampal cingulum (HC) bundle. Furthermore, we examined whether amyloid deposition moderates this process (fig1).

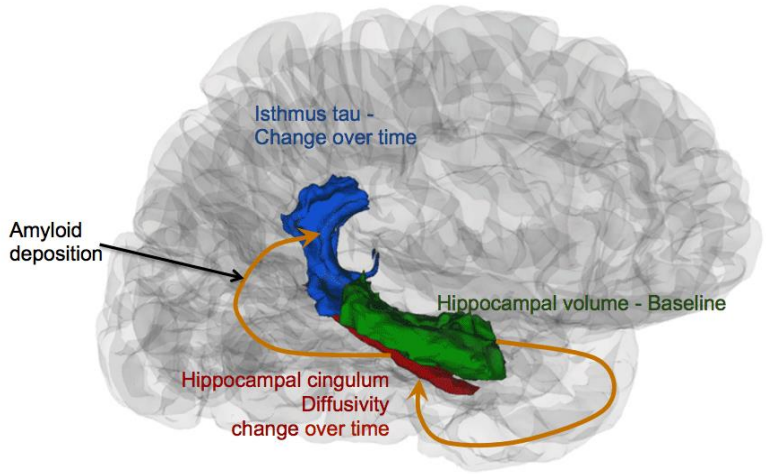

Methods:: Two hundred fifty-six clinically normal participants from the Harvard Aging Brain Study completed baseline DTI, PIB-PET scanning and neuropsychological assessment (mean age:73.45 years; mean cognitive follow-up:5.11 years; mean MRI follow-up:2.89 years) Of these participants, 110 subjects underwent Flortaucipir-PET scanning at ~2.32 ± 1.32 years from MRI baseline (mean follow-up:2.75 years (n=41)). Tract of interest was the HC and control tract was the uncinate fasciculus (UF). Tau region of interest was the isthmus; inferior temporal (IT) cortex the control region. Linear mixed models examined whether i) baseline HV predicts change in HC diffusion, ii) baseline HC diffusion predicts isthmus tau accumulation and interacts with amyloid status and iii) HC diffusion predicts memory in high isthmus tau persons. Memory scores were derived from a factor analysis. Age, gender and education were included as covariates.
Results: Baseline HV predicted diffusion changes in the HC, not in the UF. Baseline HC, not UF, diffusion predicted changes in isthmus tau, not IT tau. Amyloid positive individuals showed a stronger association between HC integrity and isthmus tau change then amyloid negative. HC diffusion predicted change in memory performance in high isthmus tau compared to low tau persons. All associations were right lateralized (fig2, table).

Effect of tract integrity on tau accumulation is amyloid-driven

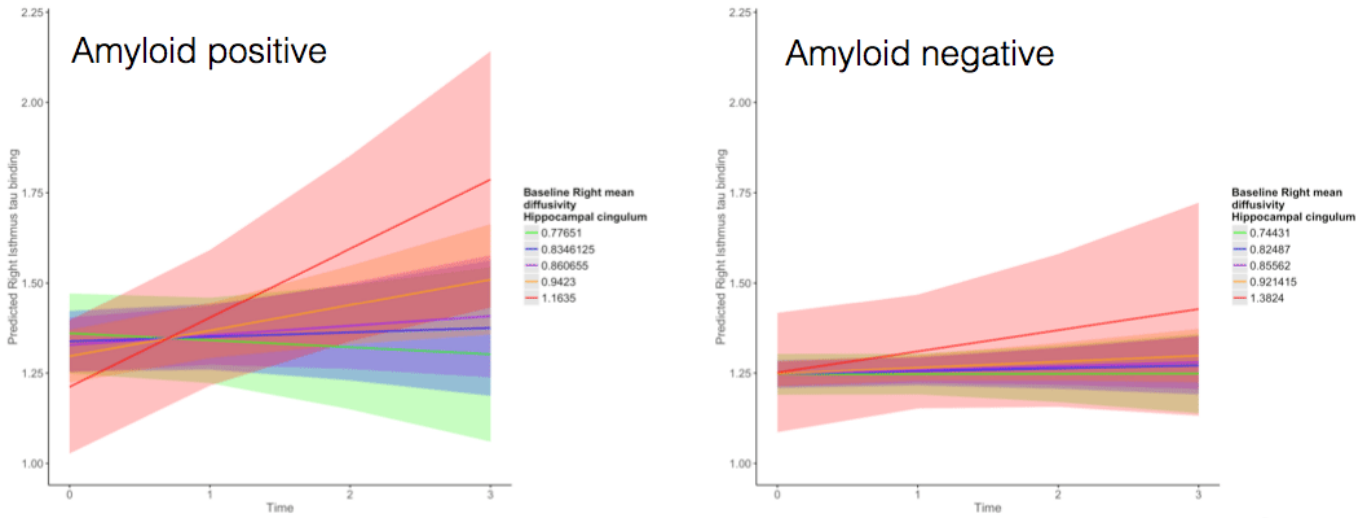

Within Aβ+
Beta=0.545(0.22)
p=0.0338

MD hippocampal cingulum x time x Aβ
p=0.030

Within Aβ-
Beta=0.091(0.10)
p=0.393

LME Models	Hippocampal cingulum		Uncinate fasciculus	
	Estimate (SE)	p-value	Estimate (SE)	p-value
I. HCV predicting diffusion (observations=392)				
• Left	$-6.2e^{-04}$ ($7e^{-04}$)	0.396	$2.3e^{-04}$ ($1.8e^{-03}$)	0.194
• Right	$-1.80e^{-03}$ ($8e^{-04}$)	**0.027**	$4.9e^{-04}$ ($4.8e^{-04}$)	0.312
II. Diffusion predicting isthmus tau (observations=151)				
• Left	0.217 (0.26)	0.417	-0.022 (0.08)	0.789
• Right	0.213 (0.09)	**0.037**	0.126 (0.14)	0.379
III. Diffusion x amyloid predicting isthmus tau (observations =149)				
• Left	-0.183 (0.55)	0.739	0.393 (0.34)	0.252
• Right	0.513 (0.23)	**0.030**	0.563 (0.38)	0.148
VI. Diffusion predicting IT tau (observations = 151)				
• Left	0.014 (0.22)	0.952		
• Right	0.066 (0.11)	0.565		
V. Diffusion x tau predicting memory (observations = 600)				
• Left	0.239 (0.35)	0.497		
• Right	-0.599 (0.25)	**0.015**		

Note: Linear Mixed effects models for the chain of events and their control regions. All models were covaried for age, gender and education and their interaction with time (if p<0.10). Age was centered at 73.45 years, education at 15.80 and female was the reference for gender. Abbreviations: LME: Linear Mixed Effects models; HCV: Hippocampal volume; IT = inferior temporal. All shown models use the mean diffusivity metric (multiplied by 1000, threshold at FA > 0.2). Tau values are in standardized uptake value ratio's with the cerebellum grey as reference region and corrected for partial volume effects. Amyloid deposition (PIB) is dichotomized at DVR-FLR=1.20

Discussion: These findings suggest that tau pathology propagates from the medial temporal to the limbic lobe via specific connections and this is potentiated by amyloid. This chain of events is associated with memory decline. Exploring these relationships in patient populations will be the next step in understanding the spatial pattern of tau propagation.

Keywords: Tau, propagation, connectivity, memory, longitudinal

Greater regional cortical thickness is associated with selective vulnerability to atrophy in Alzheimer's disease, independent of regional amyloid load

Chunfei Li[1], Ranjan Duara[2,4], David A. Loewenstein[3,4,5], Mercedes Cabrerizo[1], Warren Barker[2,4], Malek Adjouadi[1,4]

[1]Center for Advanced Technology and Education, School of Engineering, Florida International University, Miami, FL, USA
[2]Wien Center for Alzheimer's Disease & Memory Disorders, Mount Sinai Medical Center, Miami, FL, USA
[3]Psychological Services and Neuropsychology Laboratory, Mount Sinai Medical Center, Miami, FL, USA
[4]Florida ADRC (Florida Alzheimer's Disease Research Center at Gainesville, Miami Beach, Miami and Boca Raton, FL), Gainesville, Miami and Boca Raton, FL, USA
[5]Center on Aging and Department of Psychiatry and Behavioral Sciences, Miller School of Medicine, University of Miami, Miami, FL, USA

Background/Objective: Thinning of the cortex in specific brain regions has been described in both early and preclinical Alzheimer's disease (AD)[1], whereas among cognitively normal (CN) elderly, greater amyloid load has been associated with greater temporal lobe volumes[2]. We further explored these observations by studying the relationships between cortical thickness (CTh), amyloid load and the severity of regional atrophy in AD.

Methods: MRI scans (3-D, T1-weighted) were used to delineate 68 cortical regions among CN (n=251; age = 75.3 ± 6.6 years) and AD (n= 162; age= 74.7± 7.8 years) subjects in the ADNIGO/ADNI2 cohort. The severity of regional atrophy from CN to AD (Atr(%)$^{CN-AD}$) was calculated for each brain region. AV45 PET were linearly registered onto post-processed T1-weighted MRI images, and regional Uptake Value Ratios (rSUVR) (target to cerebellum) were calculated, following segmentation and parcellation. Pearson Partial Correlation (PPC) were calculated to examine the association of the mean regional CTh among CN individuals to Atr(%)$^{CN-AD}$, correcting for regional mean SUVR in corresponding regions.

Results: Regions with the greatest CTh among CN subjects were aggregated in limbic regions (e.g. entorhinal cortex, temporal pole, insula cortex) which also tended to have the lowest rSUVRs. In contrast, CTh was lower in many neocortical regions (e.g., pericalcarine, precuneus, superior parietal), which had the highest rSUVRs (Figs.1 and 2). Regional CTh was positively correlated to the severity of atrophy in each region , before ($r = 0.662$, $p = 4.309e-10$), as well as after ($r = 0.535$, $p = 2.226e-06$) partitioning out the effect of regional SUVR (Fig. 1).

Conclusions: Brain regions with greater cortical thickness at baseline have greater regional neurodegeneration, not mediated by regional amyloid load. This phenomenon may represent an aspect of brain/cognitive reserve. Alternatively, genetic factors mediating regional cortical thickness developmentally, may also mediate selective vulnerability to atrophy.

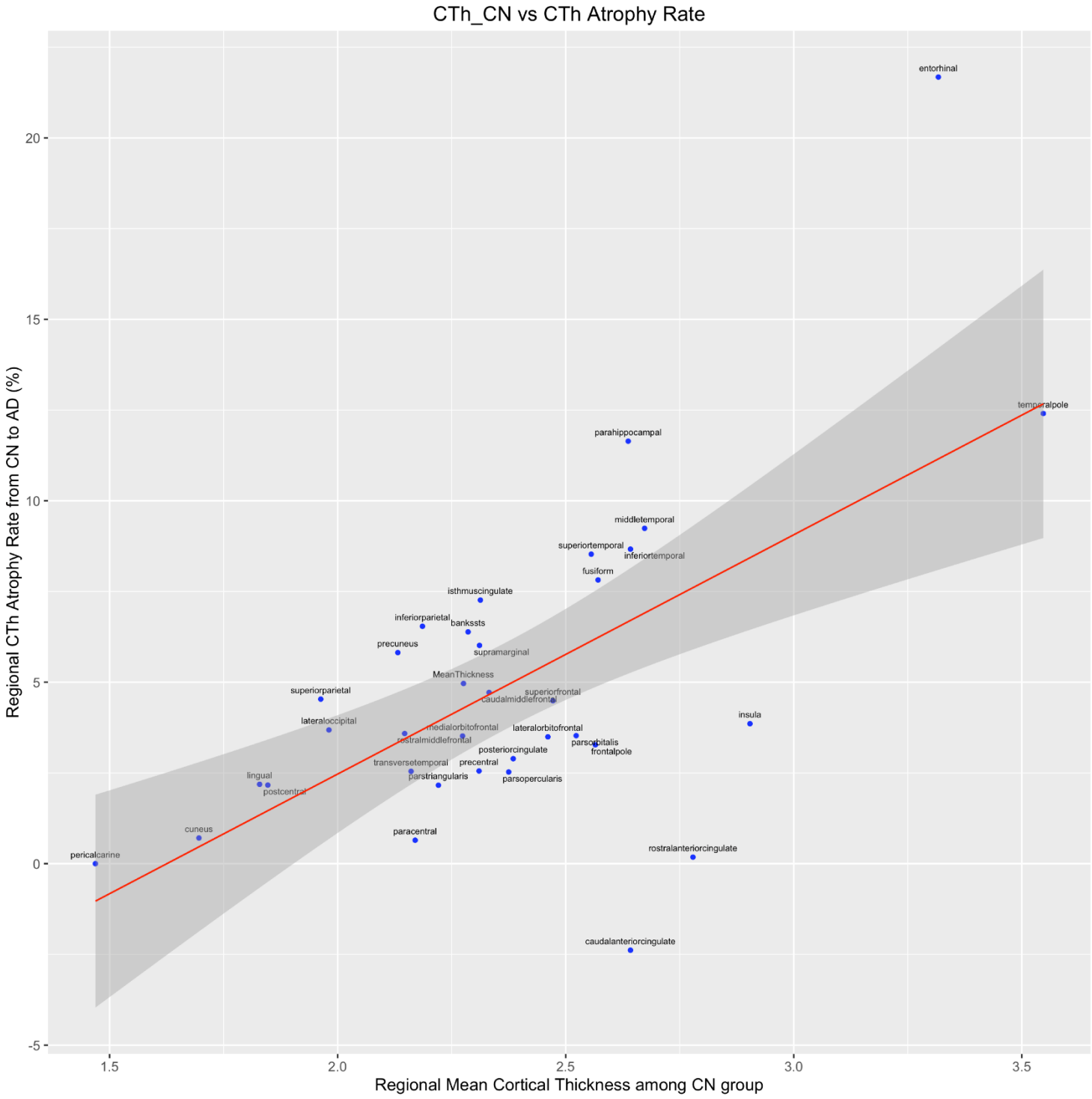

Fig. 1. Plot of regional Cortical Thickness and % Atrophy with the estimated linear regression model. Results were similar for the left and right hemisphere, so only left hemisphere ROI's were plotted. Atrophy Rate = -11.287+ 6.775*CTh; r = 0.662, adjusted R-squared= 0.4302

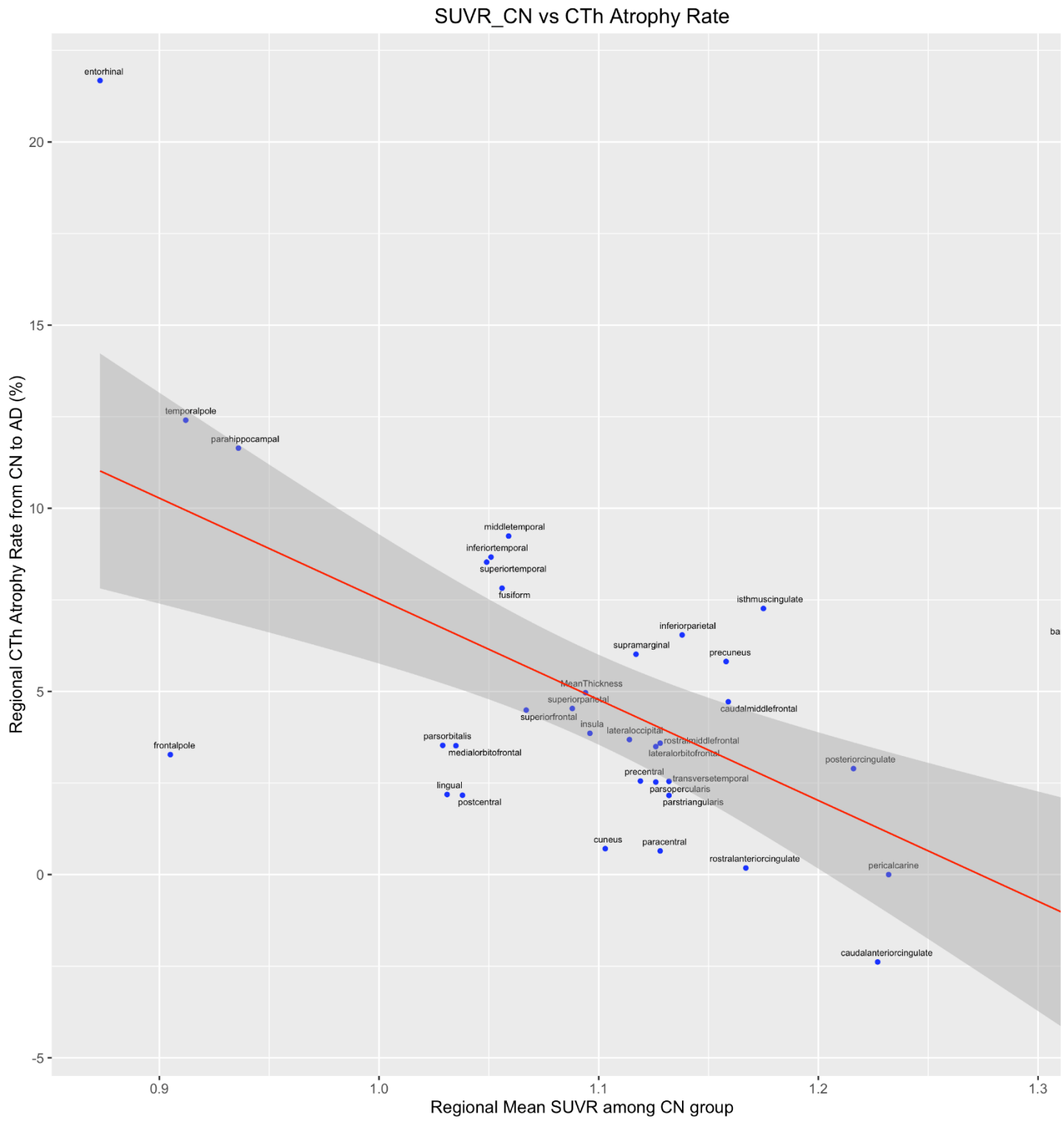

Fig. 2. Plot of regional SUVR and % Atrophy with the estimated linear regression model. Only left hemisphere ROIs are plotted. AtrophyRate = 33.627-26.33*SUVR_CN; r = -0.570, a*djusted R-squared*: 0.315

Keywords: Alzheimer's disease, selective vulnerability, cortical thickness, regional amyloid load, regional atrophy

Distinctive clinical significance of hemorrhagic and amyloid imaging markers in patients with clinical-radiological cerebral amyloid angiopathy in memory clinic patients

Young Kyoung Jang[1], Jin San Lee[1], Ko Woon Kim[1], Sang Won Seo[1,2]

[1]Department of Neurology, Samsung Medical Center, Sungkyunkwan University School of Medicine, Seoul, Korea
[2]Neuroscience Center, Samsung Medical Center, Seoul, Korea

Cerebral amyloid angiopathy is a cerebrovascular disease caused by amyloid β accumulation in the cortical and leptomeningeal vessel walls. However, only few studies examined the clinical significance of hemorrhagic and amyloid β imaging markers in patients with clinical cerebral amyloid angiopathy. We, therefore, aimed to investigate the effects of lobar cerebral microbleeds and cortical superficial siderosis on cortical thickness and cognitive impairment.

372 participants were divided into two groups according to the median number of lobar cerebral microbleeds and cortical superficial siderosis. Cortical thickness was measured by surface based methods. We also included 114 clinical-radiological cerebral amyloid angiopathy patients who underwent amyloid β PET and neuropsychological tests. Linear mixed effects model was performed in order to investigate the longitudinal effects of parenchymal amyloid β positivity.

Older age, Apolipoprotein E ε4 allele, poorer cognitive status, and more severe deep and periventricular white matter hyperintensities were the most prominent in probable cerebral amyloid angiopathy followed by possible cerebral amyloid angiopathy and non-cerebral amyloid angiopathy groups. Multiple lobar cerebral microbleeds were associated with impairment in all cognitive domains, while cortical superficial siderosis was associated with impairment in attention, frontal executive function and mini mental state examination. Furthermore, 58.9% of clinically diagnosed cerebral amyloid angiopathy patients showed amyloid β PET positivity, which also affected baseline memory function and progressive decline in multiple cognitive domains. Taken together, our findings suggest that multiple lobar cerebral microbleeds and cortical superficial siderosis affect distinctively clinical features, providing new insights into their underlying pathomechanisms.

Our findings suggested that CAA might be classified into several phenotypes according to kinds of hemorrhagic markers or the Aβ PET positivity. Therefore, these results emphasize the need for further prospective therapeutic trials to determine how prevention strategies targeting CAA related neuroimaging markers might modify the natural history of cognitive impairment.
Keywords: CAA, amyloid PET

Is tau accumulation detectable before neuronal injury markers? – Analysis from tau PET imaging with [C-11]PBB3 in clinical variants of Alzheimer's disease

Masamichi Imai[1,2], Kenji Ishii[1], Mika Tanaka[1], Kenji Ishibashi[1], Kei Wagatsuma[1], Muneyuki Sakata[1], Tetsuro Tago[1], Jun Toyohara[1], Shigeo Murayama[3], Hirotaka Maruno[2,4], Hitoshi Shimada[5], Makoto Higuchi[5], Tetsuya Suhara[5]

[1]*Neuroimaging Research, Tokyo Metropolitan Institute of Gerontology, Tokyo, Japan*
[2]*Department of Radiology, Toranomon Hospital, Tokyo, Japan*
[3]*Department of Neurology, Tokyo Metropolitan Geriatric Hospital, Tokyo, Japan*
[4]*Okinaka Memorial Institution for Medical Research, Tokyo, Japan*
[5]*Clinical Research Cluster, National Institute of Radiological Sciences, National Institutes for Quantum and Radiological Science and Technology, Chiba, Japan*

Background: Past clinico-pathological studies and recent tau PET imaging studies have suggested that neurofibrillary tangle or tau pathology is closely linked to clinical symptoms. Current neuropathological model of Alzheimer's disease (AD) assumes that tau accumulation may precede neuronal injury. The purpose of this study is to examine if tau PET imaging with ^{11}C-PBB3 can detect tau pathology concurrently or separately with hypometabolism/atrophy with ^{18}F-FDG PET/structural MRI. We focused on patients with local variant of AD in which different stages of AD pathology are most likely to coexist region by region.

Methods: We studied two cases of posterior cortical atrophy (PCA) and two cases of logopenic variant of primary progressive aphasia (lvPPA) meeting the criteria for probable AD dementia or mild cognitive impairment due to AD, and 23 amyloid negative cognitively normal subjects as control. In each subject PET images with ^{11}C-PBB3, ^{11}C-PiB, ^{18}F-FDG and 3D MRI images were obtained. All the images were co-registered and SUVR PET images in reference to cerebellar cortex were used for further evaluation with visual inspection, ROI analysis, and SPM statistical analysis.

Results: In PCA patients, ^{11}C-PBB3 accumulation was detected in bilateral occipito-parietal region. In lvPPA patients, remarkable ^{11}C-PBB3 accumulation was observed in bilateral temporo-parietal cortex left-side dominantly. Hypometabolic and atrophic area appeared to be more restricted to the area with tau deposition (Figure 1). On the other hand, in the most severely hypometabolic/atrophic regions ^{11}C-PBB3 accumulation did not necessarily be the highest, but seemed to be relatively declined (Figure 2).

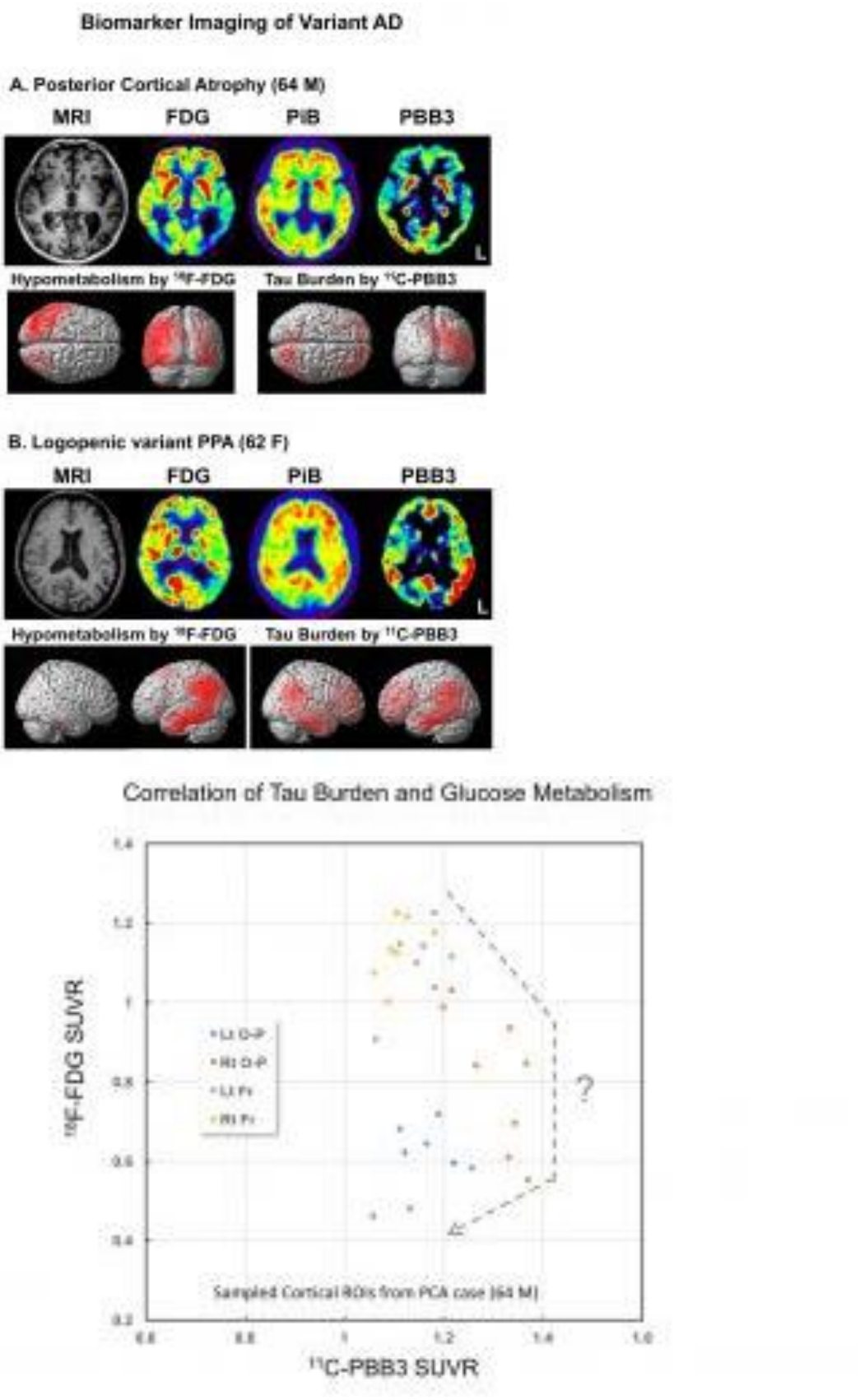

Conclusion: Our results suggest that tau related pathology in AD evaluated by ^{11}C-PBB3 is detectable before the emergence of hypometabolism and atrophy. In the regions with advanced stage of AD pathology, ^{11}C-PBB3 binding may decline presumably due to atrophy and/or tracer's binding characteristics against variable tau conformations. Further longitudinal and histopathology studies are required.

Keywords: tau. PBB3. clinical variant of Alzheimer's disease.

Investigation of gait speed and ß-amyloid in older adults from the Harvard Aging Brain Study

Dylan R. Kirn[1], Rachel F. Buckley[1,3,4,5], Bernard J. Hanseeuw[1], Rebecca E. Amariglio[1,2,3], Reisa A. Sperling[1,2,3], Keith A. Johnson[1,2,3]

[1]*Department of Neurology, Massachusetts General Hospital, Boston, MA, USA*
[2]*Department of Neurology, Brigham and Women's Hospital, Boston, MA, USA*
[3]*Harvard Medical School, Boston, MA, USA*
[4]*Florey Institutes of Neuroscience and Mental Health, Melbourne, Australia*
[5]*Melbourne School of Psychological Sciences, University of Melbourne, Melbourne, Australia*

Background: Recent evidence from post-mortem studies suggest that AD pathology may not only influence decline in cognition, but physical functioning as well. A negative relationship between gait speed(GS) and striatal ß-Amyloid(Aß) has been shown cross-sectionally, and so we aimed to investigate the effect of baseline neocortical and striatal Aß on GS change. We hypothesized that increasing baseline Aß would relate to poorer cross-sectional GS, and also slower GS over four years.

Methods: 287 older adults(73yrs±6.4) underwent baseline PiB-PET imaging and GS measurements, and had an additional GS measurement at their third yearly assessment. GS(meters/second) was measured using a 30ft course, with one turn. GS change slopes were extracted from a GS-by-time linear mixed model. Neocortical Aß burden was represented by a summary distribution volume ratio (DVR) of frontal, lateral and retrosplenial(FLR) tracer uptake, while striatal Aß reflected a composite of caudate and putamen DVRs. PiB groups were calculated according to both FLR/STR status (FLR-,FLR+/STR-,FLR+/STR+). Linear regression analyses were run to determine whether GS (cross-sectionally or longitudinally) would be predicted by either neocortical or striatal Aß, after accounting for age and gender.

Results: Neither neocortical nor striatal Aß were found to associate with cross-sectional GS (ß=0.03, p=0.46, ß=0.08, p=.12, respectively). In addition, no relationship was observed between neocortical Aß and GS change (ß=0.003, p=.15;$ß_{age}$=-.0006, p<.001), or striatal Aß and GS change (ß=.004, p=.16;$ß_{age}$=-.0006, p<.001). An ANCOVA showed that GS change did not differ according to PiB group (F=0.96,*p*=.39).

Conclusion: This is the first study to examine the longitudinal relationship between GS and Aß. Our analysis did not reveal an association between these outcome measures, however, this may be due to relatively subtle changes in gait speed over four years. While our preliminary findings support age-associated decline in gait speed, a longer follow-up will be needed to elucidate the involvement of proteinopathy.
Keywords: amyloid, gait speed, striatum, older adults

Greater [F-18]THK-5351 binding in medial and ventral temporal lobe is associated with altered microstructure and reduced myelin

Andrew Merluzzi[1], Nagesh Adluru[1], Andrew Schoen[1], Douglas Dean[1], Vikas Singh[1], Bradley Christian[1], Tobey Betthauser[1], Patrick Lao[1], Todd Barnhart[1], Murali Dhanabalan[1], Sanjay Asthana[1], Andrew Alexander[1], Sterling Johnson[1], Barbara Bendlin[1]

[1]*University of Wisconsin - Madison, Madison, WI, USA*

Background: Amyloid plaques and neurofibrillary tangles (NFTs) are not unilateral predictors of dementia, suggesting that other mechanisms contribute to the development of cognitive decline. Neuronal microstructure and brain connectivity may play an important role in this process, particularly as NFTs begin to develop. As such, we hypothesized a relationship between NFTs measured by THK-5351 binding in temporal lobe structures and altered microstructure and myelin in adjacent regions.

Methods: Cognitively healthy participants underwent THK-5351 PET imaging, diffusion tensor imaging (DTI), and mcDESPOT to detect myelin water fraction (MWF Analysis: n=11, age=67.2 ± 2.2 years, 54% female, 45% *APOE* ε4 positive; DTI Analysis: n=17, age=68.8 ± 1.6 years, 59% female, 41% *APOE* ε4 positive). Distribution volume ratios (DVR) of THK-5351 binding were obtained from bilateral hippocampus and fusiform gyrus, and were used as predictors in voxelwise linear regressions for fractional anisotropy (FA), mean diffusivity (MD), and MWF in SPM12 (controlling for age, sex, and *APOE* ε4). Biological Parametric Mapping (BPM) in SPM8 was used to ascertain the effect of tau on the microstructural metrics on a regional basis.

Results: Significant associations were found between hippocampal and fusiform THK-5351 binding and microstructure and myelin. Specifically, on a regional basis, THK-5351 was associated with reduced MWF in several temporal lobe structures, including the hippocampus and cingulum bundle (Figure 1 A/B). Similarly, on a voxelwise basis, THK-5351 was associated with reduced FA in the cingulum bundle (Figure 1 C/D). THK-5351 was also associated with increased MD in the left hippocampus (Figure 1 E/F).

Conclusions: THK-5351 binding was associated with altered microstructure and reduced myelin in a cognitively healthy middle-aged population, findings that may prove useful in identifying the early processes leading to cognitive decline in those with tau accumulation. This provides insight into the relationship between Alzheimer's disease pathologies and brain microstructure in the preclinical stage.

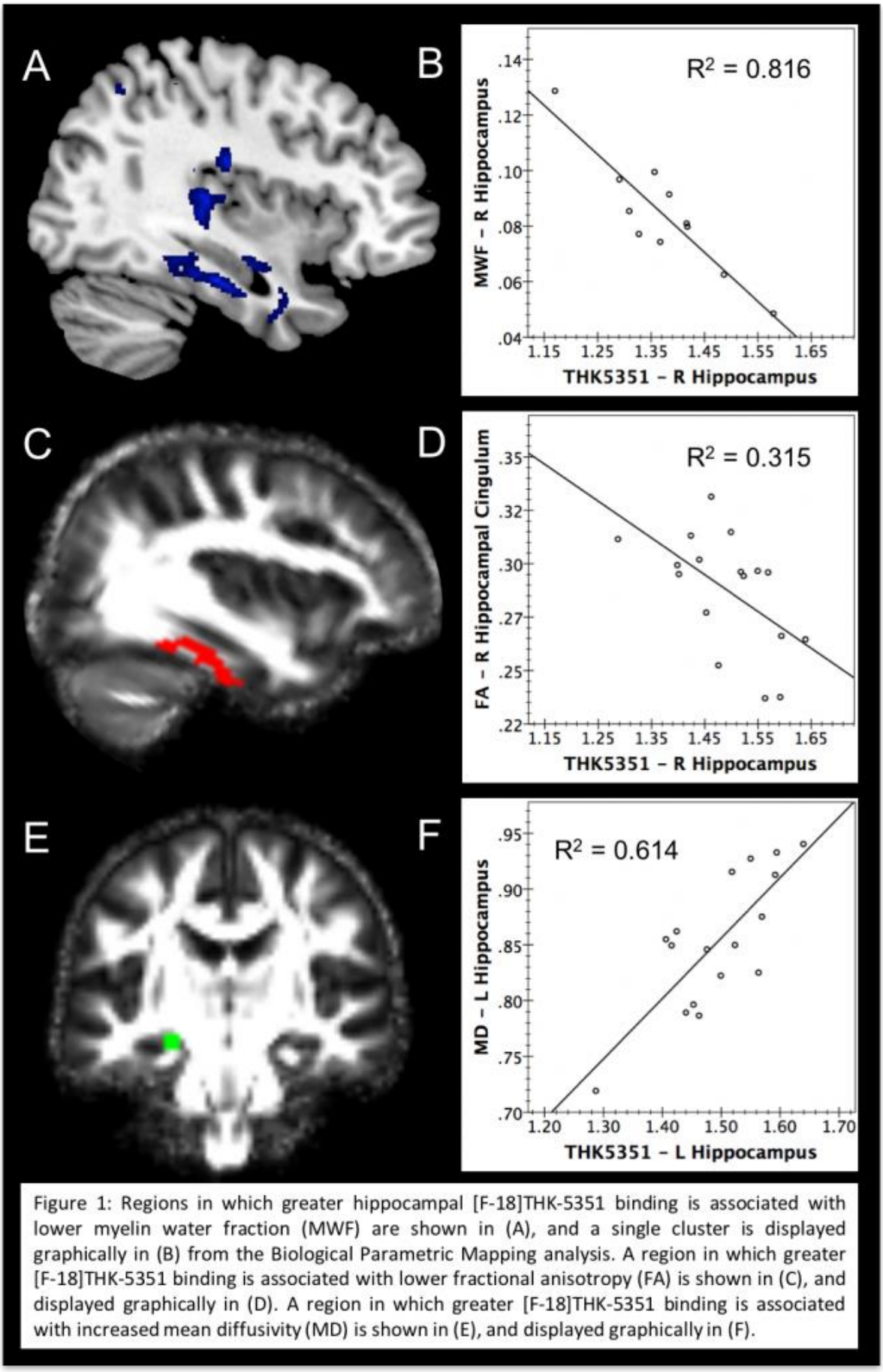

Figure 1: Regions in which greater hippocampal [F-18]THK-5351 binding is associated with lower myelin water fraction (MWF) are shown in (A), and a single cluster is displayed graphically in (B) from the Biological Parametric Mapping analysis. A region in which greater [F-18]THK-5351 binding is associated with lower fractional anisotropy (FA) is shown in (C), and displayed graphically in (D). A region in which greater [F-18]THK-5351 binding is associated with increased mean diffusivity (MD) is shown in (E), and displayed graphically in (F).

Keywords: THK5351, connectivity, DTI, myelin, tau

Contribution of neuritic and diffuse plaques to signal derived from CN-Flutemetamol: a preliminary study in AD autopsy brains

Milos Ikonomovic[1], Eric Abrahamson[1], Christopher Buckley[2], Chester Mathis[1], WIlliam Klunk[1], Gill Farrar[2]

[1]*University of Pittsburgh, Pittsburgh, PA, USA*
[2]*GE Healthcare, Amersharm, United Kingdom*

Background: Specificity and sensitivity of Flutemetamol (Vizamyl) PET are high for detecting neuritic amyloid-beta plaques (NP), however several false-positive results indicate that this radiotracer may also detect diffuse plaques (DP). Using the fluorescent derivative of Flutemetamol (CN-Flutemetamol) applied to AD brain tissue sections, we have detected both NP and DP, although NP appeared to have brighter fluorescence than DP. The current study explores quantitatively this relation in brain areas affected differentially by NP and DP.

Methods: Tissue sections from the frontal cortex (FC, variable proportions of NP and DP) and caudate (CD, all DP) from ten AD cases were processed using CN-Flutemetamol. We measured CN-Flutemetamol positive plaque load, expressed as percent area occupied by plaques, and integrated density, a measure that integrates both size and fluorescence intensity of labeled plaques per defined field.

Results: All plaques (DP and NP in the FC and DP in the CD) were labeled with CN-Flutemetamol. CN-Flutemetamol-labeled total plaque load was similar in CD and FC (CD = 3.79 ± 0.64; FC = 5.81 ± 1.18; 2-tailed t-test $p = 0.15$), however, the integrated density in FC was greater than in the CD (CD=5024 ± 490.3; FC=11742 ± 568.2; 2-tailed t-test $p<0.0001$).

Discussion: For two regions with comparable plaque area coverage, but with different involvement of NP and DP, the region with a preponderance of NP yields greater overall CN-Flutemetamol fluorescence signal when area coverage and signal intensity are calculated as a single value (integrated density). This implies that in PET imaging studies, brain regions with high densities of NP exhibit greatest Flutemetamol retention. However, DP can contribute to Flutemetamol PET signal in regions with very high DP area coverage. Thus, Flutemetamol PET may correlate better with NIA-AA 2012 AD neuropathology criteria that incorporate both CERAD (NP) and Thal phases (all types of Aβ plaques).
Keywords: Flutemetamol, amyloid-beta, diffuse plaques, neuritic plaques, PET

PET tau and amyloid synergy in default mode network determines the clinical status in predementia stages of Alzheimer's disease

Tharick Pascoal, Sulantha Mathotaarachchi, Min Su Kang, Kon Pin Ng, Jean-Paul Soucy, Serge Gauthier, Pedro Rosa-Neto

[1]*Mcgill University, Montreal, QC, Canada*

Although abnormal levels of amyloid-β and tau proteins have been constantly associated with dementia, the link between amyloid-β plaques and neurofibrillary tangles as determinants of clinical status remains an unsolved question in Alzheimer's disease (AD). Here, we tested the hypothesis that the synergistic interaction between, rather than the independent or additive effects of, amyloid-β plaques and neurofibrillary tangles determines clinical status in the predementia stages of AD. We assessed 80 ADNI individuals (41 cognitively normal individuals and 39 mild cognitive impairment) with magnetic resonance, florbetapir amyloid-β and AV1451 tau positron emission tomography imaging as well as clinical status assessed with the Clinical Dementia Rating Scale Sum of Boxes. A voxel-based interaction model assessed the main and interactive effects of amyloid-β and tau positron emission tomography on clinical status, accounting for age, gender, years of education, *APOE ε4* status, diagnosis and grey matter density at every voxel. We further carried out an analysis of variance to compare the synergistic model with the mediation and additive models. We found that the synergism between amyloid-β and tau pathologies in the precuneus, posterior cingulate, inferior parietal, lateral temporal and medial prefrontal cortices were associated with worse clinical status in the predementia stages of AD ($P < 0.001$). In addition, analysis of variance strongly supported that the model with the interaction term best described clinical status, as compared to reduced models testing (1) only amyloid-β; (2) only tau; and (3) amyloid-β plus tau with P values < 0.0001 in all three cases. These results highlight the concept that the synergy between amyloid-β and tau determines clinical status in the predementia stages of AD. Importantly, the regions where such a synergy determined worse clinical status were confined to the functional hubs of the brain's default model network, which are postulated fundamental to the large-scale brain organization.

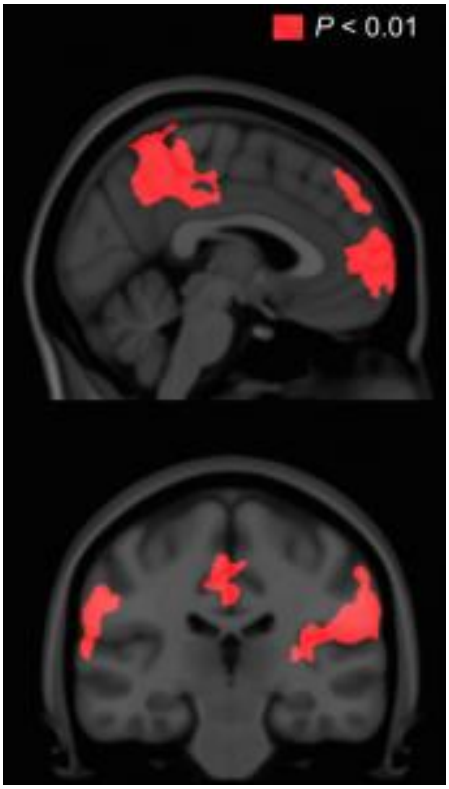

Keywords: Amyloid PET, tau PET, protein-protein interaction

Staging of amyloid-β, tau, regional atrophy rates and cognitive change in a non-demented cohort

Evan Fletcher Fletcher[1,2], Alice Renaud[3], Abhninandan Nandi[1], Charles DeCarli[1,2]

[1]*IDeA Laboratory, UC Davis, Davis, CA, USA*
[2]*Department of Neurology, UC Davis, Sacramento, CA, USA*
[3]*Northeastern University, Boston, MA, USA*

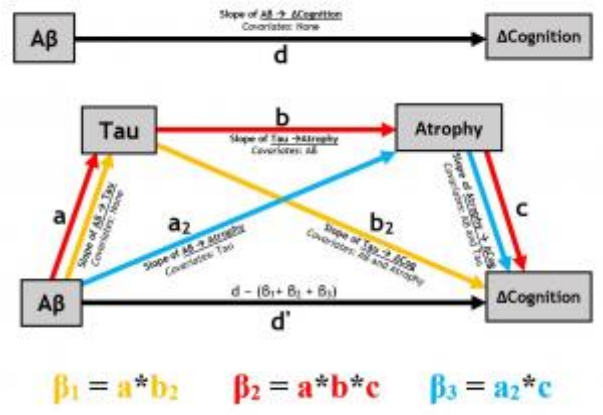

Figure 1.

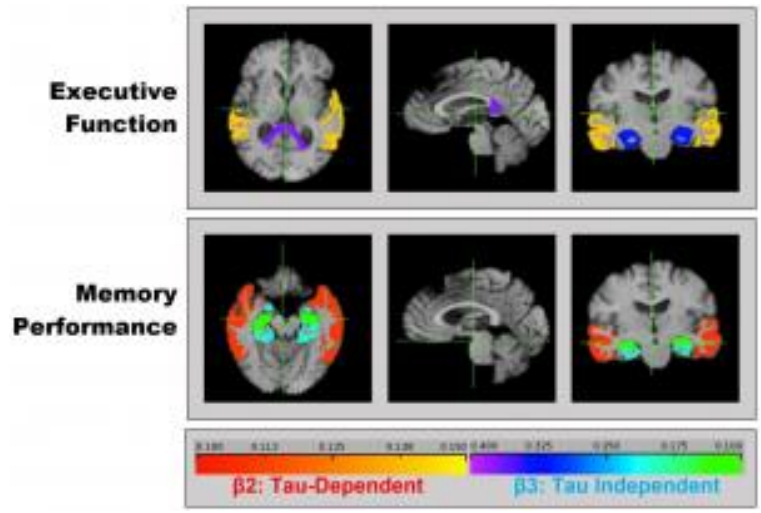

Figure 2

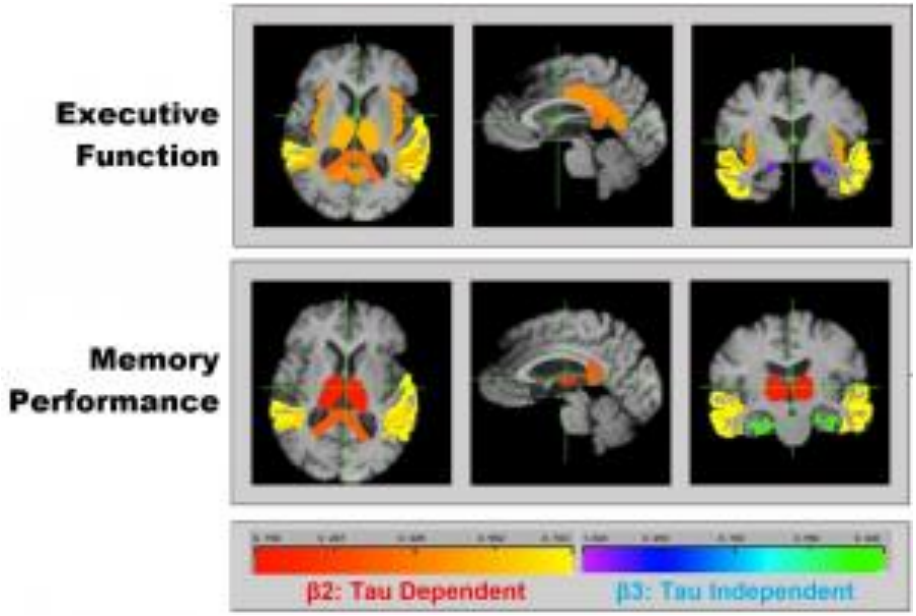

Figure 3

Background: Despite extensive study, questions remain about the sequencing of biomarker events, including amyloid-β, tau, atrophy and cognitive decline, in association with the progression of Alzheimer's pathology. Moreover, current models emphasize the temporal nature of evolution in biomarker abnormalities while neglecting the issue of differences in anatomical distribution known to accompany Alzheimer's pathology.

Subjects and Methods: We tested both biomarker chronology and anatomical variation in a non-demented cohort of ADNI-2, using regressions and serial mediation models (Fig. 1), incorporating baseline CSF tau with regional 2-year longitudinal atrophy, to mediate the effects of baseline CSF amyloid-β (Aβ) concentration on 2-year cognitive change.

Results: In cognitive normals there were no mediations but Aβ correlated with atrophy rates in medial temporal (MTL: amygdala, entorhinal cortex, parahippocampal gyrus and hippocampus), lateral temporal regions (LTR: inferior, middle and superior temporal gyri) and also with change in executive and memory function.
In mild cognitive impairment (MCI) different mediation models of Aβ effects on cognitive change were significant for anatomically distinct regions that may reflect different dynamics of the interaction of Aβ, tau and atrophy (Figs 2-3). These regions corresponded roughly with the Braak stages of tau deposition. Mediation by MTL atrophy alone (without tau) was significant in both early and late MCI. Mediation by tau --> neocortical atrophy was seen first in LTR in early MCI (Fig. 2), spreading to many other neocortical regions of atrophy by late MCI (Fig. 3).

Discussion: Our results thus suggest that different mediation models are sensitive to differing interactions of Aβ, tau and longitudinal atrophy by brain location, pointing to topographical as well as disease state differences in the sequencing of the effects of Aβ and tau on atrophy and cognition. These differences suggest that future sequential biomarker models should take into account both temporal (i.e. disease stage) and spatial (anatomical regions) dimensions.

Keywords: mediation, amyloid-beta, tau, regional atrophy, biomarker models

Increased level of CSF neurofilament light chain is associated with amyloidosis in transgenic rat model of Alzheimer's disease

Min Su Kang[1,2,6], Eduardo R. Zimmer[1,5], Monica Shin[1,2,6], Sulantha Mathotaarachchi[1,2], Tharick Pascoal[1,2], Kok Pin Ng[1,2], Henrik Zetterberg[7], Jean-Paul Soucy[3], Judes Poirier[6], Serge Gauthier[1,2,6], A. Claudio Cuello[4], Pedro Rosa-Neto[1,2,3,6], Kaj Blennow[5]

[1]Translational Neuroimaging Translational laboratory, Montreal, QC, Canada
[2]McGill University Research Centre for Studies in Aging, Verdun, QC, Canada
[3]McConnell Brain Imaging Centre - McGill University, Mont, QC, Canada
[4]McGill University - Department of Pharmacology, Mont, QC, Canada
[5]Department of Biochemistry, Federal University of Rio Grande do Sul, Porto Alegre, BR
[6]Douglas Mental Health Institute, Verdun, QC, Canada
[7]Department of Psychiatry and Neurochemistry, Institute of Neuroscience and Physiology, The Sahlgrenska Academy at University of Gothenburg, Gothenburg, Sweden

Background: Alzheimer's disease (AD) is a progressive neurodegenerative disease that has the characteristics of multiple pathologies: amyloidosis, neurofibrillary tangles (NFTs), and atrophy. Recent findings revealed higher cerebrospinal fluid (CSF) neurofilament light (NfL) levels of AD patients and APPPS1 mouse model. NfL is a novel fluid biomarker for neuronal injury as it is part of major cytoskeleton proteins. However, its association with regional amyloidosis needs further investigations. Here, we utilized McGill-R-Thy1-APP transgenic rat (Tg) model that accumulates amyloid pathology without NFTs or cell depletion. Our aim of the study is to investigate the increased level of CSF-NfL and its association with amyloid accumulation. We hypothesized that the level of CSF-NfL is greater in Tg compared to WT and it is associated with amyloidosis in the AD vulnerable regions.

Methods: A total of 28 (11 WT, 17 Tg) rats underwent CSF collection (10 to 17 months). A subset of Tg (6) also received a PET scan with NAV4694 at 17 months. CSF-NfL concentration was measured using a novel ultrasensitive Single molecule array (Simoa) method based on two UmanDiagnostics antibodies directed against the rod domain of NfL that is conserved in rodents. NAV4694-PET was acquired with a 90-minute dynamic scan followed by 9-minute transmission scan. The non-displaceable binding potential was generated using cerebellar grey matter as a reference region. The PET image was processed using MINC-toolkit. The statistical analysis of group comparison and voxel-wise parametric map were performed using R and glim_image, respectively.

Results: CSF-NfL was increased in Tg compared to WT; $t(193)=2.539$, $p=0.0119$. CSF-NfL was significantly associated with the amyloidosis in corpus callosum, fornix, hippocampus, entorhinal cortex, thalamus and striatum.

Conclusion: Our results revealed that the amyloid pathology alone is sufficient to cause neuronal degeneration, monitored as increased CSF-NfL that also correlates with amyloidosis in AD vulnerable regions in the rat model.

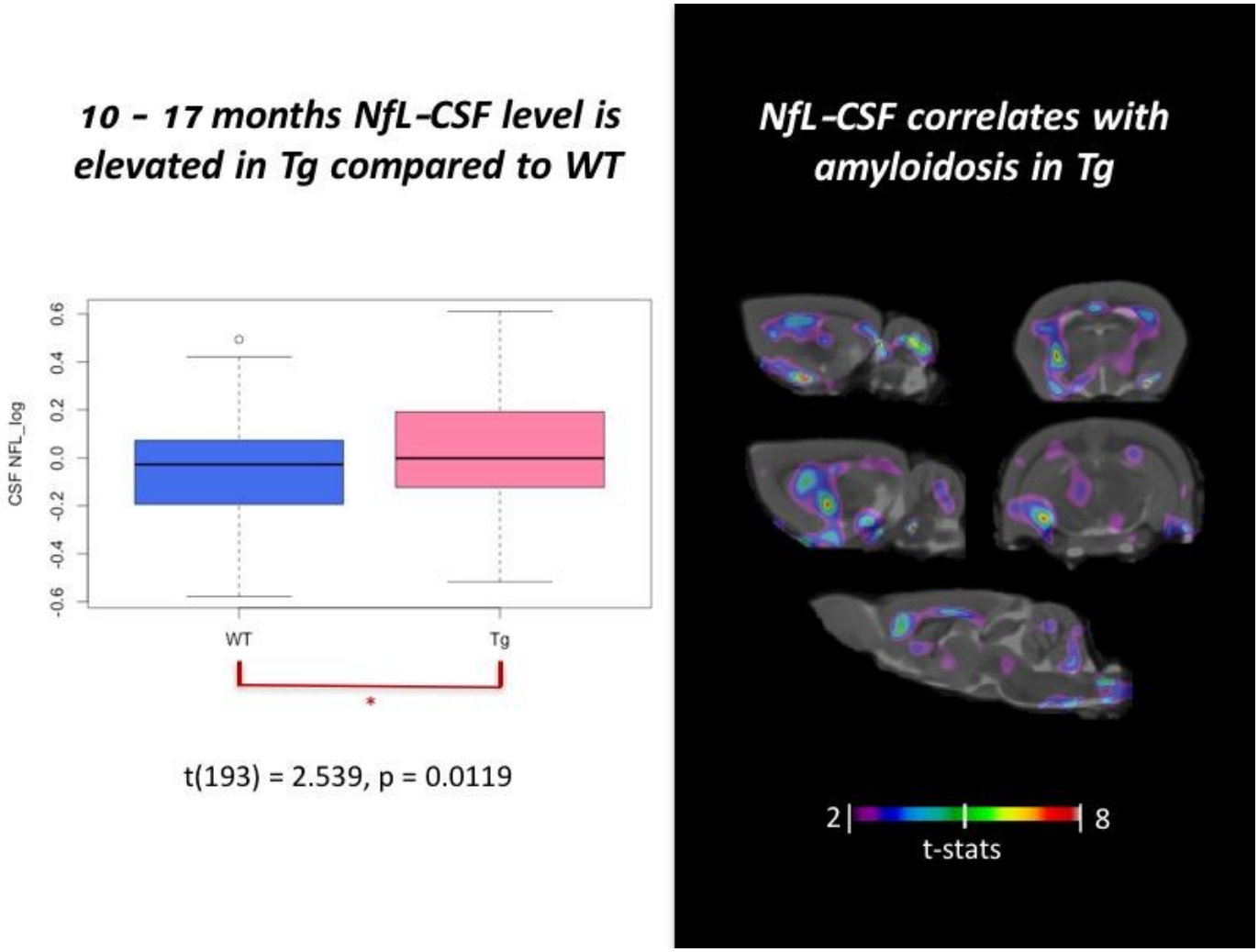

Keywords: CSF, neurfilament light chain, amyloidosis, animal model, biomarker

Thursday, January 12, 2017 - 10:15 am - 10:45 am

SESSION 4: Nauropathology II: PET to Autopsy Correlations

SESSION 4 **Nauropathology II: PET to Autopsy Correlations**	**CHAIRS:** **Melissa Murray, *Mayo Clinic*** **Teresa Gomez-Isla, *Massachusetts General Hospital***
Neuropathology and biochemical correlations of [F-18]AV-1451 and [C-11]PiB PET imaging in a subject with Alzheimer's disease	Milos Ikonomovic *University of Pittsburgh*
Neuroimaging-pathologic correlation of [F-18]-AV-1451 in an autopsy confirmed Parkinson's disease case	Marta Marquie-Sayagues *MassGeneral Institute for Neurodegenerative Disease*
Multimodal evaluation of 18F-AV-1451 PET in an autopsy-confirmed corticobasal degeneration patient	Corey McMillan *Perelman School of Medicine at the University of Pennsylvania*
Discussion	

Neuropathology and biochemical correlations of [F-18]AV-1451 and [C-11]PiB PET imaging in a subject with Alzheimer's disease

Milos Ikonomovic, Eric Abrahamson, Julia Kofler, William Paljug, Manik Debnath, Julie Price, Carl Becker, Chester Mathis, Oscar Lopez, William Klunk

University of Pittsburgh, Pittsburgh, PA, USA

Objectives: Imaging-autopsy analyses show that PiB PET corresponds to fibrillar amyloid-beta (Abeta) plaques. Neuropathology validation of AV-1451 PET in subjects with Alzheimer's disease (AD) is lacking. We report the first postmortem neuropathology evaluation of AV-1451, and comparison to PiB PET, in an AD subject.

Methods: The brain of a 94 y.o. subject with clinically probable AD and a history of PiB and AV-1451 PET scans (two years and one year prior to death, respectively) was examined postmortem. Abeta, Tau, and p-Tau immunoreactive pathology by area fraction (fixed left hemisphere, LH), and ELISA concentrations of insoluble Abeta, Tau, and p-Tau (frozen right hemisphere, RH), were correlated with region-matched, atrophy-corrected SUVR values.

Results: Subject was PiB+ (GLB6~2.16). AV-1451 retention was highest in striatum and insular, cingulate and temporal cortex. Neuropathology was complex, with age-related tau astrogliopathy, hippocampal sclerosis, TDP-43 and α-synuclein inclusions, and cerebral vascular pathology in addition to Abeta and tau pathologies (Thal phase=3, Braak stage=5, CERAD score=2). In the LH, PiB correlated with Abeta plaque load ($r=0.41$, $p=0.031$) but not tau pathology, while AV-1451 correlated with PHF-1 ($r=0.66$, $p=0.0002$), AT180 ($r=0.54$, $p=0.004$), and AT8 ($r=0.42$, $p=0.025$) pathology, and Abeta plaque load ($r=0.47$, $p=0.01$). In the RH, PiB correlated with insoluble Abeta1-42 ELISA ($r=0.61$, $p<0.001$) and weakly with pSer199 and pSer396 ELISA ($r=0.37$ and 0.39, both $p=0.05$). AV-1451 correlated with total tau (0.64, $p=0.0003$), pSer396 (0.61, $p=0.001$), pSer199 ($r=0.42$, $p=0.03$), and insoluble Abeta1-42 ($r=0.75$, $p<0.0001$) ELISAs. PET retention values of the two ligands correlated in the LH (0.38, $p=0.0038$) and the RH (0.65, $p=0.0002$).

Conclusions: AV-1451 PET corresponded to measures of p-Tau pathology load and brain concentration. Associations of AV-1451 with PiB and measures of Abeta could be related to substantial co-distribution of Tau and Abeta pathology in this case.

We thank Avid Radiopharmaceuticals for the provision of AV-1451 precursor.
Keywords: [F-18]AV-1451, [C-11]PiB, amyloid, tau, PET

Neuroimaging-pathologic correlation of [F-18]-AV-1451 in an autopsy confirmed Parkinson's disease case

Marta Marquie-Sayagues[1,2], Avery C. Meltzer[1,2], Eline Verwer[3], Marc D. Normandin[3], Michael A. Schwarzschild[1,2], Stephen N. Gomperts[1,2], Keith A. Johnson[2], Matthew P. Frosch[4], Teresa Gomez-Isla[1,2]

[1]*MassGeneral Institute for Neurodegenerative Disease, Charlestown, MA, USA*
[2]*Massachusetts General Hospital, Department of Neurology, Boston, MA, USA*
[3]*Massachusetts General Hospital, Department of Radiology, Boston, MA, USA*
[4]*Massachusetts General Hospital, C.S. Kubik Neuropathology Center, Boston, MA, USA*

Introduction: PET tracer -AV-145 preferentially binds to neurofibrillary tangles in Alzheimer's brains and those that form as a function of age. Its ability to bind tau lesions in other tauopathies remains controversial. Some studies report increased *in vivo* -AV-1451 retention, predominantly in basal ganglia and midbrain, in patients clinically diagnosed with PSP and CTE, but others notice similar patterns in older adults regardless of their clinical diagnosis, including controls whose brains are not expected to harbor tau pathology. While midbrain signal seems heavily influenced by -AV-1451 off-target binding to neuromelanin-containing neurons in substantia nigra, the underlying substrate of *in vivo* -AV-1451 retention in basal ganglia remains intriguing. Objective: We examined the correlation of *in vivo* and postmortem AV-1451 binding patterns in an autopsy-confirmed Parkinson's disease (PD) case who underwent imaging 12 months prior to death and exhibited elevated *in vivo* retention predominantly in basal ganglia.

Methods: We quantified *in vivo* retention of -AV-1451 and performed autoradiography and quantitative tau measurements in multiple brain regions.

Results: PET scan showed bilateral elevated -AV-1451 retention in basal ganglia. Lower retention was also noticed in midbrain, left frontal lobe and inferior temporal lobes. Postmortem exam showed the expected neuropathologic lesions of PD and scattered neurofibrillary tangles in medial temporal lobe. No tau pathology was present in basal ganglia. Autoradiography failed to show -AV-1451 binding in multiple brain regions with exception of incidental age-related tangles in medial temporal lobe and off-target binding in substantia nigra. There was no detectable -AV-1451 binding in the basal ganglia, where the highest *in vivo* signal was observed. *In vivo* -AV-1541 retention did not correlate with postmortem biochemical tau measures.

Conclusion: *In vivo* -AV-1451 retention in basal ganglia may represent, at least in part, non-specific binding influenced by biological or technical factors that occur *in vivo* rather than underlying tau pathology.
Keywords: [F-18]-AV-1451, PET, tau, postmortem, Parkinson, basal ganglia

Multimodal evaluation of 18F-AV-1451 PET in an autopsy-confirmed corticobasal degeneration patient

Corey McMillan[1], David Irwin[1,3], Ilya Nasrallah[2], Jeffrey Phillips[1], Meredith Spindler[1], Katya Rascovsky[1], Kylie Ternes[1], Charles Jester[1], David Wolk[1], Linda Kwong[3], Virginia Lee[3], Andrew Siderowf[4], Edward Lee[3], John Trojanowski[3], Murray Grossman[1]

[1]Perelman School of Medicine at the University of Pennsylvania, Department of Neurology, Philadelphia, PA, USA
[2]Perelman School of Medicine at the University of Pennsylvania, Department of Radiology, Philadelphia, PA, USA
[3]Perelman School of Medicine at the University of Pennsylvania, Department of Pathology & Laboratory Medicine and Center for Neurodegenerative Disease Research, Philadelphia, PA, USA
[4]Avid Radiopharmaceuticals, Philadelphia, PA, USA

Background: Autoradiographic evidence suggests that the ^{18}F-AV-1451 PET radioligand binds to paired helical filaments in Alzheimer's disease (AD), but there is mixed evidence related to binding to 4-repeat misfolded tau (4Rtau) in corticobasal degeneration (CBD). Thus, *in vivo* evaluations of ^{18}F-AV-1451 in patients with autopsy-confirmation are needed.

Method: A multimodal evaluation of a 58 year-old male who participated in baseline (15 months pre-death) clinical, ^{18}F-AV-1451 PET, ^{18}F-florbetapir PET, MRI, and DTI and longitudinal (5 months pre-death) ^{18}F-AV-1451 PET. At autopsy, immunohistochemistry confirmed a diagnosis of CBD.

Results: Baseline ^{18}F-AV-1451 PET revealed the highest retention in deep grey matter areas commonly associated with CBD pathology including bilateral substantia nigra, globus pallidus, and midbrain (Figure 1.a). Follow-up ^{18}F-AV-1451 PET revealed more visible retention in bilateral frontal and posterior temporal cortical regions along with midbrain and pons (Figure 1.b). An assessment of annualized change revealed a 1-9% increase in ^{18}F-AV-1451 PET retention, which was highest in the pons, medulla, and midbrain along with bilateral frontal and right temporo-parietal cortices (Figure 1.c). Baseline ^{18}F-AV-1451 PET uptake was inversely correlated with MRI gray matter volume (r_s=-0.209;p=0.016;Figure 2.a) and DTI mean diffusivity of white matter (r_s=-0.329;p=0.032;Figure 2.b). Percent area occupied (%AO) of tau pathological inclusions was related to follow-up ^{18}F-AV-1451 PET retention (r_s=0.768;p=0.001; Figure 2.c). Specifically, a SUVR≥1.2 captured all regions with high-tau pathology (%AO≥5.0) and did not capture any regions with low-tau pathology (%AO<5.0). Additionally, ^{18}F-AV-1451 PET uptake was more highly related to thread (r_s=0.712;p=0.004) than tangle (r_s=0.630;p=0.022) pathology.

Conclusions: This multimodal assessment demonstrates that ^{18}F-AV-1451 PET correlates with 4Rtau inclusions along with MRI and DTI measures. Single case data should be interpreted cautiously and future cohort studies including direct comparisons between CBD and AD are necessary to validate ^{18}F-AV-1451 PET.

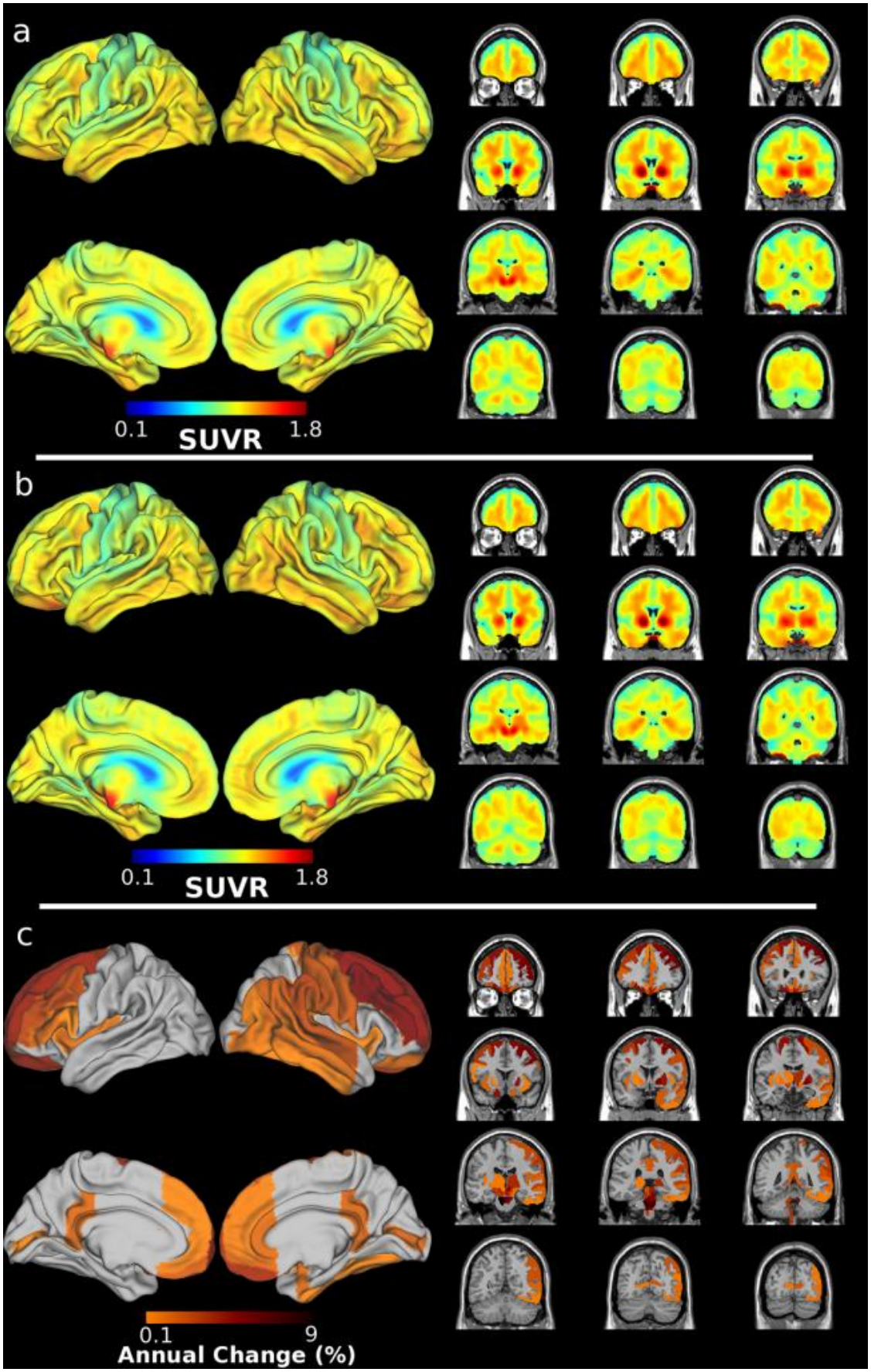

Figure 1. Regional distribution of 18F-AV-1451 PET

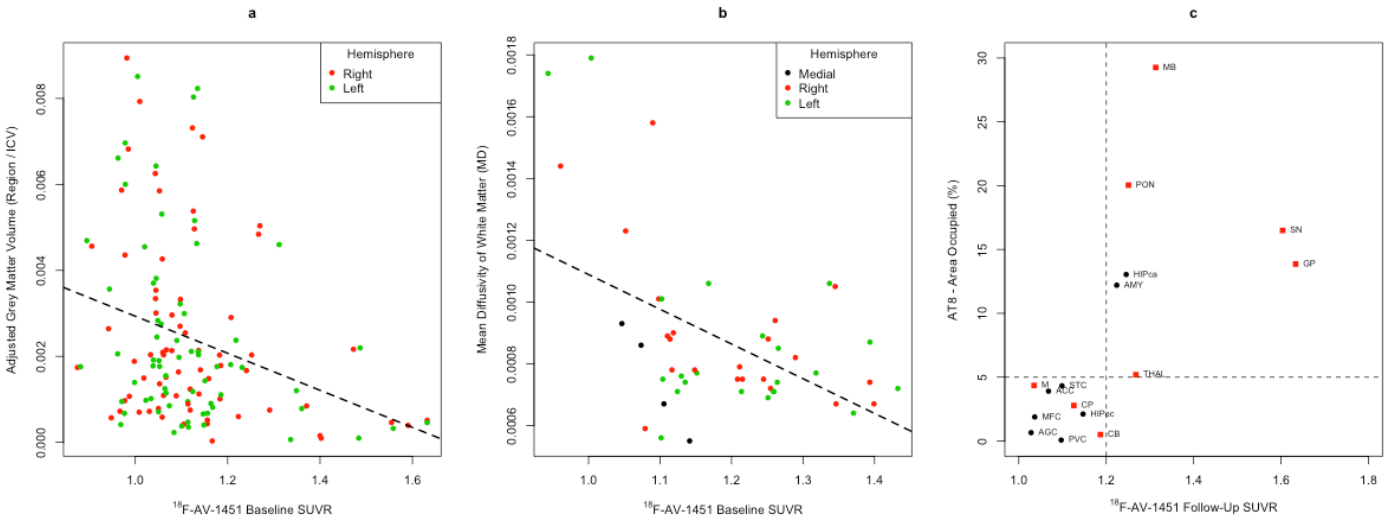

Figure 2. 18F-AV-1451 PET associations

Support: *NIH (AG043503;AG017586;AG10124), Dana Foundation & Avid Radiopharmaceuticals.*

Keywords: 18F-AV-1451 PET, Corticobasal Degeneration, tau, neuropathology, MRI

Thursday, January 12, 2017 - 11:30 am - 12:15 pm

Keynote Lecture: Thomas Beach

Tau PET for Alzheimer's Disease: Possible Promise and Pitfalls

Thomas Beach

Sun Health Research Institute, Sun City, AZ, USA

This investigative review will utilize a comparative clinicopathological viewpoint to speculate on the potential benefits, as well as the possible obstacles, for tau PET imaging of Alzheimer's disease (AD). Etiologically, the amyloid hypothesis has been dominant for 25 years but this relies largely on the existence of autosomal dominant forms of AD that are caused by mutations in genes that affect the amyloid-beta (Aβ) peptide. The universal occurrence of tangles in aging humans raises the possibility of a tangle-first scenario for most sporadic AD cases, with plaque-bearing individuals representing only a subset. The dominance of tangles over plaques, in terms of impact on cognition, is firmly established. The typical clinical presentation of AD with a simple amnestic deficit is very likely a direct effect of tangle development in the entorhinal area and hippocampus, while the progression to dementia is most strongly associated with tangle spread throughout the cerebral neocortex. Despite this, it is clear that widespread neocortical tangles in AD do not occur without widespread neocortical plaques, presenting difficulties for a simple, unifying theory. The clinical diagnosis of AD is inaccurate using neurological examination alone but biomarkers have improved this and PET imaging of Aβ and/or tau will soon allow pathology-based clinical staging of AD. These developments are expected to greatly improve clinical trial efficiency and hence progress towards disease-modifying therapies. Off-target binding of tau PET tracers is an enigma; this is not expected to seriously affect their usefulness for staging AD but may impair their application to non-AD tauopathies. Binding to iron-containing macromolecules such as hemosiderin and hemoglobin may be most explanatory but binding to melanin, mineralized deposits and lipopigments are alternate possibilities. Theoretically, molecular therapies directed against pathological tau hold at least equivalent promise as those directed against Aβ but highly prevalent comorbid pathologies, especially Lewy body disease, cerebrovascular disease and still-mysterious intrinsic aging processes may hinder any single-agent approach. Imaging-to-autopsy studies, as well as prolonged longitudinal observational studies, will be needed to determine the long-term prognostic value of both amyloid and tau PET and hence identify appropriate stages for intervention initiation. Primary prevention will have to be virtually free of serious adverse effects, and be relatively inexpensive, as treatment periods of several years will probably be needed. Secondary and tertiary prevention could utilize progressively less-innocuous and more expensive agents.

Thursday, January 12, 2017 - 01:45 pm - 02:45 pm

SESSION 5: Tau PET: Non-AD Targets

SESSION 5 **Tau PET: Non-AD Targets**	**CHAIRS:** **Gil Rabinovici** ***University of California, San Francisco*** **Brad Dickerson** ***Massachusetts General Hospital***
18F Flortaucipir binding in choroid plexus: association with race and hippocampus binding	Christopher Lee *Massachusetts General Hospital, Harvard Medical School*
[18F]Flortaucipir, aka [18F]AV-1451, Autoradiography Matches Immunofluorescent Staining From AT8 Tau Antibody in Chronic Traumatic Encephalopathy (CTE) Post-Mortem Brain Tissue Sections	Yin-Guo Lin *Avid Radiopharmaceuticals, Inc.*
Microscopic neuropathological evaluation of the binding profile of tau selective PET ligands in Alzheimer's disease and primary tauopathies	Melissa Wren *University College London*
AV-1451 tau-PET uptake in MAPT mutation carriers varies by tau isoforms	David Jones *Mayo Clinic*
18F-AV-1451 binding in familial frontotemporal lobar degeneration with tau pathology	William Kreisl *Columbia University*
Discussion	

18F Flortaucipir binding in choroid plexus: association with race and hippocampus binding

Christopher Lee[1], Marta Marquie[1], Nicolas Andrea[1], Molly LaPoint[1,2], David Jin[1], Heidi Jacobs[1], Aaron Schultz[1], Matthew Frosch[1], Teresa Gomez-Isla[1], Reisa Sperling[1,2], Keith Johnson[1,2]

[1]Departments of Neurology, Radiology, and the Athinoula A. Martinos Center for Biomedical Imaging, Massachusetts General Hospital, Harvard Medical School, Boston, MA, USA
[2]Center for Alzheimer Research and Treatment, Department of Neurology, Brigham and Women's Hospital, Harvard Medical School, Boston, MA, USA

Background: On-target ^{18}F-Flortaucipir (FTP) binding of Alzheimer's tau aggregates and off-target binding of melanocytes have been demonstrated with autoradiography (Marquie 2015). We hypothesized that if FTP binding in choroid plexus (CP) was associated with melanocytes, then FTP PET measures would be elevated in Black/African American (B/AA) participants compared to White (W).

Methods: FTP (SUVR; 80-100min,) and PiB PET were acquired in a total of 159 clinically normal participants in the Harvard Aging Brain Study, 26 B/AA and 133 W. Freesurfer FTP ROIs were sampled in CP, hippocampus (HC), amygdala (AM), inferior temporal gyrus (IT), entorhinal cortex (ER), and fusiform (FF) and corrected for the partial volume effect using GTM.

Results: Mean FTP SUVR, unadjusted for covariates, in CP was higher in Black/AA compared to White subjects (mean difference 0.47, +/-0.17, $p=0.011$) but did not differ in HC ($p>0.17$), AM ($p>0.05$), IT ($p>0.6$), ER ($p>0.8$) or FF ($p>0.7$). Elevated CP SUVR was independently associated with Black/AA race ($p=0.001$) and age ($p=0.0003$), covarying education, gender, PiB DVR and MMSE. In contrast, AM ($p>0.76$), IT ($p>0.5$), ER ($p>0.1$), and FF ($p>0.2$) SUVR were not associated with Black/AA race. However, HC SUVR was associated with Black/AA race ($p=0.003$), covarying age ($p<10^{-12}$), PiB DVR ($p=0.018$), gender, education, and MMSE; the association did reach significance when CP was included in the model.

Conclusions: These findings suggest that melanocyte binding of Flortaucipir may account for high PET signal in CP. As off-target binding affects FTP HC measurement, hippocampus FTP levels should be interpreted with caution.

Keywords: Alzheimer's disease, tau PET, choroid plexus, race

[18F]Flortaucipir, aka [18F]AV-1451, autoradiography matches immunofluorescent staining from AT8 tau antibody in Chronic Traumatic Encephalopathy (CTE) post-mortem brain tissue sections

Yin-Guo Lin[1], Qianwa Liang[1], Felipe Gomez[1], Ann Mckee[2], Mark A. Mintun[1], Giorgio Attardo[1]

[1]*Avid Radiopharmaceuticals, Inc., Philadelphia, PA, USA*
[2]*Boston University School of Medicine, Boston, MA, USA*

Objective: CTE is a progressive tauopathy characterized by abnormal tau aggregates in widespread brain regions that can occur in those with history of repetitive brain trauma. We previously evaluated the potential of AV-1451 to detect tau of CTE with fluorescent surrogates that bound tau inclusions in CTE brain sections. The use of high µM tracer concentration and alternative structures limited confidence in this previous data. Therefore, this study directly compares the autoradiography signal obtained from low M concentration of AV-1451 with AT-8 tau immunohistochemistry in CTE brain sections.

Methods: This study used sections of temporal cortex and striatum from 9 CTE brain sections (staged II, III and IV from Boston University) as well as negative and positive control brain slices from normal and Alzheimer's disease (AD), respectively, from National Disease Research Interchange. AV-1451 (20 µCi) was added to fresh frozen brain sections (10 µm thick) to obtain autoradiography images. The same brain sections were stained with phospho-Tau antibody AT8 and imaged using a NanoZoomer 2.0HT (Hamamatsu).

Results: Autoradiography signal of stage III-IV CTE sections was moderate to high in temporal cortex and well matched to AT-8 tau staining. It was low to moderate in the striatal area and matched to AT-8 in gray matter but not in white matter. Relative quantitation of autoradiography signal showed stage III-IV CTE sections with clearly more signal than normal brain sections, but at least 5-fold lower intensity than in the AD brain sections.

Conclusion: AV-1451 autoradiography demonstrates tau deposits in temporal cortex and striatum from advanced CTE brain tissue sections. However, the intensity of binding was much less in CTE than in AD sections raising the possibility that the number of tau binding sites in CTE is much lower than in AD which could make PET imaging of tau deposits difficult to achieve reliably.
Keywords: [18F]Flortaucipir, [18F]AV-1451, Autoradiography, Tau, CTE

Microscopic neuropathological evaluation of the binding profile of tau selective PET ligands in Alzheimer's disease and primary tauopathies

Melissa Wren[1,2], Kerstin Sander[1], Tammaryn Lashley[2], Nick Fox[3], Erik Arstad[1]

[1]*University College London, Institute of Nuclear Medicine and Department of Chemistry, London, United Kingdom*
[2]*University College London, Institute of Neurology, Queen Square Brain Bank for Neurological Disorders, London, United Kingdom*
[3]*University College London, Institute of Neurology, Dementia Research Centre, London, United Kingdom*

Background: Molecular imaging with positron emission tomography (PET) using tau-selective ligands may facilitate early diagnosis of the dementias and allow for assessment of potential disease-modifying interventions. Structurally diverse tau PET tracers have now been translated into clinical trials; however, it remains unclear what type of pathology the different compound classes depict, and at which sensitivity.

Aims: To understand the factors that govern tau tracer binding, and their implication for *in vivo* PET imaging.

Methods:: Tau selective ligands from two of the leading compound classes, the carbazole AV-1451, and its fluorescent analogue T726, and the quinoline THK-5117, were used to assess regional binding profiles by fluorescence microscopy, nuclear emulsion autoradiography and phosphor imaging. We used pathologically characterised tauopathy cases including Alzheimer's disease (AD), progressive supranuclear palsy (PSP), corticobasal degeneration (CBD), Pick's disease and frontotemporal dementia and parkinsonism linked to chromosome 17 (FTDP-17), together with age-matched controls. Results were correlated with underlying pathological tau immunostaining.

Results: In contrast to immunohistochemistry with the tau selective antibody AT8, imaging with T726 and THK-5117 in an AD cohort revealed large variations in the frequency of tracer binding to different types and maturities of pathological tau inclusions, and this binding varied between brain regions analyzed. Tracers from both compound classes were able to delineate neurofibrillary tangles from a mixed tau repeat FTDP-17 MAPT case, but binding was not detected in the microscopic inclusions of tissue from PSP, CBD, Pick's disease, or tau isoform specific FTDP-17 cases.

Conclusions: The results suggest that binding of tau selective ligands to the pathological inclusions found in the different tauopathies is not solely dictated by isoform composition or by the respective disease strain. Therefore, it cannot be assumed that *in vivo* PET truly reflects the distribution of tau pathology across brain areas.
Keywords: AV-1451, THK-5117, tau, PET, microscopy

AV-1451 tau-PET uptake in MAPT mutation carriers varies by tau isoforms

David Jones[1], Val Lowe[1], Jonathan Graff-Radford[1], Jeremy Syrjanene[1], Matthew Senjem[1], Christina Dheel[1], Zbigniew Wszolek[2], Rosa Rademakers[2], David Knopman[1], Ronald Petersen[1], Clifford Jack[1], Bradley Boeve[1]

[1]*Mayo Clinic, Rochester, MN, USA*
[2]*Mayo Clinic, Jacksonville, FL, USA*

Background: Tau positron emission tomography (Tau-PET) ligands have shown strong binding in Alzheimer's disease (AD) dementia cases *in vivo*. However, it is uncertain how well Tau-PET imaging performs in *MAPT* gene mutation carriers. Some *MAPT* mutations result in 3- and 4-repeat tau aggregates that are very similar to the aggregates seen in AD, while other mutations may result in tau aggregates that differ from AD.

Methods: We quantitatively (i.e., ROIs) and qualitatively (i.e., visual inspection) compared Tau-PET (AV-1451) SUVR values (cerebellar crus reference) in 9 symptomatic and 1 asymptomatic *MAPT* mutation carriers (n = 10, age range 42-67) with AD dementia subjects (n = 24, age range 54-90) and age-matched clinically normal (CN) subjects (n = 9, age range 42-67). Eight subjects had *MAPT* mutations that involved exon 10 (N279K, n=5; S305N, n=2; P301L, n=1) and two did not (V337M, n=2).

Results: Tau-PET signal was qualitatively and quantitatively different between AD, CN, and MAPT with the greatest signal intensity in AD and minimal regional signal in *MAPT* mutation carries with mutations in exon 10, each of which have primarily 4-repeat tau aggregates. However, *MAPT* mutation carriers with the mutations outside of exon 10 associated with 3- and 4- tau aggregates (V337M, n=2) had higher levels of signal relative to *MAPT* mutation carriers with mutations in exon 10 and greater than controls, but fell within the AD range (Figure 1).

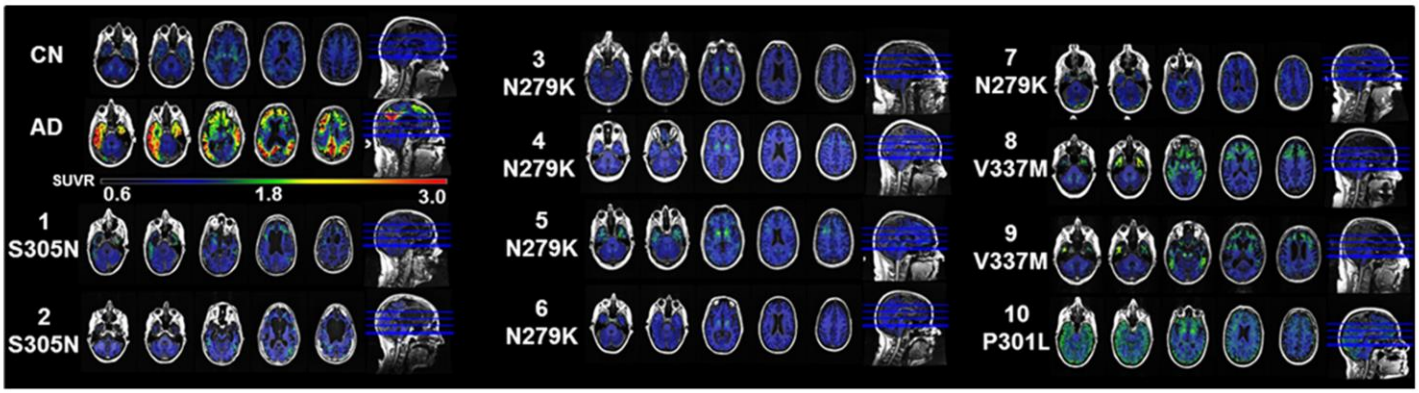

Figure 1: AV-1451 in MAPT mutation carriers and reference clinically normal (CN) and Alzheimer's disease (AD) dementia subjects. Some MAPT mutation show elevated signal in affected brain regions, but the magnitude is typically within the control range. Subjects 8 and 9 however show a higher magnitude of signal that falls in the AD range.

Conclusions: AV-1451 shows higher magnitude of binding in *MAPT* mutation carriers that harbor mutations that are more likely to produce AD-like tau pathology. Exon 10 splicing determines the balance of 3R and 4R tau isoforms with mutations in exon 10 predisposing to a greater proportion of 4R aggregates and

consequently a lower level of AV-1451 binding (Figure 2), supporting the notion that AV-1451 has specific binding properties for AD-like tau pathology.

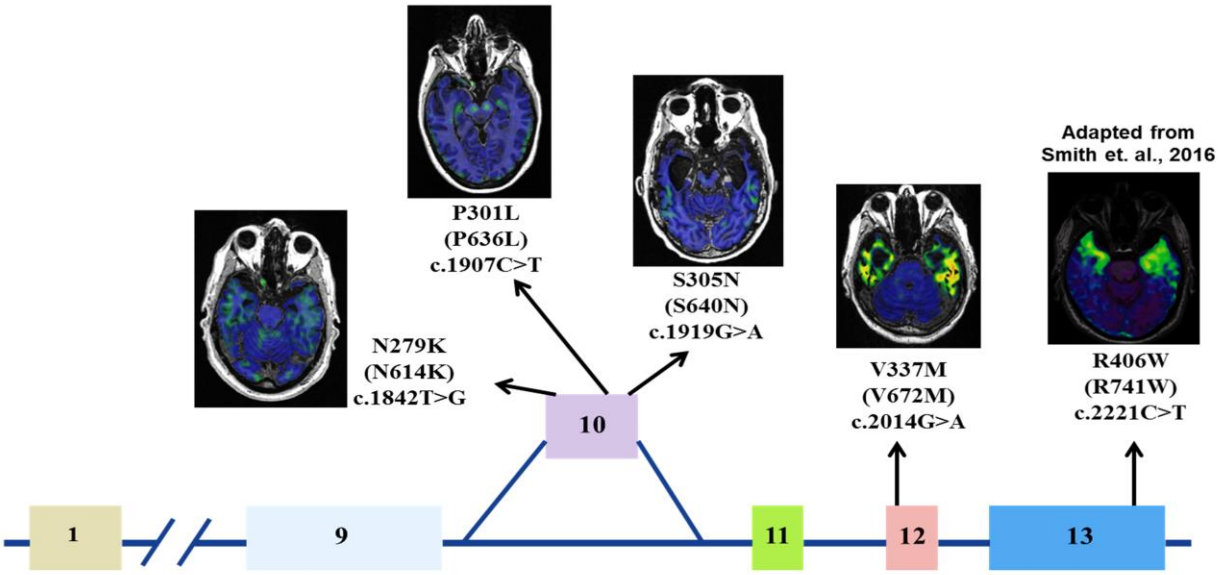

Figure 2: *MAPT* mutation location and representative AV-1451 scans. A schematic of the *MAPT* gene is displayed, highlighting the role of exon 10 splicing in determining 3R and 4R tau isoforms. The approximate mutation location and representative AV-1451 scans are indicated above for four subjects included in this analysis and one subject from the literature (adapted from Smith et. al., Brain [2016]). This schematic highlights the lack of significant AV-1451 signal in *MAPT* mutation carriers that harbor mutations that may disrupt exon 10 splicing.

Keywords: Tau-PET, AV-1451, MAPT, FTD

18F-AV-1451 binding in familial frontotemporal lobar degeneration with tau pathology

William Kreisl, Jill Goldman, Edward Huey

[1]*Columbia University, New York, NY, USA*

Background: *MAPT* mutations cause familial frontotemporal lobar degeneration with tau pathology (FTLD-tau). Alternative slicing of *MAPT* results in aggregates that are composed of different tau isoform conformations. ^{18}F-AV-1451 was developed to bind to tau aggregates found in Alzheimer's disease, which are composed of both 3-repeat (3R) and 4-repeat (4R) tau isoforms. We sought to evaluate the ability of ^{18}F-AV-1451 to detect tau aggregates in familial FTLD-tau caused by different *MAPT* mutations.

Methods: A total of seven members of three different families with *MAPT* mutations underwent PET imaging with ^{18}F-AV-1451. *MAPT* mutations were associated with either predominantly 4R (P301L) or 3R + 4R (V337M and R406W) tau aggregates. Symptomatic (n = 4) and asymptomatic carriers (n = 1) and non-carriers (n = 2) were included. PET images were acquired 80-100 min after injection of 10 mCi ^{18}F-AV-1451. Regional standardized uptake value ratios (SUVRs) were obtained by dividing uptake in target regions to that in cerebral gray matter.

Results: The three symptomatic V337M carriers (age 50-59 years, CDR = 0.5) had the greatest amount of ^{18}F-AV-1451 binding (Table 1), with highest SUVRs in orbitofrontal cortex, anterior and ventral temporal cortex, and amygdala. The asymptomatic V337M carrier (age 33 years) and the symptomatic P301L carrier (age 56 years, CDR = 1) had ^{18}F-AV-1451 binding similar to that in the two non-carriers (ages 28 and 60 years).

Conclusion: ^{18}F-AV-1451 detects tau aggregates in V337M mutation carriers and therefore may be helpful in monitoring progression in patients with 3R + 4R tauopathies. Additional scans are required to confirm the conformational specificity of ^{18}F-AV-1451 in FTLD-tau and to determine the threshold for PET positivity in 3R + 4R mutation carriers.

Table 1. Clinical characteristics, mutation type, and ^{18}F-AV-1451 binding for *MAPT* mutation family members

	Non-carriers		Carriers				
Age (years)	28	60	33	50	57	59	56
Family Mutation	R406W	V337M	V337M	V337M	V337M	V337M	P301L
Tau isoform	3R+4R	3R+4R	3R+4R	3R+4R	3R+4R	3R+4R	4R
CDR score	0	0	0	0.5	0.5	0.5	1
Ventral temporal ^{18}F-AV-1451 SUVR	0.99	1.09	1.1	1.36	1.52	1.81	1.05

Abbreviations: CDR = Clinical Dementia Rating scale, SUVR = standardized uptake value ratio

Keywords: AV-1451, FTLD-tau, MAPT

Thursday, January 12, 2017 - 03:30 pm - 04:15 pm

Poster Session 2B - *see 2A*

Thursday, January 12, 2017 - 04:15 pm - 04:30 pm

SESSION 6: Thresholds and Centiloids

SESSION 6 **Thresholds and Centiloids**	**CHAIRS:** **Keith Johnson** ***Massachusetts General Hospital*** **Sylvia Villeneuve** ***McGill University***
Defining cut-points for imaging biomarkers used in brain aging and Alzheimer's disease research	Clifford Jack *Mayo Clinic*
Further Adventures in the World of Centiloids	Robert Koeppe *University of Michigan*

Defining cut-points for imaging biomarkers used in brain aging and Alzheimer's disease research

Clifford Jack[1], Heather Wiste[1], Stephen Weigand[1], Terry Therneau[1], Val Lowe[1], David Knopman[1], Jeffrey Gunter[1], Matthew Senjem[1], David Jones[1], Kejal Kantarci[1], Mary Machulda[1], Michelle Mielke[1], Rosebud Roberts[1], Prashanthi Vemuri[1], Denise Reyes[1], Ronald Petersen[1]

[1]*Mayo Clinic, Rochester, MN, USA*

Introduction: Every biomarker exists on a continuum; however, normal/abnormal cut-points are necessary in certain situations. Our goal was to develop cut-points for amyloid PET, tau PET, FDG PET, and cortical thickness.

Methods: Clinically normal (CN) individuals in this study were participants in the Mayo Clinic Study of Aging. Cognitively impaired individuals (MCI or AD dementia) were participants in either the Study of Aging or the Alzheimer's Disease Research Center. We examined five methods for determining cut-points (**Fig 1**): (1) the threshold value beyond which the biomarker rate of change worsens reliably, (2) 95% specificity in young CN, (3) 90% sensitivity in amyloid PET positive clinically impaired, (4) accuracy in distinguishing amyloid PET positive clinically impaired from young CN, (5) accuracy in distinguishing amyloid PET positive clinically impaired from age-matched amyloid PET negative CN.

Results: The reliable worsening method produced a cut-point for amyloid PET but not for FDG PET or cortical thickness. The specificity, sensitivity, and accuracy of clinically impaired versus young CN methods all gave similar cut-points for tau PET, FDG PET and cortical thickness (**Fig 2**). These labeled the most people positive and thus we refer to these cut-points as "lenient". Cut-points defined using the accuracy of clinically impaired versus age-matched CN method labeled fewer people positive and therefore were more conservative for tau PET, FDG PET and cortical thickness (**Fig 3**). Lenient cut points do not while conservative cutpoints do incorporate the notion of "age norming."

Discussion: In the future, we will employ a single cut-point for amyloid PET (SUVR 1.42, centiloid 19) based on the reliable worsening cut-point method. We will base lenient cut-points for tau PET, FDG PET and cortical thickness on the accuracy of clinically impaired vs young CN method and base conservative cut-points on the accuracy of clinically impaired vs age-matched CN method.

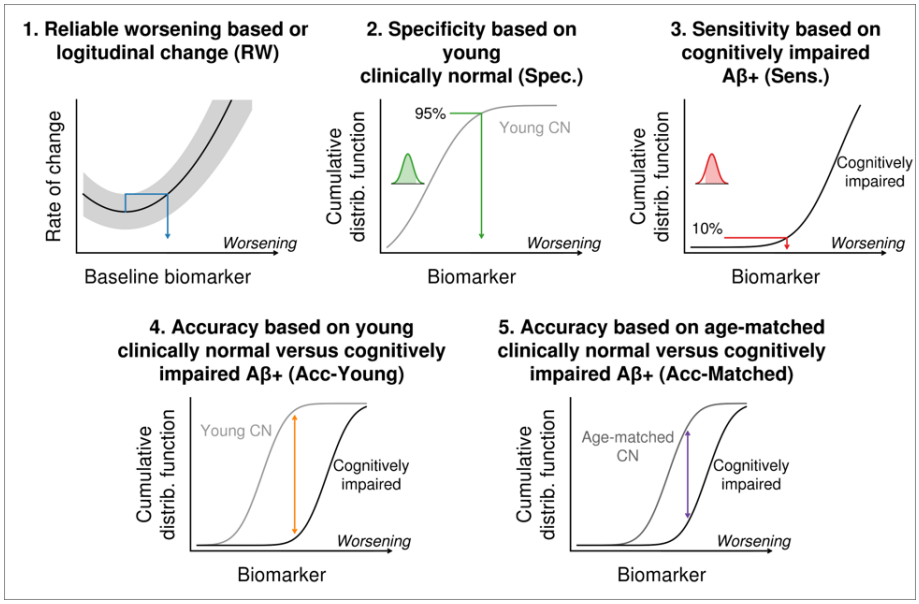

Figure 1. Cut-point methods. *Graphical summary of the five methods used for determining cut-points. In each panel, increasing numeric values of the biomarker correspond to biomarker worsening. A biomarker's cumulative distribution function (CDF) indicates a biomarker value x on the horizontal axis and the proportion of observations less than or equal x on the vertical axis.*

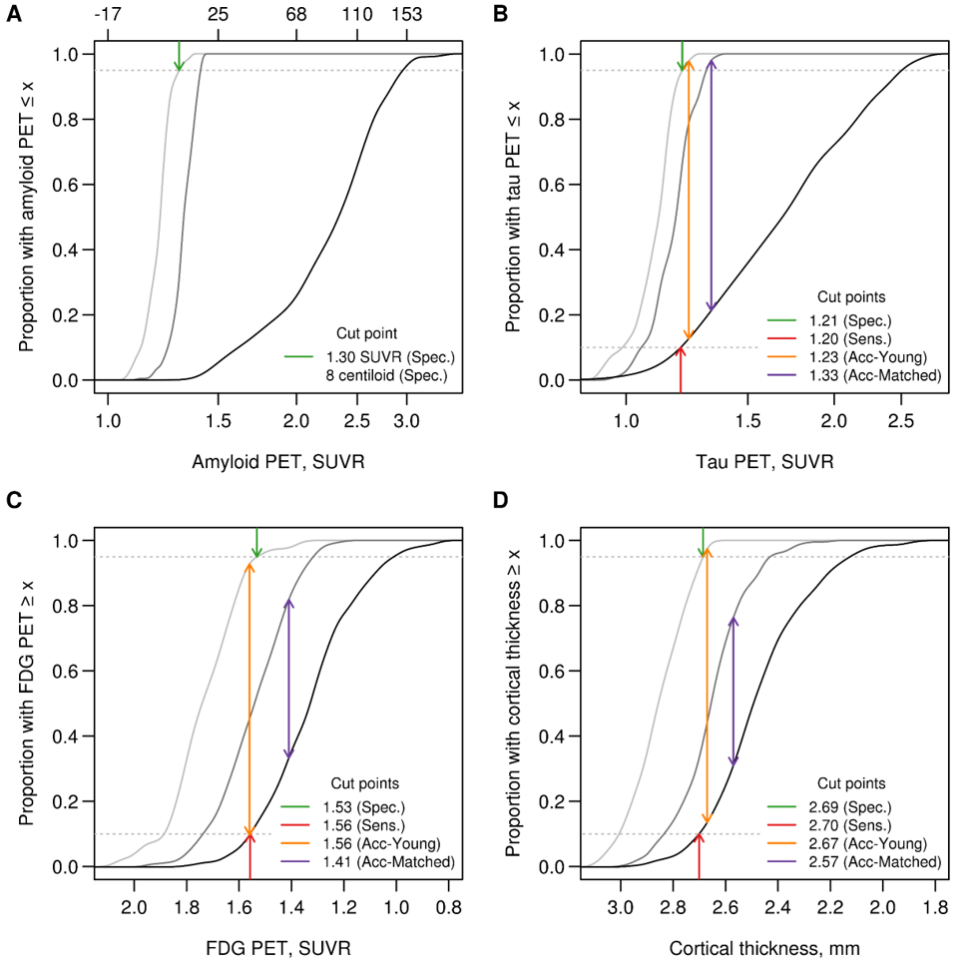

Figure 2. Specificity, sensitivity, and accuracy cut-points. *Cumulative distribution function (CDF) plots for young CN individuals (light grey), cognitively impaired individuals (black), and older CN individuals that were age- and sex-matched to the cognitively impaired group (dark grey). The arrows indicate cut-points chosen corresponding to 95% specificity (CDR = 0.95, dark green arrow), 90% sensitivity (CDF = 0.10, dark red arrow), accuracy in discriminating between young CN and cognitively impaired individuals (orange arrow), and accuracy in discriminating between age-matched CN and cognitively impaired individuals (purple arrow). Accuracy was defined as the point of maximum difference between two CDFs. Amyloid PET was used in the definition of the cognitively impaired group so only the specificity cut-point is shown. For amyloid PET (panel A), values are shown in both SUVR and centiloid units. Panel B tau PET; panel C FDG PET; panel D MRI.*

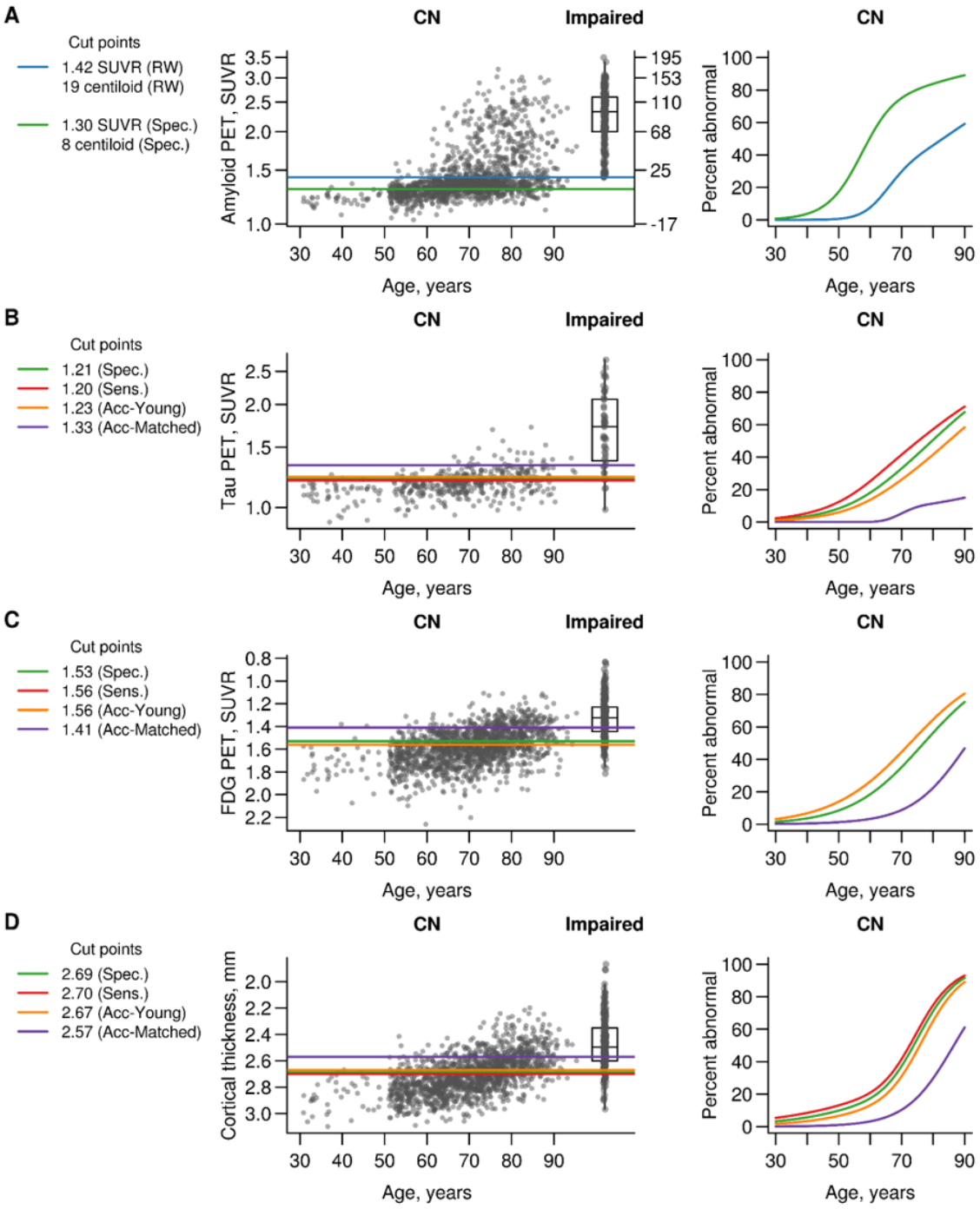

Figure 3. Biomarkers vs age. *Scatter plots of each biomarker versus age among all MCSA CN individuals with box plots of the cognitively impaired group shown for reference. The horizontal lines indicate cut-points chosen from the five methods. The colors used were as follows: reliable worsening (RW), blue (only in panel A); specificity (Spec.), green; sensitivity (Sens.), red; accuracy of cognitively impaired versus young CN (Acc-Young), orange; accuracy of cognitively impaired versus matched CN (Acc-Matched), purple. Using each of these five cut-point methods, we then label individuals as normal or abnormal and show the percent abnormal as estimated from logistic regression models. For amyloid PET (panel A), values are shown in both SUVR and centiloid units. Panel B tau PET; panel C FDG PET; panel D MRI.*

Keywords: Amyloid PET, tau PET, MRI, Alzheimer's biomarkers, Alzheimer's imaging

Thursday, January 12, 2017 - 04:30 pm - 04:30 pm

Koeppe, Robert

Further Adventures in the World of Centiloids

Robert A. Koeppe[1], Julie C. Price[2], Centiloid Working Group

[1]University of Michigan, Ann Arbor, MI
[2]Harvard University, Cambridge, MA
with Contributions from Eli Lilly/Avid, GE Healthcare, Navidea Biopharmaceuticals, and Piramal Imaging

The original Centiloid project provided a standardized method for scaling PiB data onto a 100-point scale, with "0" being the amyloid load for an "average" young control and "100" being the load for a "typical" AD patient. The original work had primary aims of providing a method for conversion of other "non-standard" methods of analysis (e.g. dynamic instead of static) or other amyloid tracers (e.g. the commonly used [^{18}F]-labeled radiopharmaceuticals) to the same 0-100 Centiloid scale.

This talk will be divided into two sections:

1) the conversion of [^{18}F]-labeled radiotracers into Centiloids, and
2) further investigation into potential sources of variability and error in the original Centiloid method.

Conversion of [^{18}F]-radiotracers: The key step in the conversion of [^{18}F]-tracers to the Centiloid scale is to acquire paired PET studies using both [^{11}C]-PiB and an [^{18}F]-compound in group of subjects including both amyloid negative and amyloid positive individuals. The standard Centiloid target VOI and reference regions are then applied to both scans to calculated pairs of SUVr measures for each individual. The regression coefficients of the relationship between the F-18 measures and the C-11 PiB measures provide the conversion of F-18 SUVr values to "PiB-equivalent" SUVr values, and hence the subsequent conversion of F-18 SUVr to Centiloids. Regression equations from studies perform by each of the companies will be presented, with emphasis on the slope of the regression line between the F-18 tracer and PiB (as a measure of signal), and the standard deviation of the amyloid-negative controls (as a measure of noise).

Centiloid 2.0: The second portion of this talk will be a brief introduction to a soon to be submitted grant to the Alzheimer's Association titled "Further Validation of Centiloid Scaling for Amyloid PET Standardization: Centiloid 2.0." The original Centiloid project did not examine the impact of different scanner platforms or of the wide anatomical variation across young to elderly and diseased brains on the original Centiloid scaling process. The two primary specific aims of the grant will be to 1) evaluate the impact of PET scanner model differences on the scaling process by scanning subjects (both control, MCI and AD) on multiple scanner models and 2) identify an advanced image normalization/VOI sampling method for the scaling process that minimizes that problems associated with varying brain anatomy in aging and disease.

FRIDAY

Friday, January 13, 2017 - 08:00 am - 08:45 am

SESSION 7: Amyloid and Tau PET in Clinical Trials

SESSION 7 **Amyloid and Tau PET in Clinical Trials**	**CHAIRS:** **Bill Jagust** ***University of California, Berkeley*** **Susan Resnick** ***National Institutes of Health***
The A4 Study: Preliminary Analyses of Baseline Tau PET Imaging	Reisa Sperling *Harvard Medical School*
Conversion of aMCI subjects to AD in relation to [18F]flutemetamol Amyloid status, and hippocampal volume in a phase III longitudinal study	David Wolk *Perelman School of Medicine at the University of Pennsylvania*
Baseline 18F Flortaucipir SUVR, but not amyloid or cognition, predicts cognitive decline over 18 months in Phase 2 trial subjects	Michael Devous, Sr. *Avid Radiopharmaceuticals*
PET amyloid and tau imaging in a Phase 3 study of solanezumab	Mark Mintun *Avid Radiopharmaceuticals*
Discussion	

The A4 Study: Preliminary Analyses of Baseline Tau PET Imaging

Reisa Sperling[1,2], Aaron Schultz[2], Dorene Rentz[1], Elizabeth Mormino[2], Eric Siemers[3], Roy Yaari[3], Sergey Schcherbinin[3], Adam Schwarz[3], Michael Devous[4], Mark Mintun[4], Michael Donohue[5], Paul Aisen[5], Keith Johnson[2]

[1]*Brigham and Women's Hospital, Boston, MA, USA*
[2]*Massachusetts General Hospital, Boston, MA, USA*
[3]*Eli Lilly and Company, Lilly Corporate Center, Indianapolis, Indianapolis, IN, USA*
[4]*Avid Radiopharmaceuticals, Philadelphia, PA, USA*
[5]*Alzheimer Therapeutic Research Institute, Keck School of Medicine, University of Southern California, San Diego, CA, USA*

Background: The advent of Tau PET imaging allows the *in vivo* detection and tracking of paired helical filament tau pathology, which may prove to be a particularly relevant outcome in secondary prevention trials in preclinical Alzheimer's disease (AD). The Anti-Amyloid Treatment in Asymptomatic AD (A4) Study is a Phase 3 trial of solanezumab vs. placebo in clinically normal older individuals with evidence of elevated amyloid accumulation on screening Florbetapir (FBP) imaging.
Methods: Tau PET imaging with 18F-Flortaucipir (FTP, aka AV1451/T807) is being acquired in a subset of participants at baseline, 18 and 36 months. FTP SUVr is evaluated in anatomically defined regions of interest (ROI) and with whole brain analyses, examining associations with FBP mean cortical SUVr and screening cognitive measures (Free and Cued Selective Reminding Test (FCSRT), Logical Memory Delayed Recall, Digit Symbol, and MMSE) with age, education, and gender covaried.
Results: FTP data (n=185; mean age=72.2±5.0; 99F/86M; MMSe=28.6±1.4) revealed a range of neocortical signal with 103/185 (56%) demonstrating SUVr >1.2 in inferior temporal regions. Significant positive associations between FBP and FTP were found in entorhinal, parahippocampal, fusiform, inferior and middle temporal, isthmus, and posterior cingulate ROI (partial r =.30 to.42; p<0.001).
Conclusion: Ongoing analyses suggest that regional Tau accumulation is significantly associated with cortical amyloid deposition and memory performance, even within the restricted ranges seen in the amyloid-positive clinically normal population eligible for A4. These preliminary findings suggest that we will be able to test the hypothesis whether decreasing amyloid accumulation can slow the spread of tau pathology and memory decline during preclinical AD.

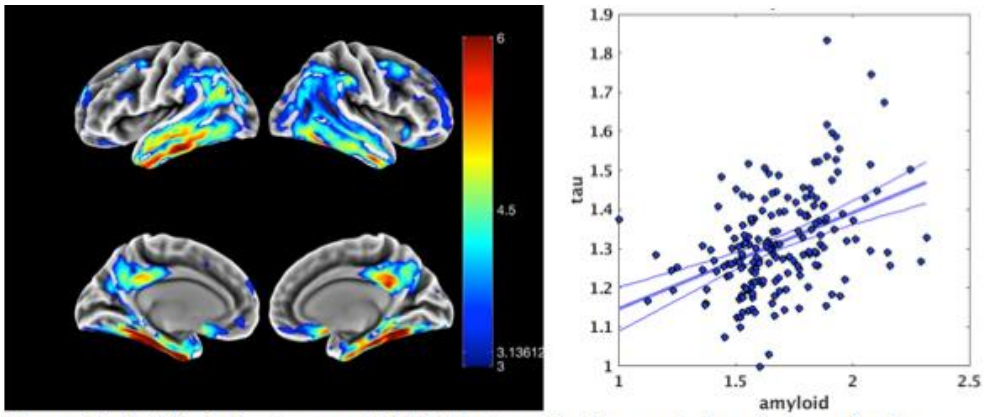

Figure. Left: Whole brain map of 18F-Flortaucipir demonstrating the voxel-wise association with mean cortical 18F-Florbetapir SUVr, adjusted for age. Right: Regression plot of 18F-Flortaucipir (tau) vs. 18F-Florbetapir (amyloid) extracted from peak voxel in left inferior temporal region (partial r= .42; p<0.00001).

Keywords: Tau PET, Amyloid PET, prevention, clinical trials, memory

Conversion of aMCI subjects to AD in relation to [18F]flutemetamol Amyloid status, and hippocampal volume in a phase III longitudinal study.

Wolk David[1], Andrea Cherubini[2], Chris Buckley[3], Michelle Zanette[4], Paul Sherwin[4]

[1]*University of Pennsylvania, Philadelphia, PA, USA*
[2]*Institute of Molecular Bio-imaging and Physiology, Rome, Italy*
[3]*GE Healthcare, Amersham, United Kingdom*
[4]*GE Healthcare, Marlborough, MA, USA*

Introduction: GE Healthcare conducted a study in which 232 patients with amnestic mild cognitive impairment (aMCI) underwent baseline MRI and amyloid PET imaging with flutemetamol to determine time to conversion to dementia in relation to baseline amyloid status. Conversion was determined by an independent committee, which reviewed the results of 6-monthly neuro-psychiatric testing for up to 36 months. While amyloid positivity was a significant and independent predictor of conversion, in a post-hoc analysis we also determined the association of hippocampal atrophy with conversion with the ultimate-aim of combining biomarkers to improve conversion prediction.

Methods: Baseline 3D T1 MRI scans from the study cohort were analysed quantitatively for hippocampal volume (hvol) estimation[1] in a post-hoc analysis. ANOVA was used to compare hvol by conversion to dementia status and amyloid status by flutemetamol image as positive/negative for amyloid by majority visual-read by five independent readers. The derived hvols were considered high if greater than-or-equal to 4.5cm^3 and low if below this value[2].

Results: Among amyloid-*negative* patients, converters had a significantly lower hvol ($p<0.0001$) than non-converters. For amyloid-*positive* patients, converters had a significantly lower hvol than non-converters ($p=0.014$).

Using PET images alone, the hazard ratio for conversion over 3y for amyloid positive subjects compared to amyloid negative subjects was 2.5:1. However, when the PET & MRI biomarkers were combined, the Hazard ratio for subjects who were amyloid positive and of low hvol compared to those who were amyloid negative and high hvol was 5.6:1, see figure 1. These results stratify the risk and rate of progression from aMCI to pAD over three years using baseline assessments of flutemetamol PET and MRI scans and demonstrate the utility of combining Aβ PET and MRI biomarkers.

References:

1. Coupé et al., NeuroImage, 54 (2011), 940–954

2.

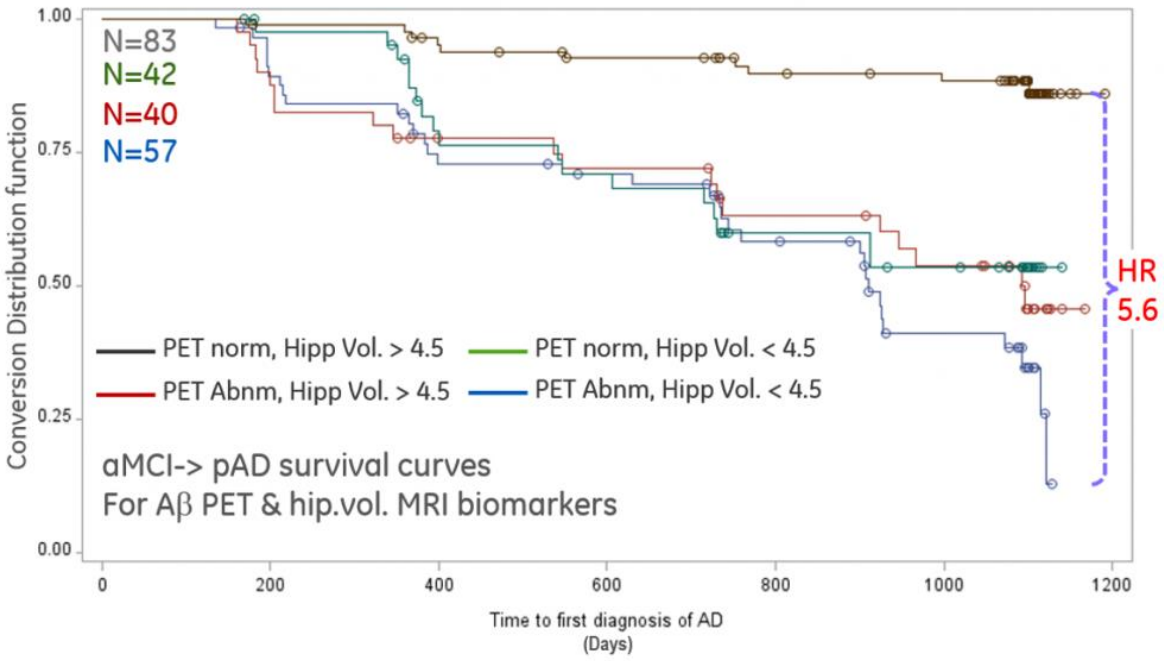

Kaplan-Meier survival plot of aMCI -> pAD conversion for majority flutemetamol visual read of amyloid PET status and threshold (4.5cc) hippocampal volume (n=222).

Keywords: aMCI, hipocampal volume, risk, conversion

Baseline 18F Flortaucipir SUVR, but not amyloid or cognition, predicts cognitive decline over 18 months in Phase 2 trial subjects

Michael D. Devous, Sr.[1], Navitsky Michael[1], Andrew Siderowf[1], Ian Kennedy[1], Abhinay D. Joshi[1], Sudeepti Southekal[1], Ming Lu[1], Michael J. Pontecorvo[1], Mark A. Mintun[1]

[1]*Avid Radiopharmaceuticals, Inc., Philadelphia, PA, USA*

Background: Literature suggests that neuropathologic tau correlates with cognitive impairment. It is unknown whether tau distributions relate to the evolution of cognitive deterioration. We examined relationships between Flortaucipir uptake and changes in cognition or function over time.

Methods: Flortaucipir scans (acquired 80-100 min post 370 MBq injection) were obtained in amyloid-positive healthy (n=5), MCI (n=47) or AD (n=30) subjects. VOI SUVr values were obtained from 1) a VOI determined by discriminant analysis to distinguish diagnostic groups (MUBADA) and 2) VOIs defined at baseline by the correlation between tau and domain-specific cognitive tests (correlation maps). SUVR values were normalized to a parametrically-derived white matter reference region. Assessments included MMSE, ADAS-Cog, a neuropsychological battery and the Functional Activities Questionnaire (FAQ). Correlations were used to compare baseline Flortaucipir SUVr, amyloid SUVR (Florbetapir) or cognitive scores to changes in cognition after 18 months.

Results: Strong correlations at baseline were seen between both Flortaucipir and Florbetapir SUVr relative to MMSE, ADAS-Cog and FAQ (Table 1). Baseline Flortaucipir MUBADA SUVr was also correlated with all 18-month cognitive and functional change measurements (ADAS p=0.047, MMSE p=0.0007, FAQ p=.0006; Table 1). However, amyloid SUVR was not correlated with 18 month changes in cognition or function, nor were baseline cognitive or functional measures correlated with changes with their respective measure. Heat map analysis (Table 2) demonstrated that for most cognitive domains, MUBADA SUVR was at least as effective as the cognitive-correlation-derived VOIs at predicting 18 month changes.

Conclusions: Baseline tau was strongly correlated with 18 month change in MMSE, ADAS-Cog and FAQ. However, neither baseline amyloid, cognitive nor functional scores related to changes at 18 months. These data suggest that tau is relevant to the evolution of cognitive and functional decline in ways not evident for either amyloid or the cognitive/functional measures themselves in MCI and AD patients.

Table 1: Relationships between tau and cognition. Baseline correlations are modeled to adjust for effects of age. 18 month change data models include both age and baseline cognition.

Baseline tau or amyloid vs baseline cognition or function

SUVr	ADAS (n=82)	MMSE (n=82)	FAQ (n=77)
Tau MUBADA	**0.52** **<.0001**	**-0.46** **<.0001**	**0.35** **0.0023**
Tau Precuneus	**0.52** **<.0001**	**-0.44** **0.0001**	**0.30** **0.0088**
Amyloid (Florbetapir)	**0.46** **<.0001**	**-0.41** **0.0002**	**0.26** **0.0245**

Baseline tau, amyloid, cognition or function vs 18 mo. Δ cognition or function

Baseline SUVr	ADAS Change (n=49)	MMSE Change (n=53)	FAQ Change (n=52)
Tau MUBADA	**0.28** **0.0468**	**-0.46** **0.0007**	**0.48** **0.0006**
Tau Precuneus	0.21 0.1529	**-0.41** **0.0032**	**0.46** **0.0009**
Amyloid (Florbetapir)	0.09 0.5391	-0.08 0.5870	-0.03 0.8301
Baseline ADAS, MMSE or FAQ scores	0.22 0.1623	-0.04 0.22	0.02 0.8915

Table 2. Relative predictive strength of baseline tau for either the MUBADA VOI or for the cognition-specific VOIs relative to 18-month change in cognition. Correlation coefficients derived from Pearson's R. Cog VOI = VOI derived from tau / cognitive test correlation maps.
Red = r $\geq$ 0.3; yellow = 0.2 $\geq$ r < 0.3; green = r < 0.2.

R	ADAS	Clock Draw	Construct praxis	DSST	Delayed Recall	Digit Span	Ideational Praxis	Immed Recall	MMSE	Orientatn	Remembr Instructns	Trails A	Trails B	Word Recall	Word Recog
MUBADA	0.30	-0.20	0.28	-0.43	-0.33	-0.20	0.29	-0.22	-0.50	0.21	0.41	0.17	0.31	0.17	-0.07
COG VOI	0.34	-0.21	0.13	-0.38	-0.26	-0.18	0.22	-0.18	-0.50	0.13	0.26	0.13	0.30	0.15	-0.05

Keywords: tau imaging, cognitive decline, progression, Amyloid, flortaucipir

PET amyloid and tau imaging in a Phase 3 study of solanezumab

Mark A Mintun[1], Michael D Devous, Sr.[1], Ming Lu[1], Michael J Pontecorvo[1], Abhinay D Joshi[1], Sudeepti Southekal[1], Andrew Siderowf[1], Mark J Lowrey[1], Marybeth Devine[1], Tyler E Benedum[1], Caitlin Pearson[1], Nathaniel C Lim[1], Adam S Fleisher[2], Karen L Sundell[2], Eric R Siemers[2]

[1]*Avid Radiopharmaceuticals, Inc., Philadelphia, PA, USA*
[2]*Eli Lilly and Company, Indianapolis, IN, USA*

Background: EXPEDITION3 is a placebo-controlled Phase 3 study assessing the effect of solanezumab, an IgG1 humanized monoclonal antibody that binds soluble amyloid-beta (Aβ) peptides, on cognitive decline over 80 weeks in patients with mild Alzheimer's disease (AD). A subset of subjects underwent amyloid PET imaging with -florbetapir (N=1839), and a subset of those also underwent tau PET imaging with -flortaucipir (N=206).

Methods: Amyloid PET scanning (20 min scans at 50 min post injection of 10 mCi -florbetapir) was done at screening and at week 80. SUVr values are calculated from standard atlas-based cortical and whole cerebellar regions. Longitudinal measures are normalized by a subject-specific MRI-derived white matter region to reduce variability in longitudinal amyloid PET estimate.

Tau PET scanning (30 min scans, 75 min post injection of 6.5 mCi 18F-flortaucipir) was done at baseline, week 40 and week 80. Flortaucipir SUVr will be calculated using a large atlas-based cortical region normalized by a parametrically derived subject-specific white matter reference region.

Solanezumab treatment effects on florbetapir amyloid and flortaucipir tau PET imaging will be evaluated with analysis of co-variance (ANCOVA) and mixed effects model repeat measurement (MMRM), respectively.

Results: Power was estimated from exploratory analyses of previous Phase 3 solanezumab amyloid PET studies and was calculated to be >90% for detection of a reduction in amyloid load as small as 2% from baseline in the treatment arm, assuming the placebo arm had no change. Based on data from a longitudinal flortaucipir Phase 2 study (Figure 1), the power for detecting the slowing of accumulation of tau deposits ranged from 28% to over 80% depending on the magnitude of the treatment effect and number of subjects completing the substudy (Table 1).

Conclusions: Imaging biomarkers are poised to play an increasing role in understanding the effect of therapeutic drugs on underlying AD pathology. Methodologies designed for assessing these results will be discussed.

***Figure 1*: PET Tau signal measured by [18F]-flortaucipir by age in subjects enrolled in a Phase 2 trial.** Data points are from subjects completing flortaucipir PET scans at baseline, 9 month and 18 month visits. Not all subjects were able to complete all visits. The SUVr on the y-axis was calculated using an atlas-based large cortical region (created with a diagnostic group discriminant analysis and labeled MUBADA) normalized by a parametrically derived subject-specific white matter reference region. The red data is for subjects with positive amyloid PET scans at baseline and the blue data are subjects with negative amyloid PET scans. In amyloid positive subjects the change in flortaucipir SUVr at the 18 month visit compared to baseline was +0.051 ± 0.0053 (LS Mean ± SE) and was statistically significant (p<0.0001).

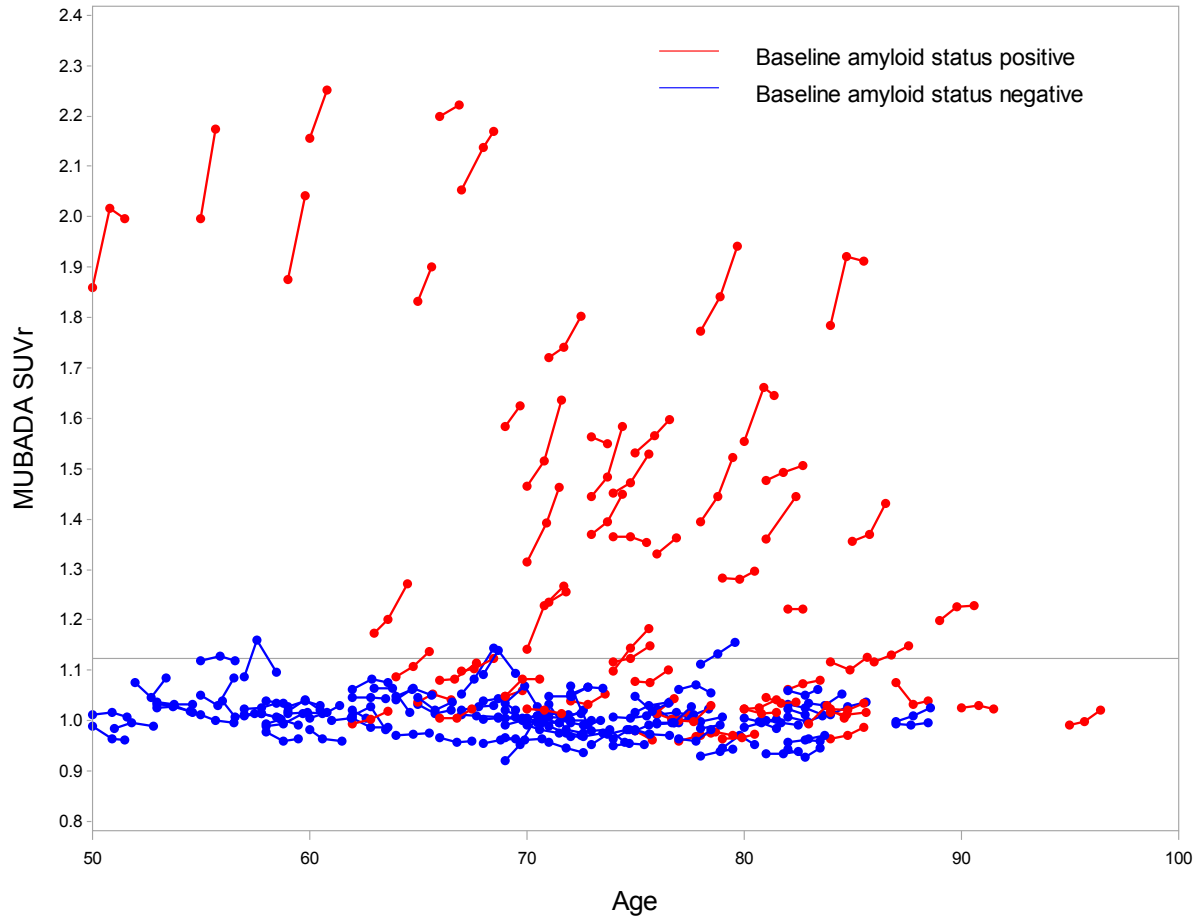

***Table 1*. Statistical Power to Detect the Possible Treatment Effect of Slowing of Tau Accumulation given Different Sample Sizes**

	% Slowing in Tau Accumulation from Treatment		
Total Number of Completers	**20% slowing**	**30% slowing**	**40% slowing**
100	28%	53%	78%
150	39%	71%	92%
200	49%	83%	97%

**Each cell displays the statistical power to detect the treatment effect with specified sample size. For example, 100 completers in total will have 78% power to detect a treatment effect of 40% slowing, between treatment and placebo groups.*

Keywords: solanezumab,mild dementia,therapeutic trial, amyloid,tau

Niemantsverdriet, Ellis - 40

Concordance improves between amyloid-PET and CSF amyloid-β for diagnosing Alzheimer's disease in a clinical setting by applying Aβ1-42/Aβ1-40 ratio

Ellis Niemantsverdriet[1], Julie Ottoy[2], Jeroen Verhaeghe[2], Charisse Somers[1], Ellen De Roeck[1], Hanne Struyfs[1], Femke Soetewey[1], Maria Bjerke[1], Tobi Van den Bossche[3,4], Sara Van Mossevelde[3,4], Johan Goeman[4], Peter Paul De Deyn[4], Peter Mariën[4,5], Jan Versijpt[6], Paul Parizel[7], Kristel Sleegers[3], Christine Van Broeckhoven[3], Leonie wyffels[2,8], Adrien Albert[8], Sarah Ceyssens[8], Sigrid Stroobants[2,8], Steven Staelens[2], Sebastiaan Engelborghs[1,4]

[1]*Reference Center for Biological Markers of Dementia (BIODEM), Laboratory of Neurochemistry and Behavior, Institute Born-Bunge, UAntwerp, Antwerp, Belgium*
[2]*Molecular Imaging Center Antwerp (MICA), UAntwerp, Antwerp, Belgium*
[3]*Department of Molecular Genetics, VIB, Antwerp, Belgium*
[4]*Department of Neurology and Memory Clinic, Hospital Network Antwerp (ZNA) Middelheim and Hoge Beuken, Antwerp, Belgium*
[5]*Clinical and Experimental Neurolinguistics, CLIN, Vrije Universiteit Brussel, Brussels, Belgium*
[6]*Department of Neurology, University Hospital Brussels, Brussels, Belgium*
[7]*Department of Radiology, Antwerp University Hospital, Antwerp, Belgium*
[8]*Department of Nuclear Medicine, Antwerp University Hospital, Antwerp, Belgium*

Background: In order to investigate the concordance between different biomarkers for Alzheimer's disease (AD) in a clinical setting, we set up a prospective longitudinal study. Evidence suggests that the concordance between amyloid PET and cerebrospinal fluid (CSF) Aβ increases when the CSF $A\beta_{1-42}/A\beta_{1-40}$ ratio is used as compared to CSF $A\beta_{1-42}$ levels alone. The present study tests this hypothesis.

Methods: Sixty-seven subjects (dementia (n=15), MCI (n=39), and cognitively healthy controls (n=13)) underwent a -AV45 (Florbetapir) PET scan, -FDG PET scan, MRI scan, and an extensive neuropsychological examination. In a subset (n=57), a lumbar puncture was performed and AD cerebrospinal fluid (CSF) biomarkers were analyzed ($A\beta_{1-42}$, $A\beta_{1-40}$, T-tau, P-tau_{181}).

Results: We detected an increased concordance in the visual, both SUVR (cerebellum (CB) or total brain white matter (WM) as reference regions), and V_t AV45 PET values when $A\beta_{1-42}/A\beta_{1-40}$ was applied. In here, no difference was found between both cortical mean SUVR values by applying the ratio. CSF biomarkers were stronger associated to AV45 PET scans with total brain WM as reference region compared to $SUVR_{CB}$.

Conclusions: The concordance between CSF Aβ and AV45 PET increases when the CSF $A\beta_{1-42}/A\beta_{1-40}$ ratio is applied. This finding is of most importance for the biomarker-based diagnosis of AD as well as for selection of subjects for clinical trials with potential disease-modifying therapies for AD.
Keywords: Florbetapir, dynamic [18F]-AV45 PET-scan, magnetic resonance image (MRI), cerebrospinal fluid (CSF), Aβ1-42/Aβ1-40 ratio

Regional visual read inspection of [18F]Flutemetamol brain images from end-of-life and amnestic MCI Subjects

Gill Farrar[1], Michelle Zanette[2]

[1]*GE Healthcare, Amersham, United Kingdom*
[2]*GE Healthcare, Marlborough, MA, USA*

Introduction: Visual interpretation of flutemetamol images relies upon review of 5 brain regions (frontal, parietal, posterior cingulate & precuneus, striatum and lateral temporal lobes). In an 'amyloid-positive' brain an elevated signal is observed in at least one region. Two different populations (end-of-life and amnestic MCI) were examined to investigate the pattern of regional read positivity in the two cohorts.

Methods: 180 EoL (mean age 81; range 59 to 95) and 232 amnestic MCI subects (mean age 71; range 53 to 91) were scanned following 185-370 MBq of intravenous flutemetamol. Images from both studies were read by two groups of 5 blinded readers who independently classified as positive or negative in each of the 5 brain regions. The majority interpretation (by at least 3 of the 5 readers) was used as the imaging endpoint.

Results: 71 positive images from the EoL study (from 106 coming to autopsy) and 97 positive images in the aMCI cohort were included in the assessment. In the EoL study widespread deposition of amyloid was observed with 76% of images positive in all 5 regions and a further 20% positive in 4 regions. In the aMCI group similar results were observed with 87% positive in 5 regions and a further 5% positive in 4 regions. In both groups, there was only a minority of cases where read positivity was observed in only 3, 2, or 1 region.

Conclusion: aMCI is one of the main patient groups assessed in clinical practice. Currently the methods for assigning a brain positive or negative for amyloid are via visual reading only. Even in this early phase of dementia the deposition of amyloid is widespread in terms of amount and topographical progression. Attempts to observe potential initial signs of amyloid deposition would have to focus on earlier populations in the dementia spectrum such as subjective cognitive decline or even earlier at risk subjects.
Keywords: [18F]flutemetamol, visual inspection, regional reads, amnestic MCI, end-of-life

Tau mediates temporal lobe structure-function relationships and disrupts memory encoding in normal aging

Shawn Marks[1], Samuel Lockhart[1], Taylor Mellinger[1], Kaitlin Swinnerton[1], Andy Horng[1], Suzanne Baker[2], William Jagust[1,2]

[1]Helen Wills Neuroscience Institute, University of California, Berkeley, Berkeley, CA, USA
[2]Life Sciences Division, Lawrence Berkeley National Laboratory, Berkeley, CA, USA

Hippocampal hyperactivity has been associated with memory impairment in both cognitively normal older adults and mild cognitive impairment. Alzheimer's pathology preferentially targets structures within the hippocampal memory network, and β-amyloid has been linked to aberrant brain activity. The role of tau in network dysfunction remains unclear. This study sought to investigate the impact of both β-amyloid and tau on the hippocampus and associated structures during episodic memory.

Forty-three cognitively normal older adults and 20 young controls participated in a functional MRI paradigm designed to emphasize lure discrimination. Participants were shown color photographs of novel, repeated, and similar (i.e. lure) objects, and told to identify them as such. A subset of elderly participants underwent PIB and AV-1451 PET scans.

Older adults performed worse on the memory task, incorrectly identifying lure stimuli as repetitions more frequently than young controls. Individual patterns of activation were identified for three trial types during memory encoding: hits (repetitions correctly identified as "old"), correct rejections (lures correctly identified as "similar"), and false alarms (lures incorrectly identified as "old"). β-amyloid was positively associated with hit deactivations, such that older adults who deactivated less had more pathology; whereas, tau was positively associated with false alarm activations. Hit deactivations and false alarm activations were combined into a composite pathological activation measure to describe memory network dysfunction. Pathological activation was negatively associated with overall task performance. Atrophy of the hippocampus and entorhinal cortex was also associated with pathological activation. Furthermore, the presence of tau, specifically in the hippocampus and entorhinal cortex, mediated the relationship between pathological activation and entorhinal cortical thickness.

These results suggest that the co-occurrence of β-amyloid and tau play a critical role in the development of age-related memory decline, particularly by leading to aberrant activity throughout the hippocampal memory network and to atrophy of crucial brain structures.
Keywords: Episodic Memory, Amyloid, Tau, fMRI

AMYPAD: A European public-private partnership to investigate the value of β-amyloid brain scans as a diagnostic and therapeutic marker for Alzheimer's disease

Frederik Barkhof[1,2], Gill Farrar[3]

[1]*VuMC, Amsterdam, Netherlands*
[2]*University College London, London, United Kingdom*
[3]*GE Healthcare, Amersham, United Kingdom*

Background: 'Amyloid imaging to prevent Alzheimer's disease' (AMYPAD) is a collaborative research initiative to improve the understanding, diagnosis and management of AD through the utilisation of β-amyloid PET imaging. The 5-year programme is part of the Innovative Medicines Initiative, a joint undertaking between the European Union and the European Federation of Pharmaceutical Industries and Associations, EFPIA. AMYPAD will have close links with its sister program EPAD (European Prevention of Alzheimer's Disease).

Goals: AMYPAD has 3 major goals: **1)** improve the diagnostic workup of people suspected to have AD and their management; **2)** understand the natural history of AD in the pre-symptomatic stage; **3)** select people for treatment trials aiming at preventing AD by ensuring a more homogeneous and appropriate enrollment. Through engagement with regulators and health technology agencies, AMYPAD aims to maximize the value of its findings for pharmaceutical companies, healthcare providers, and patients.

Methods: The above goals will be achieved via 2 large studies where amyloid scanning is the major component. Study one is a diagnostic and patient management study with 900 subjects recruited from memory clinics (300 subjective cognitive decline, 300 mild cognitive impairment and 300 possible Alzheimer's dementia).

Study two will be a natural history cohort with 3000+ subjects coming from feeder EPAD cohorts. In both cohorts repeat amyloid scanning will be performed in up to 50% of the cases to enable methodology to be developed for the longitudinal measurement of amyloid change. A total of 6000 scans will be performed split 50:50 between Neuraceq (Piramal Imaging) and Vizamyl (GE Healthcare).

Biomarker characterisation over the full dementia spectrum will support EPAD in developing clinical trial readiness cohorts to be fed into therapeutic intervention studies.

AMYPAD will also investigate areas of novel scientific interest such as the integration of MR-PET with ASL to improve quantification, integrated biomarker modelling, quantitative PET outcomes for treatment trials and diagnostic value in SCD.
Keywords: AMYPAD, amyloid PET imaging, diagnostic work-up, natural history cohorts, trial readiness

Amyloid positivity is associated with steeper declines in prospective verbal episodic memory independent of neurodegeneration in cognitively normal older adults

Murat Bilgel[1], Yang An[1], Gabriela Gomez[1], Jessica Helphrey[1], Wendy Elkins[1], Dean Wong[2], Susan Resnick[1]

[1]Laboratory of Behavioral Neuroscience, National Institute on Aging, Baltimore, MD, USA
[2]Department of Radiology and Radiological Science, Johns Hopkins University School of Medicine, Baltimore, MD, USA

Introduction: It is important to understand the distinct contributions of amyloidosis and neurodegeneration to cognitive decline in preclinical Alzheimer's disease (pcAD).

Methods: We assessed the effects of amyloid positivity as measured by Pittsburgh compound B positron emission tomography (PiB-PET) and hippocampal volume adjusted for intracranial volume (HVa) on prospective cognitive performance among 128 Baltimore Longitudinal Study of Aging (BLSA) participants (mean baseline age 76.2, SD 7.8) using data from 424 cognitively normal visits spanning 3.5 years on average. For each cognitive test, we conducted a linear mixed effects analysis whose predictors included baseline age, PiB group, HVa as well as their interactions with time, and covariates included sex, race, and cognitive reserve (computed using years of education and Wide Range Achievement Test). We also investigated the relationship between PiB positivity and prospective HVa.

Results: Baseline PiB positivity and lower HVa were independently associated with steeper longitudinal declines in verbal episodic memory and learning as measured by the California Verbal Learning Test (CVLT) sum of 5 learning trials (p=0.0004 for PiB, p=0.011 for HVa) and long-delayed free recall (p=0.017 for PiB, p=0.012 for HVa). Lower baseline HVa was also associated with steeper decline on CVLT short-delayed free recall (p=0.048). There were no associations with tests of executive function, processing speed, visual ability, or mental state. There were no differences in baseline HVa or its rate of change between the PiB groups.

Discussion: Episodic memory has consistently been shown to be the earliest cognitive domain impaired in pcAD. Given that amyloidosis and neurodegeneration are hypothesized to occur early in pcAD, our finding that amyloid positivity and lower HVa are associated with steeper declines on CVLT but not on other cognitive tests is consistent with current preclinical models. Our results suggest that amyloidosis is associated with memory decline independent of neurodegeneration.

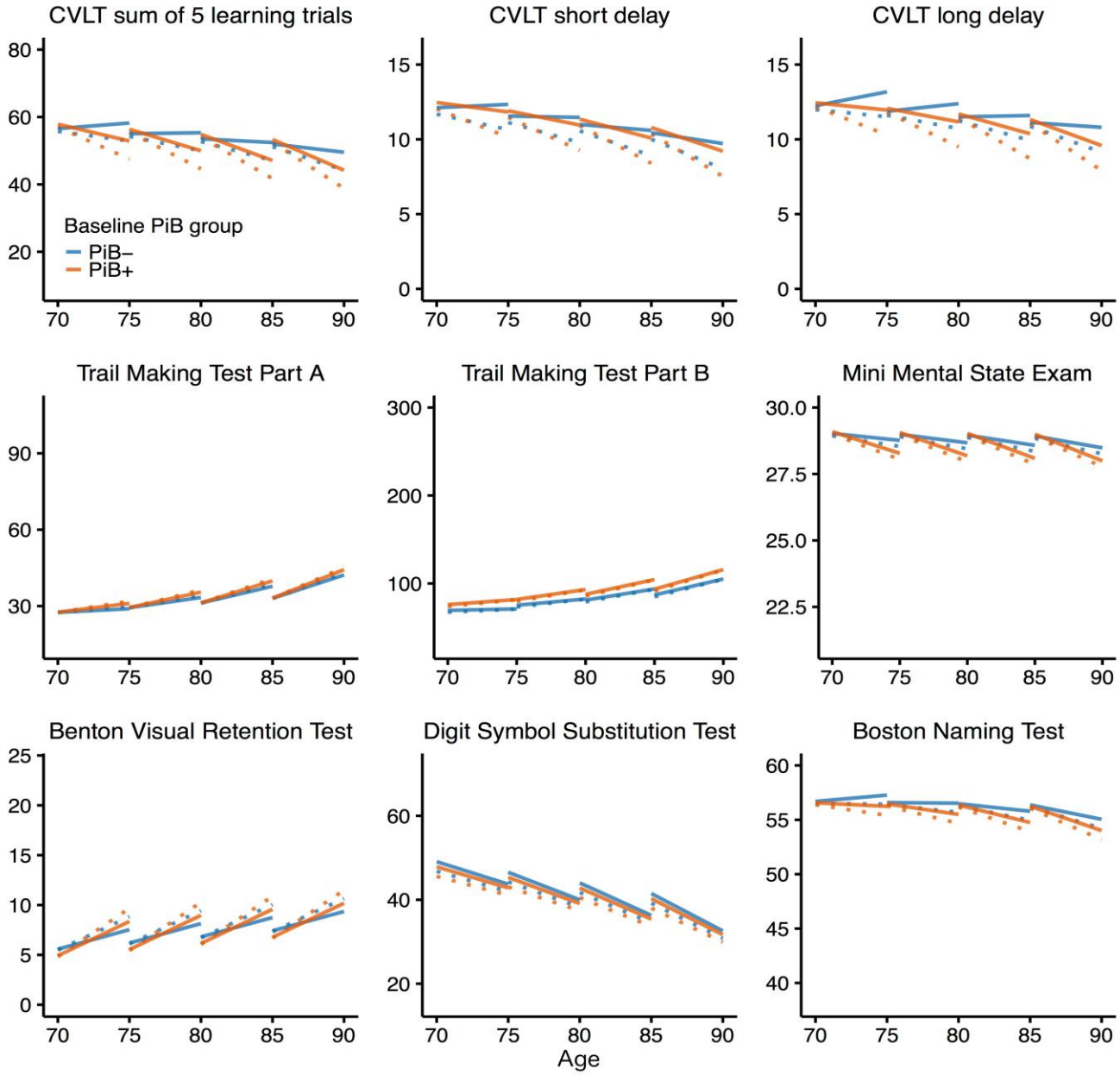

Average longitudinal cognitive trajectories as a function of age. Solid and dotted lines indicate baseline HVa one standard deviation above and below the mean, respectively. Blue and orange lines indicate PiB- and PiB+ groups, respectively. *y*-axis limits correspond to the extrema in the analyzed sample. CVLT = California Verbal Learning Test, HVa = Hippocampal volume adjusted for intracranial volume.

Keywords: PiB, cognition, hippocampus, memory

Tau burden localized in functional brain networks is associated with cognitive performance in beta amyloid positive subjects across the Alzheimer's spectrum

Arnaud Charil[1], Sergey Shcherbinin[1], Sudeepti Southekal[2], Abhinay D Joshi[2], Michael D Devous[2], Bradley B Miller[1], Adam J Schwarz[1]

[1]Eli Lilly and Company, Indianapolis, IN, USA
[2]Avid radiopharmaceuticals, Philadelphia, PA, USA

Objectives: Cognitive functions are subserved by networks of connected regions. We sought to determine whether overall tau levels within a set of predefined functional networks (FNs) predicted cognitive performance in beta amyloid positive subjects across the Alzheimer's spectrum.

Methods: Flortaucipir F18 PET (-AV-1451) images were acquired from 85 amyloid-positive subjects, and converted into SUVR units using a cerebellar crus reference region. Mean SUVR values were extracted from ROIs within 12 functional networks (FNs) independently defined based on rsfMRI (http://findlab.stanford.edu/functional_ROIs.html). Subjects underwent a battery of cognitive tests. Linear models were built to predict cognitive performance based on 1) regional (FN) SUVRs and 2) weighted whole-brain (MUBADA) SUVR as a comparator. For 1) we performed backward stepwise model selection to identify the set of FNs that best predicted variance in any given cognitive test. R^2 values were adjusted for number of predictors.

Results: The sample included 3 cognitively normal controls, 53 MCI and 29 AD subjects. Overall, more variance in cognitive scores was explained by a combination of FN predictors ($0.07<R^2<0.40$) than weighted global SUVR ($0.03<R^2<0.28$). The FN model yielded increased R^2 over weighted global SUVR in 15/17 cognitive tests, with increases of >0.1 for 8 tests (Figure). The visuospatial, ventral default mode and executive control networks were most often found to be the strongest predictors. Different tests were associated with different network tau profiles. When the weighted global SUVR was included in the same model alongside the FNs, it was retained as a significant predictor for 4/17 tests, and in all 17 the full model increased the adjusted R^2.

Conclusion: Compared to a weighted whole-brain flortaucipir SUVR measure, linear combinations of mean SUVRs from individual FNs increased the percent variance explained for different cognitive tests. Future work will examine the validity of these models in independent patient samples.

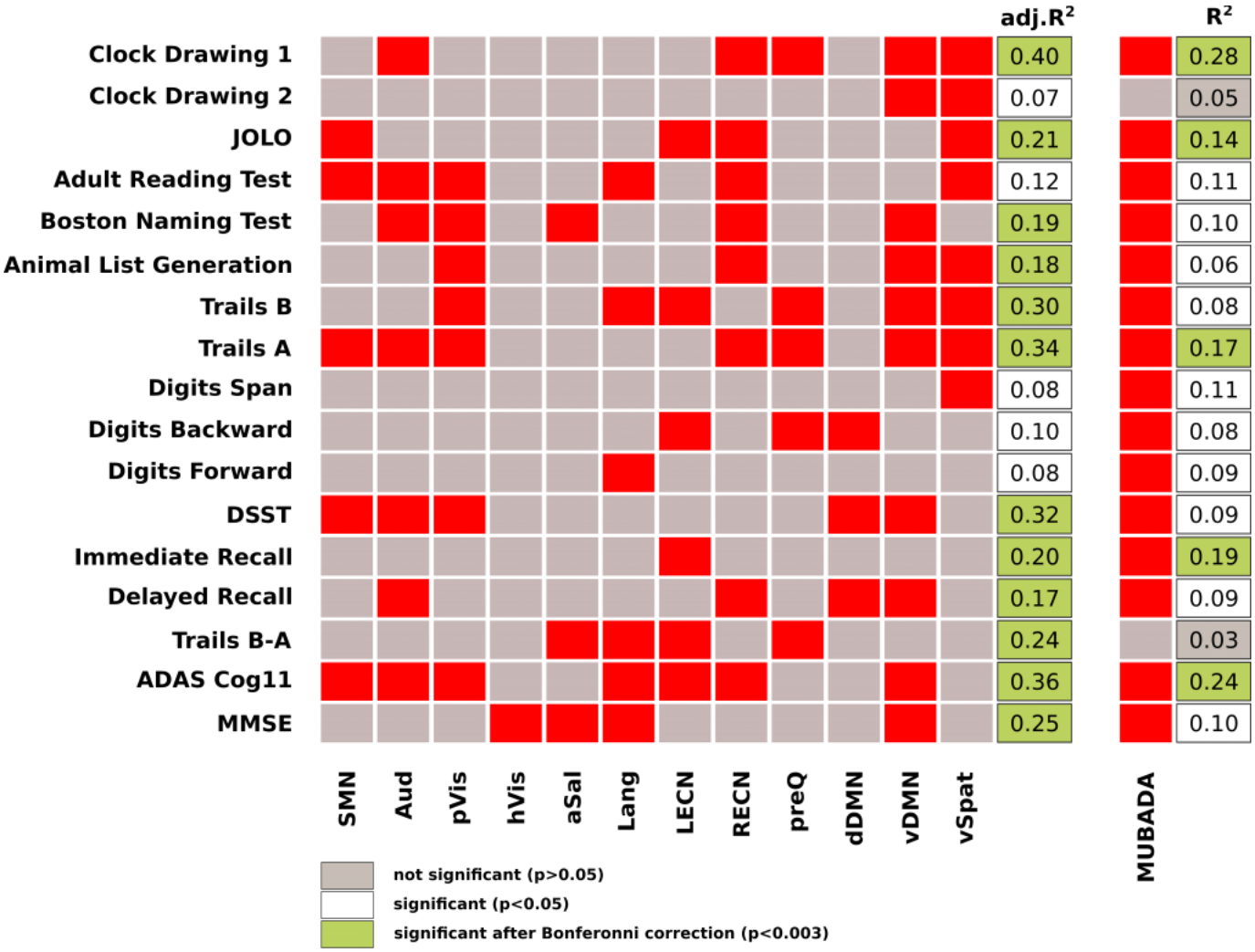

Figure: (Left) combination of functional networks whose tau burden was identified as significantly associated with the cognitive scores for each test; (right) results for the MUBADA SUVR model. Red squares represent a significant association with the cognitive test scores. [Abbreviations: JOLO = judgment of line orientation; DSST = digit symbol substitution test; SMN = sensorimotor network; Aud = auditory network; pVis = primary visual network; hVis = higher visual network; aSal = anterior salience network; Lang = language network; LECN = left executive control network; RECN = right executive control network; preQ = precuneus network; dDMN = dorsal default mode network; vDMN = ventral default mode network; vSpat = visuospatial network.]

Keywords: Flortaucipir, Tau, Functional Networks, Cognition, Alzheimer's Disease

Gait variability, an indicator of subclinical amyloid burden

Qu Tian[1], Woei-Nan Bair[1], Murat Bilgel[1], Dean Wong[2], Susan Resnick[1], Stephanie Studenski[1]

[1]*National Institute on Aging, Baltimore, MD, USA*
[2]*Johns Hopkins Medical Institutions, Baltimore, MD, USA*

Introduction: Mobility decline precedes cognitive impairment and dementia. Recent amyloid imaging evidence suggests that higher amyloid burden predicts future decline in mobility in older adults but is not associated with concurrent mobility deficits. Increased gait variability, which may precede gait slowing, may be more sensitive to increased concurrent amyloid burden.

Methods: In the Baltimore Longitudinal Study of Aging, 75 older participants without mild cognitive impairment, Alzheimer's disease, Parkinson's disease or stroke had concurrent data on amyloid imaging and gait lab characteristics (mean age=78.2yr). β-amyloid burden was measured using ^{11}C-Pittsburgh compound B (PiB) dynamic positron emission tomography. PiB+/- status was based on a previously defined mean cortical distribution volume ratio cutoff. Mean and variability (CoV=SD/mean) in gait by 3D motion analysis was determined for four domains (pace, rhythm, variability and postural control). Cross-sectional associations between PiB status and each gait characteristic were examined using linear regression models, adjusted for age, sex, body mass index, height, gait speed, and covariates related to mobility one at a time (memory, executive function, psychomotor speed, depressive symptoms, cardiovascular risk, peripheral arterial disease, ApoE ε4 status, cerebrovascular disease, knee pain).

Results: Compared to PiB-, PiB+ had higher gait speed variability and higher gait cycle time variability, independent of demographics, gait speed, and other covariates (all $p<0.05$). There were no significant associations with other gait variability measures (all $p>0.05$). Mean gait performance did not differ by PiB status, although there was a trend toward slower gait speed in PiB+ vs. PiB- ($p=0.075$).

Conclusion: This is the first evidence suggesting that in usual aging, gait speed variability and gait cycle time variability, but not mean performance, is related to amyloid positivity cross-sectionally. Increased gait variability may be a subclinical indicator of amyloid positivity.
Keywords: gait variability, subclinical amyloid burden, usual aging

Does the tau signal increase over time differ across brain regions and stage of impairment in Alzheimer's disease?

Sergey Shcherbinin[1], Mark Mintun[2], Claire Brittain[3], Ming Lu[2], Abhinay Joshi[2], Sudeepti Southekal[2], Michael Devous[2], Adam Schwarz[1]

[1]*Eli Lilly & Co, Indianapolis, IN, USA*
[2]*Avid Radiopharmaceuticals, Inc., Philadelphia, PA, USA*
[3]*Eli Lilly & Co, Windlesham, United Kingdom*

Objectives: We sought to examine longitudinal changes of regional tau accumulation over time using ^{18}F-Flortaucipir PET imaging in MCI and AD subjects.

Methods: Longitudinal ^{18}F-Flortaucipir tau images were compared to baseline images in amyloid positive MCI (N=28) and AD (N=17) subjects. SUVR values were calculated in four pre-defined atlas-based bilateral cortical (lateral temporal, occipital, frontal, and parietal) regions normalized to a white matter-based reference region (PERSI). A global weighted SUVR was calculated to approximate total tau signal for the whole cortex.

Results: At baseline, regional and global SUVR for the AD group were nominally (7-15% across regional mean values) and non-significantly larger than those for the MCI group. The largest mean signal was seen in the lateral temporal region (SUVR=1.33±0.33 for AD and 1.19±0.30 for MCI) while the frontal signal was the lowest (SUVR=1.04±0.26 for AD and 0.97±0.31 for MCI). Over 18 months, the AD group demonstrated higher increases in tau signal (in all regions and whole cortex) and the increase was more heterogeneous across regions than the MCI group. Compared with MCI, the AD group exhibited a significantly larger increase in frontal (ΔSUVR=0.06±0.05 for AD and 0.03±0.04 for MCI, $p<0.05$) and parietal (ΔSUVR=0.07±0.06 for AD and 0.03±0.05 for MCI, $p<0.03$) lobes. The strength of the signal change measured in the AD group using a mean/SD ratio of ΔSUVR (SNR) in the frontal (SNR=1.30) and parietal (SNR=1.25) lobes exceeded those pertaining to global (SNR=1.13), occipital (SNR=1.10) and temporal (SNR=0.97) ΔSUVR.

Conclusions: We observed an accelerated and less spatially uniform tau accumulation as cognitive impairment advances. In the AD group, signal in frontal and parietal regions increased more strongly than in temporal lobe and whole cortex and this frontal-parietal signal change was significantly larger than in the MCI group. Further investigation to support this preliminary analysis and to understand the possible relationship to the symptom progression is warranted.
Keywords: tau, longitudinal, accumulation, flortaucipir, heterogeneity

MRI-based amyloid imaging in Alzheimer's disease on clinical scanner

Dmitriy Yablonskiy, Yue Zhao, Tammie Benzinger, Anne Fagan, Jason Hassenstab, Nigel Cairns, Jie Wen, Andrei Vlassenko, Serguei Astafiev, Marcus Raichle, John Morris

[1]*Washington University in St. Louis, St. Louis, MO, USA*

Rational: While the primary role of the Aβ peptide in the development of Alzheimer's disease (AD) is now almost universally accepted, only PET-based measurements currently allow *in vivo* quantitative estimate of human brain amyloidosis. The aim of this presentation is to report preliminary validation of the MRI-based Gradient Echo Plural Contrast Imaging (GEPCI) technique as an efficient and non-invasive tool providing surrogate measure of Aβ accumulation in the brain.

Methods: 19 human participants with various level of cognitive decline (from normal, to preclinical, to mild AD) selected from ongoing studies of aging and dementia at the Knight ADRC at Washington University underwent GEPCI (Siemens 3T MRI) and PET PiB Aβ (Siemens PET) measurements.

Results: The correlation analysis between GEPCI measurements of *R2** relaxation rate constant and amyloid PET measurements (using PiB standardized uptake value ratio) revealed positive correlations in most cortical brain regions (Figure). The data show significant correlations not only in the areas of high amyloid accumulation (e.g. precuneus) but also in the areas of MTL. Remarkably, the strongest and most significant correlation exists in the parahippocampal cortex – the area of low amyloid accumulation in early AD stages. This shows the high sensitivity of GEPCI *R2** to Aβ accumulation in this very important area of pathological changes in early AD particularly as it relates to the formation of amyloid plaques in the cerebral cortex.

Conclusion: For the first time we demonstrate that in vivo MRI-based measurements obtained on a clinical MRI scanner can provide information on brain Aβ accumulation in human participants. Since MRI is a widely available technology, the GEPCI technique has great potential for widespread use in differential diagnosis, tracking early pathological brain changes and the evaluation of new disease-modifying therapies.

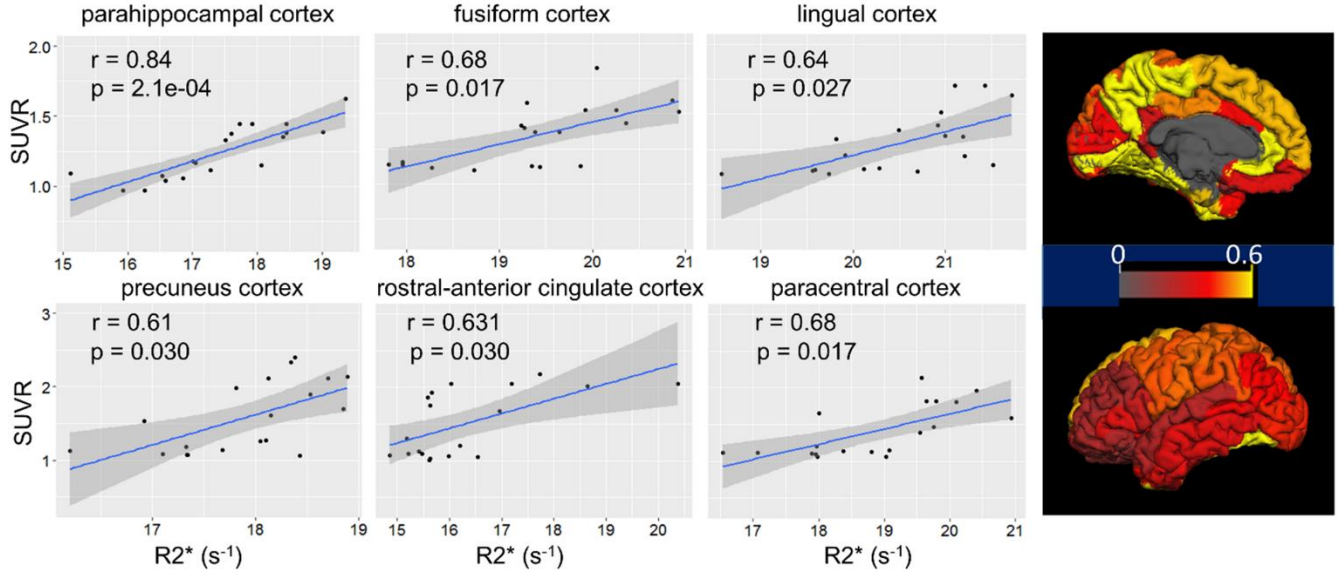

Figure. Correlations in several brain regions and on brain surface. Shaded areas are 95% confidence intervals.
Keywords: Alzheimer disease, Amyloid, MRI, GEPCI

Years to parental symptom onset predicts amyloid burden, neurodegeneration and resting state connectivity changes in healthy elderly with a parental history of Alzheimer's disease

Sylvia Villeneuve[1,3,4], Jacob W. Vogel[3,4], Julie Gonneaud[1,4], Judes Poirier[1,4], Pedro Rosa-Neto[5], Anne M. Fagan[1,2,4], Randall Bateman[5], John Morris[7], Alexa Pichet Binnette[1,3,4], Etienne Vachon-Presseau[10], Tammie L. Benzinger[6,7], Sterling Johnson[9,10], John C. Breitner[1,3], for the PREVENT-AD Research Group .[3]

[1]*Department of Psychiatry, McGill University, Montreal, QC, Canada*
[2]*Department of Neurology and Neurosurgery, McGill University, Montreal, QC, Canada*
[3]*Douglas Mental Health University Institute, Centre for Studies on Prevention of Alzheimer's Disease, Montreal, QC, Canada*
[4]*McGill Centre for Integrative Neuroscience, McGill University, Montreal, QC, Canada*
[5]*Department of Neurology, Washington University School of Medicine, St Louis, MO, USA*
[6]*Department of Radiology, Washington University School of Medicine, St Louis, MO, USA*
[7]*Knight Alzheimer's Disease Research Center, Washington University School of Medicine, St Louis, MO, USA*
[8]*Northwestern University, Chicago, IL, USA*
[9]*Wisconsin Alzheimer's Institute, University of Wisconsin-Madison School of Medicine and Public Health, Madison, WI, USA*
[10]*Alzheimer's Disease Research Center, University of Wisconsin-Madison School of Medicine and Public Health, Madison, WI, USA*

Background In dominant genetic forms of Alzheimer's disease (AD), biomarker changes follow a predictable course, with mutation carriers showing progressive biomarker change as their age approaches their family's typical age of onset. We assessed whether Aβ burden, neurodegeneration and alterations in functional connectivity appeared in a similarly predictable fashion among cognitively normal persons with a parental history of "sporadic" AD.

Methods We estimated each individual's proximity to their parent's symptom onset by subtracting their index relative's onset age from their current age . We then assessed the relationship between proximity to parental onset and cerebrospinal fluid (CSF) $A\beta_{1-42}$ (n = 102), MRI grey matter density (n = 271) and resting state functional connectivity (n = 221) in the PREVENT-AD cohort, while testing for *APOE* and gender interactions. The Aβ analyses were repeated in two independent cohorts using CSF and PIB-PET Aβ biomarkers.

Findings In PREVENT-AD, CSF $A\beta_{1-42}$ (Fig.1), grey matter density (Fig.2) and functional connectivity (Fig.3) showed increasing abnormality with greater proximity to parental onset. Interaction analyses showed that the trend for CSF $A\beta_{1-42}$, was stronger in both *APOE* e4 carriers and women. The Aβ findings were replicated in the Adult Children Study and in the Wisconsin Registry for Alzheimer's Prevention Study (Fig. 1).

Interpretation Proximity to parental symptom onset might be useful in clinical trials to track AD biomarker changes in asymptomatic individuals. As is the case in autosomal dominant AD, these results suggest that parental onset can help estimate individuals' years before onset of symptoms.

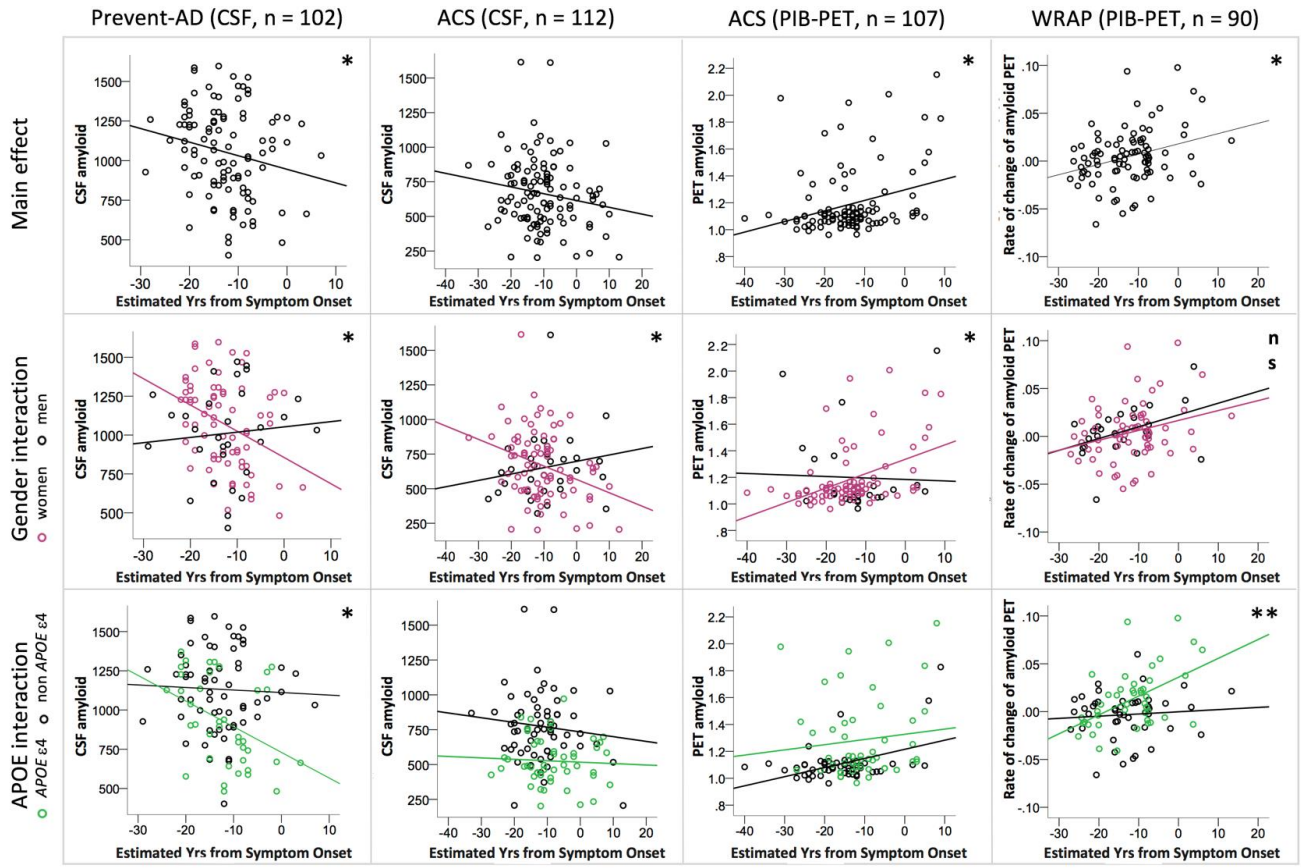

Fig 1. "Estimated Years from Symptom Onset" and amyloid burden in sporadic AD. pink=gender interactions; green=APOE interactions; * p<0.05; ** p<0.01.

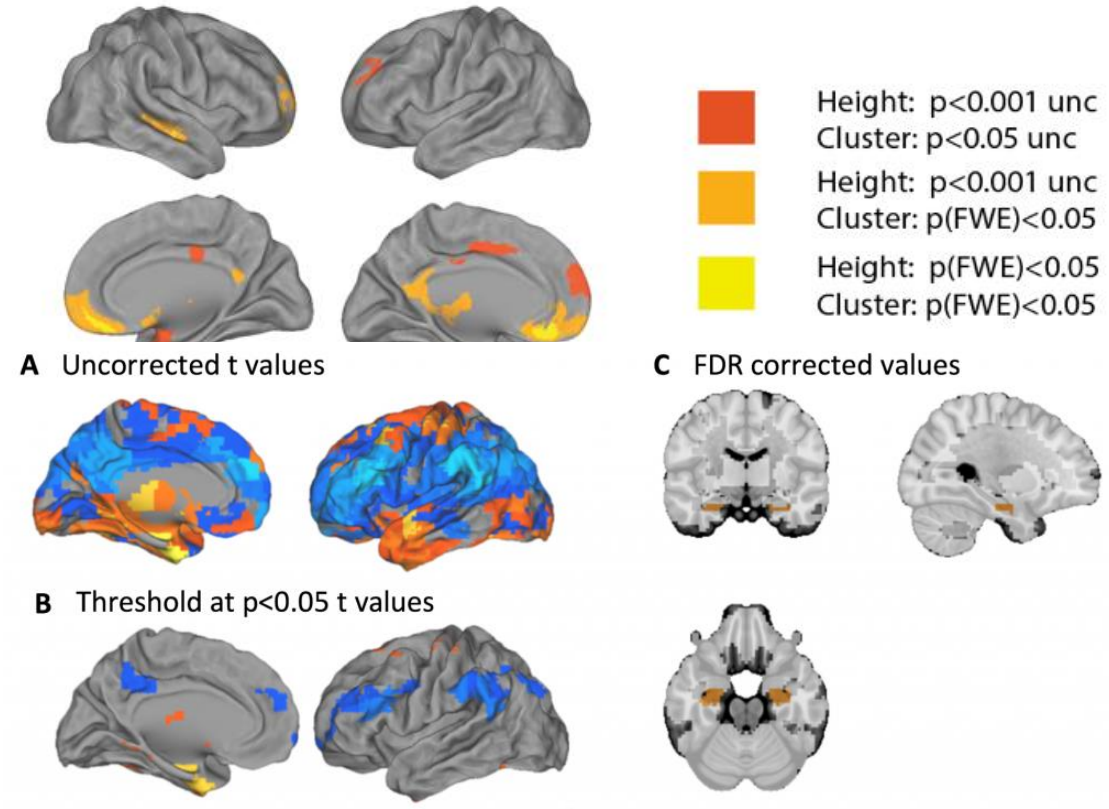

Fig.2 "Estimated Years from Symptom Onset" and grey matter density in sporadic AD.

Fig 3. "Estimated Years from Symptom Onset" and resting state connectivity in sporadic AD.

Keywords: amyloid, neurodegeneration, resting state, sporadic AD, parental onset

Clinical significance of visually equivocal amyloid PET on ADNI cohort

Minyoung Oh[1], Minjung Seo[2], Sun Young Oh[3], Jungsu S. Oh[1], Jee Hoon Roh[4], Jae-Hong Lee[4], Jae Seung Kim[1]

[1]*Department of Nuclear Medicine, Asan Medical Center, Seoul, Korea*
[2]*Department of Nuclear Medicine,Ulsan University Hospital, Ulsan, Korea*
[3]*Department of Nuclear Medicine,National Police Hospital, Seoul, Korea*
[4]*Department of Neurology, Asan Medical Center, Seoul, Korea*

Objective: We aimed to describe the clinical and imaging characteristics of subjects with visually equivocal amyloid PET images from the Alzheimer's Disease Neuro-imaging Initiative (ADNI), a prospective cohort study.

Methods: We choose subjects with florbetapir PET both at baseline and 24 month on ADNI cohort. Florbetapir PET images were visually assessed by three nuclear medicine physicians and classified as positive or negative. Images not reached consensus reclassified as equivocal. We compared the clinical and imaging characteristics according to their florbetapir PET results.

Results: Among 347 subjects, the numbers of negative/equivocal/positive florbetapir PET images were 207 (71.2±7.4y, M:F=110:97), 40 (73.4±6.6y, M:F=22:18), and, 100 (73.3±6.6y, M:F=54:46) for each. About 10% of subjects with normal cognition (CN, N=14/127), MCI (N=24/198), and AD (N=2/22) showed equivocal florebetapir PET for each. Among negative/equivocal/positive groups, CSF Aβ1-42 were positive in 25%, 80% and 98% for each. Baseline SUVR of florbetapir PET were 1.04±0.09, 1.22±0.17, 1.45±0.16, for each ($p<0.001$). During 24 month of F/U, they increased 0.93±2.88 %, 2.75±3.25 %, 2.03±3.64 % for each ($p<0.05$). SUVR of FDG PET were 6.58±0.51, 6.34±0.64, and 5.50±0.64 for each ($p<0.001$ for positive group and others). They were decreased 1.22±4.01%, 2.75±6.72% and 4.65±5.71% for each ($p<0.001$). Hippocampal volume were 7430.2±1007.3, 7105.7±1081.1, and 6565.5±1081.9 for each ($p<0.001$ for positive group and others). They were decreased 2.78±3.89%, 5.60±5.80% and 7.21±5.14% for each ($p<0.001$). Immediate recall of Rey auditory verbal learning test scores were 42.39±11.72, 38.42±13.78, and 32.75±10.16 for each ($p<0.05$). They decreased -1.17±8.39, -0.90±7.50, and 2.69±7.35 ($p<0.05$). In the equivocal group, subjects with MCI (N=24/40) showed more rapid change of SUVR of florbetapir PET and hippocampal volume than CN (N=14/40).

Conclusion: About 10% of subjects showed visually equivocal result of amyloid PET. They represented moderate amyloid accumulation and intermediate neurodegeneration with relatively rapid aggravation.
Keywords: Florbetapir, amyloid PET, equivocal, ADNI

Severity of lifetime trauma is related to hippocampal tau deposition in Vietnam war veterans with PTSD

Susan Landau[1], Andy Horng[1], Thomas Neylan[2], William Jagust[1], Jacqueline Hayes[2], Paul Aisen[4], Ronald Petersen[5], Dallas Veitch[2], Clifford Jack[5], Charles DiCarli[8], Andrew Saykin[6], Jordan Grafman[7], Duygu Tosun[2], Michael Weiner[2]

[1]Univ of California, Berkeley, CA, USA
[2]Department of Veterans Affairs Medical Center, Center for Imaging of Neurodegenerative Diseases, San Francisco, CA, USA
[3]Univ of California, San Francisco, CA, USA
[4]Alzheimer's Therapeutic Research Institute, University of Southern California, Los Angeles, CA, USA
[5]Mayo Clinic, Rochester, MN, USA
[6]Indiana Alzheimer Disease Center, Indiana University School of Medicine, Indianapolis, IN, USA
[7]nPsychiatry and Behavioral Sciences & Cognitive Neurology/Alzheimer's Disease Research Center, Northwestern University, Chicago, IL, USA
[8]kImaging of Dementia and Aging (IDeA) Laboratory, University of California, Davis, CA, USA

Objective: Posttraumatic stress disorder (PTSD) is associated with poor cognitive performance, structural and functional abnormalities in several regions including the hippocampus, and an increased risk of dementia late in life. Here we examined AV1451 PET and other neuroimaging biomarkers in Vietnam War Veterans with PTSD (and traumatic brain injury (TBI) in some cases) to determine the possible contribution of tau to PTSD symptoms.

Methods: Veterans with and without a history of PTSD (and/or TBI) participated in neuroimaging (florbetapir-PET, AV1451-PET, MRI) and clinical evaluations that were similar to ADNI. Partial volume corrected AV1451 means were calculated within a bilateral medial temporal region (entorhinal cortex, hippocampus) and neocortical regions relative to cerebellar cortex. Current and lifetime traumatic stress symptoms were assessed with the Clinician-Administered PTSD Scale (CAPS).

Results: In 24 individuals with AV1451 (4 control, 18 PTSD with/without TBI, 2 TBI), medial temporal AV1451 did not differ across subject groups (Figure 1). In 18 individuals with PTSD (14 cognitively normal, 4 MCI; all male, age=68.8+/-3.2yrs, edu=14.4+/-2.5yrs), lifetime (but not current) PTSD symptom severity correlated with medial temporal AV1451 retention ($p=0.05$; Figure 2) but not neocortical AV1451, while adjusting for age, education, and hippocampal volume. Finally, medial temporal AV1451 retention in PTSD subjects was not related to amyloid positivity, presence of TBI, degree of self-reported lifetime alcohol use, antidepressant use, depression, or memory function.

Conclusion: These preliminary findings show a relationship between medial temporal tau and PTSD severity, suggesting that chronic PTSD may increase vulnerability to tau accumulation in regions relevant to memory and emotional processing, which may underlie future risk of cognitive decline and/or dementia. Alternatively, medial temporal tau accumulation that is common in mid to late life may predispose individuals with stress exposure to manifest PTSD symptoms.

Figure 1.

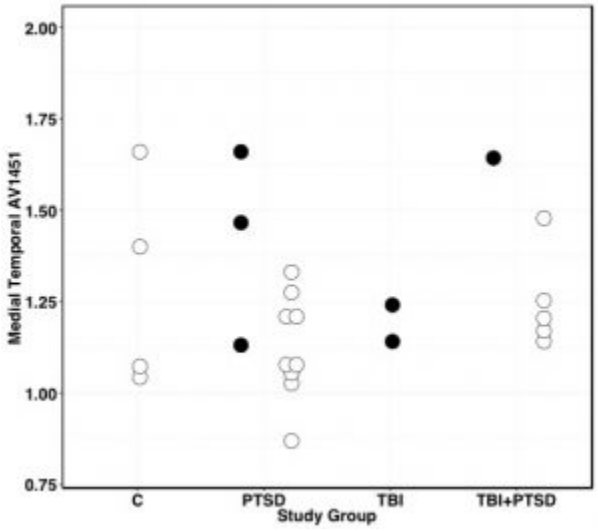

Figure 2. Datapoints with no border indicate cognitively normal subjects, datapoints with a black border indicate MCI subjects.

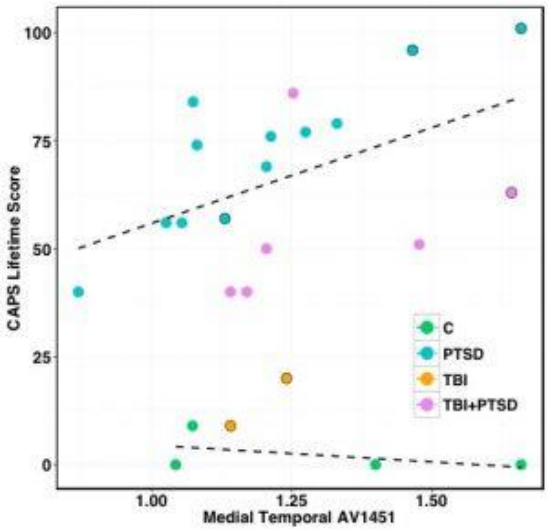

Keywords: Tau, Hippocampus, PTSD

Relationships between tau and glucose metabolism differ by amyloid status in aging

Jenna Adams[1], Samuel Lockhart[1], William Jagust[1,2]

[1]*Helen Wills Neuroscience Institute, University of California, Berkeley, Berkeley, CA, USA*
[2]*Lawrence Berkeley National Laboratory, Berkeley, CA, USA*

Relationships between tau and glucose metabolism may offer insights into how neurodegeneration evolves. We performed tau PET imaging using AV-1451, and FDG- and PIB-PET in a sample of 50 cognitively normal older adults (PIB- n=28; PIB+ n=22). We extracted partial volume corrected SUVRs for AV1451 and FDG in 62 cortical ROIs defined in native space with FreeSurfer. We performed partial correlations controlling for age and sex across all ROI combinations to determine associations between tau and FDG in the PIB- and PIB+ groups separately. Results showed that compared to the PIB- group, the PIB+ group demonstrated negative correlations between tau and FDG in many cortical ROIs; the strongest included significant (p<0.05) negative associations between tau in the entorhinal cortex and FDG in regions such as the isthmus cingulate (r=-0.51), precuneus (r=-0.55), and inferior parietal lobe (r=-0.51). Within MTL ROIs (bilateral entorhinal, hippocampus, parahippocampal gyrus), we found both significant positive and negative associations between tau and FDG which depended upon PIB status and differed by ROI. To examine these relationships, we used linear regression models predicting FDG, with tau, PIB classification (+/-), and the tau*PIB interaction as predictors. We found significant tau*PIB interactions (model p<0.05, interaction p<0.01) in most MTL ROIs. These interactions were particularly interesting in the left hippocampus, where tau in multiple MTL regions was associated with increased hippocampal metabolism in PIB+ (with positive b values 0.24 to 0.51) but decreased hippocampal metabolism in PIB-. These results indicate that tau may have different effects in different parts of the brain, and that this relationship depends on Aβ. In cortical regions, regardless of Aβ, tau is associated with reduced metabolism. In the hippocampus, tau in multiple MTL regions is associated with reduced hippocampal metabolism in the absence of Aβ, but with increased hippocampal metabolism in the presence of Aβ.
Keywords: tau, glucose metabolism, amyloid beta, older adults

Relationships between NREM-sleep fragmentation and changes in brain structure, metabolism, amyloid burden and cognitive performance in healthy older adults

Géraldine Rauchs[1], Claire Andre[1], Cléménce Tomadesso[1], Florence Mezenge[1], Pierre Branger[2], Morgane Fossey[1], Robin de Flores[1], Alice Laniepce[1], Francis Eustache[1], Gaël Chetelat

[1]Inserm-EPHE-University of Caen Normandy, research unit U1077, GIP Cyceron, Caen, France
[2]Neurology Department, Caen University Hospital, Caen, France

Background: Sleep fragmentation (SF) increases with age, and is related to cognitive impairment and a heightened risk of dementia. The mechanisms underlying these associations are still unclear, but emerging evidence suggests that a disruption of non-rapid eye movement (NREM) sleep, prevailing during the first half of the night, could exacerbate amyloid deposition. Our objective was to investigate the relationships between NREM-SF, changes in brain structure, metabolism and amyloid deposition, and cognitive performance.

Methods: 30 healthy older adults (mean age ± SD: 72.4 ± 7 y) underwent a detailed neuropsychological assessment, a structural MRI, FDG and florbetapir-PET scans (n=25 for this latter) to assess grey matter (GM) volume, brain glucose metabolism, and amyloid deposition respectively. Sleep-wake activity was recorded for one week with actigraphy (MotionWatch8, CamNtech). We computed the mean level and the variability of SF across nights, over the first half of the night. Correlations with neuroimaging data were performed using the SPM12 software, controlling for age, body mass index, anxiety, depression, and the other SF parameter (i.e. variability when the mean level was considered, and conversely).

Results: The mean level of NREM-SF was negatively correlated to brain glucose metabolism in the ventromedial prefrontal cortex (VMPFC), the accumbens and caudate nuclei, and the hypothalamus ($p<0.001$), and was associated to lower cognitive performance, especially for executive functioning and episodic memory ($p<0.05$). Variability of NREM-SF was negatively correlated to VMPFC GM volume, and positively correlated to amyloid burden in the VMPFC ($p<0.001$).

Discussion: These results suggest that, in cognitively normal older adults, a higher NREM-SF is related to brain alteration, mainly in the VMPFC known to be early affected in ageing, and by amyloid deposition in Alzheimer's disease. This may increase the risk of cognitive decline, further highlighting the importance of screening for sleep disturbances and of preserving sleep quality in elders.
Keywords: sleep; amyoid; atrophy; hypometabolism; cognition

Is microglial activation protective in mild cognitive impairment?

Grazia Daniela Femminella[1], Melanie Dani[1], Melanie Wood[1], Zhen Fan[1], Valeria Calsolaro[1], Ruth Mizoguchi[1], Rebecca Atkinson[1], Trudi Edginton[2], Adam Waldman[1], Rainer Hinz[3], David Brooks[1,4], Paul Edison[1]

[1]*Department of Medicine, Imperial College London, London, United Kingdom*
[2]*Department of Psychology, University of Westminster, London, United Kingdom*
[3]*Wolfson Molecular Imaging Centre, University of Manchester, Manchester, United Kingdom*
[4]*Department of Nuclear Medicine, Aarhus University, Aarhus, Denmark*

Introduction. Amyloid plaques and neurofibrillary tangles are characteristic features of Alzheimer's disease, and neuroinflammation has been proposed to be the link between amyloid deposition, tangle formation and neuronal damage. While microglial activation plays a significant role in Alzheimer's disease, the *in vivo* relationship between neuroinflammation and amyloid deposition and its role in mild cognitive impairment subjects is still debated. Here we investigated the role of microglial activation in mild cognitive impairment subjects using a second-generation translocator protein PET tracer, PBR28.

Methods. Thirty subjects (nine controls and twenty-one with mild cognitive impairment) underwent PBR28 and Flutemetamol PET scans, structural MRI and neuropsychometric evaluation. For PBR28 PET, distribution volumes (V_T) were calculated for each brain region, while amyloid load was estimated using 90–120 min target region:cerebellar uptake ratios. Region of interest analysis was performed for both tracers. Volumetric analysis of MRI was performed using Freesurfer. Voxel-wise correlations between PBR28 uptake and hippocampal volume were interrogated using statistical parametric mapping software.

Results. We detected microglial activation in one third of mild cognitive impairment subjects, mainly evident in the frontal, parietal and occipital cortices. 40% of mild cognitive impairment subjects showed widespread amyloid deposition compared with healthy controls. PBR28 uptake in different cortical areas was positively correlated with hippocampal volume.

Conclusions. We report increased PBR28 binding in a cohort of subjects with mild cognitive impairment, which is in accordance with early onset of neuroinflammatory changes in the brain. This was associated with higher hippocampal volume, suggesting that microglial activation can play a significant protective role in early stages of neurodegenerative diseases.
Keywords: mild cognitive impairment, inflammation, PBR28, flutemetamol

ß-Amyloid PET imaging of neurodegenerative disorders in a Chinese specialty hospital

HW Qiao[1], John Seibyl[2], Y Han[1], W Mao[1], EH Xu[1], J Lu[1], Kenneth Marek[2], Gilles Tamagnan[2], Piu Chan[1]

[1]Xuanwu Hospital, Beijing Capitol University, Beijing, CN
[2]Molecular Neuroimaging, LLC, New Haven, CT, USA

Objective: The objective of this study was to assess brain ß-amyloid with florbetapir PET in healthy controls (HC) and subjects with Subjective Cognitive Deficit (SCD), Alzheimer's Disease (AD), Parkinson disease (PD) and other neurodegenerative disorders patients at a large Chinese specialty hospital.

Methods: PET brain imaging was completed in 32 subjects: eight HC (age 53-79, MMSE 28-30), seven SCD subjects (age 50-67, MMSE 27-30), six mild to moderate AD subjects (age 58-79, MMSE 8-22), seven PD subjects (age 61-75, MMSE 11-30), and four other neurodegenerative disease subjects (DLB, MSA, FTD) (age 51-71, MMSE 15-25). Image quantitation was performed using a standardized florbetapir image analysis algorithm and compared with visual interpretation by an experienced reader. Composite SUVrs were compared across cohorts against abnormality thresholds (between 1.1-1.2).

Results: Cortical composite SUVrs were greater than 1.2 in 3/4 moderate AD subjects compared to 0/8 HC, 0/7 SCD, 0/2 subjects with mild AD. Quantitation in the PD subjects showed 2/7 greater than 1.2. Of the four other subjects 1/2 of the DLB subjects and the single FTD subject were greater than 1.2. Visual assessment showed complete concordance with quantitation at a 1.2 SUVr cut-off. At the lower threshold of 1.1, 2 /32 cases were discordant between assessment approaches.

Conclusions: These data represent the largest PET amyloid experience to date in a Chinese neurodegenerative disorder clinical cohort. In this ongoing study, the numbers of amyloid positive PET scans in clinically diagnosed AD and PD is roughly similar to reports from the literature. The lack of amyloid in healthy subjects and subjective cognitive deficit may reflect the modest sample size. Both quantitative and visual approaches give consistent assessments of brain amyloid status. The range of values for composite SUVr in this Chinese cohort is similar to published data in other cohorts using identical image analysis strategies.

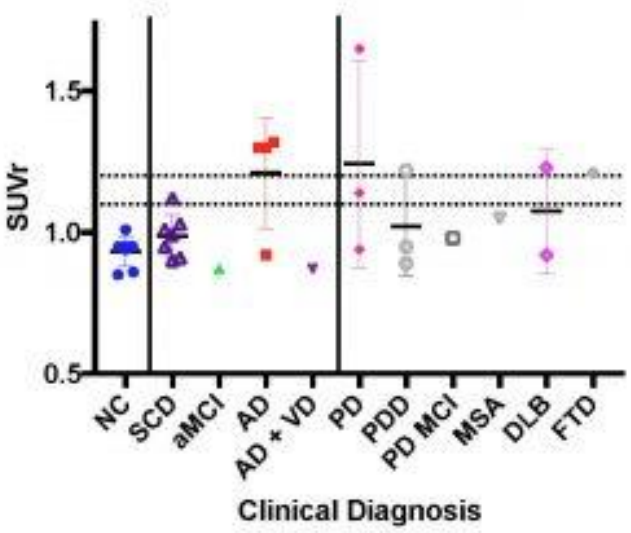

Keywords: PET, amyloid, subjective cognitive deficit, SUVr quantitation

Potential for Braak staging based on quantitative analysis of THK 5351 PET images

Christopher Buckley[1], Elisabeth Lysvic[2], Grethe Dalsgaard[1], Nobuyuki Okamura[3]

[1]*GE Healthcare, Amersham, United Kingdom*
[2]*Oslo University Hospital, Oslo, NO*
[3]*Tohoku University, Tohoku, Japan*

Introduction & Methods: Braak staging through analysis of PET tau agents has the potential to identify subjects who may respond optimally to Alzheimer's disease modifying therapies. For this reason, a quantitative analysis scheme has been created for THK3531 PET images.
Images from 11 healthy volunteers (4 young healthy (YHV) and 7 elderly healthy (EHV)), 4 amnestic Mild Cognitive Impairment (aMCI) and 12 Alzheimer's Disease (AD) subjects were imaged at Tohoku University. Subjects were administered 185Mbq of THK5351 and underwent Dynamic PET imaging. 40-60minute post-injection images were derived from these. T1-weighted 3D MRI were also performed.
The PET images were co-registered to the MR images, followed by spatial normalisation of the MRIs to MNI-152 space. The inverse of the normalisation transforms were applied to an atlas developed to represent the Braak regions. This atlas was applied to PET images to obtain $SUVR_{CER}$ for the regions implicated in stages II-VI.
Results: The results of the analysis were combined in a box-plot denoting the $SUVR_{CER}$ values for the YHVs, EHVs, aMCI & AD subject images (see figure 1).

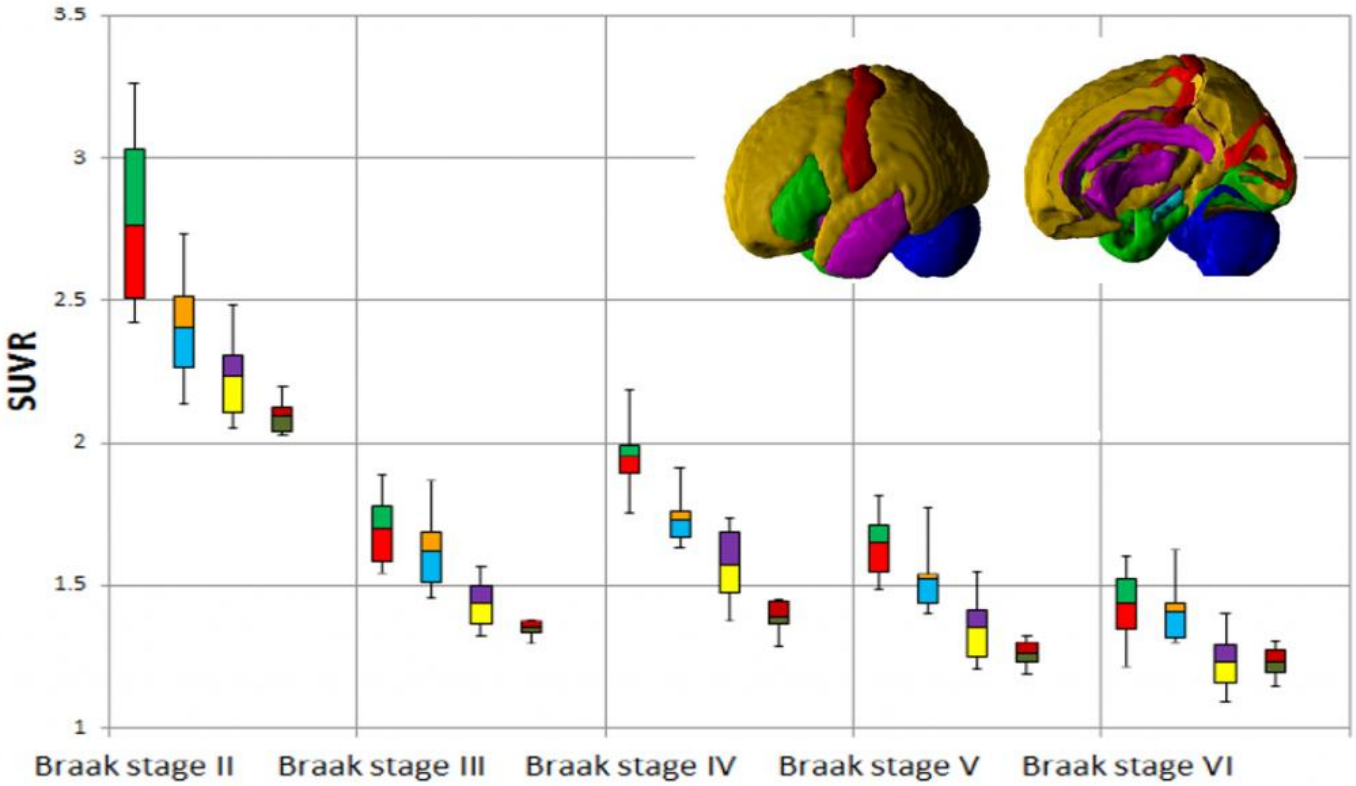

Figure 1. SUVR (cerebellum reference) by Braak stage region determined for 27 subjects. Box plot colours: Young healthy volunteers (brown/dark green), Elderly Healthy (purple/yellow), aMCI(orange/light-blue) & AD (green/red). The inset is a 3D representation of the staging atlas. Stages: II-light blue, III-green, IV-purple, V-gold, VI-red and blue is the cerebellum.
Discussion: While the subject numbers in this study are relatively small, the atlas does show differentiation

between the groups in the regions implicated in Braak stages II to V. Future work will consist of accumulating more images from clinically well-characterised subjects to create statistically valid SUVR thresholds for these regions and use these on individual scans to non-evasively estimate Braak staging in living subjects.

References

1. Braak et al. Acta Neuropathol (1991) 82:239 - 259
2. Mandal et. al. J Alzheimers Dis. (2012) 31 (0 3) 169-188

Keywords: Tau, Braak, VOI, Atlas

Both odor identification and amyloid status predict memory decline in older adults

William Kreisl[1], Peng Jin[1], Seonjoo Lee[1], Ezra Dayan[1], Shankar Vallabhajosula[2], Gregory Pelton[1], Leslie Shaw[3], D. P. Devanand[1]

[1]*Columbia University Medical Center, New York, NY, USA*
[2]*Weill Cornell Medicine, New York, NY, USA*
[3]*Perelman School of Medicine at the University of Pennsylvania, Philadelphia, PA, USA*

Background: Odor identification can be inexpensively tested using the 40-item University of Pennsylvania Smell Identification Test (UPSIT), and odor identification deficits have been shown to predict cognitive decline in older adults. We sought to compare the predictive utility of odor identification to that of central nervous system amyloid status for future memory decline.

Methods: Eighty-four adults (age 68.4 ± 7.4 years; 58 with amnestic mild cognitive impairment and 26 controls) had UPSIT, cognitive testing, and PET imaging with ^{11}C-Pittsburgh Compound B (PIB) and/or lumbar puncture at baseline, plus at least 6 months' follow-up. Amyloid-positivity was defined as either PIB uptake in composite gray matter ≥ 1.4 times that in cerebellum or CSF $A\beta_{42}$ < 250 pg/mL. Logistic regression and Receiver Operating Characteristic Curve analysis were conducted to test predictability of amyloid-positivity and UPSIT on memory decline.

Results: At follow-up, 67% of participants showed memory decline. After correcting for age, gender, and education, both amyloid-positivity (OR = 3.11; 95% CI = 1.01, 9.55; p = 0.0473) and UPSIT score <35 (OR = 3.95; 95% CI = 1.25, 12.49; p = 0.0192) predicted memory decline. Combining amyloid status and UPSIT score did not improve prediction of decline. UPSIT score correlated with PIB binding (r = -0.4582, p < 0.0001), and concordance between low UPSIT score and positive amyloid status was 62%.

Conclusion: Both UPSIT score and amyloid status predict memory decline. The moderate concordance between UPSIT and amyloid status suggests that plaque burden alone does not drive the relationship between odor identification and memory decline, and is consistent with neuropathological findings that neurofibrillary tangle pathology is prominent in the olfactory bulb in the early stages of AD. UPSIT may have utility as a low-cost, non-invasive alternative to amyloid PET or lumbar puncture in predicting memory decline.
Keywords: PIB, amyloid, olfaction, memory decline

Relationship between neuroticism and biomarkers of AD pathology in familial Alzheimer's disease

Yakeel Quiroz[1,2], Ana Baena[2], Daniel Norton[1], Danielle Cosio[1], Aaron Schultz[1], Jennifer Gatchel[1], Reisa Sperling[1], Keith Johnson[1], Francisco Lopera[2]

[1]*Massachusetts General Hospital, Boston, MA, USA*
[2]*Grupo de Neurociencias, Universidad de Antioquia, Medellin, MA, Colombia*

Objective: Neuroticism, a personality trait characterized by the tendency to experience negative emotions, is associated with increased risk for dementia and cognitive impairment. However, it is unclear whether this is because neuroticism worsens cognitive performance independently of dementia, or because dementia-related processes contribute to neuroticism. We investigated whether neuroticism is associated with genetic predisposition to Alzheimer's disease (AD), and with biomarkers of AD pathology. We hypothesized that cognitively unimpaired individuals with autosomal-dominant AD would have elevated levels of neuroticism, and that these would be related to increased tau and amyloid accumulation, as measured by PET imaging.

Methods: Eighteen cognitively unimpaired individuals of the Colombian kindred with early-onset autosomal-dominant AD (aged 25 to 44) traveled to Boston for PET imaging. Eight were carriers of the Presenilin-1 (*PSEN-1)* E280A mutation and ten were non-carrier family members. All participants were blind to genetic status, and all carried a 50% risk of developing early onset AD. All participants completed the NEO Five-Factor Inventory, and underwent PiB and AV1451 PET imaging. PiB PET cerebral-to-cerebellar DVRs and AV1451-PET cerebral-to-cerebellar SUVRs were compared based on mutation status. Both PiB and AV1451 utilized structural ROIs as defined by Freesurfer. Groups were matched for age, sex, education level, and neuropsychological test performance.

Results: Mutation carriers had higher levels of neuroticism compared to non-carriers ($p=0.05$), and neuroticism in carriers only was associated with increased levels of tau in entorhinal ($r=0.77$, $p=0.04$) and inferior temporal cortices ($r=0.87$, $p<0.001$). Other personality traits did not relate to AD pathology or differ between groups.

Conclusions: Initial findings from this ongoing study revealed that neuroticism is elevated in cognitively unimpaired individuals with autosomal-dominant AD, years before clinical onset, and it is related to tau accumulation. Further research with a larger sample size is needed to understand the underlying mechanisms explaining these associations.
Keywords: Personality, neuroticism, autosomal-dominant Alzheimer's disease, preclinical

Functional network integrity predicts cognitive decline in preclinical Alzheimer's disease

Rachel Buckley[1,2,3,4], Aaron Schultz[3,5,6], Trey Hedden[4,5], Kathryn Papp[3,4,9], Bernard Hanseeuw[3,4,5], Gad Marshall[3,4,9], Jorge Sepulcre[5,7], Emily Smith[8], Dorene Rentz[3,4,9], Keith Johnson[3,4,5,9,10], Reisa Sperling[3,4,9], Jasmeer Chhatwal[3,4,9]

[1]*Florey Institutes of Neuroscience and Mental Health, Melbourne, MA, USA*
[2]*Melbourne School of Psychological Science, University of Melbourne, Melbourne, Australia*
[3]*Department of Neurology, Massachusetts General Hospital, Boston, MA, USA*
[4]*Harvard Medical School, Boston, MA, USA*
[5]*Department of Radiology, Bost, MA, USA*
[6]*Department of Psychiatry, Bo, MA, USA*
[7]*Gordon Center for Medical Imaging, Division of Nuclear Medicine and Molecular Imaging, Department of Radiology, Massachusetts General Hospital and Harvard Medical School, Bost, MA, USA*
[8]*Department of Psychiatry, University of Texas Southwestern Medical Center, Dallas, TX, USA*
[9]*Center for Alzheimer Research and Treatment, Department of Neurology, Brigham and Women's Hospital, Boston, MA, USA*
[10]*Division of Nuclear Medicine and Molecular Imaging, Massachusetts General Hospital, B, MA, USA*

Objective: To examine the utility of resting-state functional connectivity MRI based (rs-fcMRI) measurements of network integrity as a predictor of future cognitive decline in preclinical Alzheimer's disease (AD).

Methods: 237 clinically-normal older adults (aged 63–90 years, Clinical Dementia Rating = 0) underwent baseline β-amyloid (Aβ) imaging with Pittsburgh compound-B (PiB)-PET, and structural and rs-fcMRI. Seven networks were chosen for analysis, including four cognitive networks (default, salience, dorsal attention, and frontoparietal control), and three non-cognitive networks (primary visual, extrastriate visual, motor). Using linear and curvilinear mixed models, baseline connectivity in these networks was used to predict longitudinal changes in a preclinical Alzheimer cognitive composite (PACC), both alone and in interaction with Aβ burden. Median neuropsychological follow-up was three years.

Results: Baseline connectivity in the default (p=0.0005), salience (p=0.0009) and control networks (p=0.004) predicted longitudinal PACC decline, in contrast to connectivity in the dorsal attention (p=0.51) and all non-cognitive networks (ps=0.41-0.59; see Fig 1). Default, salience, and control network connectivity was also synergistic with Aβ burden in predicting curvilinear decline (ps<0.0001) with combined higher Aβ and lower connectivity predicting the steepest decline in PACC performance (see Fig 2).

Conclusions: In clinically-normal older adults, lower functional connectivity predicted a more rapid decline in PACC scores over time, particularly when coupled with increased Aβ burden. Among examined networks, default, salience and control networks were the strongest predictors of rate of change in PACC scores, with the inflection point of greatest decline beyond the fourth year of follow-up. These results suggest rs-fcMRI may be a useful predictor of early, AD-related cognitive decline in clinical research settings.

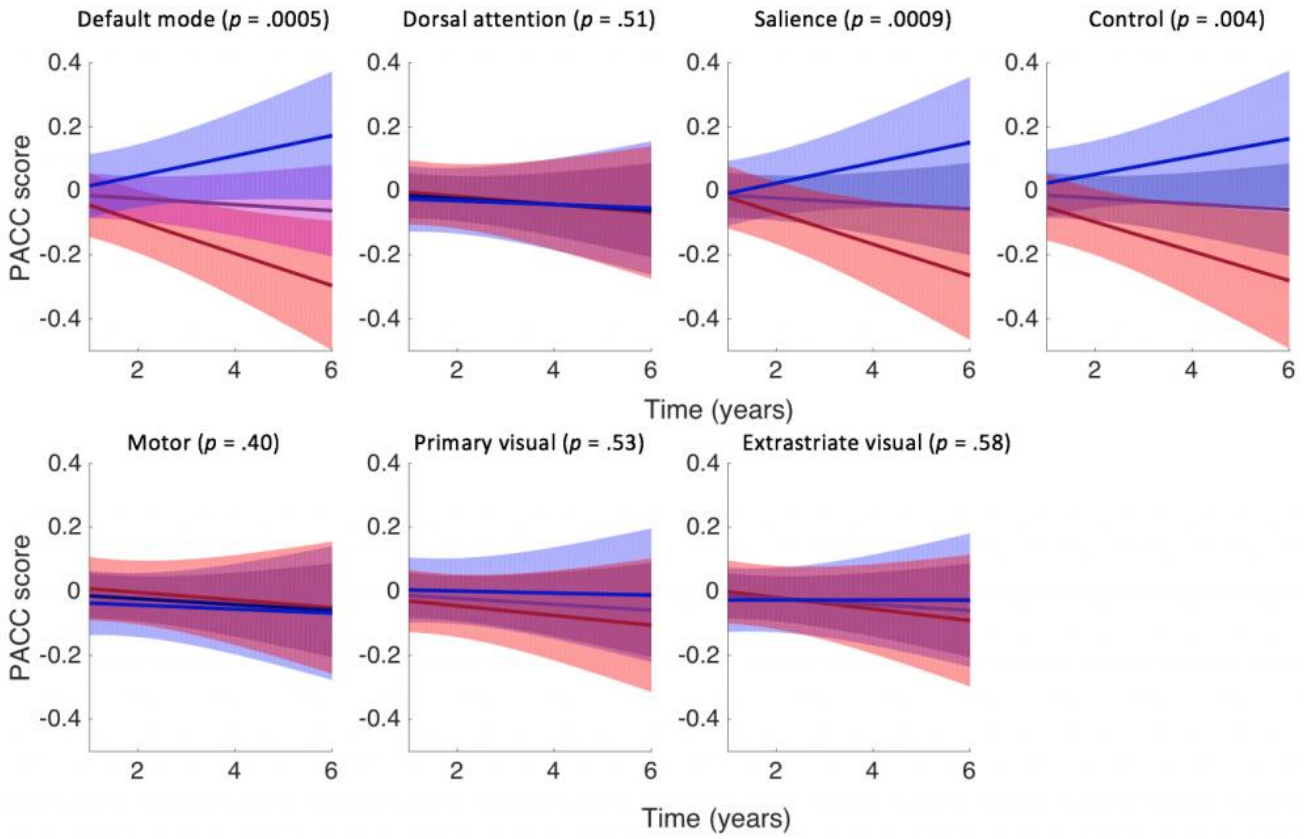

Fig 1. Model estimates of PACC decline according to rs-fcMRI networks

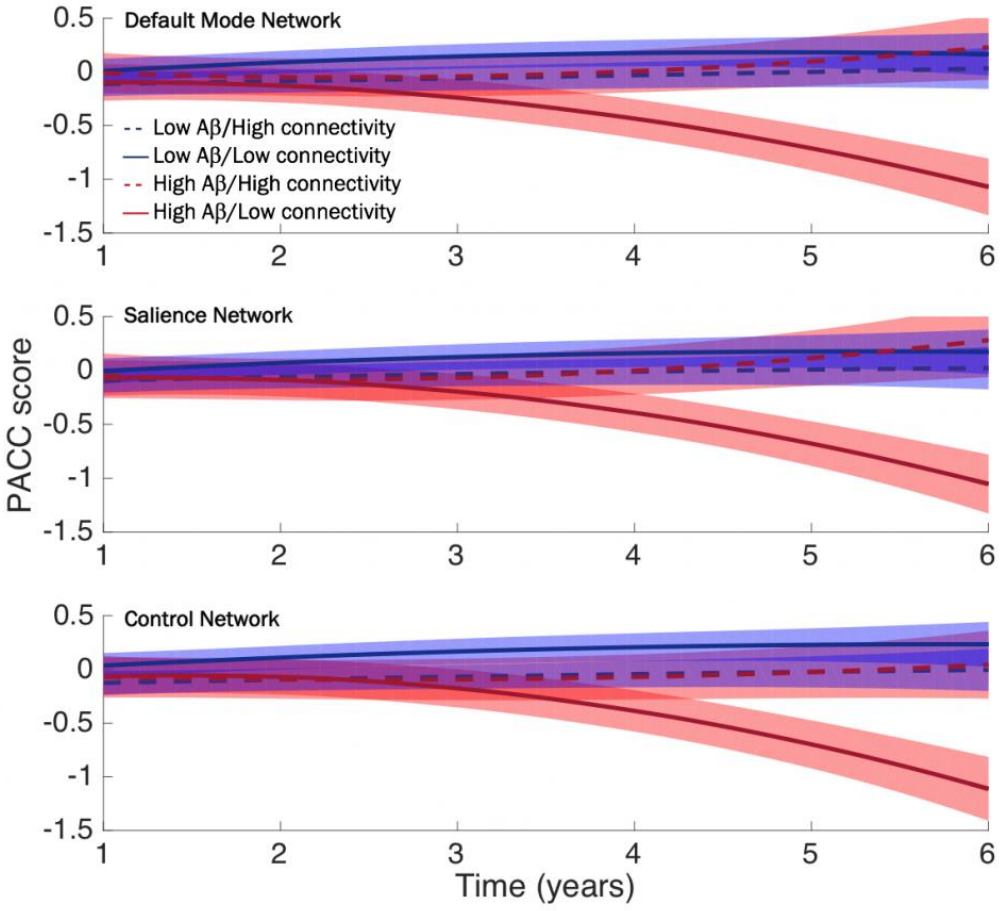

Fig 2. Non-linear model estimates of PACC slopes according to default, salience or control networks by amyloid interaction

Keywords: functional connectivity, cognitive decline, preclinical, amyloid, resting-state MRI

Subjective cognitive concerns exhibit region-specific relationships with tauopathy in the Harvard Aging Brain Study

Rachel Buckley[1,2,3,4], Bernard Hanseeuw[2,4,5], Patrizia Vannini[3,4,5], Elizabeth Mormino[3,4], Dorene Rentz[3,4,7], Reisa Sperling[3,4,7], Keith Johnson[3,4,5,7,8], Rebecca Amariglio[3,4,7]

[1]*Florey Institutes of Neuroscience and Mental Health, Melbourne, Australia*
[2]*Melbourne School of Psychological Science, University of Melbourne, Melbourne, Australia*
[3]*Department of Neurology, Massachusetts General Hospital, Boston, MA, Australia*
[4]*Harvard Medical School, Boston, MA, USA*
[5]*Department of Radiology, Massachusetts General Hospital, Boston, MA, USA*
[6]*Department of Psychiatry, Massachusetts General Hospital, Boston, MA, USA*
[7]*Center for Alzheimer Research and Treatment, Department of Neurology, Brigham and Women's Hospital, Boston, MA, USA*
[8]*Division of Nuclear Medicine and Molecular Imaging, Massachusetts General Hospital, Boston, MA, USA*

Introduction: Subjective cognitive concerns (SCC) are associated with early signs of abnormal biomarkers in Alzheimer's disease (AD), but until now, SCC has not been investigated in relation to region-specific tau deposition. We examined relationships between SCC, β-amyloid, entorhinal cortical (EC) tau, an area that exhibits very early signs of tauopathy, and inferior temporal (IT) tau, a region posited as more likely to manifest AD-related tauopathy.

Methods: 135 clinically-normal older participants (76yrs, *SD*=6.9) participating in the Harvard Aging Brain Study underwent AV1451-PET and PiB-PET. An SCC composite was created using z-transformed subscales from the Memory Functioning Questionnaire, the Everyday Cognition battery and a seven-item questionnaire. β-amyloid burden was used continuously according to a summary distribution volume ratio of frontal, lateral and retrosplenial tracer uptake. AV1451 measures were computed as standardized uptake value ratios, and partial volume corrected (PVC). Three separate models were run, focusing on main and interactive effects of β-amyloid, EC and IT tau on SCC, controlling for age, sex, education, and Geriatric Depression Scale score.

Results: SCC was associated with β-amyloid after accounting for demographics (β=0.22,*p*=.008). SCC also positively associated with EC PVC tau (β=0.36,*p*<.0001; see Fig 1). IT tau did not significantly predict SCC (β=0.10,*p*=.26; see Fig 2). An interactive effect of β-amyloid and EC tau on SCC was not significant (*p*=.22). A full *post-hoc* model suggested that EC tau was the only significant biomarker predictor, accounting for the largest variance in the model (38%).

Discussion: Greater EC tau and β-amyloid were singularly associated with greater SCC, however, synergistic relationships were not apparent. We argue that while SCC is clearly related to neuroimaging markers of tau and β-amyloid, it is possible that SCC, considered here as an aggregate composite, is a behavioral manifestation of a range of aetiologies. Future studies will examine which SCC symptoms are more indicative of AD-related pathology.

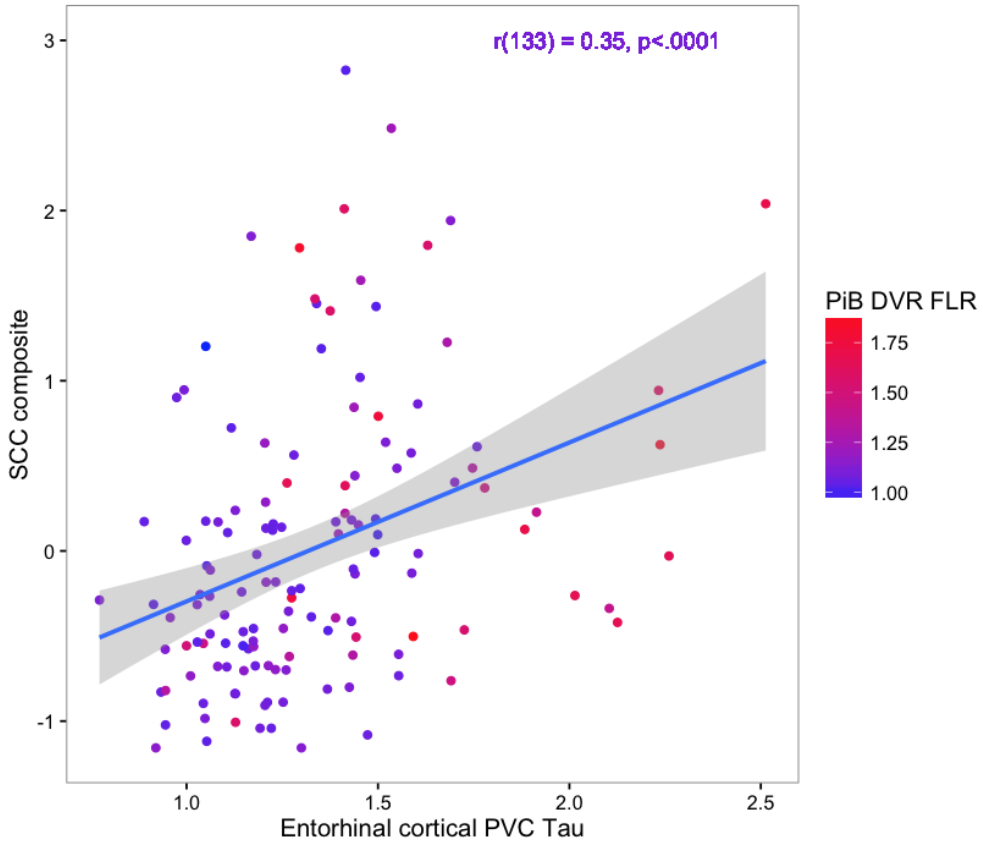

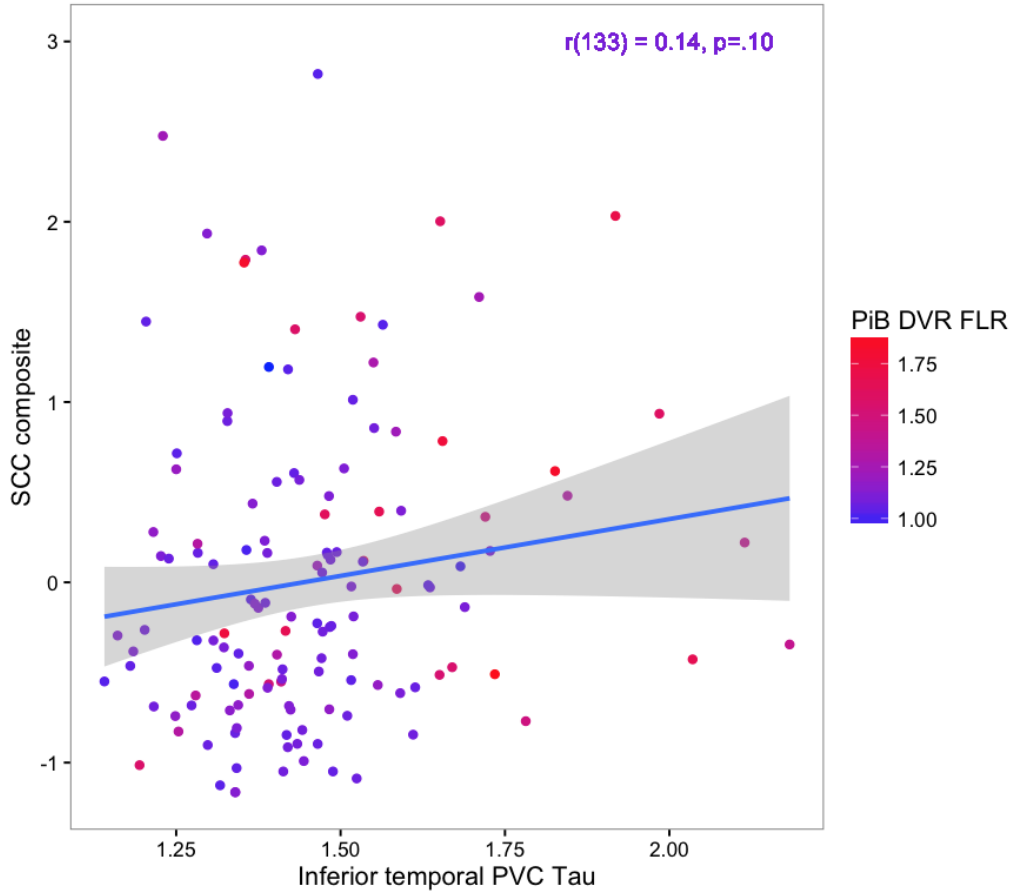

Keywords: subjective cognitive concerns, amyloid, tau, PET imaging

Longitudinal Measures of Cognition and Clinical Status are Associated with Tau Deposition in Early Symptomatic Stages of AD

Shannon Risacher[1,2], Kacie Deters[1,2], Adam Schwarz[3,4], Andrew Saykin[1,2]

[1]*Center for Neuroimaging, Department of Radiology and Imaging Sciences, Indiana University School of Medicine, Indianapolis, IN, USA*
[2]*Indiana Alzheimer Disease Center, Indiana University School of Medicine, Indianapolis, IN, USA*
[3]*Eli Lilly and Company, Indianapolis, IN, USA*
[4]*Department of Psychological and Brain Sciences, Indiana University, Bloomington, IN, USA*

Introduction: flortaucipir (AV-1451) is a novel PET tracer to visualize tau deposition *in vivo*. One group of interest is early stage individuals who are more mildly symptomatic than traditional amnestic mild cognitive impairment. We sought to investigate the relationship between clinical and biomarker measurements and tau deposition in these individuals.

Methods: 32 individuals from ADNI were included (9 significant memory concerns (SMC), 23 early mild cognitive impairment (EMCI)). flortaucipir scans and longitudinal CDR-Sum of Boxes (CDRsb), MMSE scores, florbetapir scans, and structural MRIs were downloaded from each visit from the initial ADNI-2 visit to the time of the flortaucipir scan. Florbetapir scans were processed with intensity normalization to the cerebellum and a composite ROI of eroded cerebral white matter, cerebellum, and brainstem for cross-sectional and longitudinal measures, respectively; SUVR was extracted from the whole cortex and precuneus. MRI scans were processed using Freesurfer v5.1 and mean hippocampal, hippocampal subfield, and total cortical grey matter volumes were extracted. Measures from the baseline visit, visit closest to the flortaucipir scan, and the slope of change between these visits (Δ), along with demographics, *APOE* genotype, and time between visits were entered into a step-wise linear regression model to determine the strongest associated measures with medial temporal lobe (MTL), lateral temporal lobe (LTL), and parietal lobe flortaucipir SUVR, normalized to the cerebellum crus.

Results: ΔMMSE was associated with tau in all regions (Table 1; $p<0.01$), while *APOE* and concurrent cortical amyloid were also associated with MTL and parietal tau, respectively ($p<0.05$). In amyloid-positive participants (n=15), ΔMMSE and Δhippocampal volume were associated with MTL and LTL tau ($p<0.05$), while ΔMMSE and ΔCDRsb were associated with parietal tau ($p<0.05$).

Discussion: These findings support the association between the emergence and progression of cognitive symptoms and tau deposition in early stages of AD.

Table 1. Step-wise Linear Regression Results

All SMC, EMCI							
	R^2	Variable 1	B	p	Variable 2	B	p
MTL	0.619	ΔMMSE	-0.214	0.002	*APOE*	0.118	0.031
LTL	0.692	ΔMMSE	-0.324	<0.001	n/a		
Parietal	0.864	ΔMMSE	-0.324	<0.001	Cortical AV45	0.383	0.025
Amyloid-positive SMC, EMCI							
	R^2	Variable 1	B	p	Variable 2	B	p
MTL	0.923	ΔMMSE	-0.270	0.002	ΔHippVol	-0.003	0.010
LTL	0.981	ΔMMSE	-0.461	<0.001	ΔHippVol	-0.001	0.042
Parietal	0.984	ΔMMSE	-0.450	<0.001	ΔCDR	0.269	0.008

Keywords: flortaucipir (AV-1451), early stage disease, amyloid PET, magnetic resonance imaging, Alzheimer's Disease Neuroimaging Initiative (ADNI)

Determining smallest detectable difference from longitudinal data – Application to hippocampal volume data from ADNI

Aniket Joshi[1], Dai Feng[2], Richard Baumgartner[2]

[1]Novartis Institute for Biomedical Research, Cambridge, MA, USA
[2]Merck Research Laboratory, Rahway, NJ, USA

Introduction: Hippocampal loss measured with MRI has been postulated to be a sensitive marker of Alzheimer's disease (AD) progression and is typically evaluated as a group mean difference between baseline and follow-up scans. At a subject level, the longitudinal change is a combination of two components; physiological change due to aging/progression and within-subject variability (related to test-retest). We apply random effects ANOVA model to estimate these two components from longitudinal ADNI hippocampal volume data. Furthermore, using the within-subject variability, we propose a threshold for true physiological change at a subject level and assess if this threshold can determine transitions from normal (NL) to mild cognitive impairment (MCI), and MCI to AD.

Methods: We model the hippocampal volume data using one-way random analysis of variance with 3 components; mean longitudinal change, subject-specific random effect, and within-subject variability (see equations below). From this model, we can calculate the smallest detectable difference (SDD). The method was applied to baseline and 12-month ADNI hippocampal data (Schuff et al, 2009). The model parameters were estimated using NL and MCI non-converters.

Results and Conclusion: The mean one year hippocampal change for NL and MCI non-converters was 43 mm^3 and 64 mm^3, respectively. The Bland-Altman plots show a large variability over one year. Though group mean hippocampal volumes reduction is significantly higher for converters compared to non-converters, at subject level this trend is not consistent. Thus, from this dataset, the hippocampal volume change does not appear to be a predictive marker of the disease at subject level.

The SDDs obtained for NL and MCI non-converters were 189 mm^3 and 175 mm^3, respectively. Change greater than SDD for a subject can be attributed to true physiological change at 95% confidence level. This approach can be applied to other ADNI longitudinal biomarkers to determine a conservative threshold for physiological change at subject level.

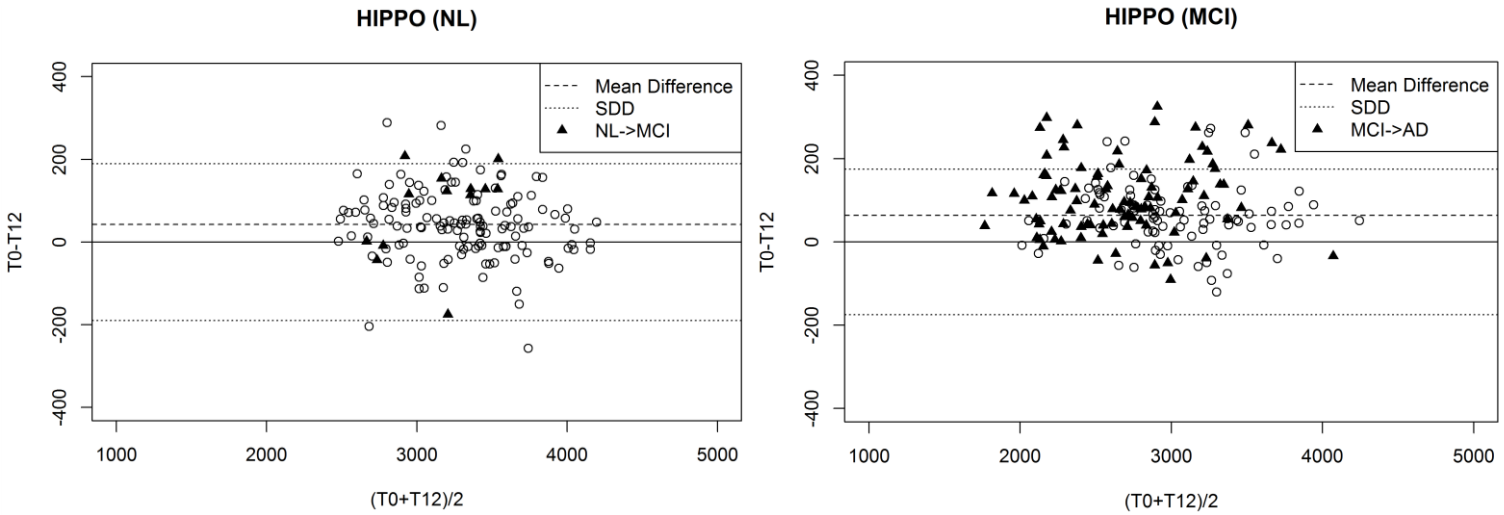

Bland-Altman plots for hippocampal volume longitudinal change from baseline (T_0) to 12-month follow-up (T_{12}). The dotted lines represent smallest detectable difference (SDD) and the dashed line denotes the mean difference. The solid symbols represent the converters from NL to MCI (left) and MCI to AD (right)

Modeling Longitudinal Change with Random Effects ANOVA:

The hippocampal volume is modeled as follows :

$$Y_{ij} = \mu + s_i + r_j + e_{ij},$$

where,

Y_{ij} is the hippocampal volume of the i' th subject at j' th timepoint.

μ is the population mean of the hippocampal volume

$s_i \sim N(0, \sigma_s^2)$ is random subject - specific effect

r_j represents the longitudinal change at timepoint j as fixed effect. It is assumed that at baseline $(j = 1), r_1 = 0$.

$e_{ij} \sim N(0, \sigma_e^2)$ is measurement error associated with within subject variability.

For a subject i, the longitudinal change between 12 - month scan $(j = 2)$ and baseline $(j = 1)$ is

$$Y_{i2} - Y_{i1} = r_2 + (e_{i2} - e_{i1}) = r_2 + \Delta e_i$$

$$\Delta e_i \sim N(0, 2\sigma_e^2)$$

SDD is estimated as follows :

$SDD = \sqrt{2}\, z_{1-\alpha/2} \hat{\sigma}_e$ (Barnhart et al., 2009)

where $z_{1-\alpha/2}$ is the $1 - \alpha/2$ quantile of standard normal distribution

(with $\alpha = 0.05$, $z_{1-\alpha/2} = 1.96$)

Keywords: smallest detectable difference, progression biomarker, hippocampal volume change, ADNI

Additive effects of subjective cognitive decline and amyloid-β burden predict cognitive decline in healthy elderly individuals

Jacob Vogel[1], Monika Varga Dolezalova[1], Renaud La Joie[2], Shawn Marks[1], Henry Schwimmer[1], Susan Landau[1], William Jagust[1]

[1]*Helen Wills Neuroscience Institute, University of California, Berkeley, CA, USA*
[2]*Memory and Aging Center, University of California, San Francisco, CA, USA*

Background Brain amyloid-β (Aβ) and subjective cognitive decline (SCD) are both predictors of longitudinal cognitive decline in cognitively intact elderly individuals. However, the relationship between these variables and cognitive decline remains unexplored.

Methods A data-driven SCD measure was extracted from the Geriatric Depression Scale(GDS) using principle axis factor analysis on data from 347 healthy, non-depressed (GDS < 11) elderly individuals from the Berkeley Aging Cohort Study. This sample was also used to generate cognitive factor scores. PiB-PET scans were acquired from participants with at least three cognitive testing sessions (n=136) to determine the presence (PiB+) or absence (PiB-) of Aβ pathology. Cognitive decline was measured using mixed effects modeling. Models included age, gender, education, a composite score summarizing subsyndromal depression, and the interaction between each of these covariate and time, as covariates of no interest.

Findings A significant three-way time x Aβ status x SCD interaction was found for episodic memory ($p<0.005$) and global cognition ($p<0.01$). SCD and presence of Aβ at baseline demonstrated additive effects on change in cognition over time, where PiB+ individuals exhibiting SCD demonstrated the steepest cognitive decline.

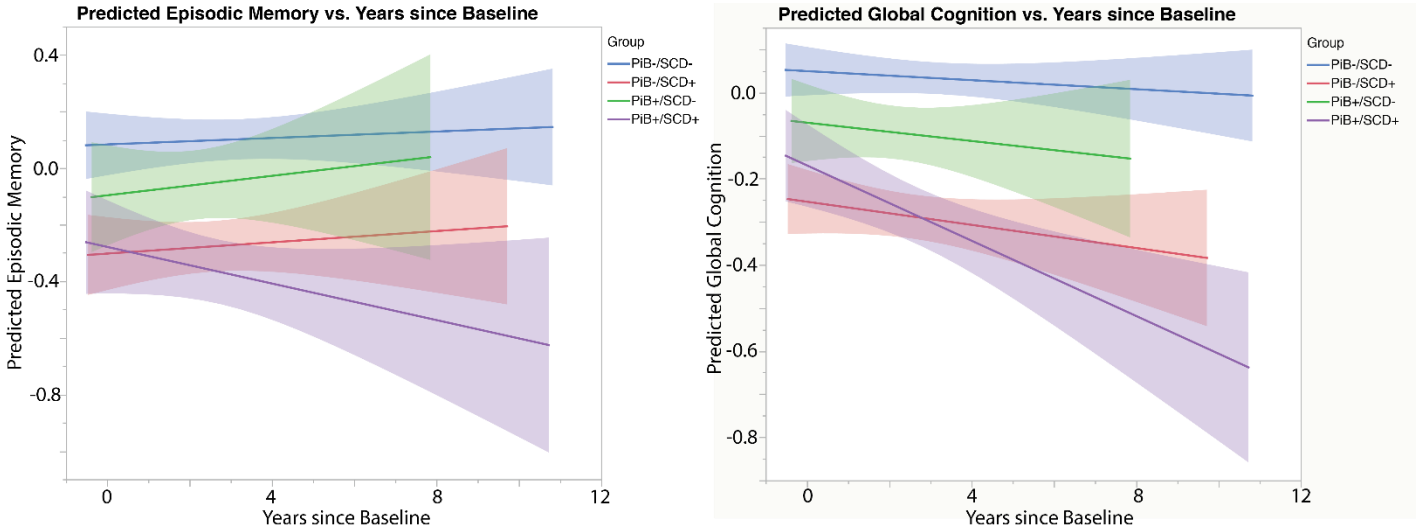

Figure 1 Model results visualizing the three-way interaction between time (years since baseline, x-axis), SCD and β-amyloid (PiB) status on longitudinal cognitive measurements (left, episodic memory; right, global cognition). For the purpose of visualization, participants were binarized into SCD+ or SCD- groups based on a median split. Participants were then further split based on their SCD and PiB status as follows: PiB-/SCD- (blue), PiB-/SCD+ (red), PiB+/SCD- (green), PiB+/SCD+ (purple). PiB+/SCD+ demonstrated the steepest cognitive decline in both episodic memory (left) and global cognition (right). A main effect of SCD is also observable in both plots.

Additionally, significant conditional effects of SCD ($p<0.05$) and time ($p<0.001$) on episodic memory were observed, as well as significant conditional effects of SCD ($p<0.01$), time ($p<0.001$) and SCD x time ($p<0.05$;) on global cognition.

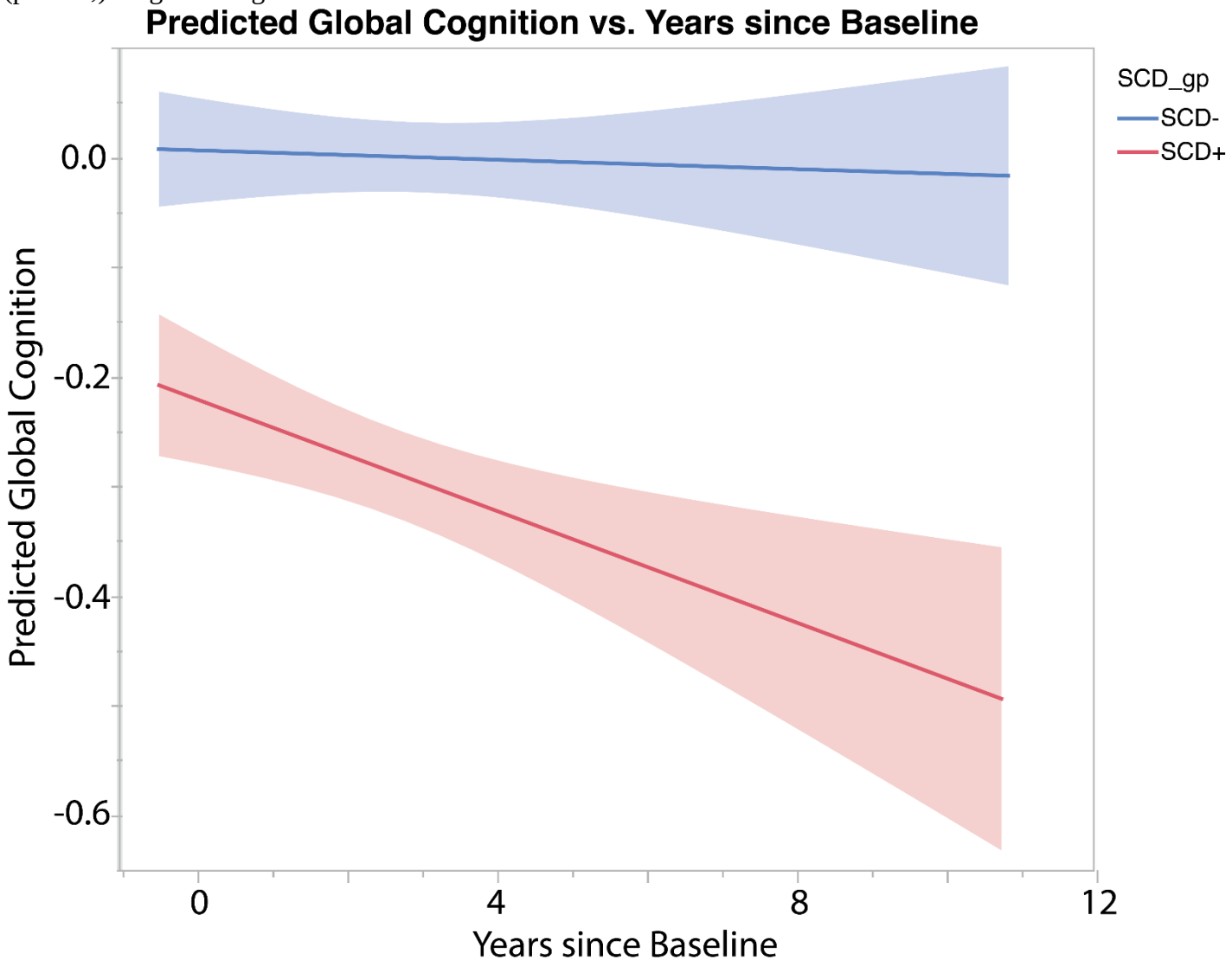

Figure 2: Model results visualizing the conditional two-way interaction between time (years since baseline, x-axis), and SCD (y-axis) on measurements of longitudinal global cognitive. For the purpose of visualization, participants were binarized into SCD+ or SCD- groups based on a median split. Participants exhibiting more pronounced SCD (red) at baseline showed reductions in global cognition over time compared to participants with less intense SCD at baseline, adjusting for covariates.

Interpretation Our results suggest that the presence of SCD in combination with brain Aβ is predictive of cognitive decline over time. These findings have implications for clinical trials, suggesting individuals with evidence for both Aβ and SCD are at higher risk for cognitive decline than those that exhibit one or the other. The conditional effects observed suggest SCD alone to predict change in global cognition over time, but that neither SCD or amyloid can fully explain changes in cognition observed in this cohort.

Keywords: amyloid, SCD, cognition, longitudinal, aging

Amyloid-β associated cortical thinning of the lateral temporo-parietal cortex predicts symptom severity over time in amnestic MCI patients

Federico d'Oleire Uquillas[1], Heidi I.L. Jacobs[2], Michael Properzi[1], Aaron P. Schultz[1,3], Molly R. LaPoint[1], Bernard Hanseeuw[2,4], Keith A. Johnson[2,3,4], Reisa A. Sperling[1,3,4], Patrizia Vannini[2,3,4]

[1]Department of Neurology, Massachusetts General Hospital, Harvard Medical School, Boston, MA, USA
[2]Department of Radiology, Massachusetts General Hospital, Harvard Medical School, Boston, MA, USA
[3]Athinoula A. Martinos Center for Biomedical Imaging, Massachusetts General Hospital, Harvard Medical School, Boston, MA, USA
[4]Department of Neurology, Brigham and Women's Hospital, Harvard Medical School, Boston, MA, USA

Introduction: While previous studies in Alzheimer's disease (AD) dementia have shown β-amyloid (Aβ)-associated cortical thinning in medial and lateral temporal cortices, it remains unknown whether similar patterns can be detected in mild cognitive impairment (MCI). Here we explored the neuroanatomical correlates of amyloid pathology in MCI patients, and investigated whether these structural correlates predict changes in symptom severity.
Methods: Forty-one patients with amnestic MCI underwent MRI and PiB-PET scans. Baseline PIB-DVR (from AD-vulnerable regions) was regressed vertex-wise on baseline cortical thickness, covarying for age. Results were cluster-wise corrected (p<0.05). Cortical thickness values were then extracted from each region and used in linear mixed effects models (LMEs) to investigate associations with clinical progression over time using the Clinical Dementia Rating Sum-of-Boxes (CDR-SB). All LMEs included age, gender and their interaction with time. PiB-DVR>1.2 indicated Aβ+ status (N=21). The fit of complex models was compared with simpler models using ANOVA. Results were Bonferroni-corrected (6 models, p<0.0083).
Results: Aβ burden was negatively associated with thickness of the right lateral temporo-parietal cortex (LTP) and right entorhinal cortex (EC). Interaction of Aβ-status × LTP-thickness × time, but not Aβ-status × EC-thickness × time, on CDR-SB was significant (p=0.0017)–an effect driven by Aβ+ patients (p<0.0001) . Model fit comparisons showed that this three-way interaction predicted CDR-SB change better than assessing the independent effects of the two-way interactions (p=0.0039).
Conclusion: Cortical thinning of the LTP predicted CDR-SB change, and this was particularly evident in Aβ+ patients. These Aβ-associated cortical regions are similar to those found in previous studies looking at the association of CSF-Aβ and cortical thickness in MCI. These spatial patterns also overlap with the distribution of Tau pathology in the brain. Our findings support the hypothesis that neocortical Aβ is associated with distal cortical thinning of memory-related regions, and that these processes occur even before diagnosis of clinical AD.

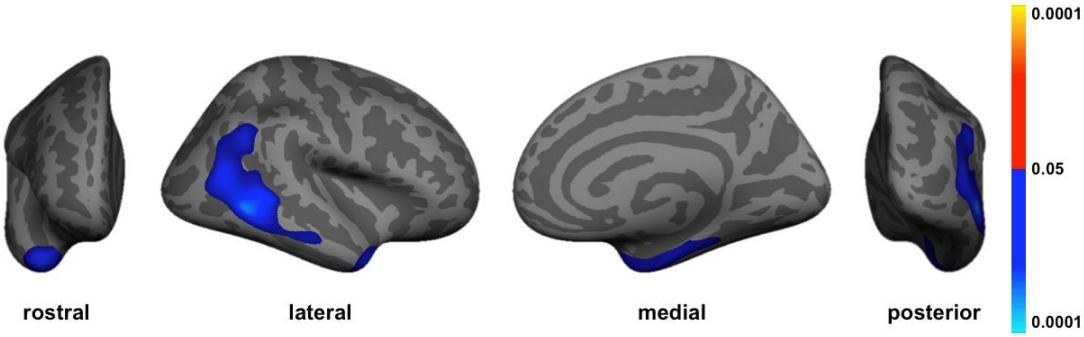

Figure 1. Association map of amyloid-β on cortical thickness across the entire cortical mantle after correcting for multiple comparisons. Right hemisphere shown.

Figure 2.
Two-way interaction of CDR-SB over time by right lateral temporo-parietal cortical thickness in Aβ+ patients shows that the lower the cortical thickness in this region the greater the increase in CDR-SB over time. This interaction was not significant in Aβ- patients.
CDR-SB, Clinical Dementia Rating Sum of Boxes.

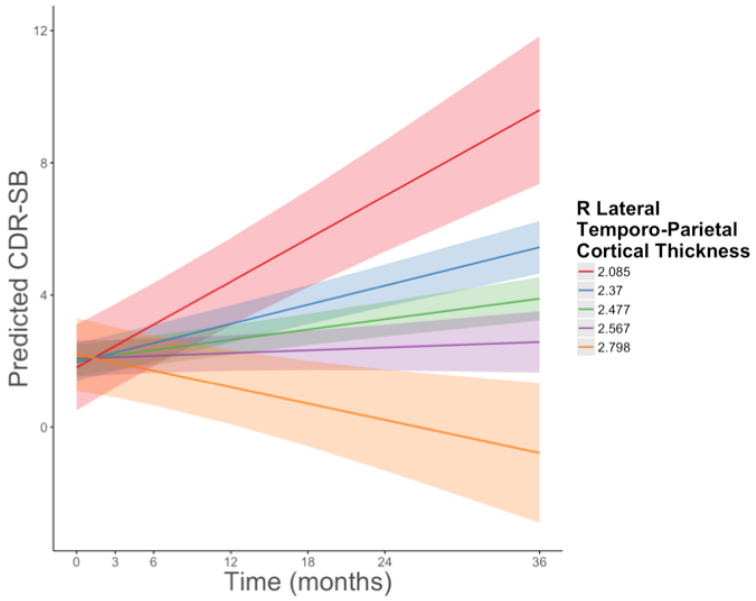

Table 1

Dependent variable:	**CDR-SB (N=134)**	
	Estimate	p-value
I. LME model with only Aβ Status × Time	0.06 (0.01)	**<0.0001****
II. LME model with only r.EC Thickness × Time	-0.05 (0.02)	0.0119*
III. LME model with only r.LTP Thickness × Time	-0.25 (0.04)	**<0.0001****
IV. LME model with both Aβ Status and r.EC Thickness × Time		
Aβ Status × Time	0.06 (0.01)	**<0.0001****
r.Entorhinal Cortical Thickness × Time	-0.004 (0.02)	0.8229
V. LME model with both Aβ Status and r.LTP Thickness × Time		
Aβ Status × Time	0.03 (0.01)	0.0515
r.Lateral Temporo-Parietal Cortical Thickness × Time	-0.17 (0.05)	**0.0019****
VI. LME model with interaction of Aβ Status, r.LTP Thickness, and Time		
Aβ Status × Time	0.79 (0.24)	**0.0011****
r.Lateral Temporo-Parietal Cortical Thickness × Time	-0.04 (0.07)	0.5448
Aβ Status × r.Lateral Temporo-Parietal Cortical Thickness	3.07 (2.72)	0.2663
Aβ Status × r.Lateral Temporo-Parietal Cortical Thickness × Time	-0.30 (0.09)	**0.0017****

All LME models included age, gender and their effect by time as covariates. Aβ-PiB and gender are a dichotomous variable, and age and cortical thickness measures are continuous. Females are used as the reference group for gender. Age, as a control variable, was centered at the group mean (72.43). LME, linear mixed-effects model; CDR-SB, Clinical Dementia Rating Sum of Boxes; r.EC, right entorhinal cortex; r.LTP, right lateral temporo-parietal; Aβ, amyloid-β; PiB, Pittsburgh compound B; r, right. *p<0.05, **p-value significant at Bonferroni-level p<0.0083.

Keywords: cortical thickness, amyloid, mild cognitive impairment (MCI), symptom severity, CDR Sum-of-Boxes

Does high baseline amyloid predict declines in activity participation and need for cognition over four years? Results from the Dallas Lifespan Brain Study

Allison Parker[1], Sara Festini[1], Michelle Farrell[1], Denise Park[1]

[1]*Center for Vital Longevity, University of Texas at Dallas, Dallas, TX, USA*

Introduction: Lower amyloid deposition has been associated with high lifetime cognitive engagement (Landau et al., 2012), and other studies suggest high activity levels defer an Alzheimer's disease diagnosis (Wilson et al., 2007). These relationships may occur because individuals withdraw from activities as neuropathology spreads. We examined whether baseline amyloid positivity in cognitively normal adults predicted a decline in activity level and need for cognition over a four-year interval.

Method: Participants (*N*=184) from the Dallas Lifespan Brain Study (ages 30-89) with F-18 Florbetapir PET imaging completed engagement surveys both at baseline and four years later. Baseline amyloid status (positive or negative) was used to predict changes in self-reported need for cognition and activity participation, measured by six subscales of the Victoria Longitudinal Study Activity Lifestyle Questionnaire. Linear mixed models included amyloid status, APOE e4 status, gender, and time as factors, age and education as covariates, and participant as a random effect.

Results: Analysis of need for cognition revealed a significant Amyloid x Time interaction. Amyloid positive individuals exhibited a decline in need for cognition over 4 years, whereas amyloid negative individuals did not. Importantly, this relationship remained even after controlling for baseline episodic memory performance and change in episodic memory. The Amyloid x Time interaction was not significant for any of the activity subscales. There were, however, marginal main effects of amyloid status on hobbies (p=.053) and self-maintenance activities (p =.098). Amyloid positive individuals reported lower levels of hobbies and self-maintenance activities across time points.

Conclusion: Amyloid positive, but not Amyloid negative, individuals exhibited decline over four years in need for cognition and reported less engagement in self-maintenance and hobbies across time points. These results indicate that amyloid pathology may contribute to withdrawal from engagement in cognitively stimulating activities in healthy adults.
Keywords: Amyloid, Need for Cognition, Engagement Activities

Amyloid-β related memory decline is modified by years of school education in cognitively normal subjects: A study of PiB PET and cognitive reserve

Takashi Kato[1,2], Iwata Kaori[2], Izumi Kuratsubo[2], Yoshitaka Inui[1], Naohiko Fukaya[1], Kengo Ito[1], Akinori Nakamura[2], Study Group MULNIAD[2]

[1]Department of Radiology, National Center for Geriatrics and Gerontology, Obu, Japan
[2]Department of Clinical and Experimental Neuroimaging, National Center for Geriatrics and Gerontology, Obu, Japan

A number of studies have demonstrated evidence of cognitive deficits (especially decline of episodic memory) in association with amyloid-beta deposition in cognitively normal elderly people. The purpose of this study was to investigate effects of cognitive reserve on the amyloid-related memory decline.

Subjects selected from in-house studies were 61 cognitively normal (CN) subjects (age: 69.8±5.7 (60-82) y.o., years of school education (YSE): 12.2±2.4 (9-18) years). They underwent a test of logical memory-II (LM-II) of Wechsler memory scale revised. Distribution volume ratio (DVR) image was calculated from dynamic PiB PET using simplified reference tissue mode 2. The DVR images spatially normalized using DARTEL method. Statistical analyses of the DVR images were performed with SPM8 for multiple regressions to assess the relationship with memory, age, and YSE. Correlation and regression analyses among regional DVR value, age, LM-II score and YSE were performed using SPSS.

Eleven out of 61 cases were visually evaluated as positive scans. LM-II score was 16.8 ± 6. A significant correlation was observed between LM-II and YSE ($r>0.5$, $p<0.001$). The correlation between LM-II and age was not statistically significant ($r=-0.16$, $p=0.21$). A SPM analysis showed that the bilateral medial temporal DVR was inversely associated with LM-II score ($p<0.005$, ext>50). Multiple regression analyses with LM-II as a dependent variable represented that statistically significant terms were YSE ($p<0.001$) and an interaction term of YSE and regional DVR in the medial temporal lobe in all the cases (n=61). When two outlier cases showing higher DVR value in the medial temporal lobe were excluded (n=59), statistically significant terms were YSE ($p<0.001$) and medial temporal DVR value ($p=0.041$).

The results suggest that, in cognitively normal subjects, recent memory declines in associated with amyloid deposition in the medial temporal lobe, and the negative association is modified by cognitive reserve.
Keywords: preclinical AD, amyloid PET, memory, cognitively normal, cognitively reserve

Memory encoding and recalling assessed by functional Near-Infrared Spectroscopy

Sahar Jahani[1], David Harper[2], Jim Ellison[2], Antoniu Fantana[1], David Boas[1], Meryem Yucel[1]

[1]*MGH, Charlestown, MA, USA*
[2]*Mclean, Belmont, MA, USA*

Background: Alzheimer's disease (AD) is a chronic neurodegenerative disorder which is the sixth leading cause of death in the United States (NIA-NIH). Early detection of AD is the key to preventing, slowing and stopping the disease. The earliest cognitive impairments in patients with Alzheimer's disease are seen in learning and memory skills as in normal aging, however, with different underlying neurological changes (Sperling2003). This preliminary study is performed to assess the NIRS's utility to measure brain activation during memory encoding on young healthy adults.

Paired-associate learning: Paired-associate learning (PAL) the pairing of two items e.g. for face-name pairs, when the learner is prompted with the face, he responds with the appropriate name. The face-name encoding task activates the striate, fusiform, prefrontal cortices and the anterior hippocampus in young healthy adults (Sperling2001).

Data and Analysis: NIRS acquisition was performed for 19 healthy adult subjects. fNIRS data were processed by using HOMER2 and MATLAB, Mathworks, Natick, MA.Paired t-test threshold was set to 0.05 for significance.

Results and Discussion: Robust activation was obtained during both encoding and recalling by fNIRS. Encoding and retrieval of information requires use of the short term memory buffer.Broader activation during recalling novel faces compared to encoding may be due to the inherent difficulty in recalling task that requires involvement of more regions.Default mode network may be responsible for the activation during encoding of same faces in medial frontal cortex.

References

- Sperling RA et al., (2003). "fMRI studies of associative encoding in young and elderly controls and mild Alzheimer's disease." J Neurol Neurosurg Psychiatry. 74(1):44-50.
- Sperling RA, et al., (2001). "Encoding novel face–name associations: a functional MRI study." Hum Brain Map, 14:129–39.

Keywords: near infrared spectroscopy, memory, Alzheimer's

Associations between regional amyloid load, cortical thickness, APOE genotype and cognition in ADNIGO/ADNI2 participants

Chunfei Li[1], Ranjan Duara[2,4], David A. Loewenstein[3,4,5], Mercedes Cabrerizo[1], Warren Barker[2,4], Malek Adjouadi[1,4]

[1]Center for Advanced Technology and Education, School of Engineering, Florida International University, Miami, FL, USA
[2]Wien Center for Alzheimer's Disease & Memory Disorders, Mount Sinai Medical Center, Miami, FL, USA
[3]Psychological Services and Neuropsychology Laboratory, Mount Sinai Medical Center, Miami, FL, USA
[4]Florida ADRC (Florida Alzheimer's Disease Research Center at Gainesville, Miami Beach, Miami and Boca Raton, FL), Gainesville,Miami and Boca Raton, FL, USA
[5]Center on Aging and Department of Psychiatry and Behavioral Sciences, Miller School of Medicine, University of Miami, Miami, FL, USA

Background/Objective: We examined the independent effects of Aβ load and (APOEe4 (e4) genotype on cortical thickness (CTh) and cognition in AD vulnerable regions[1] among participants in the ADNI/GO/ADNI2 study.

Methods: Subjects were classified as (a) CN (n=251) early MCI (EMCI) (n=297), late (LMCI) (n= 196) and AD (n=162); (b) e4+ or e4-; (c) amyloid positive (AMY+) or negative (AMY-), based on a mean Standard Uptake Value Ratios (SUVRs) (cut point of 1.10 for mean SUVR in 34 bilateral brain regions). ANCOVA was used to determine the independent association of Aβ load and e4 status on measures of CTh and cognition for each of 12 selectively vulnerable left regions, as well as on cognitive scores across all four diagnostic groups.

Results: (1) Across all diagnostic groups, greater Aβ load was associated with reduced CTh in most AD vulnerable regions; (2) e4+ status was associated with higher Aβ load in all regions and across all diagnostic groups; (3) Higher Aβ load was associated with impaired RAVLT, MMSE and ADAS13 cognitive scores, independent of diagnosis or e4 status (Table 1 and 2); (4) Among CN and EMCI subjects, e4+ status (controlling for amyloid load), was associated with ***increased*** cortical thickness in the Entorhinal Cortex, Parahippocampal Gyrus, Inferior Temporal Gyrus and Temporal Pole, but no independent association with cognition across diagnostic groups (Table 3).

Conclusions: The current findings suggest that Aβ load has an independent effect on reducing CTh and on impairing cognitive performance in all diagnostic groups. The effect of e4+ status on CTh and cognition is almost exclusively mediated via its effect on increasing SUVR in all brain regions. However, CTh in limbic regions is increased among CN and EMCI subjects who are e4+, independent of the effect of Aβ load, perhaps representing brain/cognitive reserve or genetic mechanisms[2].

TABLE 1: Regional Cortical Thickness and Cognition as a Function of ADNI Diagnosis and Amyloid Load Status Adjusting for ApoE4 Status

	CN AMY- 165 AMY+ 86	**EMCI** AMY- 149 AMY+ 148	**LMCI** AMY- 66 AMY+ 130	**AD** AMY- 19 AMY+ 143	**F[a] Amyloid**	**F E4 Status**	**F[a] Diagnosis**	**F[a] DX by Amyloid**
Age	74.51(6.84)[b] 76.75(5.74)	69.19(7.4) 73.46(6.83)	73.68(9.42) 73.61(7.29)	77.49(8.15) 74.38(7.71)	10.64**[c]	29.92***	15.79***	4.78**
Regional Cortical Thickness (left hemisphere)								
Entorhinal	3.34(0.38) 3.27(0.37)	3.32(0.46) 3.26(0.43)	3.17(0.52) 2.96(0.52)	2.77(0.74) 2.58(0.49)	14.59***	2.51	42.18***	1.56
Parahippocampal	2.67(0.34) 2.58(0.41)	2.66(0.36) 2.67(0.31)	2.52(0.39) 2.5(0.4)	2.44(0.39) 2.31(0.35)	6.74**	4.08*	15.6***	1.23
Inferior temporal	2.66(0.16) 2.61(0.16)	2.66(0.18) 2.61(0.19)	2.61(0.18) 2.57(0.23)	2.57(0.26) 2.39(0.24)	31.18***	13.07***	13.86***	3.13*
Temporal pole	3.56(0.33) 3.53(0.36)	3.48(0.37) 3.5(0.34)	3.5(0.35) 3.35(0.45)	3.08(0.63) 3.11(0.51)	2.46	3.51.	23.19***	1.99
Medial orbitofrontal	2.28(0.15) 2.27(0.18)	2.27(0.14) 2.23(0.16)	2.23(0.17) 2.22(0.17)	2.25(0.2) 2.19(0.16)	8.14**	3.95*	4.57**	1.3
Superior frontal	2.48(0.17) 2.46(0.17)	2.52(0.15) 2.49(0.15)	2.45(0.17) 2.42(0.16)	2.37(0.17) 2.36(0.18)	3.79.	1.82	15.17***	0.14
Rostral Middle Frontal	2.15(0.14) 2.15(0.15)	2.18(0.13) 2.15(0.12)	2.14(0.14) 2.11(0.13)	2.09(0.16) 2.07(0.15)	1.87	0.02	8.2***	0.64
Superior Parietal	1.96(0.17) 1.96(0.17)	2.01(0.14) 2.01(0.14)	1.97(0.16) 1.94(0.16)	1.95(0.12) 1.86(0.18)	6.08*	0.8	10.02***	1.69
Inferior Parietal	2.19(0.16) 2.18(0.17)	2.23(0.14) 2.21(0.15)	2.2(0.14) 2.13(0.16)	2.18(0.18) 2.02(0.2)	20.82***	0.75	10.67***	4.78**
Supramarginal	2.31(0.18) 2.31(0.18)	2.37(0.15) 2.34(0.16)	2.3(0.17) 2.26(0.17)	2.26(0.19) 2.16(0.18)	10.98***	3.44.	16.51***	1.71
Precuneus	2.14(0.17) 2.12(0.17)	2.19(0.14) 2.15(0.15)	2.14(0.16) 2.1(0.15)	2.11(0.14) 1.99(0.18)	16.55***	0.97	10.33***	1.92
Posterior Cingulate	2.38(0.18) 2.4(0.18)	2.41(0.17) 2.39(0.17)	2.4(0.17) 2.37(0.17)	2.39(0.22) 2.31(0.18)	4.25*	0.4	1.7	1.66
Cognition Test								
MMSE	29.13(1.24) 28.88(1.22)	28.62(1.39) 28.03(1.69)	28.35(1.5) 27.24(1.9)	22.74(2.9) 22.77(2.7)	6.19*	1.64	218.36***	2.47.
RAVLT immediate	45.96(10.3) 44.2(10.97)	41.7(11.15) 37.24(9.98)	36.59(12.1) 31.49(9.7)	23.58(7.0) 22.15(7.0)	10.56**	0.53	97.83***	1.35
RAVLT percent forgetting	35.83(28.4) 36.97(26.7)	42.56(29.5) 51.44(29.3)	55.34(32.1) 73.47(29.2)	87.63(20.0) 90.43(19.9)	5.97*	3.2.	77.19***	3*
ADAS-COG13	8.73(4.44) 9.78(4.69)	11.26(5.05) 14.18(5.58)	14.71(6.4) 19.53(7.5)	29.53(7.31) 31.82(8.98)	21.28***	0.37	214.73***	2.81*

[a] F value is adjusted for E4 Status

[b] Values are represented as mean(SD), upper is for AMY- group and lower is for AMY+ group

[c] p<.1; *p<.05; **p< .01; ***p< .001

TABLE 2: Regional Cortical Thickness, Cognition and ApoE4 Status Across Diagnostic Groups Controlling for Global Amyloid Load

	CN E4- 184 E4+ 67	**EMCI** E4- 169 E4+ 128	**LMCI** E4- 92 E4+ 104	**AD** E4- 54 E4+ 108	**F Amyloid**	**F[a] E4 Status**	**F[a] Diagnosis**	**F[a] DX by E4**
Age	75.77(6.35)[b] 73.93(6.98)	72.07(7.31) 70.33(7.49)	74.96(8.55) 72.46(7.42)	76.43(8.57) 73.9(7.28)	19***[c]	29.12***	12.89***	0.44
Regional Cortical Thickness (left hemisphere)								
Entorhinal	3.3(0.38) 3.35(0.37)	3.22(0.46) 3.37(0.41)	3.11(0.54) 2.96(0.51)	2.69(0.6) 2.55(0.48)	5.64*	0.02	68.18***	4.84**
Parahippocampal	2.62(0.38) 2.68(0.34)	2.64(0.32) 2.7(0.34)	2.5(0.39) 2.52(0.39)	2.37(0.38) 2.31(0.34)	2.29	1.71	25.56***	1.08
Inferior temporal	2.63(0.15) 2.68(0.17)	2.62(0.19) 2.65(0.19)	2.57(0.21) 2.59(0.22)	2.42(0.27) 2.41(0.24)	25.75***	9.99**	32.41***	0.5
Temporal pole	3.53(0.35) 3.6(0.32)	3.45(0.37) 3.53(0.34)	3.42(0.4) 3.38(0.44)	3.11(0.53) 3.1(0.52)	1.57	1.55	32.87***	1.1
Medial orbitofrontal	2.27(0.15) 2.28(0.18)	2.25(0.15) 2.25(0.15)	2.22(0.16) 2.22(0.18)	2.17(0.18) 2.21(0.15)	11.92***	4.83*	4.78**	0.53
Superior frontal	2.46(0.18) 2.5(0.16)	2.51(0.14) 2.5(0.16)	2.44(0.17) 2.42(0.16)	2.33(0.15) 2.37(0.19)	2.98.	2.01	22.2***	1.49
Rostral Middle Frontal	2.14(0.15) 2.15(0.14)	2.18(0.12) 2.15(0.13)	2.13(0.14) 2.11(0.12)	2.05(0.16) 2.08(0.15)	0.59	0	14.73***	1.8
Superior Parietal	1.95(0.16) 2(0.17)	2.02(0.14) 2(0.14)	1.96(0.16) 1.94(0.16)	1.88(0.18) 1.87(0.18)	3.03.	0.57	18.66***	1.7
Inferior Parietal	2.18(0.16) 2.21(0.18)	2.22(0.15) 2.22(0.15)	2.18(0.16) 2.13(0.15)	2.06(0.2) 2.03(0.21)	14.18***	0.1	25.75***	2.11.
Supramarginal	2.3(0.18) 2.34(0.17)	2.35(0.15) 2.36(0.16)	2.29(0.17) 2.26(0.17)	2.17(0.19) 2.17(0.18)	6.26*	2.08	30.71***	0.99
Precuneus	2.12(0.16) 2.16(0.17)	2.17(0.14) 2.16(0.15)	2.12(0.16) 2.1(0.16)	2.03(0.17) 2(0.18)	9.64**	0.36	22.49***	1.39
Posterior Cingulate	2.37(0.18) 2.42(0.18)	2.41(0.17) 2.38(0.17)	2.38(0.16) 2.38(0.18)	2.33(0.2) 2.31(0.18)	1.56	0.16	5.47***	2.03
Cognition Test								
MMSE	29.1(1.24) 28.88(1.21)	28.49(1.4) 28.1(1.7)	27.92(1.66) 27.34(1.98)	22.85(2.54) 22.72(2.7)	7.68**	2.07	329.04***	0.42
RAVLT immediate	45.84(10.6) 44.01(10.5)	40.41(10.9) 38.24(10.5)	34.59(11.7) 31.99(9.9)	22.02(7.3) 22.46(6.9)	23.43***	0.09	114.99***	0.79
RAVLT percent forgetting	36.2(29.04) 36.26(24.2)	44.84(29.3) 49.82(30.2)	57.73(33.6) 75.89(26.5)	88.56(24.3) 90.87(17.4)	15***	2.77.	92.83***	3.29*
ADAS-COG13	8.99(4.46) 9.36(4.8)	12.05(5.33) 13.61(5.64)	16.4(7.46) 19.21(7.3)	31.45(8.3) 31.59(9.1)	38.61***	0.1	301.44***	1.18

[a] F value is adjusted for Global Amyloid Load

[b] Values are represented as mean(SD), upper is for E4- group and lower is for E4+ group

[c] p<.1; *p<.05; **p< .01; ***p< .001

TABLE 3: Regional Cortical Thickness, Cognition and ApoE4 Status among combined CN and EMCI Groups Controlling for Global Amyloid Load

	E4- (353)	E4+ (195)	F_SUVR	F_E4[a]
Regional Cortical Thickness (left hemisphere)				
Entorhinal	3.27(0.42)[b]	3.36(0.4)	7.02**[c]	10.89***
Parahippocampal	2.63(0.35)	2.7(0.34)	3.26.	7.07**
Inferior temporal	2.62(0.17)	2.66(0.18)	15.36***	11.98***
Temporal pole	3.49(0.36)	3.56(0.33)	3.2.	6.56*
Medial orbitofrontal	2.26(0.15)	2.26(0.16)	11.87***	1.41
Superior frontal	2.48(0.16)	2.5(0.16)	1.4	1.32
Rostral Middle Frontal	2.16(0.14)	2.15(0.13)	0.01	0.56
Superior Parietal	1.98(0.16)	2(0.15)	0.06	1.84
Inferior Parietal	2.2(0.15)	2.22(0.16)	1.69	3.05.
Supramarginal	2.32(0.17)	2.35(0.17)	0.87	4.65*
Precuneus	2.15(0.15)	2.16(0.16)	3.09.	1.68
Posterior Cingulate	2.39(0.17)	2.4(0.18)	0.08	0.21
Cognition Test				
MMSE	28.81(1.37)	28.37(1.6)	15.35***	4.11*
RAVLT immediate	43.24(11.09)	40.23(10.83)	16.3***	2.83.
RAVLT percent forgetting	5.57(2.38)	5.36(2.57)	5.95*	0.02
ADAS-COG13	3.99(2.81)	4.17(2.41)	2.42	0.06

[a] F value is adjusted for Global Amyloid Load

[b] Values are represented as mean(SD)

[c] p<.1; *p<.05; **p< .01; ***p< .001

Keywords: Alzheimer's Disease, Regional Amyloid Load, Cortical Thickness, APOE genotype, Cognition

Regional uptake of FDDNP and exposure to professional fighting

Sarah Banks[1], Vladimir Kepe[2], Frank DiFilippo[2], Bern Lee[1], Jorge Barrio[2], Charles Bernick[1]

[1]*Cleveland Clinic Lou Ruvo Center for Brain Health, Las Vegas, NV, USA*
[2]*Cleveland Clinic, Cleveland, OH, USA*
[3]*University of California Los Angeles, Los Angeles, CA, USA*

Background: Exposure to repeated traumatic head injury has been associated at autopsy with increased tau. In football players, there is some evidence to suggest that PET tracers including FDDNP can demonstrate pathology during life. We used FDDNP to assess active and retired professional boxers and mixed martial arts fighters.

Methods: Fighters were recruited from a large, ongoing longitudinal study, the Professional Fighters Brain Health Study. This analysis represents the first 34 fighters, who ranged in age from 19 to 66 years, with a mean of 40 years. We used the MIAKAT kinetic analysis software to analyze FDDNP PET data. Fighters also underwent cognitive tests, and structured interview.

Results: While there were several relationships between exposure to fighting and FDDNP uptake in cortical and subcortical regions, these did not survive correcting for age. There was also an interesting relationship between nonverbal memory and FDDNP uptake in the amygdala.

Discussion: This preliminary evidence shows some limited support for increased regional uptake of FDDNP in fighters with more exposure. With ongoing data collection from normal controls and more fighters, we will be able to elucidate the relationship with age.
Keywords: FDDNP; brain injury; tau; amyloid; sports

Tau imaging in professional fighters

Sarah Banks, Karthik Sreenivisan, Charles Bernick

Cleveland Clinic Lou Ruvo Center for Brain Health, Las Vegas, NV, USA

Background: Repeated traumatic brain injury sustained in sports has been associated with neurodegenerative disease, and specifically with tauopathy. ^{18}F-AV1451, a PET tracer that binds to certain forms of tau, has been shown to follow the expected trajectory of spreading tauopathy in Alzheimer's patients. In a symptomatic retired football player, PET tracers that bind to tau have been shown to have increased uptake in regions that show increased tau at autopsy.

The Professional Fighters' Brain Health Study is a longitudinal study of professional boxers and mixed martial arts fighters. For the current study, we added ^{18}F-AV1451 scans to the usual battery which includes cognitive testing, demographic and clinical data collection, and MRI scanning. We expected fighters who showed extensive fight history, or those with poor scores on cognitive tests, to show more extensive uptake in regions known to be vulnerable to tau deposition in autopsy proven cases of CTE.

Methods: 12 professional fighters were scanned as part of a larger study with further recruitment planned. Mean SUVR values were extracted for FreeSurfer-defined regions. Given the small n we concentrated on the hippocampus, amygdala and thalamus bilaterally, and assessed correlations with age and number of fights. For regions that were significant, we performed a secondary analysis looking at correlations with cognitive test scores.

Results: Number of fights correlated with uptake in the amygdala bilaterally (left r=.622, right r=.746) and this effect was independent of age. Uptake in both amygdalae correlated negatively with processing speed score (left r=-.653, right r=-.585).

Discussion: These data suggest increased tau deposition in professional fighters with extensive fight experience, and that this is not an effect only of age. Furthermore, those fighters with the most tau deposition in the amygdala performed worse on a processing speed test. Further analysis with larger datasets will be important to clarify the meaning of this finding.
Keywords: tau, sports, head trauma, cognition

Clinical utility of amyloid PET in amnestic mild cognitive impairment.

Ko Woon Kim[1], Jin San Lee[1], Young Kyoung Jang[1], Sang Won Seo[1,2]

[1]Department of Neurology, Samsung Medical Center, Sungkyunkwan University School of Medicine, Seoul, Korea, Seoul, Korea
[2]Neuroscience Center, Samsung Medical Center, Seoul, Korea, Seoul, Korea

Background & Objective: Mild cognitive impairment (MCI) refers to a transitional zone between normal ageing and dementia. Despite clinical trials, a standard treatment strategy for MCI patients has not been established. Previous amyloid PET studies also showed that just 50-60% MCI patients had amyloid positivity, which predicted their worse clinical outcomes. The purpose of this study is to examine how an amyloid PET scan helps guide doctors in treating mild cognitive impairment (MCI) patients.

Methods: Data on all amyloid PET scan from May 2009 through May 2016 were retrieved from Samsung medical center. We compared pre-PET intended management to post-PET actual management recorded 90 days after the scan. Examples of changes in management include: use of Alzheimer's drug therapy, other drug therapy such as ginkgo biloba.

Among 168 MCI patients, the overall treatment change rate was 61%. In contrast, treatment non-change rate was 39%. Of the 39% patients with treatment non-change, amyloid positive group occupied as high as 52% compared amyloid negative group occupied only 29%. Of the 61% patients with treatment change, amyloid positive group was 44% and amyloid negative group was 41%.

Results of this study showed amyloid PET data could influence physicians' decision for MCI. Especially, physicians confidently started choline esterase inhibitors when amyloid PET result was positive. However, when amyloid PET showed a negative result, physicians hesitated stop choline esterase inhibitors. Future multi-center studies will be required to ascertain the clinical roll of brain amyloid PET that is an important factor to change treatment plan for MCI patients.
Keywords: MCI, amyloid PET, treatment

Relationships between [11C]PIB, [18F]AV1451 PET, and gray matter volumes within functional networks in Alzheimer's disease

Jungho Cha[1], Alexandre Bejanin[1], Renaud La Joie[1], Nagehan Ayakta[1], Suzanne L. Baker[3], Mustafa Janabi[3], James P. O'Neil[3], Bruce L. Miller[1], William J. Jagust[2,3], Gil D. Rabinovici[1,2]

[1]Memory and Aging Center, Department of Neurology, University of California, San Francisco, San Francisco, CA, USA
[2]Helen Wills Neuroscience Institute, University of California, Berkeley, Berkeley, CA, USA
[3]Life Science Division, Lawrence Berkeley National Laboratory, Berkeley, CA, USA

The objective of this study was to assess the relationships between amyloid and tau accumulation and gray matter volumes across the cortex and within functional networks in patients with Alzheimer's Disease (AD). We included forty-seven patients (mean age 62.9±8.2 yrs, mean MMSE 22.7±5.5) with a clinical diagnosis of probable AD and positive amyloid (PIB) PET. T1-weighted MRI was used to measure modulated gray matter volumes (mGM). PIB 90-minute DVR and AV1451 80-100 minutes SUVR were created using a cerebellar gray matter reference region. We assessed bivariate Spearman correlations between modulated gray matter volumes (mGM, SPM12), PIB DVR, and AV1451 SUVR across all cortical regions (210 regions-of-interest from the Human Brainnetome Atlas), and within 13 functional network templates from the Stanford FIND Lab (dorsal/ventral default mode networks (DMN), left/right executive controls networks (ECN), precuneus, auditory, language, anterior/posterior salience, higher visual, primary visual, visuospatial, and sensorimotor networks).

We found a positive correlation between PIB and AV1451 (ρ=0.40, p<0.001) across all cortical regions **(Figure 1)**. Both AV1451 (ρ=-0.33) and PIB (ρ=-0.12) were negatively correlated with mGM (p<0.001), though correlation with AV1451 was greater than with PIB (Z=15.95, p<0.001).

Figure 1. Relationships between [18F]AV1451 SUVR, [11C]PIB DVR, and modulated gray matter volumes across the cortex using Human Brainnetome atlas (Fan et al., 2016). Histograms of each variable across the cortex appear along the diagonal. ρ values are colored red if p < 0.05.

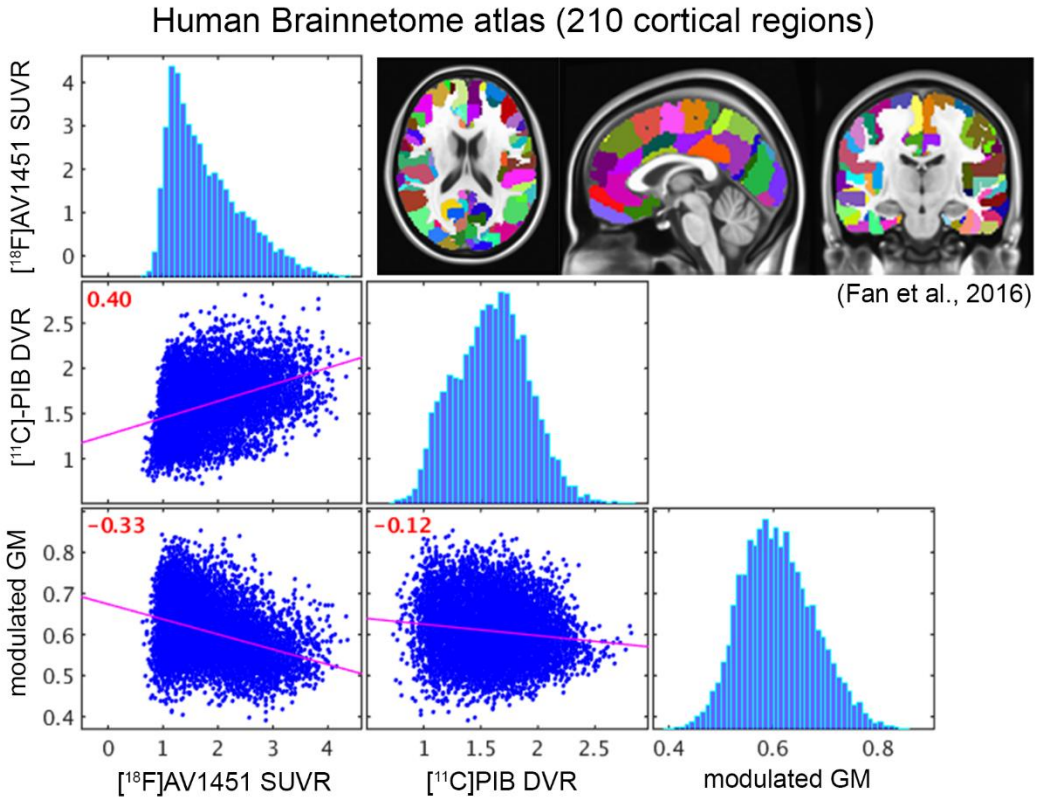

In all 13 functional networks, there were positive correlations between AV1451 and PIB (average ρ = 0.45, p<0.05). AV1451 was negatively correlated with mGM in dDMN, left ECN, right ECN, anterior salience, language, higher visual, and primary visual network, while PIB only showed associations with mGM in right ECN **(Figure 2)**. No significant correlations between mGM and PIB or AV1451 were found in other networks.

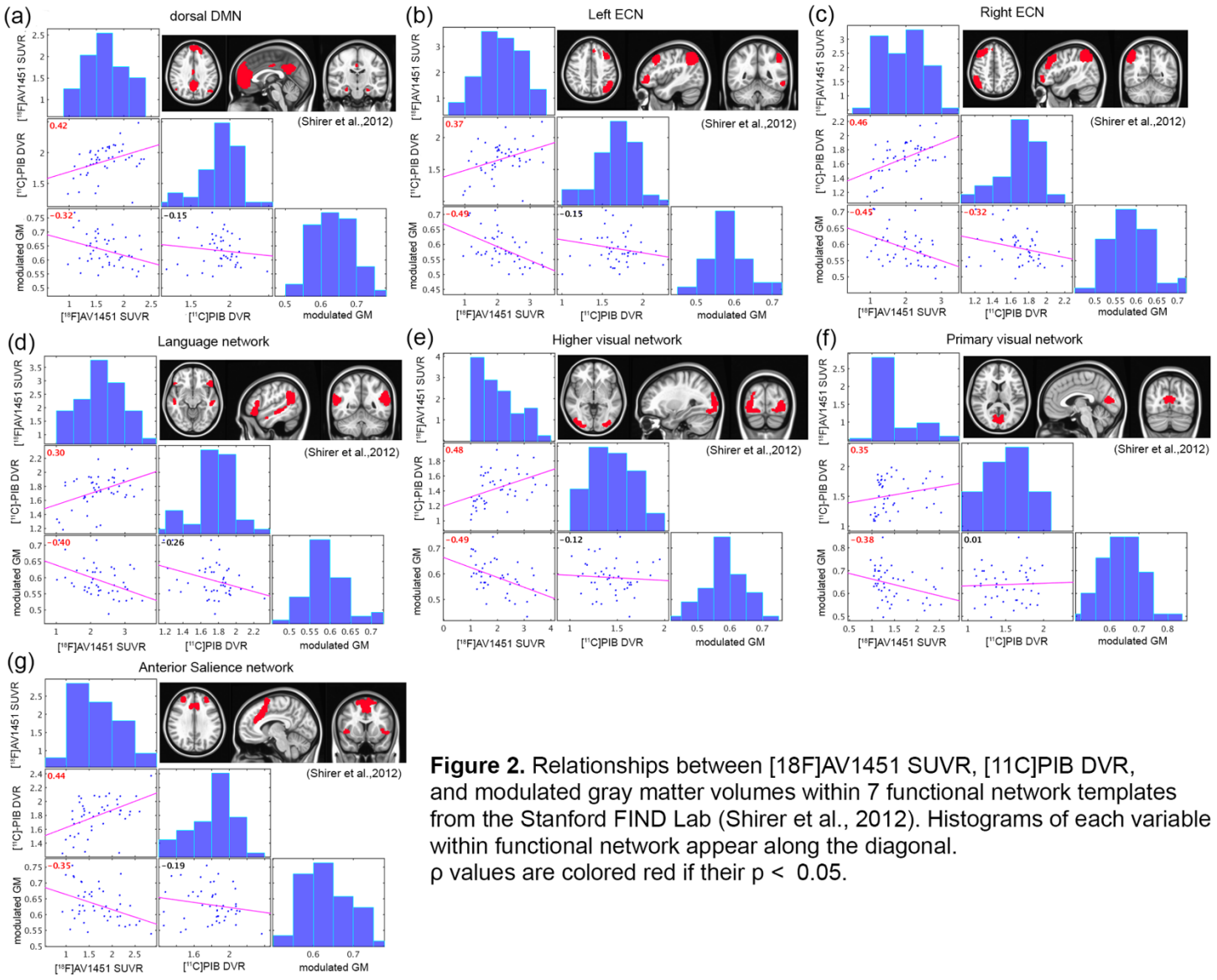

Figure 2. Relationships between [18F]AV1451 SUVR, [11C]PIB DVR, and modulated gray matter volumes within 7 functional network templates from the Stanford FIND Lab (Shirer et al., 2012). Histograms of each variable within functional network appear along the diagonal.
ρ values are colored red if their p < 0.05.

In conclusion, we found significant correlations between tau and amyloid accumulation across the cortex, but tau was more strongly linked to gray matter loss within cognitive networks. These results are consistent with AD being an amyloid-facilitated tauopathy, in which network-based spread of tau drives neurodegeneration and ultimately cognitive decline.

Keywords: [18F]AV1451, [11C]PIB, Neurodegeneration, Functional network, Alzheimer's disease

Prevalence of amyloid PET positivity according to APOE genotype in subcortical vascular cognitive impairment

Jin San Lee[1], Seonwoo Kim[2], Heejin Yoo[2], Seongbeom Park[1], Yeongsim Choe[1], Young Kyoung Jang[1], Rik Ossenkoppele[3], Ko Woon Kim[1], Yeshin Kim[1], Hyemin Jang[1], Hee Jin Kim[1], Key-Chung Park[4], Duk L. Na[1], Sang Won Seo[1]

[1]*Department of Neurology, Samsung Medical Center, Sungkyunkwan University School of Medicine, Seoul, Korea*
[2]*Biostatistics Team, Samsung Biomedical Research Institute, Seoul, Korea*
[3]*Department of Neurology and Alzheimer Center, VU University Medical Center, Amsterdam, Netherlands*
[4]*Department of Neurology, Kyung Hee University School of Medicine, Seoul, Korea*

Objectives: We compared the prevalence of amyloid positivity on PET between patients with subcortical vascular cognitive impairment (SVCI) and cognitively normal (CN) subjects. We also investigated the effects of APOE genotyping on the prevalence of amyloid positivity in CN subjects and SVCI patients.
Methods: A total 373 subjects (224 SVCI patients from the Samsung Medical Center and 149 CN subjects from the Australian Imaging, Biomarker & Lifestyle Flagship Study of Ageing dataset) who underwent ^{11}C-Pittsburgh compound B or ^{18}F-florbetaben PET scans were included in this study. All study participants were genotyped for the APOE ε2/ε3/ε4 alleles. Statistical analyses to compare between the groups were performed by chi-square test (Fisher's exact test) or Student's *t*-test. Multivariate logistic regression model was used to determine the prevalence of amyloid positivity according to age.
Results: The prevalence of amyloid positivity was significantly higher in SVCI patients than in CN subjects (34.4% vs. 24.2%, p=0.036). In comparison with non-carriers, the APOE ε4 carriers had significantly higher amyloid positivity in the SVCI and CN groups. Interestingly, the APOE ε2 carriers seemed to have higher amyloid positivity than the APOE ε3/ε3 groups in SVCI patients although their relationships were not significant. Furthermore, there were interaction of APOE ε2 and groups (SVCI and CN) for amyloid positivity (p=0.031).
Conclusion: Our findings support that the APOE ε2 might promote the accumulation of cerebral amyloid angiopathy (CAA) in the cerebral vasculature, as shown in the previous studies that higher level of Aβ was associated with the increased risk of hemorrhages in CAA with APOE ε2 patients.

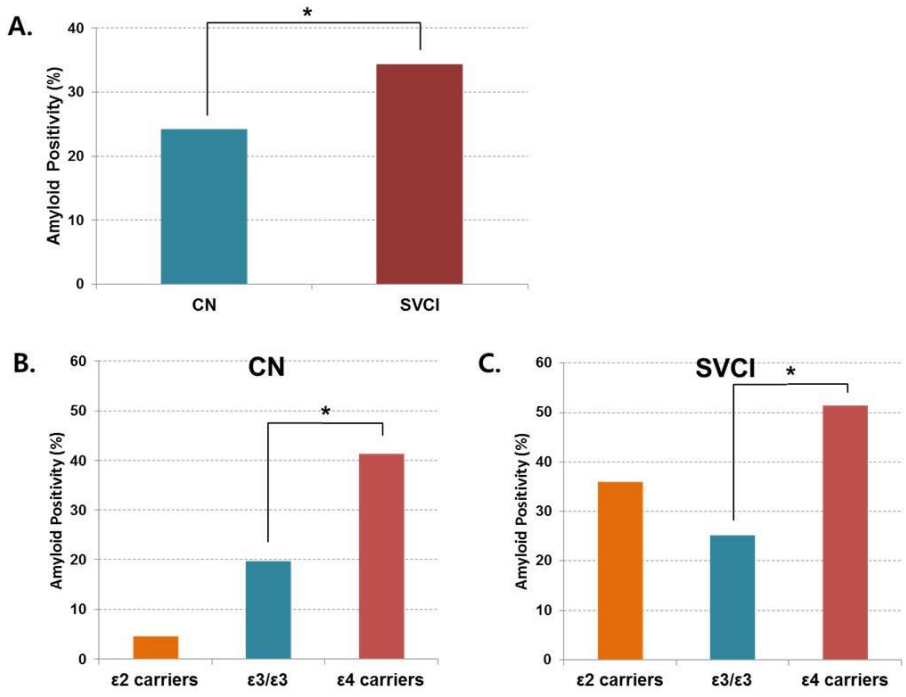

Figure 1. Comparision of amyloid positivity according to cognitive status (A) and APOE genotype (B, C)

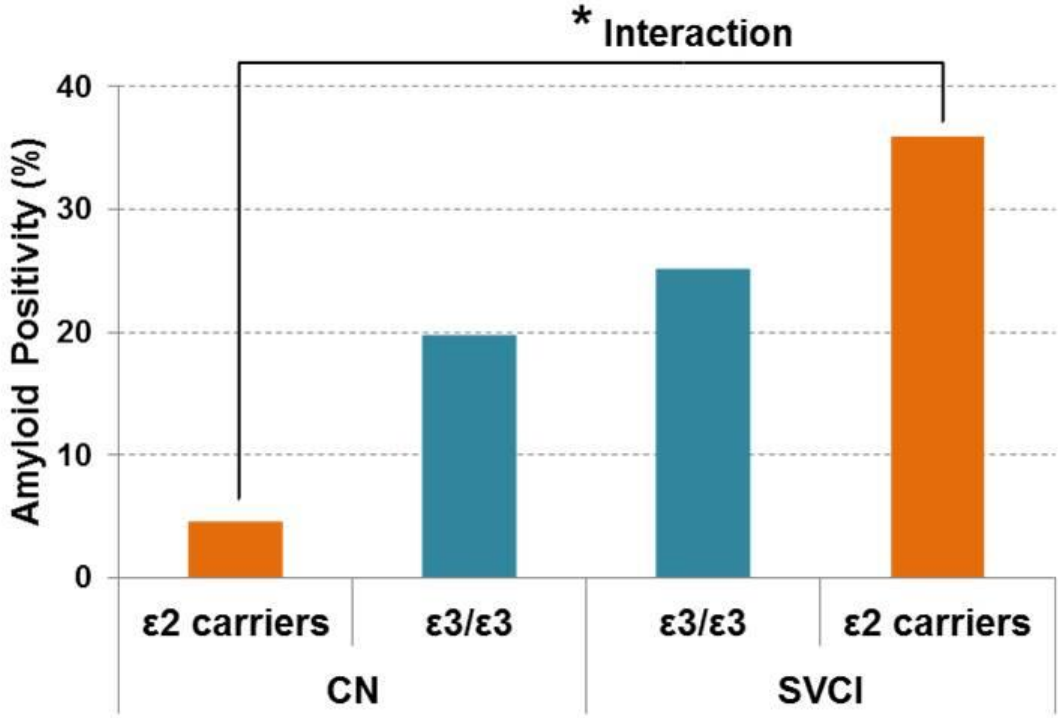

Figure 2. Interaction of APOE ε2 and groups (CN and SVCI) for amyloid positivity

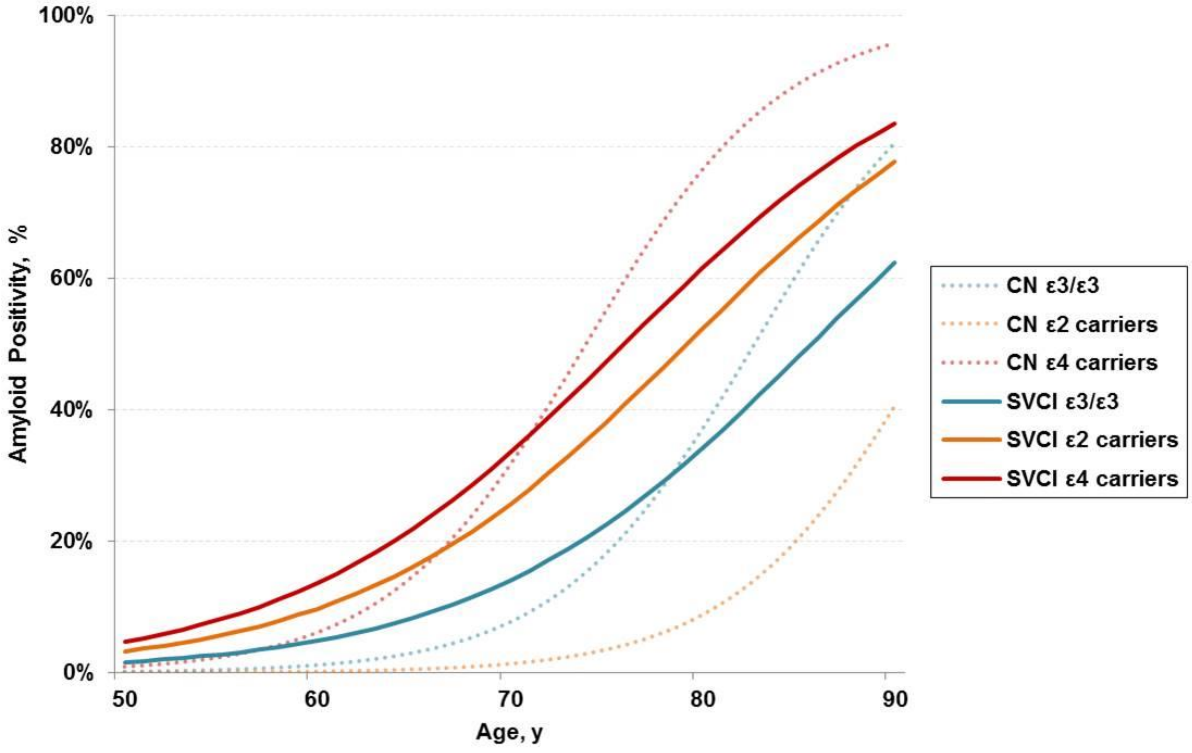

Figure 3. Association of age with prevalence estimates of amyloid positivity according to cognitive status and APOE genotype

Keywords: Subcortical vascular cognitive impairment, Amyloid positivity, APOE genotype, Cerebral amyloid angiopathy, Alzheimer's disease

Genetic drivers of resilience in asymptomatic Alzheimer's disease

Timothy Hohman, Logan Dumitrescu

[1]*Vanderbilt University Medical Center, Nashville, TN, USA*

Background: Asymptomatic Alzheimer's disease (AD) is characterized by the presence of autopsy-confirmed pathological AD (plaques and tangles) without the clinical manifestation of cognitive impairment. My lab has leveraged biomarker, neuroimaging, and cognitive data to build a robust metric of resilience that predicts protection from future cognitive decline, brain atrophy, and clinical progression (Hohman et al, *Neurology*, in press). The current project applied this measure of resilience as an endophenotype in a predicted gene expression analysis to identify novel genetic effects that promote resilience from cognitive decline, particularly in the presence of enhanced biomarkers of AD neuropathology.

Methods: Participants were drawn from the AD Neuroimaging Initiative (ADNI; n=686), the National Alzheimer's Coordinating Center (NACC; n=479), and the Rush Memory and Aging Project/Religious Orders Study (ROS/MAP, n=713). A partial-least squares latent variable model was used to calculate a continuous metric of resilience representing better or worse cognitive performance given an individual's level of cerebrospinal fluid biomarkers (ADNI) or an individual's burden of plaques and tangles (NACC/ROS/MAP). PrediXcan, a technique to "impute" gene expression, was leveraged to assess the association between tissue-specific gene expression and resilience. Analyses adjusted for age and sex while correcting for multiple comparisons ($\alpha=1x10^{-6}$).

Results: Lower predicted expression of GTP Binding Protein 2 (*GTPBP2)* in the cerebellar cortex was associated with higher levels of resilience in all three datasets (Fixed effects $\beta=-0.27$, $p=8.8x10^{-7}$). The effect was particularly strong among individuals who were biomarker positive, and among those individuals who met neuropathological criteria for AD.

Conclusions: Model system work has highlighted the role of *GTPBP2* in neurodegenerative cascade, particularly when ribosomal protein production has been stalled. Our results further highlight the potential role of *GTPBP2* in neurodegeneration and suggest that brain expression of *GTPBP2* may be particular relevant to the clinical manifestation of disease in the presence of AD neuropathology.
Keywords: Asymptomatic AD, Resilience, Biomarkers, Neuropathology, Genetics

Heterogeneity of amyloid-related cognitive decline in clinically normal older adults

Kate Papp[1], Dorene Rentz[1,2], Rebecca Amariglio[2], Aaron Schultz[2], Keith Johnson[1,2], Reisa Sperling[1,2], Elizabeth Mormino[2]

[1]*Brigham and Women's Hospital, Boston, MA, USA*
[2]*Massachusetts General Hospital, Boston, MA, USA*

Background: Previous work indicates that a subset of clinically normal older adults with elevated amyloid (Ab) on PET imaging are at risk of cognitive decline. However, how cognition declines by cognitive domain remains unclear. We therefore sought to examine Aβ-related decline across different cognitive domains in participants from the Harvard Aging Brain Study.

Methods: Clinically normal older adults (mean age=73.67, 63-90) underwent baseline imaging (PiB-PET; dichotomized into Aβ-/Aβ+ groups) and annual neuropsychological testing for up to 5 years (mean follow up=3.6±1.1 years). We constructed cognitive composites for Memory, Semantic Processing, and Executive Functions. Linear mixed models controlling for age, sex and education were used to examine cognitive decline in Memory (*6-trial SRT DR, Logical Memory DR*), Semantic Processing (*BNT, category fluency*), and Executive Functions (*TMTB-A, Digit Symbol Coding*).

Results: The Aβ+ group declined across all cognitive domains in comparison with the Aβ- group. Estimated mean annual z-score change for the Aβ+ group was as follows: Memory (beta= -0.08, p=0.001), Semantic Processing (beta= -0.09, p

Conclusions: Elevated amyloid was associated with longitudinal decline across multiple cognitive domains. Furthermore, our findings that Memory, Semantic Processing, and Executive Functions independently capture Aβ-related early decline provides evidence for the heterogeneity of the preclinical AD cognitive phenotype.
Keywords: cognition, amyloid

Predicting the rate of amyloid accumulation using multimodal data

Yan Jin[1], Shuai Huang[1], the ADNI[2]

[1]*University of Washington, Seattle, WA, USA*
[2]*Washington University in St. Louis, St. Louis, MI, USA*

Background: Alzheimer disease (AD) is the most common form of dementia and its incidence increases exponentially with age. Amyloid PET enables the early detection of brain amyloidosis, and the rate of amyloid accumulation is an important biomarkers especially in anti-amyloid clinical trials. In this project, we investigate the feasibility of predicting the longitudinal rate of amyloid accumulation based on multimodal data including APOE genotypes, FDG-PET, MRI volumetrics, and demographics. Specifically we adopt a widely used machine learning technique, RuleFit, to perform the predictive modeling and compare with traditional regression approaches.

Methods: Multimodal biomarker data was obtained from the Alzheimer's Disease Neuroimaging Initiative (ADNI) database. 1737 subjects in total are included in this study. Rate of amyloid accumulation was estimated based on longitudinal Florbetapir scans from ADNI-GO/2 cohort. RuleFit, an ensemble method that uses LASSO penalization to combine predictions from individual trees, was applied to establish the model for prediction of amyloid accumulation rate. The mean squared errors (MSE) of the RuleFit model was estimated and compared to three other popular regression models.

Results: The five most important rules found by the RuleFit algorithm is reported in Tab. 1. The importance score (Impo.) describes the relative importance of the respective input variables, while the support (Supp.) represents the percentage of the samples that satisfy the corresponding rules. Fig. 1 demonstrates the relative importance of selected biomarkers. Tab. 2 reports the MSE and R squared of the RuleFit model in comparison with other models. The performance of RuleFit model is better, where particularly it explains 75% of total variance.

Conclusion: RuleFit is a promising machine learning technique that can characterize the relationship of multiple biomarkers to the longitudinal accumulation of amyloid plaques. The predictive model may be used to improve participant selection in future longitudinal studies of AD progression and AD therapy/prevention trials targeting amyloid.

Table 1: 5 most important rules in RuleFit model

IMPO.	SUPP.	RULE
100	0.17	AGE>64.55; ADAS13>16.50
52.64	0.42	MidTemp>1.25
47.41	0.38	APOE4≠0; MMSE>19.50
44.30	0.50	APOE4=0; Ventricles<3.95
34.35	0.20	WholeBrain<70.20; MidTemp<1.28
33.07	0.35	ADAS13>12.50; Entorhinal>0.23

Table 3: prediction accuracy comparison

	$\overline{MSE}(10^{-3})$	$\sigma^2(MSE)(10^{-4})$	R^2
RULEFIT	6.74	0.81	0.75
LINEAR REGRESSION	26.25	18.09	0.36
LASSO REGRESSION	6.79	5.33	0.68
RANDOM FOREST	6.81	3.98	0.71

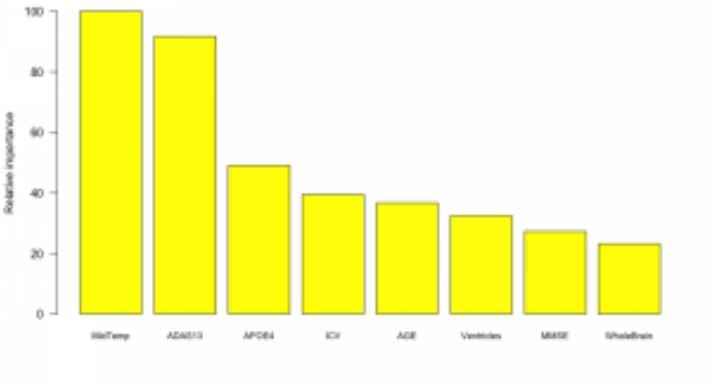

Keywords: RuleFit, AV45, Prediction, ADNI

PET based network analysis reveals temporal lobe as a hub for tau propagation in MCI

Sulantha Mathotaarachchi[1,2], Tharick Pascoal[1,2], Monica Shin[1,2], Min Su Kang[1,2], Vladimir Fonov[1,2], Andrea Benedet[1,2], Serge Gauthier[1], Pedro Rosa-Neto[1,2]

[1]McGill University, Montreal, QC, Canada
[2]Translational Neuroimaging Laboratory, McGill University Research Center for Studies in Aging, Verdun, QC, Canada

Introduction: The Braak and Braak neurofibrillary tangle(NFT) staging of Alzheimer's suggests a symmetric pathway for tau propagation. However, it remains to be established whether patterns of NFT deposition follows specific brain networks. We propose a data-driven minimum spanning tree (MST) based approach for determining the underlying structure of the NFT network. MST networks are constructed to incorporate the minimum number of connections required to reach all nodes of a network and believed to represent the backbone structure of a network. We hypothesize that the abnormal NFT occurs in the set of anatomical brain regions interconnected with the temporal lobe.

Methods: AV1451 images were acquired for 41 cognitively normal (CN) and 38 mild cognitive impairment (MCI) individuals from the ADNI cohort and the SUVr maps were generated using cerebellum gray matter as the reference region. CN and MCI, TAU networks were then constructed using 745 nodes distributed across the brain cortex. Subsequently, the minimum spanning tree networks were generated and the average degree distribution was calculated for 55 cortical regions.

Results: In MCI individuals, the right inferior temporal gyrus and the left medial frontal orbital gyrus showed a considerably high average degree distribution compared to the other brain regions. They also showed an increase when comparing the same regions in CN individuals (Figure 1, 2, https://www.youtube.com/watch?v=AA9SbnGmCKw)

Discussion: Our results indicate that in MCI, the main hubs of the brain tau networks are asymmetric, predominantly temporal in the right and orbitofrontal on the left hemisphere. These asymmetric hubs, suggests independent propagation in both hemispheres. As a caveat, the current study includes a cross-sectional analysis and a longitudinal study is required to validate the findings.

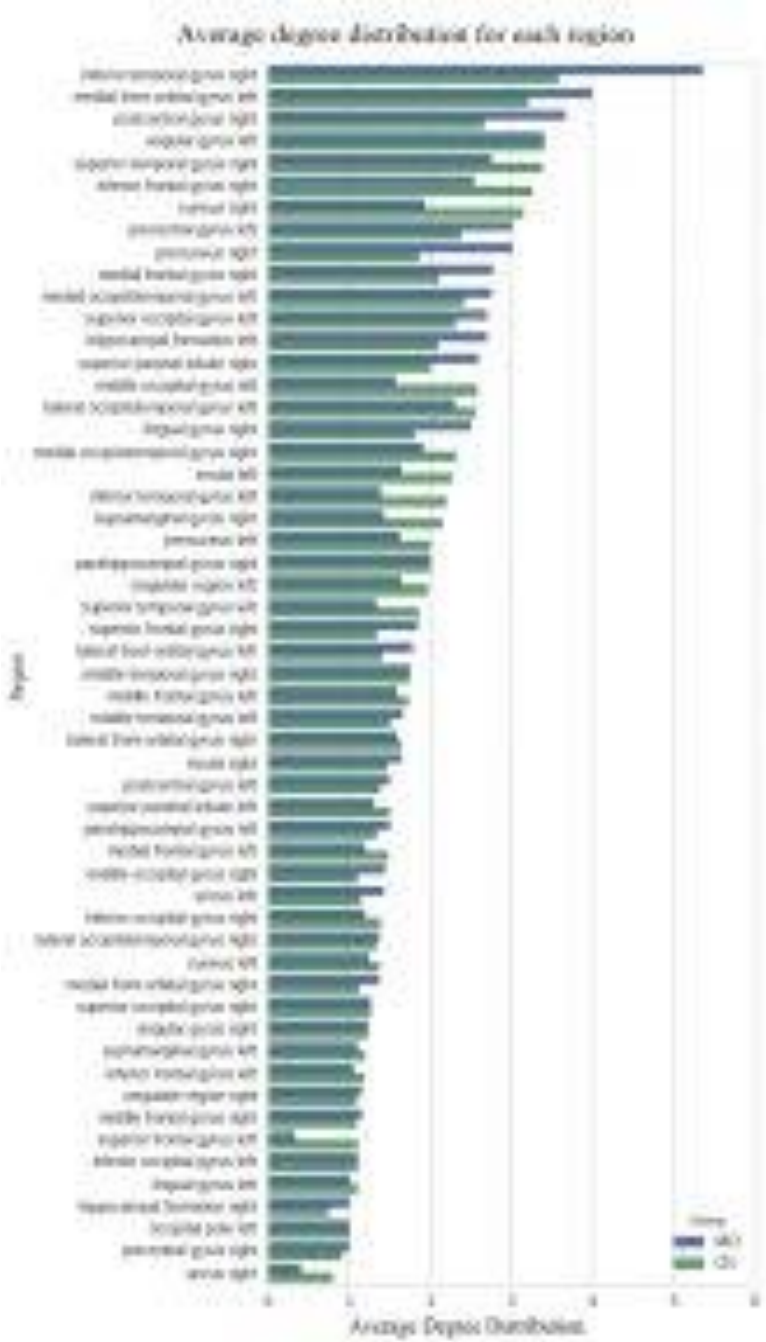

Figure 1. Average degree distribution for each cortical region.

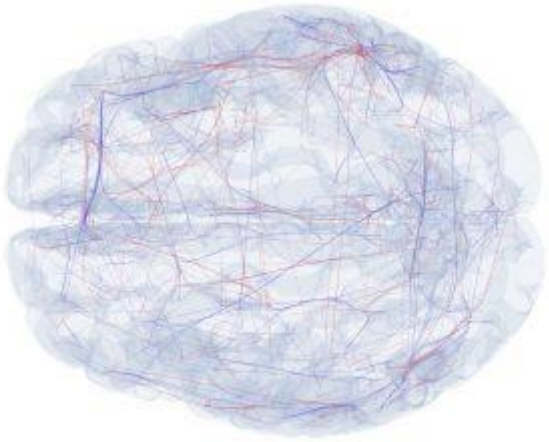

Figure 2. Blue - CN MST network; Red - MCI MST network

Keywords: tau, network, brain, minimum spanning tree

Regional tau correlates of instrumental activities of daily living and apathy in mild cognitive impairment and Alzheimer's disease dementia

Gad Marshall[1,2], Jennifer Gatchel[4], Nancy Donovan[4,5], Aaron Schultz[3], J. Alex Becker[3], Jasmeer Chhatwal[2], Bernard Hanseeuw[2], Kathryn Papp[1,2], Rebecca Amariglio[1,2], Dorene Rentz[1,2], Reisa Sperling[1,2], Keith Johnson[1,3]

[1]Department of Neurology, Center for Alzheimer Research and Treatment, Brigham and Women's Hospital, Harvard Medical School, Boston, MA, USA
[2]Department of Neurology, Massachusetts General Hospital, Harvard Medical School, Boston, MA, USA
[3]Department of Radiology, Massachusetts General Hospital, Harvard Medical School, Boston, MA, USA
[4]Department of Psychiatry, Massachusetts General Hospital, Harvard Medical School, Boston, MA, USA
[5]Department of Psychiatry, Brigham and Women's Hospital, Harvard Medical School, Boston, MA, USA

Background: Instrumental activities of daily living (IADL) impairment and apathy co-occur in mild cognitive impairment (MCI), worsen in mild Alzheimer's disease (AD) dementia, and are associated with regional atrophy, hypoperfusion, and hypometabolism in vivo, as well as greater tau burden in post-mortem studies.

Objective: To explore the association between IADL, apathy, and in vivo regional tau, visualized by T807 PET, in MCI and AD dementia.

Methods: Twenty-four subjects (13 MCI, 11 AD dementia) underwent assessments of IADL using the informant-based Functional Activities Questionnaire (FAQ) and apathy using the Apathy Evaluation Scale Clinician report (AES-C). Tau burden was assessed using T807 PET in 9 cortical and subcortical regions and cortical amyloid burden was assessed using Pittsburgh Compound B PET. Unadjusted correlations were performed to assess the relationship between FAQ, AES-C, and tau burden. Regions with associations of $p \leq 0.01$ were entered into regression models assessing the relationship between tau burden and FAQ or AES-C (dependent variables) in separate models, adjusting for age and sex (and depression in apathy models). Models were repeated with an interaction between tau and amyloid.

Results: Greater tau burden in dorsolateral prefrontal (partial r (pr)=0.56, p=0.005), supramarginal (pr=0.55, p=0.005), inferior temporal (pr=0.54, p=0.006), lateral temporal (pr=0.50, p=0.01), and entorhinal cortex (pr=0.50, p=0.01) was associated with greater IADL impairment. Greater dorsolateral prefrontal tau burden (pr=-0.52, p=0.02) was associated with greater apathy. The interaction between tau and amyloid was not significant, while independent associations with both tau and amyloid were retained (amyloid: IADL p=0.006; apathy p=0.08).

Conclusions: Our results suggest that IADL impairment in AD is associated with widespread tau burden, while apathy is associated with frontal tau. That said, both IADL impairment and apathy may be serving as a proxy of global cognition. Therefore, these findings need to be replicated in a larger sample adjusting for cognition to better inform specific treatments.
Keywords: Alzheimer's disease, apathy, instrumental activities of daily living, mild cognitive impairment, tau

Friday, January 13, 2017 - 10:15 am - 11:15 am

SESSION 8: Preclinical AD

SESSION 8 **Preclinical AD**	**CHAIRS:** **Reisa Sperling** ***Harvard Medical School*** **Elizabeth Mormino** ***Harvard Medical School***
Implementing and testing the new A/T/N classification in AIBL participants combining fluid (CSF) and different Aβ and tau imaging radiotracers	Victor Villemagne *University of Melbourne*
The Relationship of Elevated Medial Temporal Lobe and Diffuse Brain Tau-PET Signal in Clinically Normal Participants	Val Lowe *Mayo Clinic*
Prevalence and incidence of amyloid positivity in cognitively normal elderly individuals	Neelesh Nadkarni *University of Pittsburgh*
Longitudinal tau accumulation is associated with cognitive decline in normal elderly	Bernard Hanseeuw *Harvard Medical School*
Baseline amyloid burden predicts cognitive decline four years later in healthy adults: The value of a dose-response analysis	Michelle Farrell *University of Texas at Dallas*
Discussion	

Implementing and testing the new A/T/N classification in AIBL participants combining fluid (CSF) and different Aβ□ and tau imaging radiotracers

Samantha C Burnham[1,2], Christopher C Rowe[3], Pierrick Bourgeat[4], Vincent Doré[3,4], Greg Savage[5], Simon Laws[2], Qiao-Xin Li[6], Steven Collins[6], Ralph Martins[2], Olivier Salvado[4], Colin L Masters[6], Victor L Villemagne[3,6]

[1]*eHealth, CSIRO Health and Biosecurity, Perth, WA, Australia*
[2]*Edith Cowan University, Perth, WA, Australia*
[3]*Department of Molecular Imaging & Therapy, Austin Health, Melbourne, VIC, Australia*
[4]*eHealth, CSIRO Health and Biosecurity, Brisbane, QLD, Australia*
[5]*Department of Psychology, Macquarie University, Sydney, NSW, Australia*
[6]*The Florey Institute of Neuroscience and Mental Health, Melbourne, VIC, Australia*

Background: Extending their previous two-biomarker approach, Jack and colleagues (*Neurology, 2016*) have proposed a new classification scheme based on a triad of biomarkers: "A" (Aβ-amyloid), "T" (tau), and "N" (neuronal injury). We implemented and tested the A/T/N classification in AIBL participants.

Methods: Two-hundred and ninety AIBL participants (218 HC, 45 MCI, and 27 AD) underwent Aβ imaging (either ^{11}C-PiB, ^{18}F-florbetapir, ^{18}F-flutemetamol, or ^{18}F-NAV4694) and 3D MRI, where 146 of them had "T" status determined by CSF p-tau and 144 by tau imaging (either ^{18}F-AV1451, ^{18}F-THK5351 or ^{18}F-THK5317). A binary high(+)/low(-) classification was adopted for each marker. The A/T/N distribution in each clinical group and the relationship with cognition were explored.

Results: Application of the A/T/N classification showed that 51% of HC, 20% of MCI and 15% of AD had no marker abnormality, while 1% of HC, 22% of MC and 56% of AD presented with all three abnormal markers.

In HC, 12% were A+ and 12% N+ (*T- SNAP*), with 8% being T+. In MCI, 11% were A+T-N-, while 4% and 2% were A-T+N- and A-T-N+, respectively. When considering two-biomarker abnormality, only 1% of HC were A-T+N+ (*T+ SNAP*), while 20% of MCI were A+T-N+, 15% A+T+N-, and 4% A-T+N+. In AD, 19% were A+T-N+ and 7% A+T+N-.

Increasing biomarker abnormality was associated with increasing cognitive impairment. When only one biomarker was abnormal, A+T-N- HC and MCI had worse performance than A-T+N- and A-T-N+. Interestingly, when two biomarkers were abnormal, A+T-N+ had worse cognitive performance than A+T+N- and A-T+N+, as well as significantly faster cognitive decline than A-T-N-.

Conclusions: The new proposed A/T/N categories allows a more comprehensive classification of the aging population. That said, translation of the new A/T/N classification into research and clinical practice will require larger series and longer follow-up, to fully assess its clinical and prognostic performance.
Keywords: tau imaging, Aβ-imaging, CSF, cognitive performance

The relationship of elevated medial temporal lobe and diffuse brain Tau-PET signal in clinically normal participants

Val Lowe[1], Emily Lundt[1], Heather Wiste[1], Ping Fang[1], Matthew Senjem[1], Bradley Boeve[1], Keith Josephs[1], Mukesh Pandey[1], Melissa Murray[2], Kejal Kantarci[1], David Jones[1], Christopher Schwarz[1], David Knopman[1], Ronald Petersen[1], Clifford Jack[1]

[1]Mayo Clinic, Rochester, MN, USA
[2]Mayo Clinic, Jacksonville, FL, USA

Background: Medial temporal lobe (MTL) uptake on tau-PET is seen in AD dementia but also in the aging population. Some AD dementia patients have much less MTL tau-PET signal compared to other isocortical signal. The relationship of these findings to the development of AD dementia needs to be better understood.

Methods: Tau-PET with AV-1451 was performed on 439 CN participants ages 50-94. For each cortical region, we defined abnormal tau-PET as cortical-to-cerebellar crus gray matter ratio (SUVr) greater than the 95th percentile among 71 CN participants ages 30-49. We included enthorinal cortex, parahippocampal gyrus, and hippocampus as MTL regions. All other cortical regions were considered extra-MTL regions. Off-target regions, such as pallidum, were excluded. The number of CNs with and without abnormal MTL regions and those with or without extra-MTL abnormities were determined. We characterized the age, PiB and APOE status of the groups.

Results: Of CN participants, 37% (163/439) had MTL abnormalities. Of those with MTL findings, 95% (155/163) had extra-MTL abnormality with most having more than one (Figure 1). Of the 276 without an MTL abnormality, 29% (81/276) had extra-MTL abnormalities (Figure 2). Participants having MTL abnormalities tended to be older ($p<0.001$) and have elevated amyloid ($p<0.001$). Among those having MTL abnormalities, no age or PiB differences were seen between the groups with or without extra-MTL abnormalities. There were no significant differences in the percentage of APOE e4 carriers.

Conclusions: MTL tau-PET signal is often associated with abnormal extra-MTL tau-PET signal in CN participants and likely represents neurofibrillary tangle development in participants likely to develop AD dementia. Tau-PET signal exclusively outside of the MTL is seen in 29% of CN participants and could be the initial finding in a unique subset of participants in the AD dementia pathway. These findings need to be evaluated with longitudinal data.

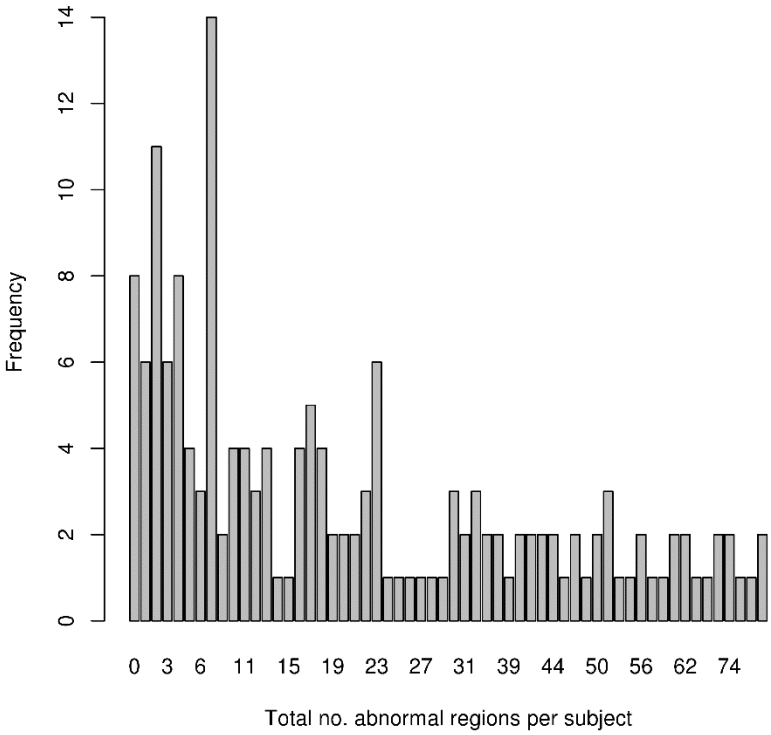

Figure 1. Numeric distribution of regional abnormalities outside medial temporal lobe (MTL) among those having any MTL abnormality

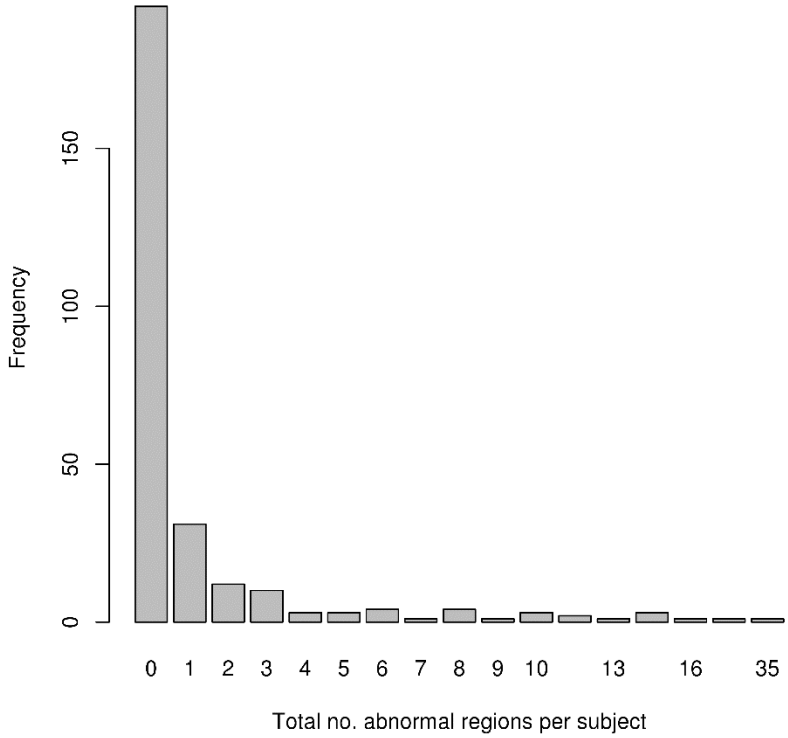

Figure 2. Numeric distribution of regional abnormalities outside medial temporal lobe (MTL) among those having no MTL abnormality

Keywords: tau-PET, medial temporal lobe (MTL), AD

Prevalence and incidence of amyloid positivity in cognitively normal elderly individuals

Neelesh Nadkarni[1,5], Dana Tudorascu[2,4], Beth Snitz[3,5], Edythe Halligan[3], Annie Cohen[4,5], Howard Aizenstein[3,4], Oscar Lopez[3,4,5], William Klunk[4,5]

[1]*Division of Geriatric Medicine, Department of Medicine, University of Pittsburgh, Pittburgh, PA, USA*
[2]*Division of Internal Medicine, University of Pittsburgh, Pittsburgh, PA, USA*
[3]*Department of Neurology, University of Pittsburgh, Pittsburgh, PA, USA*
[4]*Department of Psychiatry, University of Pittsburgh, Pittsburgh, PA, USA*
[5]*Alzheimer's Disease Research Center,, Pittsburgh, PA, USA*

Aims: We estimated the prevalence of amyloid positivity at baseline, and incidence of amyloid positivity in participants without an amyloid positive baseline scan in the Amyloid Pathology and Cognition in Normal Elderly study cohort.

Methods: Community-dwelling elderly individuals (n=98), screened for psychiatric and neurologic conditions, were deemed CN based on their performance on standardized tests of cognition. Participants underwent Pittsburgh-B (PiB)-PET scan at baseline and a subset had repeat scans over subsequent 1-10 years (average: 6). Amyloid positivity was defined as regional PiB(+) (any one ROI) and global PiB(+) (average of 6 ROI) using established PiB-SUVR cutoffs. Person-years were calculated for each PiB(-) individual as years to conversion to a PiB(+) scan (amyloid positive converters) or total number of years of follow-up of persistently PiB(-) scans (non-converters). Incidence rates were derived by dividing the observed incidence by sum of person years.

Results: In this sample of CN elderly individuals, mean (SD) age was 73.6 years (5.7 years), 64% were female, 21.25% were APOE-ε4 carriers and 83% white. There were no significant differences between the global PiB(+) and PiB(-) group on demographic measures and MMSE scores. Regional PiB(+) participants were older (p=0.019), but were otherwise similar to PiB(-) participants. Regional amyloid positivity was observed in 25 (25.51%) and global amyloid positivity was observed in 19 (19.4%). Of the 75 PiB(-) participants at baseline, 19 (25.33%) progressed to regional PiB(+), and 14 (18.67%) progressed to global PiB(+). Incidence rate of regional and global amyloid positivity was 19/239 (8 cases per 100 person- years) and 14/258 (5.4 cases per 100 person-years) respectively.

Conclusion: Estimates of prevalence and incidence of amyloid positivity in CN elderly individuals can inform the design of future secondary prevention trials targeting MCI and AD.
Keywords: amyloid positivity, prevalence, incidence rate

Longitudinal tau accumulation is associated with cognitive decline in normal elderly

Bernard Hanseeuw, Alex Becker, Aaron Schultz, Jorge Sepulcre, Beth Mormino, Kate Papp, Heidi Jacobs, Danielle Cosio, Jasmeer Chhatwal, Trey Hedden, Reisa Sperling, Keith Johnson

Massachusetts General Hospital, Boston, MA, USA

Background: Early PET data have shown associations between PHF tau and cognitive performance, including in clinically normal (CN) older adults. Recently acquired serial tau-PET data allowed us to assess the association between longitudinal tau imaging and change in cognition.

Methods: Forty-three CN (age=65-90; MMSE≥26) had Flortaucipir-PET (FTP, cortical white matter reference), cognitive assessment (Preclinical Alzheimer Cognitive Composite (PACC) within a 3-months delay , and were subsequently followed during 24 months . Linear regressions investigated the association between tau and cognitive performance at baseline. Linear mixed models with random intercepts and slopes investigated the association between cognitive decline, baseline tau, and annual change in tau. Analyses were conducted in bilateral inferior temporal gyri, restricted to the voxels with the highest signal (SUVr>1.06=97.5th percentile of all cortical voxels). Analyses were adjusted for age, sex, and education.

Results: Elevated baseline tau signal was associated with low baseline cognition (Fig.1; Estimate=-5.8±2.90, p=0.050). High baseline tau predicted cognitive decline in the following two years (Fig.2; Estimate=-6.2±1.74, p=0.001). Change in tau also predicted cognitive decline (Fig.3; Estimate=-24.3±6.23, p=0.00015). A tau increase of 0.01 SUVr was thus associated with a cognitive decline of 0.243 z-scores on the PACC. Cognitive decline was more strongly related to change in tau (p=0.022) than to baseline tau (p=0.100) when both predictors were simultaneously modeled. Change in tau was significantly associated with change in each individual PACC component (Logical Memory: Estimate=-17.7±9.1, p=0.037; Free and Cued Selective Reminding Test (/96): Estimate=-27.2±9.1, p=0.003; MMSE: Estimate=-46.6±12.5, p=0.0003; Digit-Symbol: Estimate=-11.6±4.2, p=0.006).

Conclusion: Cognitive decline in CN is associated with temporal tau accumulation, beyond the association with baseline tau. Serial tau-PET imaging is a promising marker to predict cognitive deterioration and track disease progression. Larger samples are required to further explore the longitudinal associations between tauopathy and cognition.

Fig.1 Baseline tau predicts baseline cognition

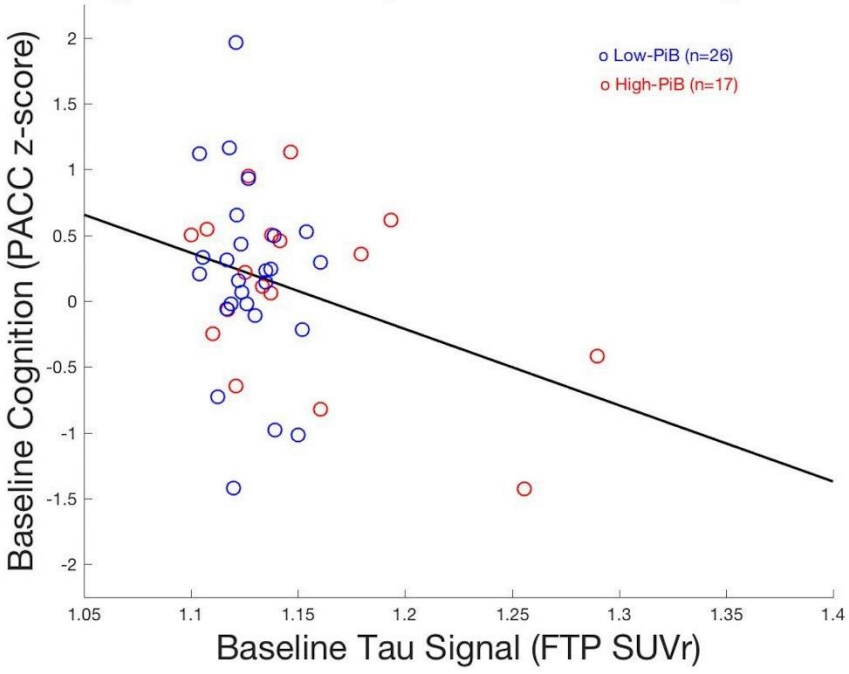

Fig.2: Baseline tau predicts change in cognition

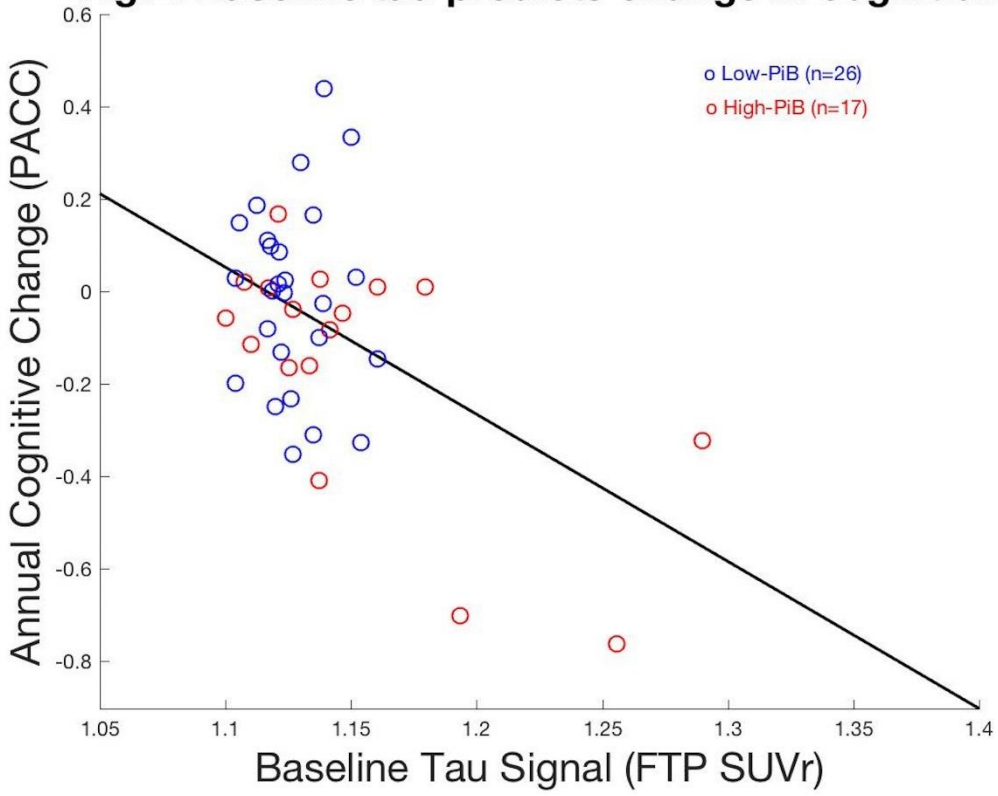

Fig.3: Change in tau predicts change in cognition

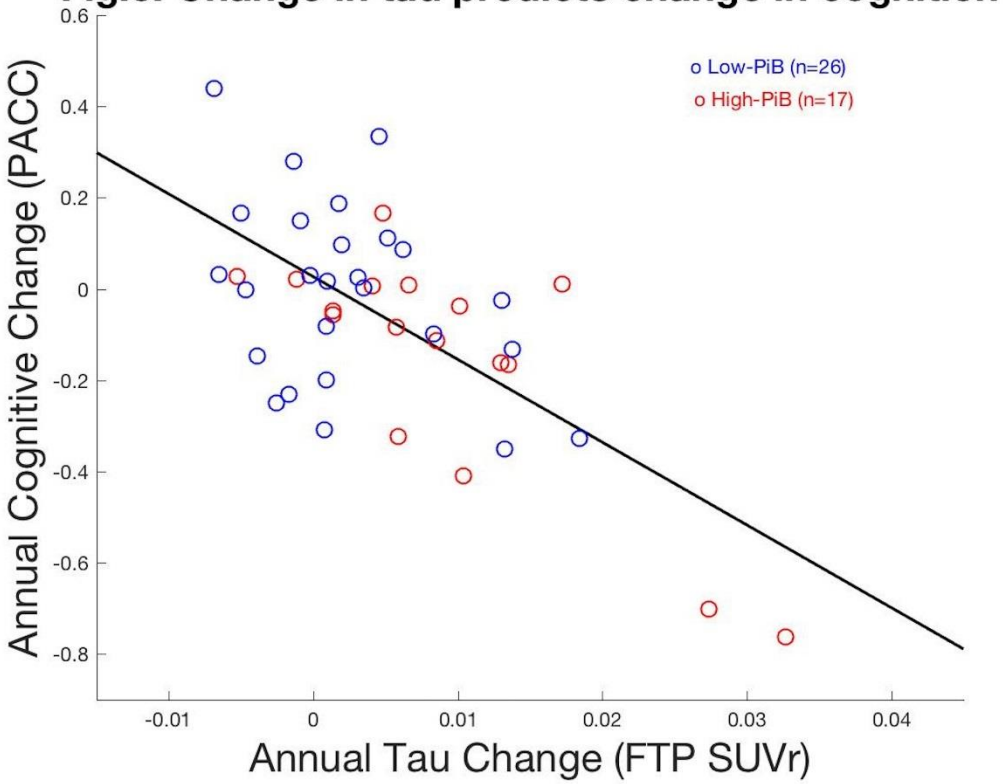

Keywords: Tau accumulation; Longitudinal PET imaging, Preclinical Alzheimer Cognitive Composite; Clinically Normal;

Baseline amyloid burden predicts cognitive decline four years later in healthy adults: the value of a dose-response analysis

Michelle E. Farrell[1], Kristen M. Kennedy[1], Karen M. Rodrigue[1], Gagan S. Wig[1], Gérard N. Bischof[2], Xi Chen[1], Sara B. Festini[1], Denise C. Park[1]

[1]*University of Texas at Dallas, Dallas, TX, USA*
[2]*University Hospital Cologne, Cologne, Germany*

Background: Longitudinal studies in cognitively-normal adults have largely treated amyloid as a categorical variable, reporting greater cognitive decline for amyloid-positive adults compared to amyloid-negative adults. We examined whether a continuous, dose-response relationship between amyloid burden and cognitive decline was present in middle-aged and older adults, with increasing baseline amyloid burden predicting increasing rates of cognitive decline.

Methods: Participants (*n*=174, age=40-89) completed amyloid imaging (f-18-Florbetapir) at baseline and cognitive assessments at baseline and a 4-year follow-up. Linear mixed models assessed SUVR, Time and SUVR x Time effects on episodic memory, reasoning, processing speed, vocabulary and MMSE performance. Age, sex, education, APOE, and the random effect of intercept were included as covariates.

Results: The primary analysis yielded significant SUVR x Time interactions in episodic memory (*p*=.001), processing speed (*p*=.04), vocabulary (*p*=.004), and MMSE (*p*=.028), but not reasoning. Figures 1A-1D show that increasing SUVR projects a steeper trajectory of decline. A sub-group analysis of older adults (ages 60-89) yielded similar effects. In middle-aged adults (ages 40-59), increasing SUVR predicted vocabulary decline (*p*=.021). When amyloid was treated as a categorical variable (positive/negative), significantly greater decline was observed for amyloid positive than negative adults in episodic memory (*p*=.010) and vocabulary (*p*=.011), but processing speed was mitigated to a trend (*p*=.082) and MMSE was non-significant (*p*=0.364).

Conclusions: The results indicate that there is a significant dose-response relationship between baseline amyloid burden and cognitive decline over 4 years in episodic memory, processing speed, vocabulary and MMSE performance. Furthermore, continuous SUVR provided a more sensitive predictor of the trajectories of cognitive decline than amyloid positivity. The magnitude of SUVR potentially provides useful information about expected preclinical disease trajectory.

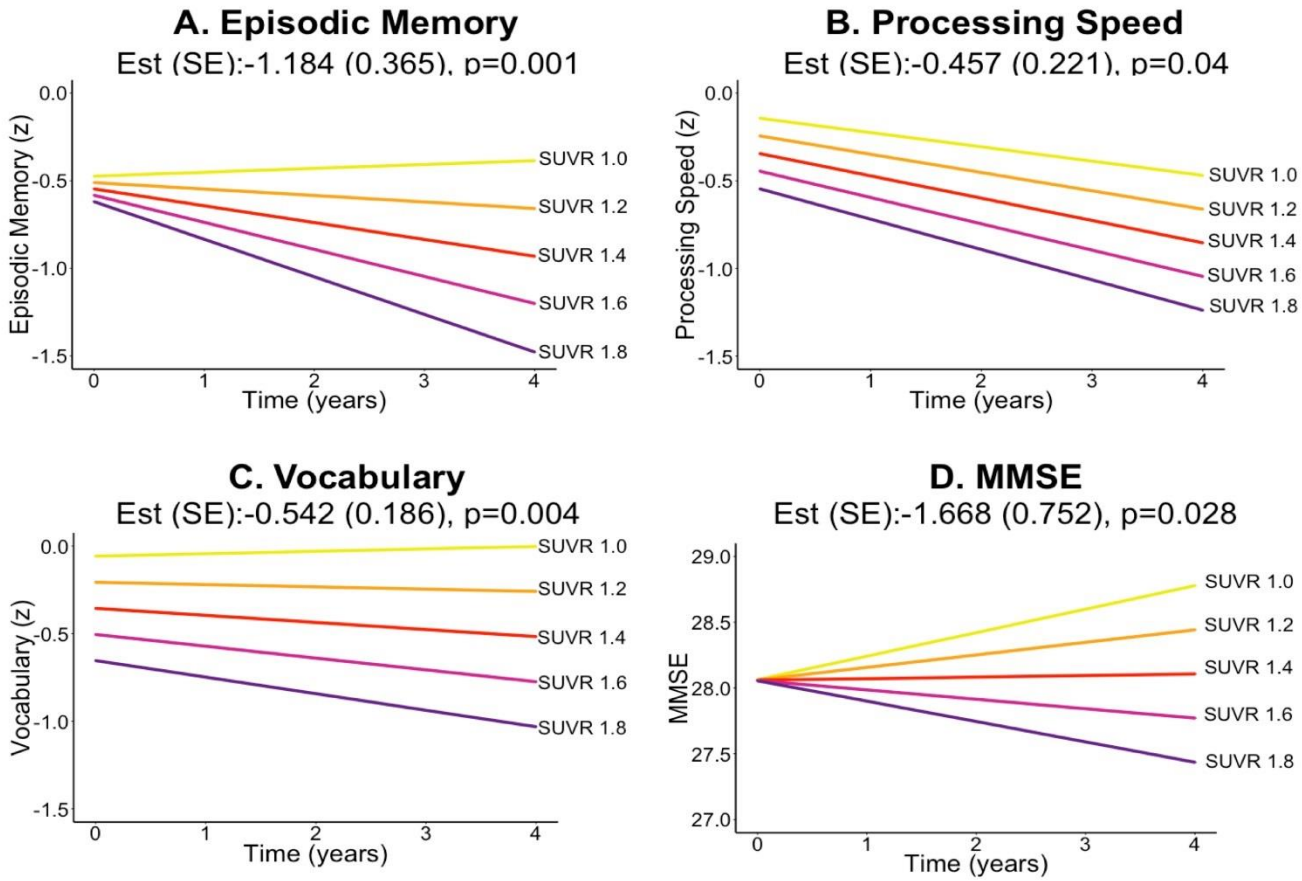

Figure 1. Model Projections of the Impact of Increasing Baseline Amyloid Burden on Cognitive Change Trajectories over Four Years. To evaluate the significant SUVR x Time interactions, estimated means were computed using simple slope analysis for each time point based on increasing values of SUVR. Across (a) episodic memory, (b) processing speed, (c) vocabulary, and (d) MMSE, the model projected that high levels of SUVR predicted cognitive decline, while negative or low levels of SUVR predicted modest or no cognitive decline (or in the case of MMSE, a practice effect).

Keywords: cognition, longitudinal, aging, memory, preclinical

Friday, January 13, 2017 - 12:00 pm - 12:45 pm

Keynote Lecture

Alzheimer's disease clinical trials: 2017 update—Staying the course? Correcting the course? Shifting the paradigms used in trials?

Howard Feldman

University of California, San Diego, La Jolla, CA

The National Alzheimer Project Act (2011-present) set out an ambitious roadmap of therapeutic development that would be needed to reach a cure by 2025, with an estimated 30 new therapeutic drugs in early testing and with a projection of the number of trials with known targets, novel targets and repurposed medicines. However, there have not been any successful late phase clinical AD trials resulting in regulatory approval since 2003. There have been over 200 trials reach phase 2 or beyond, however, all those advancing to phase 3 have had a null or inconclusive result. There is voiced concern that that the opportunity for new therapies by 2025 is getting smaller, however, there are course corrections that can be made to change the outcome.

This presentation will provide some directions that could improve the likelihood of more successful development. The conceptual considerations include the need and approach to more rigorously pursuing proof of concept, diversifying target selection and combinatorial approaches, redefining the disease as a syndrome with multiple etiologies, proteinopathies and contributing factors, and deploying innovative trial designs which allow for more rapid screening seeking larger effect sizes. Central to each of these considerations, is the need for accelerated pace of discovery and research into amyloid and tau PET, novel MRI measures, dynamic CSF biomarkers to address synaptic and cellular function, and blood measures to more rapidly screen populations at risk.

Friday, January 13, 2017 - 02:15 pm - 03:15 pm

SESSION 9: Amyloid, Tau, and Neurodegeneration

SESSION 9 **Amyloid, Tau, and Neurodegeneration**	**CHAIRS:** **Clifford Jack** ***Mayo Clinic*** **Tammie Benzinger** ***Washington University at St Louis***
Neocortical Tau and hippocampus volume reflect distinct processes in preclinical Alzheimer's disease	Elizabeth Mormino *Massachusetts General Hospital*
Do neurodegeneration or amyloid pathology contribute to the relationship between AV-1451 and cognitive symptoms in Alzheimer's disease?	Alexandre Bejanin *University of California, San Francisco*
Comparing the contributions of tau and neurodegenerative biomarkers to cognitive decline	Susan Landau *University of California, Berkeley*
Differential genotypic variance in PET and CSF measures of amyloid burden: Findings from the DIAN Study	Jasmeer Chhatwal *Massachusetts General Hospital*
Relationships between AV1451-PET and CSF biomarkers in a heterogeneous clinical sample	Renaud La Joie, *University of California, San Francisco*
Discussion	

Neocortical Tau and hippocampus volume reflect distinct processes in preclinical Alzheimer's disease

Elizabeth Mormino[1], Aaron Schultz[1], Kathryn Papp[1], Molly LaPoint[1], Bernard Hanseeuw[1], Trey Hedden[1], Dorene Rentz[1], Reisa Sperling[1], Keith Johnson[1]

[1]*Massachusetts General Hospital, Boston, CA, USA*

Objective: To explore neocortical Tau and hippocampus volume as a function of age and Aβ status, as well as the contributions of these biomarkers to memory among older clinically normal (CN) participants.

Methods: We examined 143 CN participants from the Harvard Aging Brain Study that underwent Amyloid PET with PIB, Tau PET with AV1451, structural MRI and memory performance within 1 year (mean age=75.5±6.9, age range=55-90). Effects related to age and Aβ status were compared for inferior temporal Tau and hippocampus volume. Hierarchical regression was used to assess the unique contributions of inferior temporal Tau, hippocampus volume, and age to memory performance for Aβ- and Aβ+ groups separately.

Results: Age was related to hippocampus volume, regardless of Aβ status (within Aβ-: r= -0.63; within Aβ+: r= -0.52) (**Figure 1A**). Aβ+ showed significantly higher inferior temporal Tau than Aβ- (r= 0.42); age was related to inferior temporal Tau in Aβ- (r= 0.35) but not within Aβ+ (r= 0.04)(**Figure 1B**). Although inferior temporal Tau was related to hippocampus volume among Aβ+ (r= -0.29), the strength of this relationship was smaller than the association between age and hippocampus volume in Aβ+ (r= -0.52). Among Aβ-, 5.0% of the total variance in memory was explained by age, inferior temporal Tau, and hippocampus volume, with age accounting for the most unique variance (ΔR^2=1.84%). Among Aβ+, 31% of the total variance in memory was explained by age, inferior temporal Tau, and hippocampus volume, with inferior temporal Tau accounting for the most unique variance (ΔR^2=20%)(**Figure 2**).

Conclusions: These results suggest that hippocampus volume largely reflects non-AD age-related etiologies whereas neocortical Tau is a more specific marker of early AD processes among older CN. Further simultaneous evaluation of Tau and hippocampus volume among CN is essential to clarify the interpretation of these markers in preclinical staging criteria.

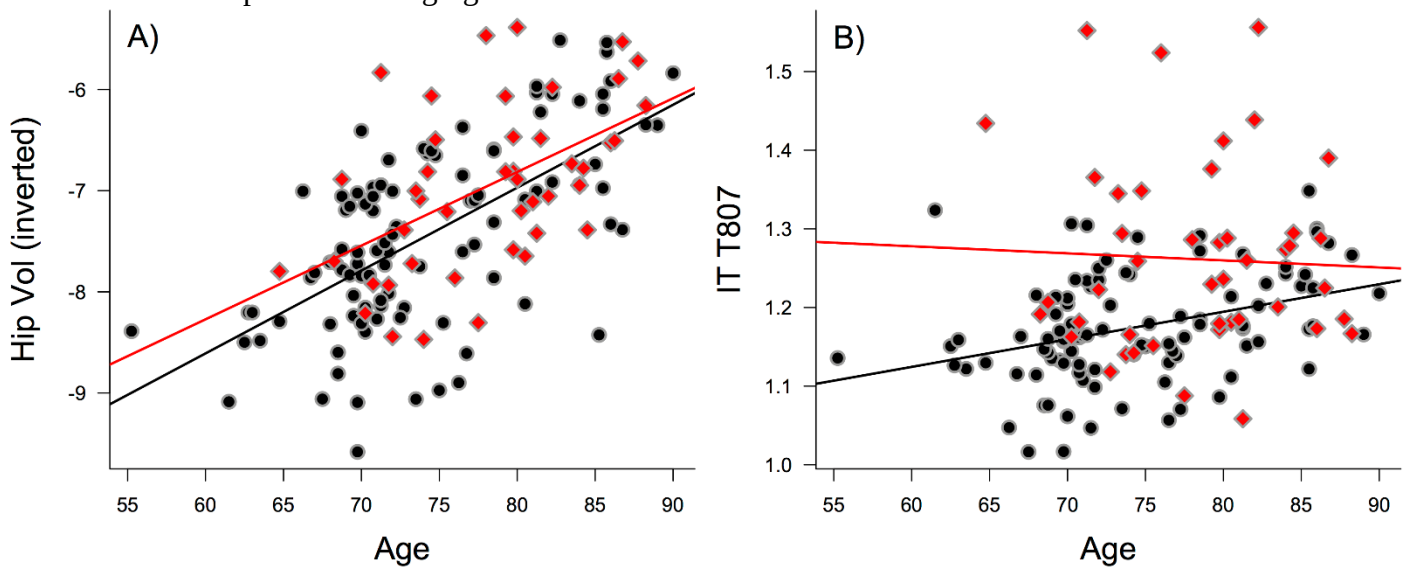

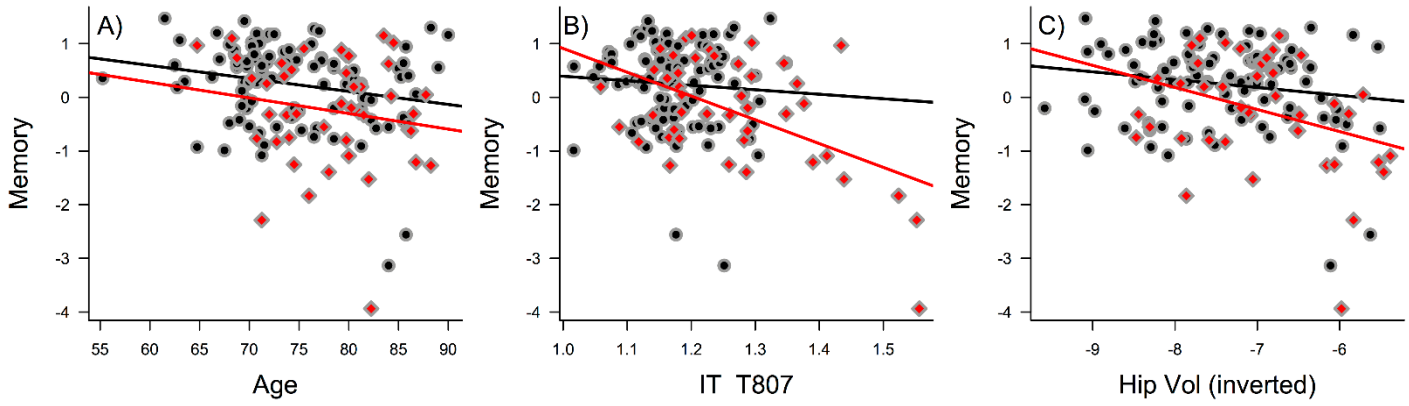

Keywords: AV1451, PIB, hippocampus volume, memory, preclinical AD

Do neurodegeneration or amyloid pathology contribute to the relationship between AV-1451 and cognitive symptoms in Alzheimer's disease?

Alexandre Bejanin[1], Daniel R. Schonhaut[1], Renaud La Joie[1], Joel H. Kramer[1], Suzanne L. Baker[2], James P. O'Neil[2], Bruce L. Miller[1], William J. Jagust[2,3], Gil D. Rabinovici[1,3]

[1]*Memory and Aging Center, University of California San Francisco, San Francisco, CA, USA*
[2]*Life Sciences Division, Lawrence Berkeley National Laboratory, Berkeley, CA, USA*
[3]*Helen Wills Neuroscience Institute, University of California Berkeley, Berkeley, CA, USA*

Objective: To test the relationship between cognition and tau pathology in Alzheimer's disease (AD) and to assess whether neurodegeneration or amyloid pathology mediate this relationship.

Methods: Forty patients with heterogeneous AD phenotypes (5 with Aβ-PET+ mild cognitive impairment and 35 with Aβ-PET+ probable AD dementia, including 12 posterior cortical atrophy and 8 logopenic-variant primary progressive aphasia) underwent 3T MRI, ^{11}C-PiB-PET and ^{18}F-AV1451-PET, and episodic and semantic memory, language, executive and visuo-spatial functions assessment. Raw cognitive scores were converted to W-scores (age-adjusted Z-scores) and averaged to compute composite scores for each cognitive domain. Independent regressions were performed between ^{18}F-AV-1451 SUVR and each domain and Biological Parametric Mapping (BPM) was used to further control for local grey matter volumes, PIB-DVR, or both. Partial correlations and mediation analyses were performed in the regions showing an association between cognition and both ^{18}F-AV-1451 SUVR and grey matter volume/PIB-DVR. The average direct effect (ADE) and average causal mediation effect (ACME), reflecting direct and indirect effects ^{18}F-AV-1451 on cognition, were computed using the mediation R package (non-parametric bootstrapping, 5000 simulations).

Results: Decreased cognitive performance in each domain was related to increased ^{18}F-AV-1451 SUVR in specific brain regions conforming to established brain-behavior relationships (Figure 1).

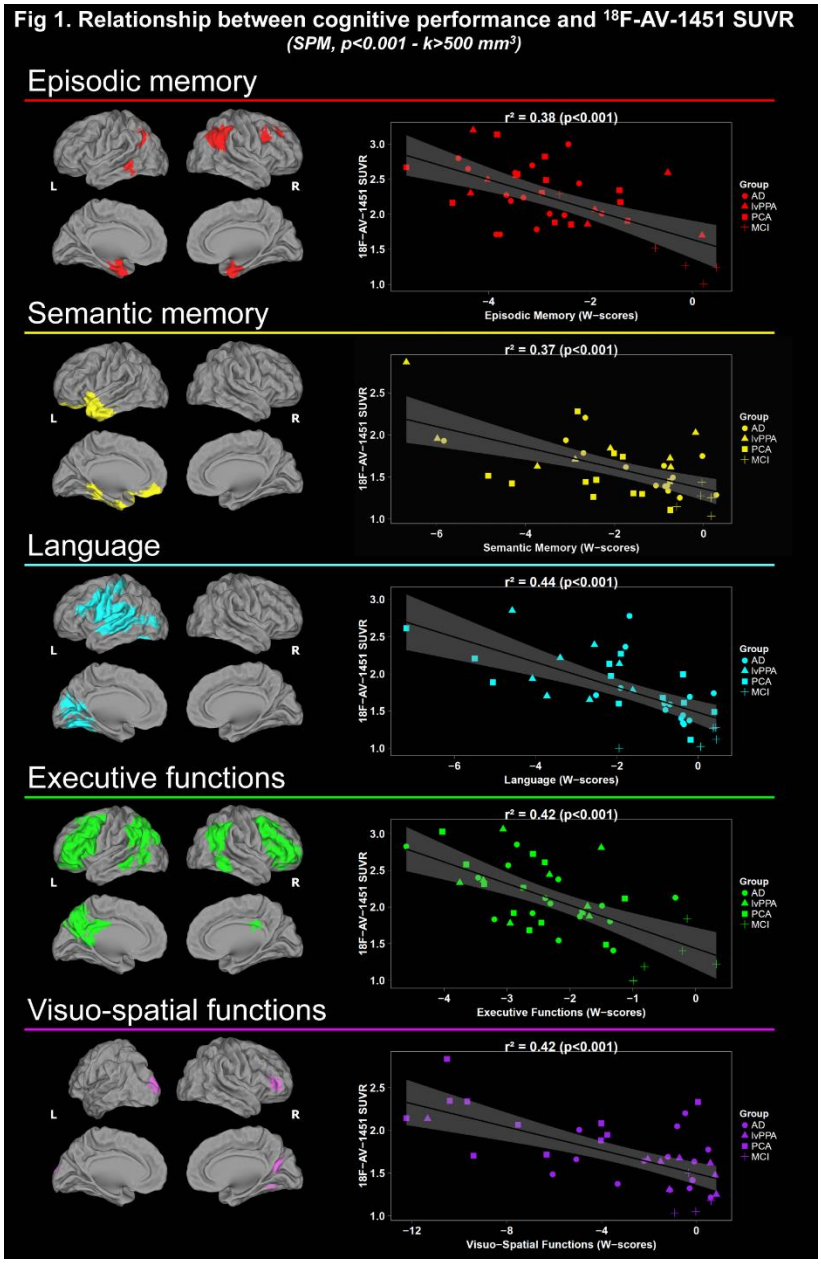

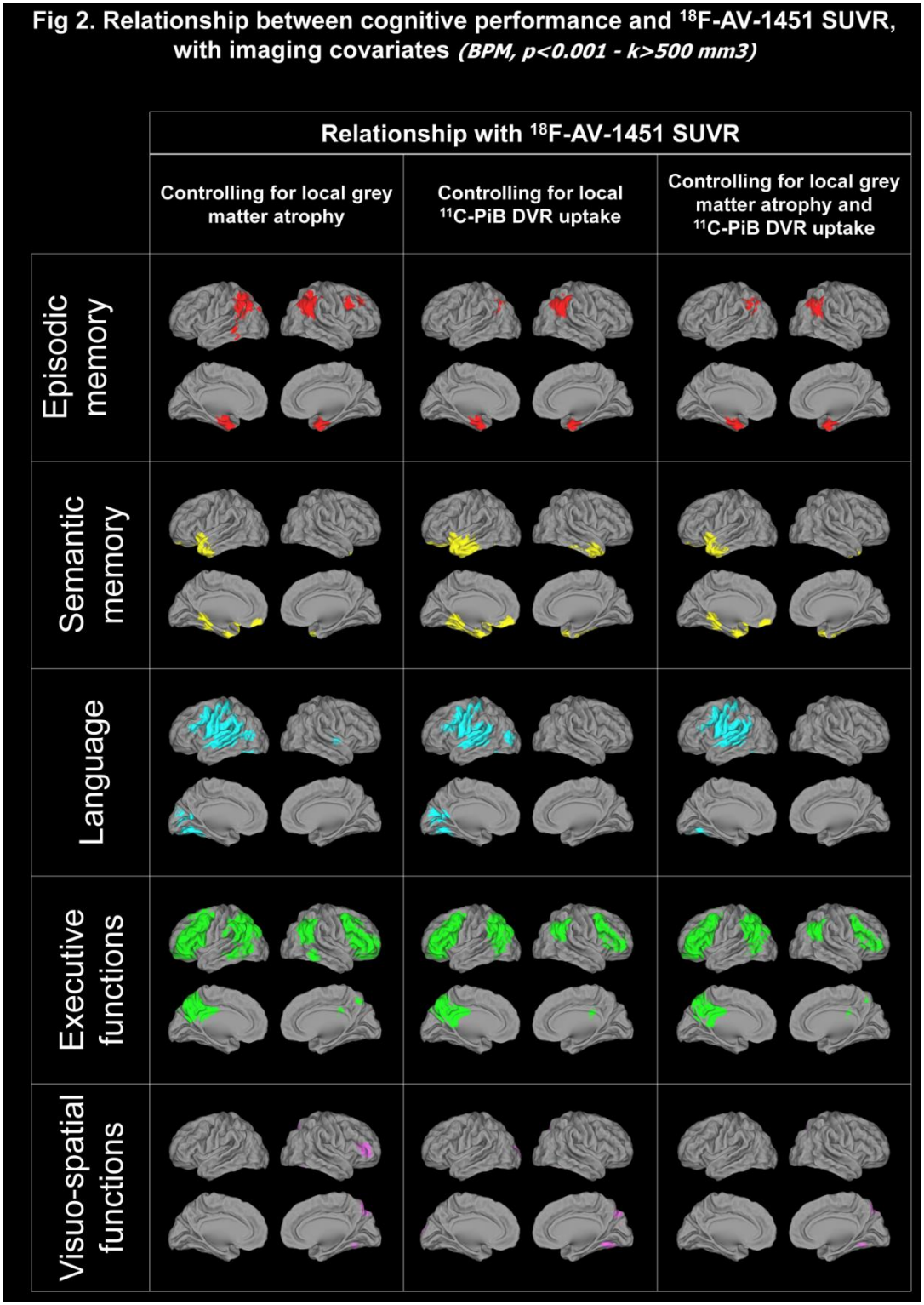

This pattern of regional associations remained essentially unchanged when grey matter volume or ^{11}C-PiB-DVR maps were added as covariates (Figure 2).

Mediation analyses revealed both direct effects (ADE) of ^{18}F-AV-1451 on cognitive performances and mediating effects (ACME) of grey matter atrophy on these relationships (Figure 3).

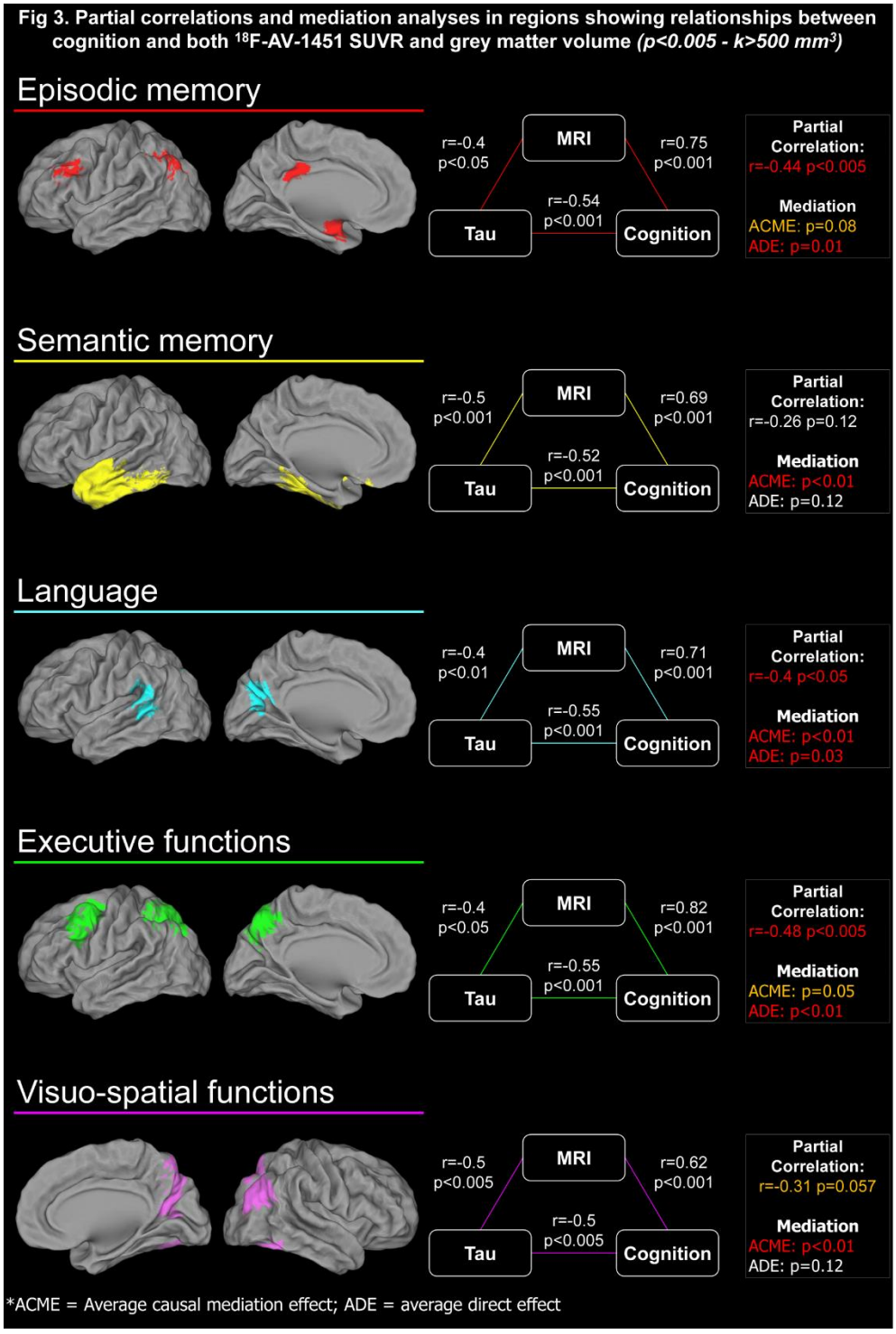

Discussion: Tau shows distinct regional correlations with performance in specific cognitive domains. The relationships between tau and cognition in AD are not related to amyloid burden, but are in part mediated by grey matter volumes. These results suggest that tau pathology may lead to cognitive deficits through a variety of mechanisms, including, but not limited, to neuronal loss.

Keywords: tau, cognition, atrophy, amyloid, mediation analyses

Comparing the contributions of tau and neurodegenerative biomarkers to cognitive decline

Susan Landau, Andy Horng, William Jagust

[1]*Helen Wills Neuroscience Department, University of California, Berkeley, CA, USA*

Objectives: Tau deposition and neurodegeneration are hypothesized downstream effects of amyloid deposition in Alzheimer's disease but their relative contributions to cognitive decline are poorly understood. Here, we compared the relationship of these measurements to retrospective longitudinal cognitive decline across individuals at different levels of disease severity, and stratified by amyloid status.

Methods: Participants included 74 ADNI subjects (38 normal, 15 EMCI, 16 MCI, 5 AD) with AV1451-PET who had concurrent florbetpair-PET scans, as well as MRIs and FDG-PET obtained prior to AV1451. We used a Braak staging method to assess partial volume corrected AV1451 retention relative to cerebellar cortex at different levels of progression: medial temporal (Braak 1/2), lateral temporal (Braak 3/4), neocortical (Braak 5/6) regions. We also measured hippocampal volume (HV) adjusted for total intracranial volume, hypometabolism (FDG) within a set of AD-specific regions, and retrospective cognitive decline using 3.3 +/- 1.1 yrs of longitudinal ADAS-cog measurements. Regression models were adjusted for age, sex, education, and ApoE4 status.

Results: In florbetapir- subjects (n=42), no biomarker (AV1451, FDG, HV) was predictive of ADAS-cog decline. In florbetapir+ subjects (n=32; 13 normal, 4 EMCI, 10 LMCI, 5 AD), however, AV1451, FDG, and HV were all predictive of ADAS-cog decline in univariate models. Furthermore, AV1451 retention in all Braak stages was associated with ADAS-cog decline, but medial temporal AV1451 was most closely linked to decline. In a multivariate model with FDG, HV, and medial temporal AV1451, only AV1451 remained significantly associated with ADAS-cog decline (p=0.001; florbetapir status X AV1451 interaction, p = 0.01; see Figure).

Conclusion: In amyloid+ individuals at different stages of disease, neurodegeneration and medial temporal tau deposition in particular are related to ongoing cognitive decline. These findings support a model in which amyloid and tau have a synergistic influence on cognitive decline.

In florbetapir+ but not florbetapir- individuals, greater medial temporal AV1451 is associated with greater ADAS-cog decline.

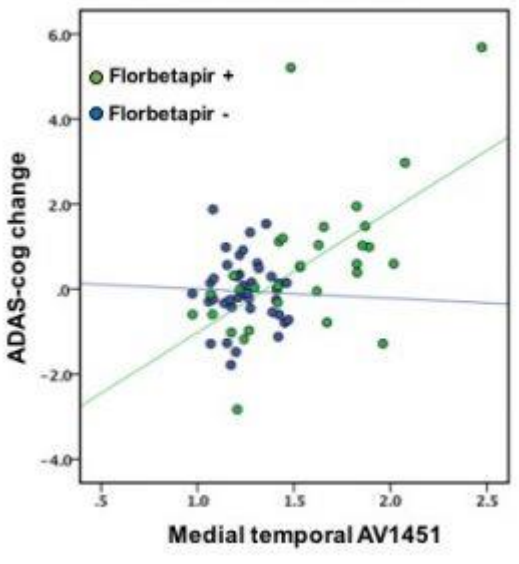

Keywords: AV1451, cognitive decline, hippocampal volume, hypometabolism

Differential genotypic variance in PET and CSF measures of amyloid burden: findings from the DIAN Study

Jasmeer Chhatwal[1], Eric McDade[2], Peter Wang[2], Tammie Benzinger[2], Anne Fagan[2], Aaron Schultz[1], Bernard Hanseeuw[1], Colin Masters[3], Adrian Danek[5], Peter Schofield[4], Martin Farlow[7], John Morris[2], Randall Bateman[1], Keith Johnson[1], Reisa Sperling

[1]*Massachusetts General Hospital, Brigham and Women's Hospital, Harvard Medical School, Boston, MA, USA*
[2]*Washington University School of Medicine, St. Louis, MA, USA*
[3]*The Florey Institute, The University of Melbourne, Parkville, Australia*
[4]*Neuroscience Research Australia, Sydney, Australia*
[5]*German Center for Neurodegenerative Disease, Tuebingen, Germany*
[6]*Mount Sinai School of Medicine, New York, NY, USA*
[7]*Indiana University School of Medicine, Indianapolis, IN, USA*

Rationale: Pathogenic mutations in Presenilin (PSEN) 1, 2 or amyloid precursor protein (APP) lead to autosomal dominant Alzheimer's disease (ADAD) by altering beta-amyloid production and deposition. Though these mutations are all highly penetrant, *in vitro* studies suggest that there is substantial molecular diversity in the amyloid species produced by each mutation. Using data from the Dominantly Inherited Alzheimer Network (DIAN), we examine inter-genotypic variance in the temporal pattern of amyloid burden assessed using both Pittsburgh Compound B (PiB) PET and cerebrospinal fluid (CSF) Aβ42.

Methods: CSF Aβ42 and PiB PET were assessed in 174 individuals (117 mutation carriers, 67 non-carriers). Thirty-seven unique PSEN1 genotypes were categorized into 7 groups based on affected topologic domain. In addition to these PSEN1 groupings, three well-represented non-PSEN1 genotypes were included in the analysis (2 APP, 1 PSEN2). We used linear mixed-effect regression models to examine interactions between estimated years to symptom onset (EYO) and genotype.

Results: Significant genotype-by-EYO interactions were observed in mean cortical PiB binding, and in a composite posterior cingulate and precuneus ROI. Intriguingly, significant inter-genotypic variance was not observed in CSF Aβ42 in the same sample. CDR sum of boxes also did not show significant genotype-by-EYO interactions, suggesting grossly similar clinical progression across genotypes.

Conclusion: These results suggest that the nature of particular ADAD mutations can lead to differential temporal patterns of amyloid burden as measured by PiB PET. The same effect was not observed in CSF Aβ42, suggesting greater inter-genotypic variance in insoluble fibrillar amyloid as compared to amyloid species measured in CSF. These results are relevant for the use of PiB PET and CSF Aβ42 in ongoing ADAD prevention trials, and, more broadly, in understanding how CSF- vs. PET-based amyloid measurements may relate to AD-related cognitive decline.

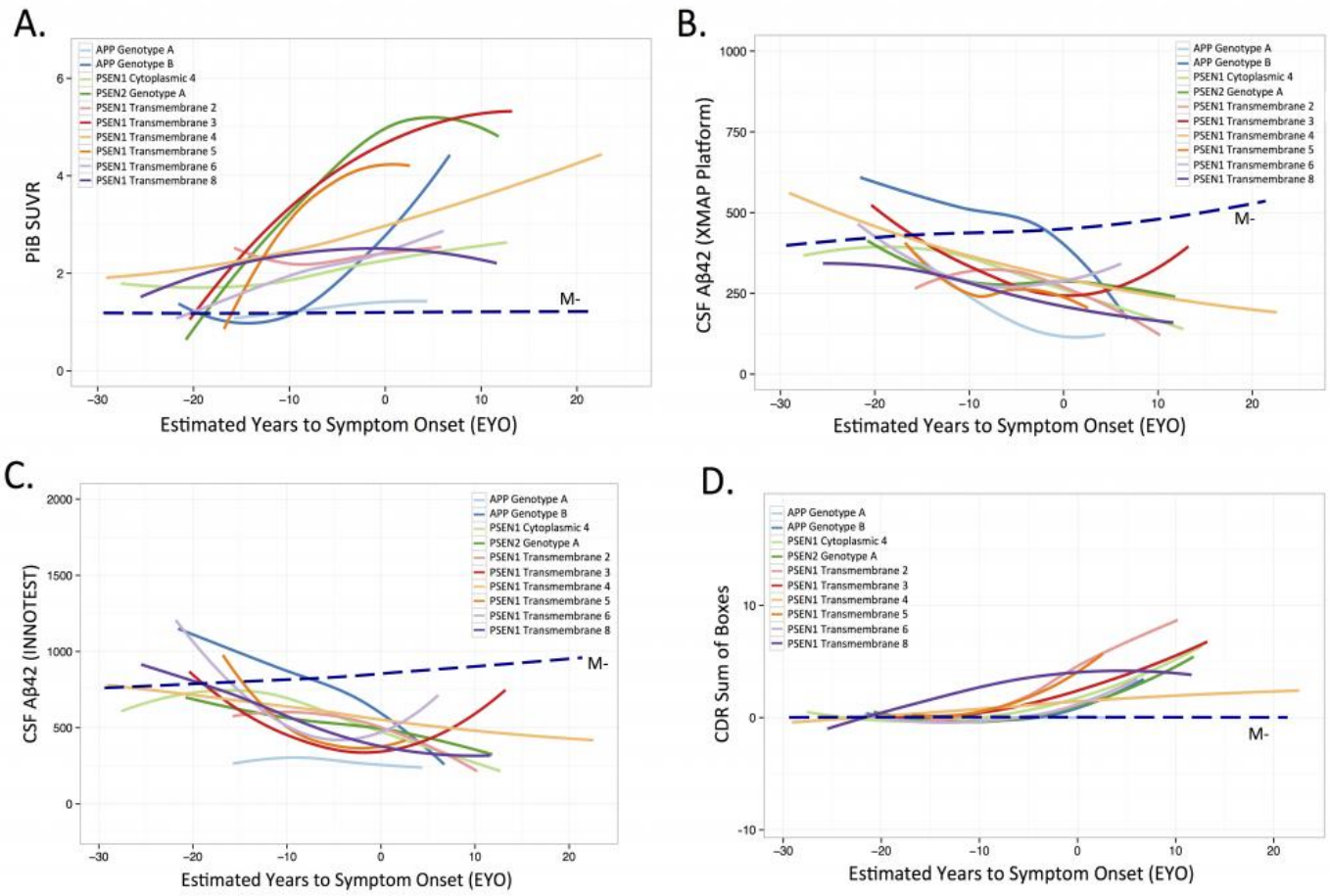

Figure 1: *Inter-genotype Variance in Measures of Amyloid Burden in ADAD.* (A) Amyloid burden in the posterior cingulate and precuneus as measured by PiB PET varies significantly across genotype category (genotype by EYO interaction, p = 0.009). (B and C) Beta-amyloid as assessed by immunoassays for CSF Aβ42 on the XMAP (B) and INNOTEST ELISA platforms (C) do not show significant variation by genotype category (genotype by EYO interaction, p > 0.8 for both comparisons). (D) Clinical Dementia Rating Scale Sum of Boxes scores across the spectrum of EYO also do not vary by genotype category (genotype by EYO interaction, p = 0.34). Trajectories illustrated using locally weighted scatter plot smoothing (LOWESS).

Keywords: Pittsburgh Compound B, Alzheimer's Disease, CSF, genetics, Presenilin

Relationships between AV1451-PET and CSF biomarkers in a heterogeneous clinical sample

Renaud La Joie[1], Alexandre Bejanin[2,3,4], Anne Fagan[1], Nagehan Ayakta[5], Suzanne Baker[1], Viktoriya Bourakova[1], Anna Karydas[5], James O'Neil[1], Julie Pham[1], Adrienne Visani[1], Howard Rosen[1], Adam Boxer[1], Bruce Miller[1], William Jagust[5,6], Gil Rabinovici[1,6]

[1]1 Memory and Aging Center, University of California San Francisco, san francisco, CA, USA
[2]2 Knight Alzheimer's Disease Research Center, Washington University in St. Louis, St. Louis, MI, USA
[3]Department of Neurology, Washington University in St. Louis, St. Louis, MI, USA
[4]The Hope Center for Neurological Disorders, Washington University in St. Louis, St. Louis, MI, USA
[5]Life Sciences Division, Lawrence Berkeley National Laboratory, Berkeley, CA, USA
[6]Helen Wills Neuroscience Institute, University of California Berkeley, Berkeley, CA, USA

Objective: To determine the relationships between AV1451-PET and cerebrospinal fluid (CSF) biomarkers in a heterogeneous sample of memory clinic patients.

Methods: We studied patients seen at UCSF Memory and Aging Center with available AV1451-PET, PIB-PET and CSF biomarkers (median between PET and lumbar puncture: 114 days). This included 19 Aβ-PET positive patients with AD and 13 patients with suspected non-AD etiologies (see Table 1). CSF samples were analyzed for total tau (T-tau), phosphorylated tau (P-tau181), and $A\beta_{42}$ at Washington University using Alzbio3 xMAP immunoassay (Fujirebio). AV1451 data were processed using Freesurfer 5.3 and SPM12. We examined associations between CSF markers and 1) global gray matter AV1451 SUVR, ii) spatial extent of elevated AV1451-uptake (i.e. the percentage of voxels with Z value > 2 compared to 41 Aβ-PET-negative healthy older adults), and iii) the topography of AV1451 using voxelwise analyses.

Results: In the full sample, both P-tau and T-tau were strongly related to AV1451-PET measures but also to PIB-PET uptake (Figure 1, black lines), these associations being mostly driven by differences between the AD and non-AD groups. When restricting the analyses to Aβ-PET-positive AD patients, significant associations were found between measures of cortical AV1451 and P-tau (Figure 1, yellow lines), but not between AV1451 and total tau or $A\beta_{42}$. On voxel-wise analysis in Aβ+ AD, P-tau was associated with AV1451 retention in cingulate, precuneus and lateral parietal areas, whereas T-tau was related to increased medial prefrontal and left temporal uptake (Figure 2).

Conclusion: In a heteregenenous clinical sample, AV1451 imaging was strongly associated with CSF measures of tau but not $A\beta_{42}$. In AD, although P-tau was the only correlate of global AV1451 metrics, P-tau and T-tau showed distinct regional correlations with AV1451 uptake, suggesting they may be capturing different elements of disease pathophysiology or stage.

	Aβ+ AD	Other patients	statistics
n	19	13	
Age	61 [57, 65]	68 [60, 74]	U = 84, p = .13
Gender: n_F / n_M	11 / 8	4 / 9	p = .17
Years of education	17 [16, 18]	16 [14.25, 18]	U = 122, p = .38
MMSE	22 [19.5, 26.3]	27 [19.5, 28]	U = 88, p=.25
CDR n_0 / $n_{0.5}$ / n_1 / n_2	1 / 8 / 9 / 2	3 / 8 / 1 / 1	U = 173.5, p=.03

Table 1. Continuous variables are presented as median [1st quartile, 3rd quartile] while exact numbers are provided for categorical and ordinal variables. Groups were compared using Mann Whitney test for continuous and ordinal variables and Fisher's exact text for categorical variables.

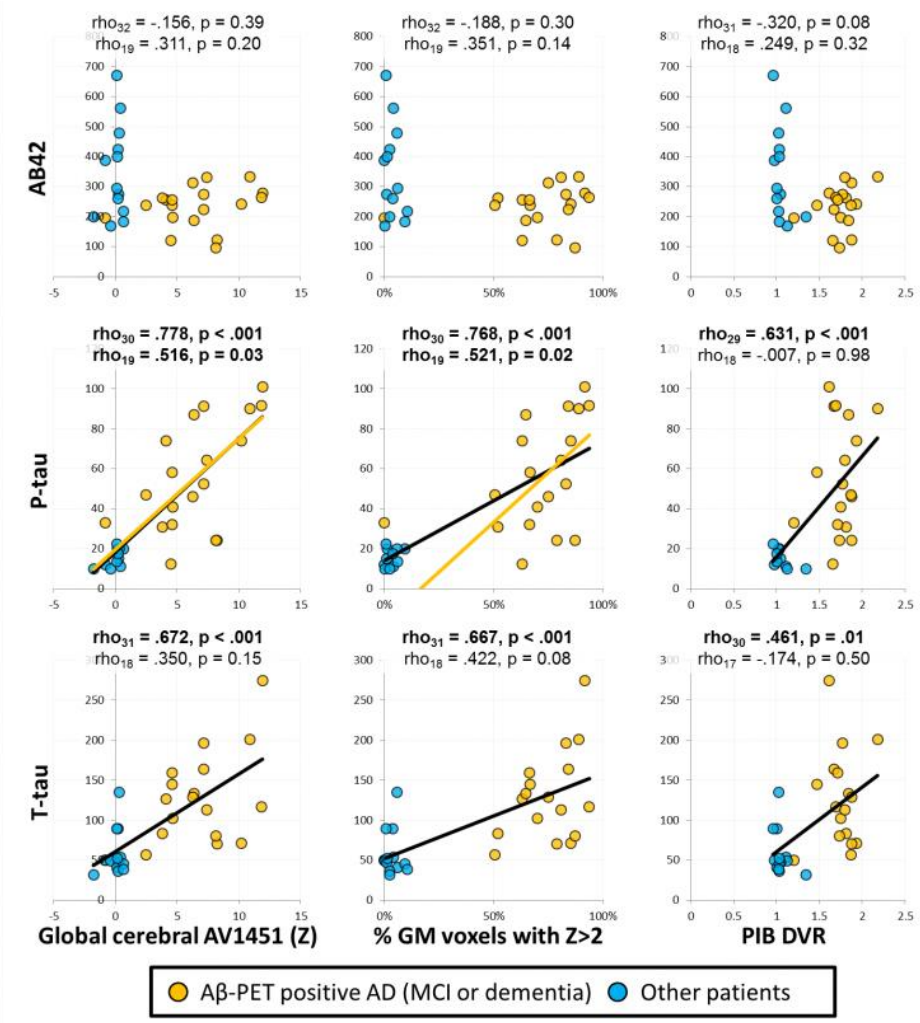

Figure 1. Correlation between CSF biomarkers and metrics of AV1451-PET (global burden and spatial extent) as well as PIB-PET. Associations were assessed using spearman correlations in the whole group (black line when p<0.05) and in the Aβ-PET-positive AD group (yellow line when p<0.05). Statistical indices are indicated for each pair of variables (top line: full sample, bottom line: Aβ-PET-positive AD group).

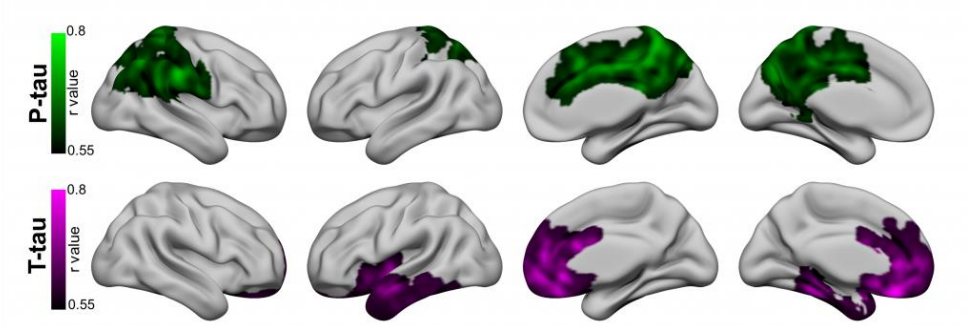

Figure 2. Areas of significant association between AV1451-uptake and P-tau or T-tau in the group of 19 Aβ-PET-positive AD patients. A combination of thresholds ($P_{uncorrected}$<0.005 at the voxel level and P_{FWE}<0.05 at the cluster level) was used.

Keywords: Alzheimer's disease, AV1451, Cerebrospinal fluid

Friday, January 13, 2017 - 04:00 pm - 04:45 pm

Poster Session 3B - *see 3A*

Friday, January 13, 2017 - 04:50 pm - 05:35 pm

SESSION 10: Amyloid and Tau PET in Distinct Populations

SESSION 10 **Amyloid and Tau PET in Distinct Populations**	**CHAIRS:** **Trey Hedden** ***Massachusetts General Hospital*** **Charles de Carli** ***University of California, Davis***
Association of regional FDG hypometabolism with age, amyloid, tau, and cardiac and metabolic conditions along the AD continuum	Prashanthi Vemuri *Mayo Clinic*
18F-AV1451 PET in patients with subcortical vascular cognitive impairment	Sang Won Seo *Sungkyunkwan University School of Medicine*
White matter hyperintensities and brain amyloid deposition: The ARIC-PET Study	Rebecca Gottesman *Johns Hopkins University*
Association of amyloid-beta plaque accumulation and glucose hypometabolism in Down syndrome demonstrates pattern associated with Alzheimer's disease	Patrick Lao *University of Wisconsin*
Discussion	

Association of regional FDG hypometabolism with age, amyloid, tau, and cardiac and metabolic conditions along the AD continuum

Prashanthi Vemuri, Val Lowe, David Knopman, Jonathan Graff-Radford, David Jones, Matthew Senjem, Heather Wiste, Mary Machulda, Ronald Petersen, Clifford Jack Jr.

[1]*Mayo Clinic, Rochester, MN, USA*

Introduction: Our goal was to understand the association of age, amyloid via PIB-PET, tau via AV1451-PET, and cardiac and metabolic conditions (CMC variable – composite of presence/absence of hypertension, hyperlipidemia, cardiac-arrhythmias, coronary artery disease, congestive heart failure, diabetes mellitus, stroke) with hypometabolism via FDG-PET in individuals along the AD continuum. We hypothesized that regional tau deposition, age, and CMC but not amyloid would be strongly coupled with regional hypometabolism.

Methods: We identified 474 individuals (52 between 30-49 years as reference group, 360 clinically normal (CN) elderly ≥50 years of whom 120 were amyloid positive, and 62 amyloid positive MCI and dementia) with Tau-PET, FDG-PET, and amyloid-PET scans from the Mayo Clinic Study of Aging and Mayo Alzheimer's disease research center. We estimated correlations between each of the variables with regional FDG-PET. We computed regional z-scores for tau and FDG based on the reference group such that higher z-scores corresponded to worse biomarkers. We used a cut-off of 2 and applied it to individuals in the 50+ group to classify regions as normal and abnormal.

Results: In CN, age and CMC were more correlated with FDG hypometabolism compared to regional amyloid and tau deposition correlations with regional FDG adjusted for age. In clinically impaired individuals, regional tau had stronger associations with regional FDG compared to regional or global amyloid or age and the associations between FDG and tau were high in the parietal, temporal, and frontal lobes ($p<0.001$). Using regional z-score cutoff of 2 for FDG and tau in 50+ CN, we found that regional tau was more often abnormal due to amyloid positivity than regional FDG.

Discussion: These results provide evidence that tau deposition may be an earlier event compared to FDG hypometabolism and FDG is more likely to be abnormal when individuals start showing clinical symptoms along the AD continuum.
Keywords: Amyloid PET, Tau PET, FDG hypometabolism, cardiac and metabolic conditions

18F-AV1451 PET in patients with subcortical vascular cognitive impairment

Hee Jin Kim[1], Hanna Cho[2], Seongbeom Park[1], Young Kyoung Jang[1], Jin San Lee[1], Hyemin Jang[1], Yeshin Kim[1], Ko Woon Kim[1], Young Hoon Ryu[3], Jae Yong Choi[3], Duk L. Na[1], Chul Hyoung Lyoo[2], Sang Won Seo[1]

[1]Departments of Neurology, Samsung Medical Center, Sungkyunkwan University School of Medicine, Seoul, Korea
[2]Department of Neurology, Gangnam Severance Hospital, Yonsei University College of Medicine, Seoul, Korea
[3]Department of Nuclear Medicine, Gangnam Severance Hospital, Younsei University College of Medicine, Seoul, Korea

Background: We aimed to evaluate the distribution and clinical significance of tau in patients with subcortical vascular cognitive impairment (SVCI).

Methods: We recruited 51 SVCI patients and 20 normal controls (NCs). We assessed imaging markers for small vessel disease such as the volume of white matter hyperintensities, number of lacunes, deep micorbleeds and lobar microbleeds. The presence of amyloid was assessed by ^{18}F-florbetaben PET. All participants underwent ^{18}F-AV1451 PET to measure paired helical filament (PHF)-tau at Gangnam Severance Hospital. Using cerebellar gray matter as a reference region, we measured regional AV1451 SUVR. We used freeSurfer-derived region of interests that approximates the anatomical definitions of the Braak stages: Braak I/II ROI corresponded to the entorhinal stage, Braak III/IV ROI to the limbic stage, and Braak V/VI ROI to the isocortical stage.

Results: NCs showed localized AV1451 uptake in the bilateral medial temporal subregions while, SVCI patients showed increased uptake in more extended areas which included the medial, inferior and lateral temporal areas; precuneus; and medial and orbitofrontal regions. When we compared AV1451 SUVR in each Braak stage ROI, SVCI patients showed higher AV1451SUVR across all the Braak stage ROIs, compared to NCs. Among the SVCI patients, those who were amyloid positive showed higher AV1451 uptake in the medial and inferior temporal regions. The higher number of lobar microbleeds was associated with higher AV1451 uptake in the inferior and lateral temporal, precuneus, and lateral parietal regions. In SVCI patients, higher AV1451 uptake correlated with worse cognitive function in language, visuospatial function, and general cognition. Path analysis showed that amyloid and lobar microbleed each contributed to increased AV1451 uptake which in turn led to cognitive impairment.

Conclusions: SVCI patients had increased tau compared to NCs. Amyloid and lobar microbleeds each contributed to increased tau, which in turn led to cognitive impairments.

Keywords: Subcortical vascular cognitive impairment,AV1451, paired helical filament tau, amyloid, small vessel disease

White matter hyperintensities and brain amyloid deposition: The ARIC-PET Study

Rebecca Gottesman[1], Zeyi Wang[1], Yun Zhou[1], Brian Caffo[1], Edward Green[2], Naresh Gupta[3], Timothy Hughes[4], Cliff Jack[5], David Knopman[5], Akiva Mintz[4], Arman Rahmim[1], A. Richey Sharrett[1], Lynne Wagenknecht[4], Dean Wong[1], Thomas Mosley[2]

[1]*Johns Hopkins University, Baltimore, MD, USA*
[2]*University of Mississippi Medical Center, Jackson, MS, USA*
[3]*Hagerstown Imaging, Hagerstown, MD, USA*
[4]*Wake Forest University, Winston-Salem, NC, USA*
[5]*Mayo Clinic, Rochester, MN, USA*

Objective: Microvascular changes in the brain have been associated with cognitive impairment and clinical dementia, but data are conflicting as to the role of brain microvascular disease in Alzheimer's Disease (AD) specifically. In this study, we evaluated the cross-sectional association between brain small vessel disease and brain amyloid, among participants in the community-based Atherosclerosis Risk in Communities (ARIC)-PET Amyloid Imaging Study.

Methods: Dementia-free participants from three U.S. communities, (n=326) aged 67-89, underwent brain MRI scans, with standardized measurement of brain infarcts and white matter hyperintensities (WMH), and florbetapir PET, with standardized uptake value ratio (SUVR) measurement in regions of interest. A global cortex SUVR measure was calculated; values above the sample median (SUVR>1.2) were considered abnormal. Logistic multivariable regressions were considered, with sequential adjustment for demographics and vascular risk factors, as well as APOE genotype. Effect modification by race and APOE status was also evaluated.

Results: The cohort was 43% black, 57% female, with mean age 75.8 years. Presence of any infarct, or any lacunar infarct, was not significantly associated with increased odds of amyloid positivity (Table 1). In the overall sample, WMH volume (per standard deviation) was associated with higher odds of elevated brain amyloid only in unadjusted models (unadjusted OR 1.41, 95% CI 1.10, 1.88), with loss of significance with further adjustment (Table 1). However, in demographic-adjusted models, WMH was associated with elevated amyloid among APOE e4 noncarriers (OR 1.39, 95% CI 1.01-1.99), but not in carriers (OR 1.09, NS; Table 2). No formal interactions by APOE or by race were identified, although associations tended to be stronger in blacks than in whites (p-interaction NS; Table 3).

Conclusions: We did not find evidence of an association between brain small vessel disease and elevated amyloid, although this may be due to lack of adequate power, in this community-based cohort.

Table 1. Associations between markers of cerebrovascular disease by brain MRI and elevated brain amyloid (defined as SUVR>1.2).

	Model 1 OR	95% CI	Model 2 OR	95% CI	Model 3 OR	95% CI
Any infarct	1.34	0.81-2.23	1.33	0.80-2.22	1.33	0.79-2.25
Any lacunar infarct	1.06	0.60-1.86	1.04	0.59-1.84	0.96	0.53-1.74
White matter hyperintensity volume (per SD)*	1.28	0.98-1.74	1.26	0.96-1.71	1.29	0.97-1.76

Model 1 : adjusted for age, sex, race, educational attainment
Model 2: Model 1 + hypertension, diabetes, current smoking, BMI
Model 3: Model 2 + APOE
*Total intracranial volume added as covariate in all models for white matter hyperintensity volume

Table 2. Association between white matter hyperintensity volume and elevated brain amyloid, stratified by APOE status.

	OR: APOE ε4 carriers (N=102)	95% CI	OR: APOE ε4 noncarriers (N=224)	95% CI
Model 1	1.09	0.64-2.16	1.39	1.01-1.99
Model 2	0.97	0.56-2.00	1.34	0.98-1.92
Model 3	NA	NA	NA	NA

Model 1 : adjusted for age, sex, race, educational attainment, total intracranial volume
Model 2: Model 1 + hypertension, diabetes, current smoking, BMI
Model 3: Model 2 + APOE

Table 3. Association between white matter hyperintensity volume and elevated brain amyloid, stratified by race.

	OR: Blacks (N=141)	95% CI	OR: Whites (N=185)	95% CI
Model 1	1.54	0.95-2.83	1.15	0.83-1.60
Model 2	1.58	0.95-2.99	1.15	0.83-1.61
Model 3	1.59	0.95-3.02	1.20	0.86-1.70

Model 1 : adjusted for age, sex, race, educational attainment, total intracranial volume
Model 2: Model 1 + hypertension, diabetes, current smoking, BMI
Model 3: Model 2 + APOE

Keywords: cerebrovascular disease, epidemiology, amyloid, white matter hyperintensities

Association of amyloid-β plaque accumulation and glucose hypometabolism in Down syndrome demonstrates pattern associated with Alzheimer's disease

Patrick Lao[1], Tobey Betthauser[1], Julie Price[2], William Klunk[2], Peter Bulova[2], Sigan Hartley[1], Regina Hardison[2], Rameshwari Tumuluru[2], Dhanbalan Murali[1], Chester Mathis[2], Annie Cohen[2], Todd Barnhart[1], Dana Tudorascu[2], Darlynne Devenny[3], Charles Laymon[2], Sterling Johnson[1], Ben Handen[2], Bradley Christian[1]

[1]*University of Wisconsin-Madison, Madison, WI, USA*
[2]*University of Pittsburgh, Pittsburgh, PA, USA*
[3]*New York State Institute for Basic Research in Developmental Disabilities, New York City, NY, USA*

Background: Amyloid-β plaques and cerebral hypometabolism are two common biomarkers for Alzheimer's disease (AD). The aim of this work was to use amyloid PET and FDG PET to provide insight into the association between these two AD biomarkers in the Down syndrome (DS) population, which is genetically predisposed to both the overproduction of amyloid-β and AD.

Methods: Twenty-three non-demented adults (38.6±7.0yrs;12M,11F) with DS underwent PiB PET scan and a subsequent FDG PET scan (124.7±102.6 days apart). Standard uptake value ratios (SUVRs) were calculated for PiB (50-70 min) and FDG (40-60 min) using cerebellar gray matter as reference region. Parametric SUVR images were spatially normalized using tracer-specific templates and analyzed in MNI space. Biological parametric mapping (BPM; MATLAB2011a,SPM5) was used to investigate associations between PiB and FDG SUVR images, adjusted and unadjusted for chronological age and sex using a linear regression model on the voxel level (8mm smoothing, cluster size >1000 voxels, α=0.001 uncorrected).

Results: PiB SUVR and FDG SUVR were negatively associated in the precuneus and temporal cortex (|r|=0.62-0.84), which survived separate correction for sex and age. There were no clusters of significant positive association between PiB and FDG SUVRs. Representative SUVR images demonstrate that subjects with low PiB retention also had uniform FDG uptake (with the exception of elevation occipital lobe uptake), and subjects with high PiB retention in the striatum and cortex had low FDG uptake in the precuneus and temporal cortex (Figure1).

Conclusions: Non-demented adults with DS demonstrated early and elevated PiB retention followed by reductions in FDG uptake. Glucose hypometabolism occurred in the precuneus and temporal cortex in a pattern typical of that seen in late-onset AD. Also similar to late-onset AD, PiB retention and metabolism were negatively associated only in these posterior regions, and not in frontal cortex.

Research Support: R01 AG031110, U54 HD090256, U01 AG051406

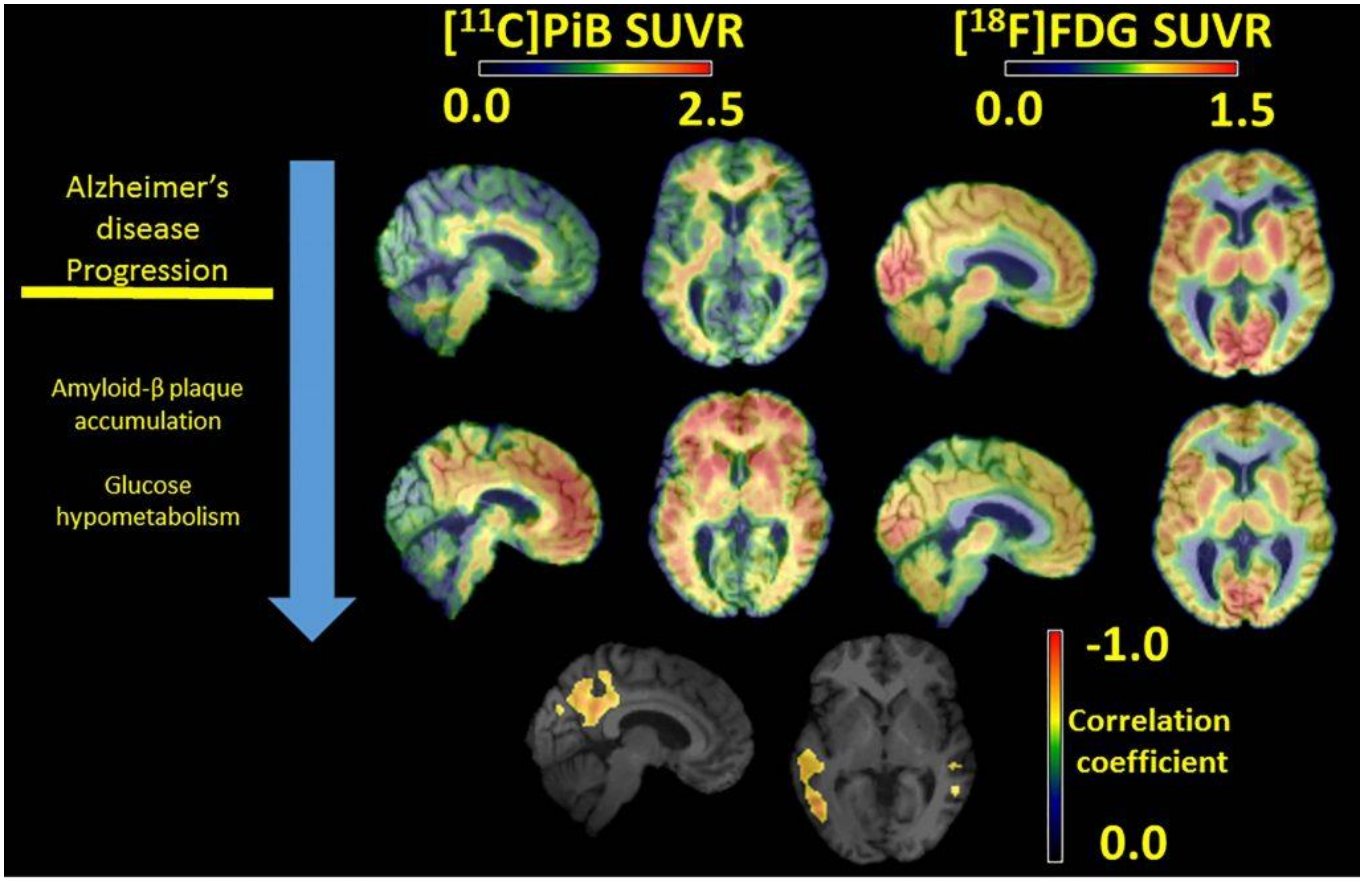

Representative [^{11}C]PiB and [^{18}F]FDG SUVR images from two non-demented adults with Down syndrome demonstrating the expected progression of Alzheimer's disease. The bottom row shows the statistically significant clusters of negative association between PiB and FDG SUVRs ($p<0.001$) from a voxel-wise analysis.

Keywords: Down syndrome, Alzheimer's disease, PiB, FDG, BPM

NOTES

Funding for this conference was made possible in part by grant R13 AG042201 from the National Institute on Aging and the National Institute of Biomedical Imaging and Bioengineering.

The 11h Human Amyloid Imaging Conference is supported through educational grants from:

PLATINUM

Lilly

For further information
concerning Lilly grant funding
visit www.lillygrantoffice.com

GOLD

GE Healthcare

Biogen

Silver

janssen
PHARMACEUTICAL COMPANIES OF Johnson&Johnson

Bronze

abbvie

MERCK

Piramal
knowledge action care

BIOCLINICA
SEE MORE CLEARLY

www.worldeventsforum.com/hai or mobile app: http://my.yapp.us/HAICONF